DYNAMIC CONTROL OF GRID POWER FLOW USING CONTROLLABLE NETWORK TRANSFORMERS

A Thesis
Presented to
The Academic Faculty

by

Debrup Das

In Partial Fulfillment
of the Requirements for the Degree
Doctor of Philosophy in the
School of Electrical and Computer Engineering

Georgia Institute of Technology
May, 2012

DYNAMIC CONTROL OF GRID POWER FLOW USING CONTROLLABLE NETWORK TRANSFORMERS

Approved by:

Dr. Deepakraj M. Divan, Advisor
School of Electrical and Computer Engineering
Georgia Institute of Technology

Dr. Saibal Mukhopadhyay
School of Electrical and Computer Engineering
Georgia Institute of Technology

Dr. Ronald G. Harley
School of Electrical and Computer Engineering
Georgia Institute of Technology

Dr. J. Rhett Mayor
School of Mechanical Engineering
Georgia Institute of Technology

Dr. Thomas G Habetler
School of Electrical and Computer Engineering
Georgia Institute of Technology

Date Approved: 11/29/2011

To my parents, my brother and my wife

ACKNOWLEDGEMENTS

I joined Georgia Tech just after completing my bachelor's degree. It was a big change for me and it was not just from the academic perspective. In retrospect, for someone who had never even visited any other country, and whose travels even within his country were few and far between, it should have been a daunting decision to make. Frankly, for me it was not. Sure I had my share of "what ifs", but the idea of doing my PhD in USA was more exciting than intimidating, it was like a dream come true. I would like to thank everyone who helped me fulfilling this dream.

I am greatly indebted to my advisor Prof. Deepak Divan for shaping up my thoughts and helping me over and over again for the last five years. His constant encouragement and advice has been invaluable to me. I am also grateful to Prof. Thomas Habetler, Prof. Ronald G. Harley, and Prof. A.P. Meliopoulos for their guidance during various stages of my PhD life. I would also like to thank Prof. Saibal Mukhopadhyay and Prof. Rhett J. Mayor for serving on my PhD defense committee and for their valuable suggestions.

I would like to acknowledge the National Science Foundation and the Southern Company for their financial support for this research work. I would also like to thank Mr. Frank Lambert, Mr. James Steinberg and Ms. Deborah King for their support and help.

I would also like to thank my fellow graduate researchers at Georgia Tech, Harjeet Johal, Yi Yang, Rohit Moghe, Rajendra Prasad Kandulla, Anish Prasai, Jyoti Sastry, Andrew Paquette, Frank Kreikebaum, Ravi Shankar Nilakantan, Jiaqi Liang, Siwei Cheng, Jorje Hernandes and Prasun Johari for their support.

I would especially like to thank Shreyas Sen, my friend and my roommate for five years in Atlanta. In addition I would like to thank all my friends for their wonderful friendship and support throughout my stay in Atlanta. My heartfelt gratitude for Aritra Banerjee, Ananda Barua, Gopal Jha, Kshitij Asthana, Tapobrata Bandopadhyay, Prabir Saha, Zannatul Ferdous, Arindam Basu, Subho Chatterjee, Proma Chatterjee, Atri Dutta, Lipilekha Dutta, Koushik Kundu, Priya Kundu, Saikat Sarkar, Payel Paul, Ayan Chakrabarti, Payel Chaterjee, Samit Ghosh, Rimi Hazra, Risa Ghosh, Padmanava Sen, Arup Polley, Rita Bui, Nand Jha, Neha Jha, Mrinmoy Ghosh, Chandan Dasgupta, Neena Majumdar, Bevin George Perumana and Jithu Susan Mathew. It was a pleasure to get to know you all.

Last but not the least I would like to thank my parents, my brother and my wife for their unconditional love and support.

TABLE OF CONTENTS

LIST OF FIGURES

LIST OF TABLES

LIST OF SYMBOLS AND ABBREVIATIONS

CNT	controllable network transformer
LTC	load tap changer
DVQS	dual virtual quadrature sources
TACC	thin ac converter
HAF	hybrid active filter
FACTS	flexible ac transmission systems
BTB	back-to-back converter system
OPF	optimal power flow
PWM	pulse width modulation
D	duty cycle
K_0	DC component of D
K_2	amplitude of the second harmonic component of D
Φ	phase of the second harmonic component of D

SUMMARY

The objective of the research is to develop a cost-effective, dynamic grid controller called the controllable network transformer (CNT) that can be implemented by augmenting existing load tap changing (LTC) transformers with an AC-AC converter. The concept is based on using a fractionally rated direct AC-AC converter to control the power through an existing passive LTC. By using a modulation strategy based on virtual quadrature sources (VQS), it is possible to control both the magnitude and the phase angle of the output voltage of the CNT without having any inter-phase connections. The CNT architecture has many advantages over existing power flow controllers, like absence of low frequency storage, fractional converter rating, retro-fitting existing assets and independent per-phase operation making it potentially attractive for utility applications.

The independent control of the magnitude and the phase angle of the output voltage allow independent real and reactive power flow control through the CNT-controlled line. In a meshed network with asymmetric network stresses this functionality can be used to redirect power from critically loaded assets to other relatively under-utilized parallel paths. The power flow controllability of CNT can thus be used to lower the overall cost of generation of power. The solid state switches in the CNT with fast response capability enable incorporation of various additional critical functionalities like grid fault ride through, bypassing internal faults and dynamic damping. This bouquet of features makes the CNT useful under both steady state and transient conditions without compromising the grid reliability.

CHAPTER 1

1. OBJECTIVE OF THE RESEARCH

1.1 Introduction

The US grid is at the brink of a profound change. The increased load demand, increasing penetration of highly stochastic renewable energy and limited transmission investments has significantly increased the stress level on the grid. The energy outlook of the customers has also changed significantly over time, thereby creating an increased demand for better quality, high reliability and environmentally friendly energy. The slow electromechanically controlled grid of the previous century needs to be revamped drastically in order to make it capable of fulfilling the new objectives of the energy delivery system.

The electricity grid can be generally divided into three sectors – generation, transmission and distribution. The traditional grid, which was more radial in structure, had most of its controls located at the generation sector. However, with increasing requirement of high reliability, the grid shifted to a more radial structure. The lack of controllability of transmission lines gave rise to problems such as congestions. Traditionally congestion is tackled by building more transmission capacity. However, various market forces and regulatory requirements of today make it very difficult to build new transmission lines. Dynamic control of power flow has thus become an increasingly important need for the electricity grid. Increased penetration of stochastic renewable

resources like wind and solar energy has further raised the need of dynamic power flow control.

One of the methods of tackling this problem is to transform the present grid in a cost effective way into a smart and controllable grid which is fast, adaptive, self-healing, efficient and reliable. This research outlines the development of a dynamic power flow controller, which can be realized by retro-fitting an existing grid asset, making it more smart and controllable.

1.2 Objective

The objective of the research is to develop a cost-effective, dynamic grid controller called the controllable network transformer (CNT) that can be implemented by augmenting existing load tap changing (LTC) transformers with an AC-AC converter. The concept is based on using a fractionally rated direct AC-AC converter to control the power through an existing passive LTC. By using a modulation strategy based on virtual quadrature sources (VQS), it is possible to control both the magnitude and the phase angle of the output voltage of the CNT without having any inter-phase connections. This strategy helps with avoiding generation of complex fault modes and disturbances, which may arise as a result of coupling between phases. The independent control of the magnitude and the phase angle of the output voltage allow independent real and reactive power flow control through the CNT-controlled line. In a meshed network with asymmetric network stresses this functionality can be used to redirect power from critically loaded assets to other relatively under-utilized parallel paths. The power flow controllability of CNT can also be used to implement power transfer contracts between

two control areas. The solid state switches with fast response capability enable incorporation of various additional critical functionalities like grid fault ride through, bypassing internal faults and power oscillation damping in the CNT. This bouquet of features makes the CNT useful under both steady state and transient conditions without compromising the grid reliability.

The main advantage of the CNT is derived from its design, which uses only a fractionally rated converter to control the power through the line. The converter rating is expected to be only 20-40% of the LTC rating. This reduces the cost and complexity of the converter to a great extent, especially in context of unavailability of robust high-power, solid-state devices. The direct converter does not require any low-frequency storage capacitor, which also reduces the cost of implementation of the converter significantly. The reliability of the CNT is ensured to be at least that of the LTC, as its converter is provided with a fast bypass option, which can be activated in case of internal faults.

1.3 Outline of Chapters

The dissertation begins by outlining the problem statement in Chapter 2. Some of the existing problems in the transmission sector are analyzed. A comprehensive literature survey of power flow controllers is presented. Limitations of the existing techniques are highlighted and desired features for a new power flow control technology are outlined. The chapter also gives a short history of development of direct AC-AC converters.

Chapter 3 introduces the Controllable Network Transformer (CNT) – the proposed power flow controller. The salient features of the technology and its benefits compared to

existing power flow controllers are highlighted. The basic operation of the power flow controller is described and an analytical, steady-state model of the device is developed. This model is verified in simulation. The model is also used to define control boundaries of the power flow controller. A low voltage experiment validating the basic principle of operation is demonstrated.

Chapter 4 shows the potential impact of the CNT on large power networks. A modified loadflow algorithm is developed for networks with CNTs. The ability of CNTs in improving network dynamic stability is also analyzed.

The problem of optimal placement and control of CNTs in a large network is tackled in Chapter 5. The developed techniques are run on test systems to analyze the potential benefit of the CNT technology compared to present power flow control technologies.

The third harmonic filter for the CNT is designed in Chapter 6. The methodology for optimal design of such a filter is also highlighted.

Chapter 7 gives the details of design, implementation and testing of a medium voltage CNT prototype. The loss calculations of the CNT converters are also presented along with the dynamic power flow control demonstration.

Finally, Chapter 8 summarizes the contribution of this research and suggests some of the possible future works.

CHAPTER 2

2. ORIGIN AND HISTORY OF THE PROBLEM

The electricity transmission system is an extensive, interconnected network of high voltage power lines that transport electricity from the generators to the consumer. The U.S. grid, which presently spans the country with more than 160,000 miles of lines, was built incrementally over the last 125 years. Since the introduction of competition in the wholesale electricity market in the early ‘90s, the transmission system has essentially been transformed into an interstate highway system for enabling wholesale electricity commerce. Nondiscriminatory transmission access to wholesale energy suppliers is ensured by the seven independent system operators (ISOs) and the regional transmission organizations (RTOs).

In order for the electricity market to be successful, it is pertinent that the grid be able to deliver electricity reliably to the consumers at the lowest possible cost. However, presently the transmission sector is plagued by several problems and issues, which should be addressed in order for it to operate efficiently.

2.1 Increasing Load Demand

Increasing automation in industrial, commercial and residential sectors has led to a 2.5% average annual increment of electricity consumption over the past two decades. The projections for future electricity demand also point towards increased electrification. Figure 2.1 shows the steady increase in electricity consumption in the U.S. over the last 20 years [1].

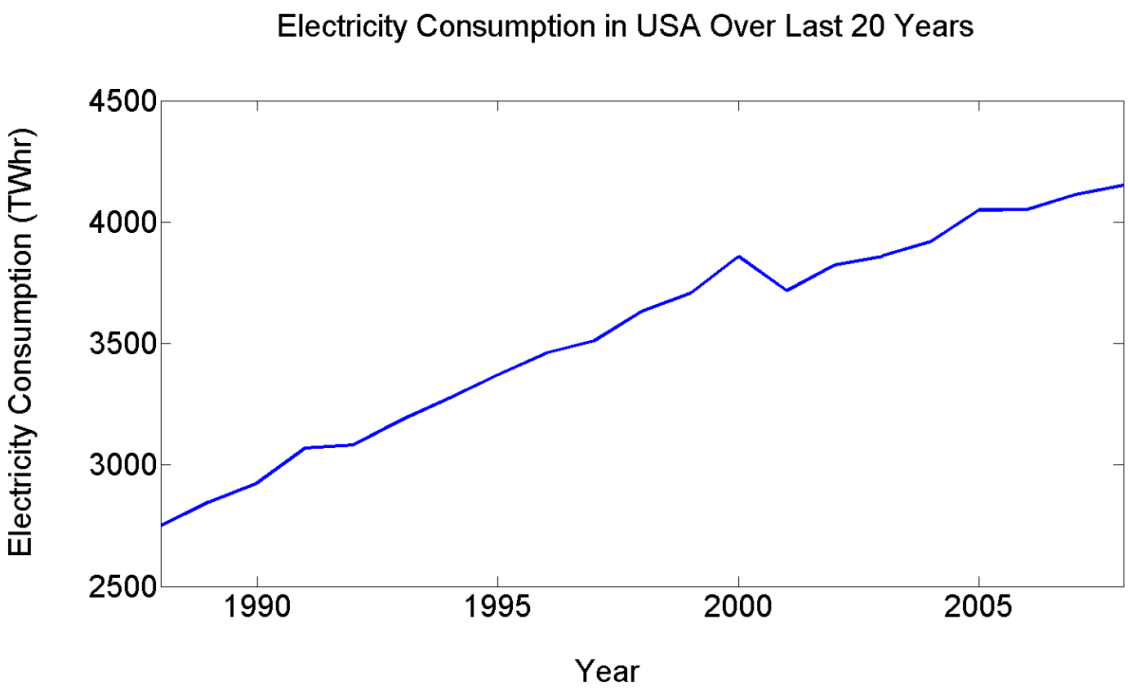

Figure 2.1: Electricity consumption in USA over last 20 years

The seemingly imminent shift of the automotive industry towards electrically powered technologies is expected to have a significant impact on the electricity demand, especially in the residential sector. The transmission system has to keep up with this increased electricity demand. One possible way of controlling the ever increasing electricity demand is to adopt more energy efficient technologies. Although some efficiency improvement programs have been adopted both at the federal as well as the state level, the large scale impact of these programs is yet to be seen.

2.2 Increased Grid Interconnections

At its inception and for most part of the 20th century the transmission network was conceived as a radial connection from energy generation sources to their loads. However, as electricity became a basic infrastructure requirement, reliable delivery of electricity to

customers became increasingly important. The eventual establishment of reliability policies, which mandated utilities to deliver electricity reliably to their customers, forced utilities to incorporate multiple changes both in the operation as well as in the planning sector. In the operation sector, the concept of N-1 and N-2 contingency operation became the benchmarks, whereby utility systems were required to operate safely even with one or two of the worst possible contingencies. This stringent requirement in utility operations translated to redundancy and overbuilding in utility planning.

Reliability of transmission systems can be increased in a cost-effective manner by interconnecting neighboring systems, as it ensures alternate paths of energy flow in case of contingencies without extensive built-out. As a result most transmission systems shifted from a radial structure to a more meshed network. Although meshed networks are highly reliable, they possess one serious drawback – their power flow cannot be easily controlled. Also because of the inherent asymmetry of the meshed networks' path impedances, energy flow through the parallel paths is unevenly distributed, leading to asymmetrical stresses on the transmission assets. The throughput of a meshed transmission network is limited by the first line that reaches its thermal limit. These transmission line congestions increase the cost of electricity significantly. It is estimated that the cost of congestion in 2008 for Pennsylvania-New Jersey-Maryland (PJM) interconnection alone was $2.1 billion [2].

2.3 Increased Grid Dynamics

The growing concern over climate deterioration because of increased industrialization and CO_2 emissions has generated significant public interest in green energy. As many as 29 US states have already adopted policies like renewable portfolio standards (RPS) to

encourage early adoption of renewable energy [3]. Other state led initiatives include efforts like the regional greenhouse gas initiative (RGGI), and implementation of requirements that green options be included among retail electricity plans [4]. The shift from fossil-fuel-based energy to renewable energy is expected to gain further momentum if the American Clean Energy and Security Act of 2009 is implemented, which includes a national renewable electricity standard of up to 20% by the year 2020 [5]. Figure 2.2 shows the level of renewable penetration achieved in the North American power grid over the last 20 years and the projected penetration in the near future.

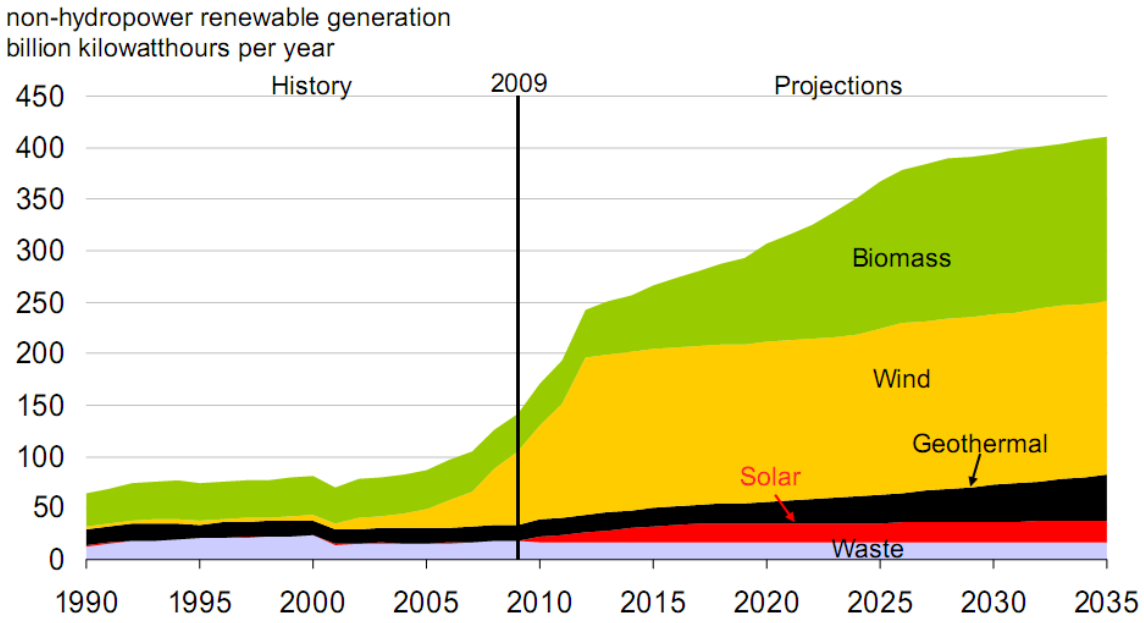

Figure 2.2: Non-hydropower renewable generation in US over the last two decades and its projection over the next two decades

Increasing penetration of renewable resources in the electric grid is expected to pose significant challenges in grid operation and planning. Unlike fossil-fuel-powered generators whose output power can be controlled by fuel injection, power from renewable resources like wind and solar depends on variables like wind speed, solar

insolation, etc. and are thus highly stochastic in nature. The grid has to be improved to handle the dynamics caused by the variability of these resources while meeting current metrics. This will be challenging, especially as the penetration of renewable resources is increased [6]. Renewable generation prefers to be sited where the most cost-effective resources are located, which are generally not close to major load centers. From the transmission planning perspective, the major challenge is to transfer the renewable energy from the generation sites to their load centers. On the other hand from the transmission operation perspective it must be ensured that the grid is capable of handling this unprecedented level of dynamics.

2.3.1 Outdated and Ineffective Transmission Investment Policies

One of the main problems of the transmission sector is that most of the benefits of transmission are not adequately accounted for in the incentive structure offered to the investors. As a result investors presently have little or no incentive to invest in transmission projects that might be beneficial for consumers and society at large. The present incentive structure is not able to capture the full benefits of transmission for many reasons.

2.3.1.1 Inappropriate Project Benefit Estimation

Regulators and policy makers calculate the benefits of a particular transmission project within a limited geographical and chronological scope [7]. In most cases while evaluating a transmission project, state regulators calculate the transmission investment benefits accrued only to the state residents. However, the North American grid being interconnected and transmission lines being mostly uncontrolled, the benefits of a

transmission line, especially that of a long interstate corridor, may also be enjoyed by neighboring states. For example if California builds a transmission corridor to purchase wind energy from Texas, the transmission project is likely to benefit states like New Mexico and Arizona through which the transmission corridor is built. However regulators in California do not have authority to charge the customers of New Mexico and Arizona for the benefits they enjoy because of the transmission project. Also regulators of New Mexico and Arizona have little incentive to charge their residents to help pay for the interstate corridor.

The choice of chronological scope for a transmission projects' benefit calculation also requires improvement. Transmission planning and cost allocation is done with a focus on benefits that will be realized within five years of the project completion. However most transmission assets have a lifetime of at least 25 years, while in many cases it can exceed 50 years. Hence capturing the benefits accrued in the first 5 years of these projects is not enough for an economic evaluation. This short term economic outlook encourages transmission patchwork rather than full scale transmission projects, which could have benefits like economies of scale. The transmission patchworks not only cause loss of financial benefit for the society, but its effects may also translate into negative environmental impact, since such patchwork may lead to many low capacity corridors rather than a few high capacity ones.

2.3.1.2 Lead Time Mismatch with Renewable Generation

Much of the transmission required presently is due to increased penetration of renewable resources, especially wind and solar generation. Bulk renewable generation

sites are often located far away from load centers. The existing transmission ties to these remote locations are often not strong enough to support bulk power transmission. Thus new renewable generation installation is often required to be accompanied by extensive transmission build-out. However, there is a significant mismatch between the lead time required to build a transmission line and that of a wind or solar plant installation [8]. While transmission line projects require 5-10 years to be planned and built, renewable generation plants can be constructed within a year or less. This gives rise to a waiting game among the transmission and renewable generation investors, which is commonly referred to as "the chicken and egg problem". On one hand the transmission investors are often reluctant to build new transmission lines without the guarantee that new renewable generation plants will be built to use the new lines, while on the other hand solar and wind plant investors are unwilling to build a generation plant without certainty that the transmission line will be built. Thus instead of transmission being planned and built on a strategic basis to create competitive renewable energy markets, the present transmission build-outs are mostly driven by individual projects on a transactional basis.

2.3.1.3 Acquisition of Real Estate

Long distant transmission projects involving transmission lines crossing different states are subject to the regulatory process of each of the governing entities. An interstate transmission project thus has to be approved by all of the associated governing bodies that control the land over which the transmission is to be built. This is one of the major problems in the western U.S., where more than half of all the land is controlled by federal agencies like the Department of the Interior, the Department of Agriculture and the Department of Defense [7]. The process of getting approval from all of the concerned

entities is a fairly long one, often taking many years. Also a particular state through which transmission is to be built may not approve the sale of land if the benefits of the project received by that state are not very high.

2.3.1.4 Free Rider Problem

The present transmission investment regulations create a "free-rider" problem [9]. Under the present policy framework, a new generator willing to connect to the grid has to pay for all the upgrade costs that result post interconnection. Often a new generator connected at a particular site may result in a transmission asset overload hundreds of mile away. The new generator in this case has to pay for all of this transmission equipment. However, this new generator is not given any credit for removing the congestion or improving the transmission network. The benefit of the investment is shared by all the users, although the cost is not. As a result most investors are willing to wait and reap the benefits of others' investment and nobody is willing to move forward with making a new investment. An analogous situation for the highway system would be requiring the next car that enters a crowded highway to pay for the full cost for adding a lane to the highway, which is clearly not a fair system as the upgrade would benefit all the system users.

The reason behind the infrastructure and operations problems is that the policy and the regulatory structure that governs the transmission industry are obsolete for today's energy industry needs. Most of these policies were designed in an era where the utilities primarily served customers using generators of their own state. Interstate energy transfer was very limited and generally was used only for contingency support. As a result, most transmission investment projects were evaluated by state regulators in the light of the

benefit accrued by the state. However with increasing interstate energy transfers because of increasing penetration of renewable resources, this business model can no longer be used.

2.3.2 Under Utilization of Existing Transmission Assets and High Cost of New Transmission

The electricity transmission sector is a very conservative industry, and reliability of power delivery is one of the major performance metrics. To achieve high reliability the utilities have gradually moved from a radial to a more meshed topology. Although radial systems are more economical for point to point delivery, a fault at any point in a radial system may result in extended outage for all the downstream customers. A meshed system on the other hand provides alternate paths of energy delivery from a source to a load in case of a fault, thus enhancing the system reliability. However, the increased reliability comes at the cost of lower controllability. Meshed systems are harder to control and they may give rise to undesired events like uneven line loading, causing congestion, loop flows, etc. To ensure reliable operation of this meshed network, the utilities have to operate such that none of the lines in the network get overloaded. As a result the total throughput of the transmission network is limited by the first line that reaches its thermal limit. The overall system loading at this point is very low, typically around 50% [10]. The situation becomes worse when the N-1 or N-2 contingency scenarios are taken into consideration. Under this situation the system reliability can be maintained by either of two methods – building new lines or installing power flow controllers.

2.3.2.1 Building New Lines

Building new lines is in most cases the easiest, albeit the most expensive method of increasing transmission system throughput without compromising its reliability. It is estimated that the cost of a new transmission line at 500 kV is about $3 million per mile [11]. Transmission projects not only require huge capital expenditure but also involve a long lead time, on the order of 5-10 years. One of the major obstacles towards construction of new lines is the acquisition of the required real estate. Moreover, the general public sentiment towards locating transmission lines near their communities has become increasingly negative. The real estate problem is much more severe in many urban centers where the cost of land required for transmission projects can be exorbitantly high. It is also claimed that increased use of land for transmission networks may adversely affect the environment.

2.3.2.2 Installing Power Flow Controllers

An alternate way of increasing transmission system throughput without jeopardizing its reliability is by increasing the overall system utilization with the help of power flow controllers. Various kinds of power flow controllers have been proposed over the years. Power flow controllers are essentially devices which can push more power through a meshed network by increasing utilization of parallel lightly loaded paths, while preventing overloading of highly loaded lines. The following section provides a brief overview of some of the major power flow controllers.

2.4 Maximizing Transmission Asset Utilization

Since it is expensive to build new transmission lines, maximizing the utilization of the existing ones are of paramount importance. Various methods are there to ensure maximal utilization of the transmission network without overloading any transmission line. These methods can be broadly classified into two categories: optimal dispatch and transmission network control using power flow controllers.

2.4.1 Optimal Dispatch

The method of optimal dispatch is the traditional and the most widely adopted method by the utilities to ensure proper utilization of the transmission network, without compromising its reliability [12]. The optimal dispatch consists of essentially monitoring the present system followed by appropriate selection of available control options. The first task is better known as State Estimation while the second is called Optimal Power Flow.

2.4.1.1 State Estimation

State Estimation is a computational procedure that uses a redundant set of measurements to compute a statistical estimate of the system operating state [13]. The state of a system is defined by a set of variables that completely defines all other system variables. In the case of a power network, the state variables are the various bus voltage magnitudes and phase angles. From the knowledge of these state variables the values of all other system variables like line currents, active and reactive power etc. can be derived as shown in (2.1)-(2.4).

$$I_{BUS} = Y_{BUS} V_{BUS} \tag{2.1}$$

$$I_i = \sum_{k=1}^{N} Y_{ik} V_k \tag{2.2}$$

$$P_i = Real\left(V_i^* \sum_{k=1}^{N} Y_{ik} V_k \right) \tag{2.3}$$

$$Q_i = -Imaginery\left(V_i^* \sum_{k=1}^{N} Y_{ik} V_k \right) \tag{2.4}$$

In (2.1)-(2.4), I_i is the current injected while P_i and Q_i are the real and reactive power injected at the i^{th} bus, in an N bus system. V_k denotes the complex voltage at the k^{th} bus while V_i^* represents the complex conjugate voltage at the i^{th} bus. The admittance of the line connecting the i^{th} and the j^{th} bus is given by Y_{ik}. The system admittance matrix is given by Y_{BUS}, while the system voltages and currents are given by V_{BUS} and I_{BUS} respectively.

In an N bus system the system state is defined by $2N-1$ real variables. Hence $2N-1$ real equations are enough for solving the system state. However, any real measurement has a nonzero error associated with it. Further at a given point one or more of the sensors might malfunction. It is thus desirable to have redundant set of measurements to overcome these problems. The state of the system is hence statistically estimated from the redundant set of measurements. Since the measured quantities are dependent on the system states, any measured quantity z_i can be expressed as (2.5).

$$z_i = h_i(x) + \varepsilon_i \tag{2.5}$$

Here x is the state of the system, $h_i(x)$ is a function specific to the measured quantity z_i, while ε_i is the associated error with the measurement. For a set of M measurements, the equation can be written in matrix form as given by (2.6). It is to be noted that a requirement for state estimation is M > 2N-1.

$$Z = H(x) + E \tag{2.6}$$

Here x is a vector of dimension Nx1, while Z, $H(x)$ and E are of dimension Mx1. The residual R is given by (2.7). By the least squares method the best estimate of the system state can be obtained by minimizing J given by (2.8), where W is a weight matrix. It can be shown that the state of the system can be solved by solving the iterative equation (2.9), where H is the matrix $\frac{\partial H(x)}{\partial(x)}$ computed at $x = x^k$.

$$R = H(x) - Z \tag{2.7}$$

$$J = (H(x) - Z)^T W (H(x) - Z) \tag{2.8}$$

$$x^{k+1} = x^k - (H^T W H)^{-1} H^T W (h(x^k) - Z) \tag{2.9}$$

2.4.1.2 Optimal Power Flow

Once the system state is approximately identified using the state estimation procedure, necessary control actions can be taken to meet certain performance criteria such as minimum operating costs, minimum losses, etc. Optimal Power Flow (OPF) is used to calculate the set points of various generators, load tap changing transformers, shunt VAR compensation banks etc., that are required to achieve the desired performance

criteria. To ensure safe and reliable system operation, limits of certain dependant variables, for example maximum line current, maximum and minimum bus voltages, etc., are introduced as constraints in the OPF.

Mathematically, the OPF can be formulated as shown in (2.10a)-(2.10f).

$$Min\ C(x,u) \tag{2.10a}$$

such that

$$P_j^{min} \leq P_j \leq P_j^{max} \qquad j \in [1, N_{gen}] \tag{2.10b}$$

$$Q_j^{min} \leq Q_j \leq Q_j^{max} \qquad j \in [1, N_{gen}] \tag{2.10c}$$

$$V_i^{min} \leq V_i \leq V_i^{max} \qquad i \in [1, N_{bus}] \tag{2.10d}$$

$$\left|S_k^{EndBus1}\right| \leq |S_k^{max}| \qquad k \in [1, N_{line}] \tag{2.10e}$$

$$\left|S_k^{EndBus2}\right| \leq |S_k^{max}| \qquad k \in [1, N_{line}] \tag{2.10f}$$

Here x is the state of the network and therefore consists of the bus voltage magnitudes and angles. The variable u is called the control variable and consists of all the independent control variables that has to be set in the network. Examples of variables that make up u are the real power and output voltage magnitude of generators. The objective of the OPF is to minimize the cost function $C(x,u)$ while satisfying the constraints (2.10b)-(2.10f). The output real and reactive powers of the j^{th} generators are represented by P_j and Q_j respectively. For the j^{th} generator, the limits of the real power are given by P_j^{max} and P_j^{min} while that of the reactive power are given by Q_j^{max} and Q_j^{min}. The bus voltage of the i^{th} bus is given by V_i. For proper voltage regulation this voltage is required

to be within V_i^{min} and V_i^{max}. The apparent powers at the two ends of the k^{th} line are given by $S_k^{EndBus1}$ and $S_k^{EndBus2}$. To ensure operation within the thermal ratings of the k^{th} line it is necessary to ensure that the apparent power flowing through either ends of the line be below the maximum permissible apparent power S_k^{max} of that line.

The operations like State Estimation and OPF are performed at a central control center with the help of an Energy Management System. The output of the OPF may be used to set the operating point of generators, shunt compensators, etc., however in most cases the utilities are required to operate reliably under *N-1* contingency condition. As a result security constrained OPF (SCOPF) is used instead of regular OPF. In SCOPF the operating margins of the system assets are reduced to ensure their safe operation even under the worst case fault scenario. The OPF or the SCOPF is performed once in every 5-15 minutes [14]. It is assumed that between the two successive OPF calculations the system does not change appreciably and hence the optimal point of operation also does not shift much. The autonomous controllers, for example the frequency-droop controller and voltage regulator of the generators, ensure that the system operates close to the OPF set optimal point for relatively small system disturbances during this time period. Also, it is to be noted that like most nonlinear optimization techniques, the OPF does not guarantee a global optima, rather the output is a local optima.

In a practical utility system, the output of generators can be controlled by the system operator very easily and smoothly, though it may involve a large time constant. As a result in the case of transmission line congestions or over-loadings a general practice is to re-dispatch the generators to mitigate the problem. This results in out-of-merit generator

dispatch thus increasing the cost of energy generation. In a meshed system, an alternate method is to use transmission line power flow controllers, some of which are discussed in the next section.

2.4.2 Transmission Network Power Flow Controllers

Apart from generator re-dispatch, power flow in a meshed system can also be controlled by controlling the transmission network. This method has the advantage that it can enable in-merit generation dispatch, thus lowering the cost of energy generation. However, often the cost and complexity of implementation of such power flow controllers may exceed the benefits incurred from them. This section reviews some of the major state of the art transmission power flow controllers and discusses their various advantages as well as limitations [15].

2.4.2.1 Basic Principles

Consider the two bus system shown in Figure 2.3. The transmission system connects a surplus generation area (*Area1*) to a deficit generation area (*Area2*). It is seen that the transmission system consists of two parallel paths – *Path1* and *Path2*. Each of these paths may be considered a simplified representation of a transmission corridor.

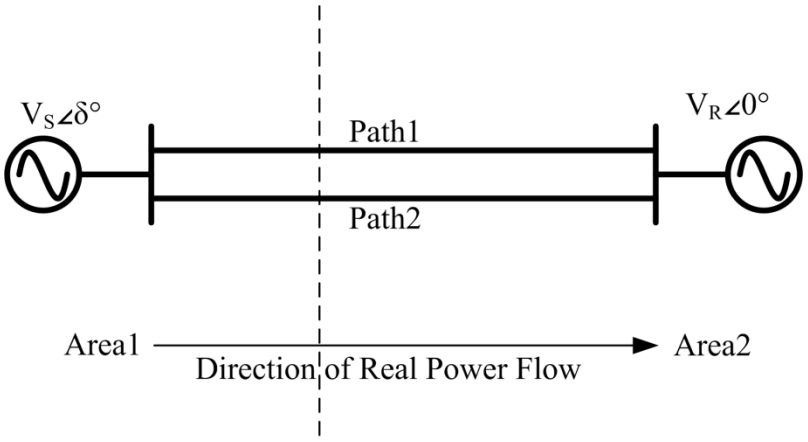

Figure 2.3: Two Bus System

In absence of any power flow controllers the power flowing through the paths are inversely related to the path impedances. The voltages at the sending and receiving end are assumed to be $V_S\angle\delta°$ and $V_R\angle0°$ respectively. If the impedance for the i^{th} path is assumed to be given by (2.11), then the real and reactive power flowing at the sending and receiving ends of the i^{th} path is given by (2.12)-(2.15).

$$Z_i = R_i + X_i = |Z_i|\angle\theta \tag{2.11}$$

$$P_i^R = \frac{|V_R|^2}{|Z_i|}\cos(\theta) - \frac{|V_s||V_R|}{|Z_i|}\cos(\theta - \delta) \tag{2.12}$$

$$Q_i^R = \frac{|V_s||V_R|}{|Z_i|}\sin(\theta - \delta) - \frac{|V_R|^2}{|Z_i|}\sin(\theta) \tag{2.13}$$

$$P_i^S = \frac{|V_S|^2}{|Z_i|}\cos(\theta) - \frac{|V_s||V_R|}{|Z_i|}\cos(\theta + \delta) \tag{2.14}$$

$$Q_i^S = \frac{|V_s||V_R|}{|Z_i|}\sin(\theta + \delta) - \frac{|V_S|^2}{|Z_i|}\sin(\theta) \tag{2.15}$$

For simplified approximate analysis, the resistance of transmission lines can be neglected with respect to its reactance. For such a simplified lossless transmission system equations (2.11)-(2.15) can be reduced to (2.16)-(2.20).

$$Z_i = X_i \tag{2.16}$$

$$P_i^R = -\frac{|V_s||V_R|}{X_i}\sin(\delta) \tag{2.17}$$

$$Q_i^R = \frac{|V_s||V_R|}{X_i}\cos(\delta) - \frac{|V_R|^2}{X_i} \tag{2.18}$$

$$P_i^S = \frac{|V_s||V_R|}{X_i}\sin(\delta) \tag{2.19}$$

$$Q_i^S = \frac{|V_s||V_R|}{X_i}\cos(\delta) - \frac{|V_S|^2}{X_i} \tag{2.20}$$

From (2.19) it is seen that the real power flowing through the i^{th} path depends on the terminal voltage magnitudes, V_S and V_R, the path impedance X_i, and the angular separation of the terminal voltages, δ. Thus real power flowing through a transmission corridor can be varied by varying one or more of these parameters. Figure 2.4 shows schematically how the various parameters may be varied for the *Path2* of the two bus system of Figure 1.3 to achieve power flow controllability through that path.

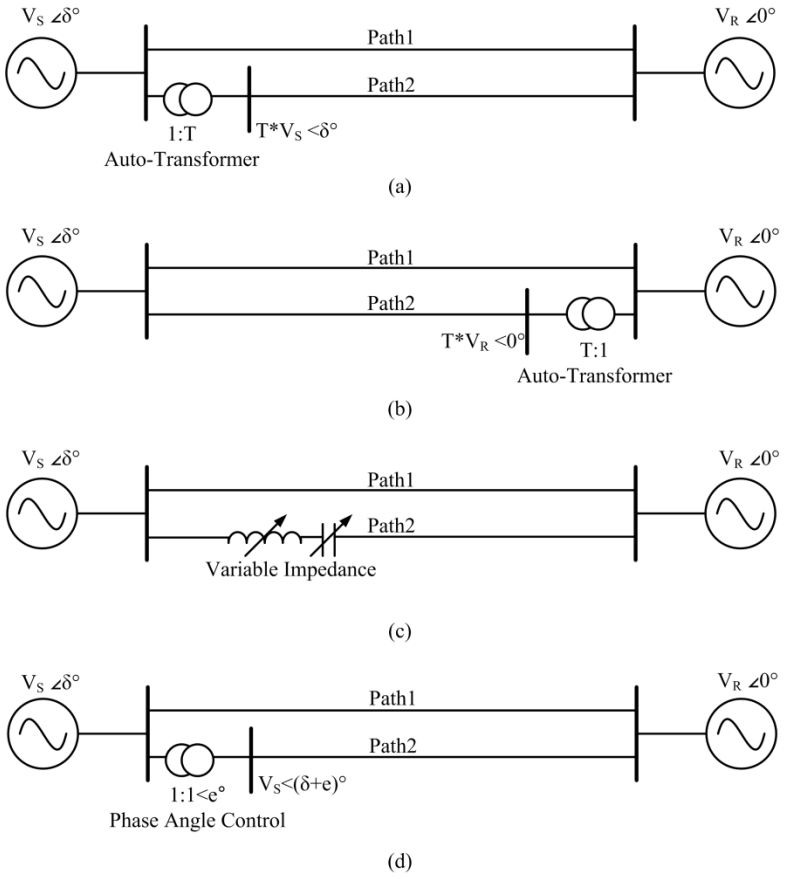

Figure 2.4: Power flow control in Path2 of the two bus system by controlling (a) $|V_S|$ with auto-transformer, (b) $|V_R|$ with auto-transformer (c) series reactance X_2 (d) voltage phase angle difference

2.4.2.2 Load Tap Changers

Load Tap Changers (LTCs) or load tap changing transformers are essentially transformers with the capability of having variable turns-ratio, as shown in Figure 2.5. LTCs are provided with multiple discrete sets of taps on one or more windings [16]. The output voltage magnitude can be varied by selecting the appropriate taps. The tap setting selection is usually obtained from the output of the OPF program, which is communicated from the control center to the transformer. The arrangement that allows the LTCs to select the desired tap dynamically can be electromechanical or solid state in

nature. The solid state LTCs usually use a set of anti-parallel thyristors to control the effective turns-ratio.

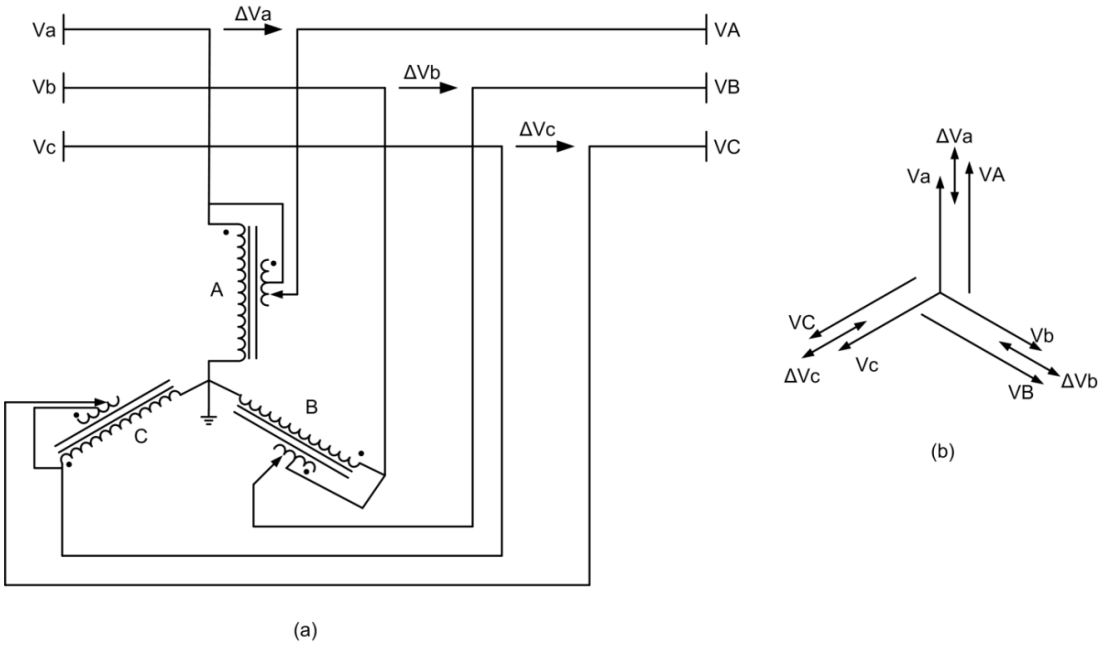

Figure 2.5: (a) Schematic of a LTC and (b) associated phasor diagram

The advantage of LTC is in its simplicity and low cost. It can effectively vary the voltage magnitude. The design of a traditional transformer has to be varied only slightly to realize a LTC. However, to comply with voltage regulation requirements the range of control achieved by LTC is very limited. Transmission networks are required to maintain the bus voltages at close to 1 per unit (pu). As a result often it is not desirable to have a LTC with more than 5-10% off-nominal tap ratio. Hence even with one 10% LTC at each end of the transmission path, the maximum change in active power flow that can be achieved in a path is only ±21%, according to (2.19). The actual achievable power flow in practical scenarios is much lower due to the voltage regulation issue. Also the electromechanical LTCs have the disadvantage of being slow devices. The solid state

LTCs are much faster, but their reliability may be lower because of the power electronic switches. LTCs are more effective in controlling the reactive power flow, since reactive power is more dependent on voltage magnitude than active power as can be seen from (2.20).

2.4.2.3 Phase Angle Regulators

The phase angle regulator (PAR) can be used to vary the effective phase angle of a transmission path. The PAR adds the phase voltage of a line with a voltage in quadrature to it, as shown in Figure 2.6 [17]. The PAR consists of two transformers – the exciter unit and the regulator unit. The exciter unit is connected as a shunt transformer with the phase to neutral voltage appearing across its primary windings. The secondary of the exciter unit is used to produce a scaled down voltage in phase with the line to neutral voltages. The primary of the regulator unit is fed using the line to line scaled down voltage, while the secondary is added in series to the transmission line, so that the induced voltage adds up to the line to neutral voltages. As can be seen from the phasor diagram in Figure 2.6, the voltage added by the regulator unit is in quadrature with the line to neutral voltage. The resultant voltage thus has a phase shift from the input voltage. By controlling the scaling level in the exciter unit it is thus possible to control the output voltage angle shift and thus the power flowing through the line.

The PAR can effectively control the real power flowing through the line since it can control the output voltage phase angle. However, it has very little control over the reactive power since it does not have much control over the voltage magnitude. Also the PAR is a more expensive device than a LTC, as it requires two transformers – one

required to handle the full rated voltage and the other the full rated current. System fault handling becomes extremely difficult since PAR works on the principle of coupling of phases. Also control of PAR in real systems involving unbalanced voltages is difficult. Like LTC, the PAR can be implemented using electromechanical slow controllers or solid state based fast controllers.

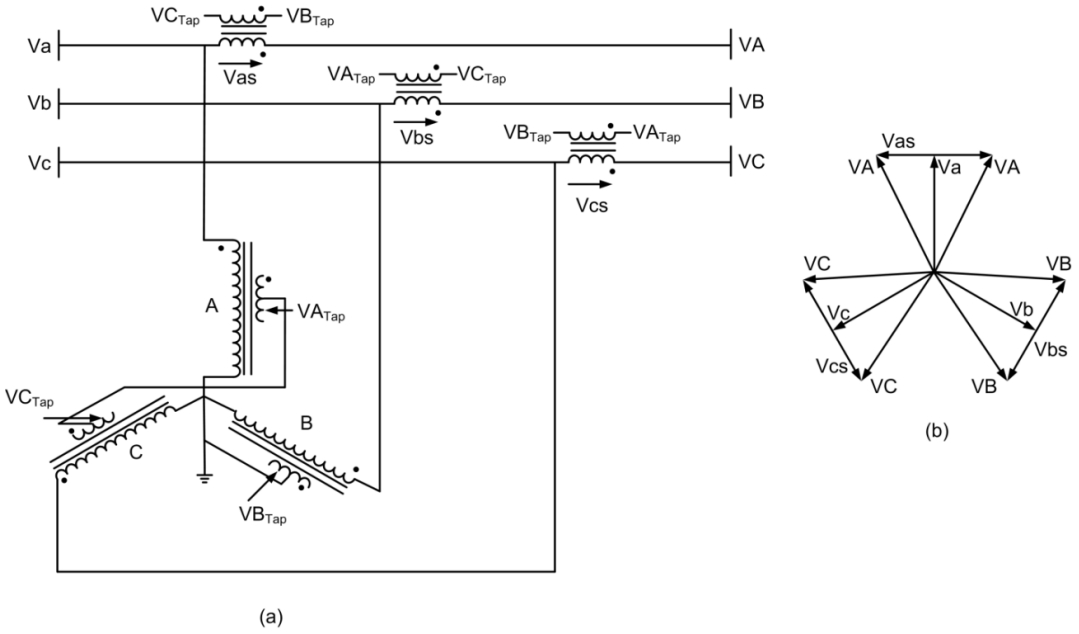

Figure 2.6: (a) Schematic of a Phase Angle Regulator and (b) associated phasor diagram

2.4.2.4 Sen Transformer

The sen transformer (ST) combines the functionality of both the LTC and the PAR. Figure 2.7 shows the schematic and phasor diagram for a ST [18]. The ST is essentially a single core three phase transformer with a Y connected primary winding and nine secondary windings. As shown in Figure 2.7, the voltage at any point in the electrical system is applied to a shunt connected single core, three phase transformer's primary windings.

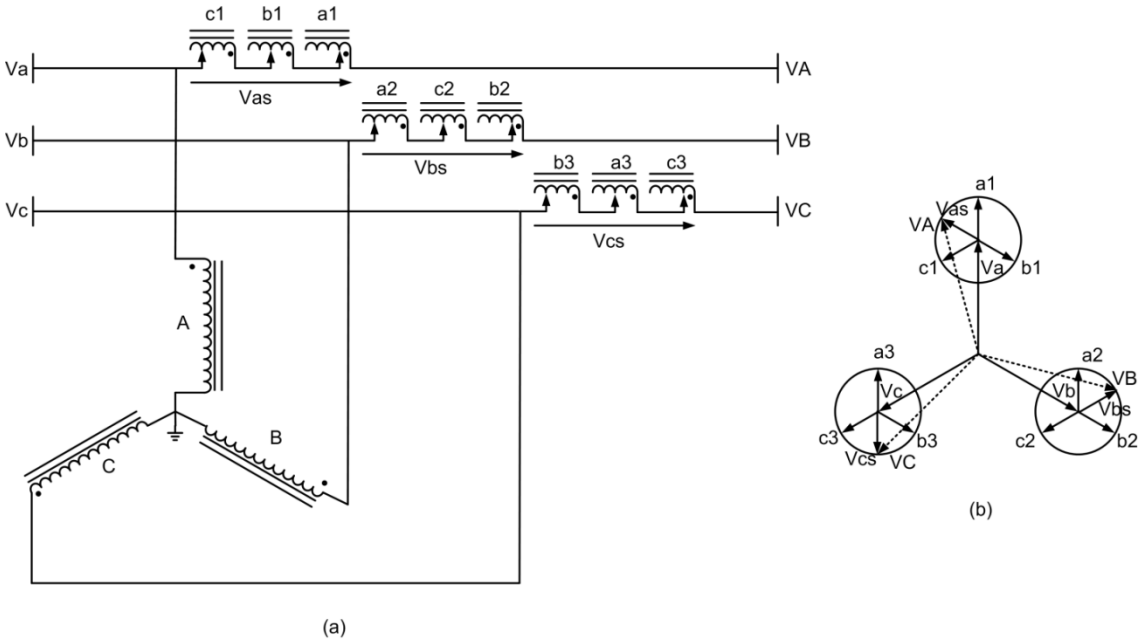

Figure 2.7: Schematic and phasor diagram for a Sen Transformer

A total of nine secondary windings (a1, c2 and b3 on the core of A-phase, b1, a2 and c3 on the core of B-phase, and c1, b2 and a3 on the core of C-phase) constitute the voltage and impedance regulating unit. By choosing the number of turns of each of the three windings, and therefore the magnitudes of the components of the three 120° phase shifted induced voltages, the compensating voltage in any phase is derived from the phasor sum of the voltages induced in a three phase winding set (a1, b1 and c1 for injection in A-phase, a2, b2 and c2 for injection in B-phase, and a3, b3 and c3 for injection in C-phase). The compensating voltage is of line frequency and is connected in series with the line through auto transformer action. To provide voltage magnitude compensation at any phase, the in-phase voltage is modified. For example to change the magnitude of A-phase, the number of turns of a1 is modified. On the other hand for out-of-phase or quadrature compensation, the number of turns in c2 and b3 is adjusted.

The ST can provide control over line power as well as bus voltage. The range of control provided by the ST is also impressive. The functionality of an ST can be compared with that of a LTC and a PAR put together. In terms of cost it is lower than an equivalent LTC added with a PAR system, since it has only one transformer. However, since its working principles are same as that of the LTC and PAR, it retains all the disadvantages of the above two. The transformer of the ST is required to handle the full rated voltage and also should be designed to handle the full fault current, making it an expensive proposition. As a result of inter-phase coupling, fault identification and isolation becomes very challenging. Also handling system imbalances becomes very difficult. Thus integration of ST in an existing system with existing distance relay protections is very challenging.

2.4.2.5 Variable Frequency Transformer

The variable frequency transformer (VFT) is essentially a continuously variable phase shifting transformer that can operate at an adjustable phase angle [19]. The core technology of the VFT is a rotary transformer with three phase windings on both rotor and stator as shown in Figure 2.8. The collector system conducts current between the three phase rotor winding and its stationary buswork. One power grid is connected to the rotor side of the VFT and another power grid is connected to the stator side of the VFT. Power flow is proportional to the angle of the rotary transformer, as with any other AC power circuit. The impedance of the rotary transformer and AC grid determine the magnitude of phase shift required for a given power transfer. Power transfer through the rotary transformer is a function of the torque applied to the rotor. The rotor inherently

orients itself to follow the phase angle difference imposed by the two asynchronous systems, and will rotate continuously if the grids are at different frequencies.

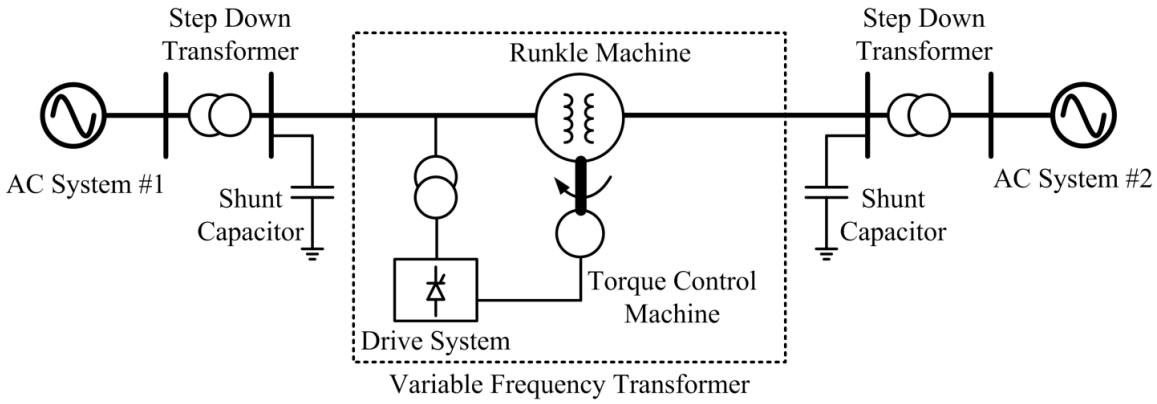

Figure 2.8: Schematic of variable frequency transformer

Torque is applied to the rotor by a drive motor, which is controlled by the variable speed drive system. When a VFT is used to interconnect two power grids of the same frequency, its normal operating speed is zero. Therefore, the motor and drive system is designed to continuously produce torque while at zero speed (standstill). However, if the power grid on one side experiences a disturbance that causes a frequency excursion, the VFT will rotate at a speed proportional to the difference in frequency between the two power grids. During this operation the load flow is maintained. The VFT is designed to continuously regulate power flow with drifting frequencies on both grids.

A closed loop power regulator maintains power transfer equal to an operator set point. The regulator compares measured power with the set point, and adjusts motor torque as a function of power error. The power regulator is fast enough to respond to network disturbances and maintain stable power transfer. Reactive power flow through the VFT

follows conventional AC circuit rules. It is determined by the series impedance of the rotary transformer and the difference in magnitude of voltages on the two sides.

The VFT has the advantage that unlike power electronic alternatives, it produces no harmonics and does not cause undesirable interactions with neighboring generators or other equipment on the grid. On the other hand the VFT being essentially a slow rotating transformer has a very large time constant of the order of 1-2 seconds. Hence it does not have the fast response of a power electronics based power flow controller. The transformer of the VFT has to be rated for full system power and also has to handle the worst case fault current. Since the rotor of the VFT has to be designed for rotational motion, the design of VFT becomes complicated and expensive. This is because it is difficult to achieve high reliability with systems in motion. Typically it is difficult to design VFTs for power levels exceeding 100 MVA. In those cases multiple VFTs are required to be in parallel, making the system more complex and expensive.

2.4.2.6 Flexible AC Transmission Systems

Flexible AC Transmission Systems (FACTS) are a family of power electronics based controllers, which can be used to achieve various grid control functionalities [15]. Like other power flow controllers, the FACTS devices vary one or more parameters among V_S, V_R, δ and X_i given in (2.19) to achieve power flow control. In this section the major FACTS power flow controllers are discussed.

2.4.2.6.1 Shunt Controllers

Voltage regulation is one of the major limitations in long distance AC power transmission. Since the transmission line is mostly inductive and most load centers

absorb real as well as reactive power, the voltage magnitude drop along a long transmission line can be significant enough to violate the voltage regulation norms. Reactive shunt compensation can be used to control the voltage profile along a transmission line and increase the real power throughput of the line. Shunt connected reactors are used to minimize line overvoltage under light loading conditions, while shunt capacitors are used to maintain voltage levels under heavy loading conditions [20].

The effect of shunt compensation is shown using the simple two bus system, provided with an ideal reactive compensator at its midpoint, as shown in Figure 2.9. For simplicity the line is assumed to be purely inductive. The sending and the receiving end voltages are assumed to be of same magnitude, hence $|V_S| = |V_R| = V$. The reactive compensator is represented by a sinusoidal voltage source, which maintains the midpoint voltage magnitude at the same level as the sending and receiving end voltage magnitudes, thus $|V_M| = V$. The reactive compensation is provided at the midpoint of the transmission line since the midpoint of the transmission line has the maximum drop in voltage magnitude.

In absence of the shunt compensator, the real power through the line is given by (2.21). Hence, the maximum power that can be transmitted through the uncompensated line is given by P^{U}_{MAX} in (2.22). In presence of the midpoint compensation, the transmission line is effectively divided into two segments, each with an impedance of X/2. The reactive compensator is assumed to inject only reactive power. Hence the real power sent from the sending end is same as the real power received at the receiving end and is given by (2.23). It is seen that the maximum power that can be transmitted through

the compensated line is twice that of the uncompensated line. The reactive power that is required to be injected from the compensator is given by (2.24).

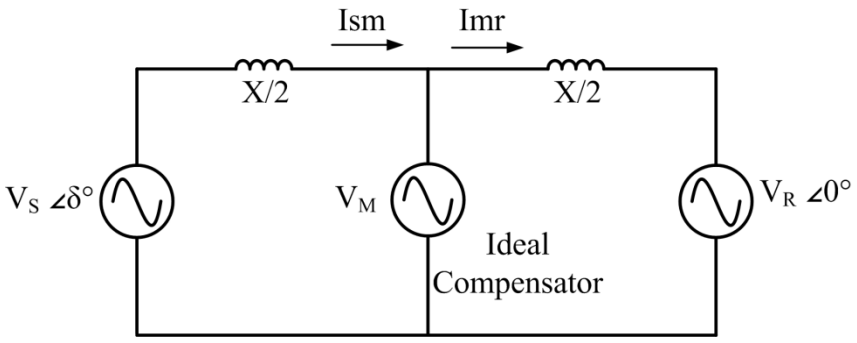

Figure 2.9: Two bus system with an ideal midpoint reactive compensator

$$P^U = \frac{V^2}{X}\sin\delta \tag{2.21}$$

$$P^U_{MAX} = \frac{V^2}{X} \tag{2.22}$$

$$P^C = \frac{2V^2}{X}\sin\left(\delta/_2\right) \tag{2.23}$$

$$Q^C = \frac{4V^2}{X}\left(1 - \cos\left(\frac{\delta}{2}\right)\right) \tag{2.24}$$

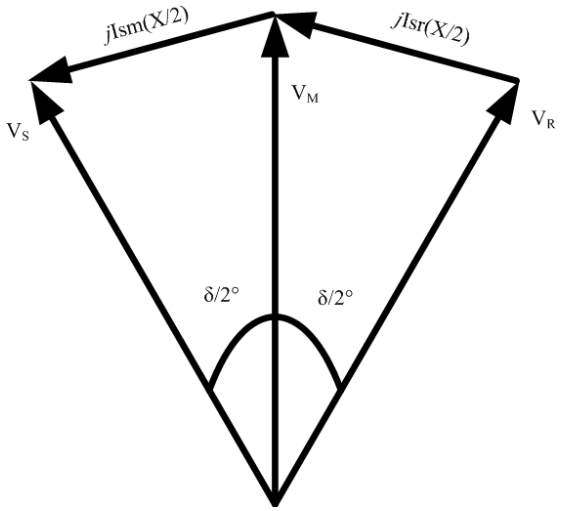

Figure 2.10: Phasor diagram for the two bus midpoint compensated system

Figure 2.10 shows the phasor diagram, while Figure 2.11 shows the relationship between the real power, reactive power compensation required and angle δ for the midpoint compensated system. It is seen from the above example that by injecting reactive power through midpoint shunt compensator the maximum real power throughput of a transmission line can be doubled. The concept can be expanded further by using multiple shunt compensators to divide the transmission line into multiple segments. Increased number of shunt compensators increases the transmittable real power through the line. However, it also increases the reactive power injection requirement as well as the cost of implementation. Shunt compensators are generally used to supply reactive VAR at steady state. They also improve the system stability margin under transient conditions.

Fixed steps of reactive compensation can be provided by shunt reactor or shunt capacitor banks. However it is desirable to have a dynamic compensator, which can be used to supply any amount of reactive power within a range. Over-excited or under-

excited synchronous generators were used earlier for this purpose. However advances in power electronics have enabled implementation of semi-conductor based compensators.

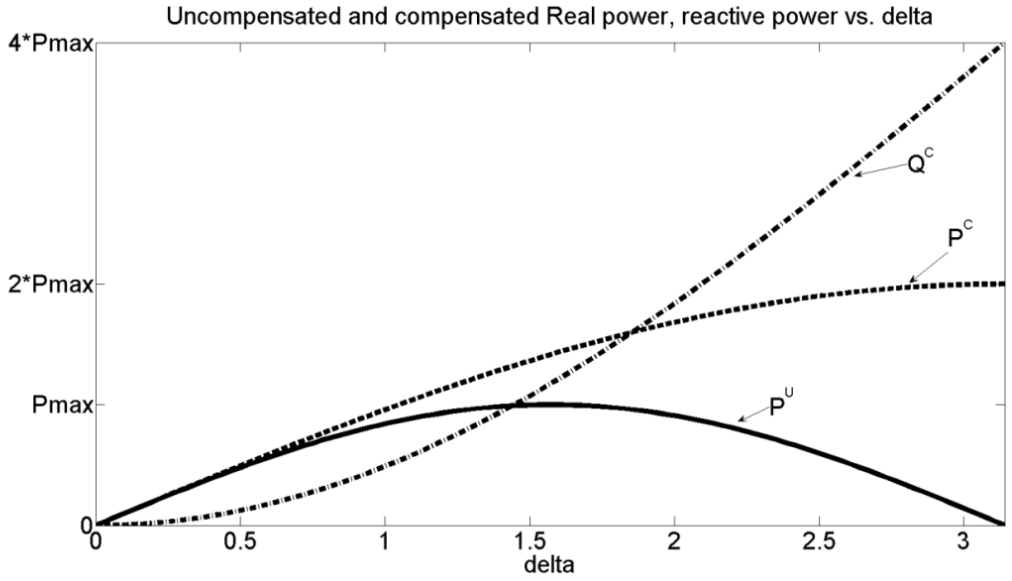

Figure 2.11: Real power transmitted in the uncompensated case (P^U), compensated case (P^C) and the midpoint reactive compensation required (Q^C)

Using a fixed reactor or capacitor and a bidirectional thyristor valve, the amount of injected reactance can be controlled. Such compensators are referred to as Static VAR Generators (SVG) [21]. Variable inductance can be realized using the circuit shown in Figure 2.12, while variable capacitance is implemented using the topology shown in Figure 2.13. The former is called thyristor controlled reactor (TCR) while the later is called thyristor switched capacitor (TSC).

Depending on the application and the required reactive power injection control range may be different. Alternate topologies like fixed capacitor-thyristor controlled reactor (FC-TCR) and thyristor switched capacitor-thyristor controlled reactor (TSC-TCR),

which are essentially derived from the TCR and TSC, may also be used. The schematic of these topologies are shown in Figure 2.14.

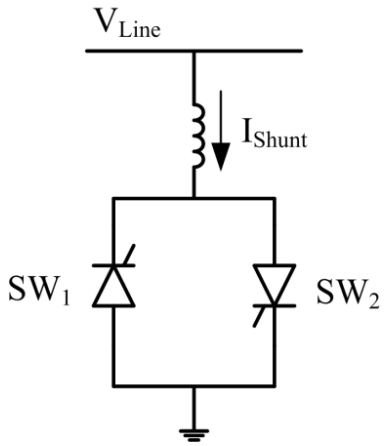

Figure 2.12: Thyristor Controlled Reactor

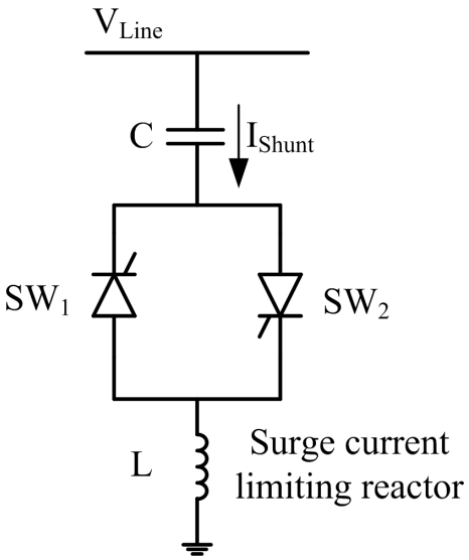

Figure 2.13: Thyristor Switched Capacitor

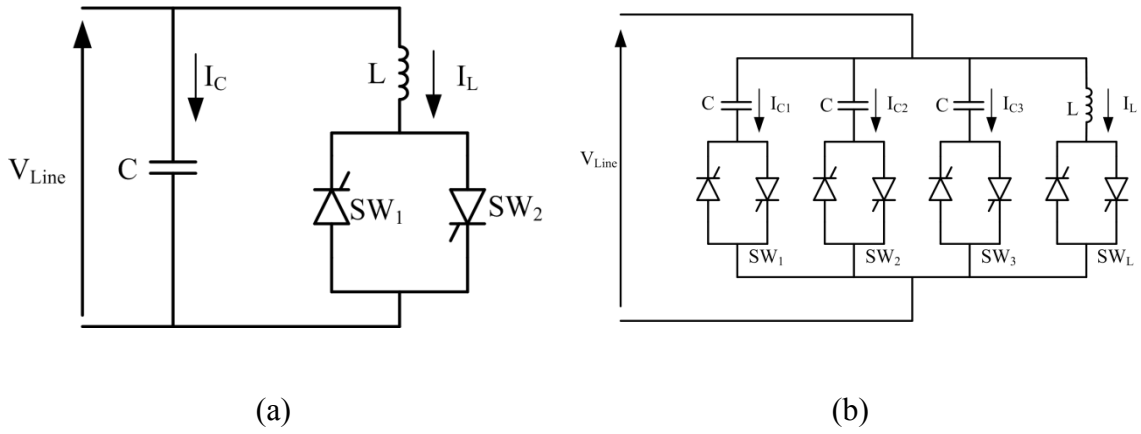

(a) (b)

Figure 2.14: Schematic of (a) FC-TCR and (b) TSC-TCR

Although SVGs are relatively easy to implement and low cost, they introduce harmonics around the switching frequency, in the power circuit. Also shunt capacitors may result in resonance with the line inductance. However the main disadvantage of the SVGs is that their ability to provide reactive support depends on the system voltage. Systems typically have low voltage when in need of reactive VAR support. The reactive injection capability of SVGs is proportional to the square of the voltage magnitude as shown in Figure 2.15. Hence when the system voltage is low and high reactive support is required, the SVGs have reduced reactive injection capability.

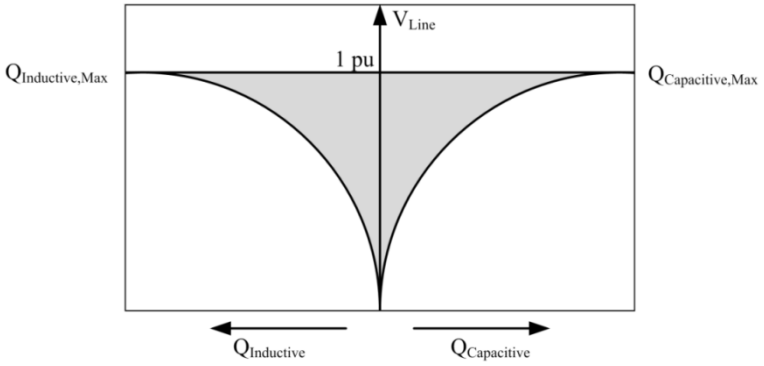

Figure 2.15: Variation of reactive power support capability of SVGs with system voltage

Static Synchronous Compensators or STATCOMs are alternate shunt compensators, which were introduced by Gyugyi in 1976. Statcoms use voltage source converters (VSCs) to inject or absorb reactive power from the system, as shown in Figure 2.16 [22]. By varying the output voltage of the three phase inverter it is possible to control the reactive power absorbed or injected by the Statcom. Hence if the output voltage amplitude is more than the system voltage, reactive power is injected into the system and vice versa. Ideally the Statcom does not draw any real power from the system. However, in practice it draws a small amount of real power to compensate for the losses. The main advantage of the Statcom over SVG is the reactive power injection range of Statcom does not vary much with system voltage, as shown in Figure 2.17. Thus a Statcom can provide full rated reactive compensation even for almost zero system voltage.

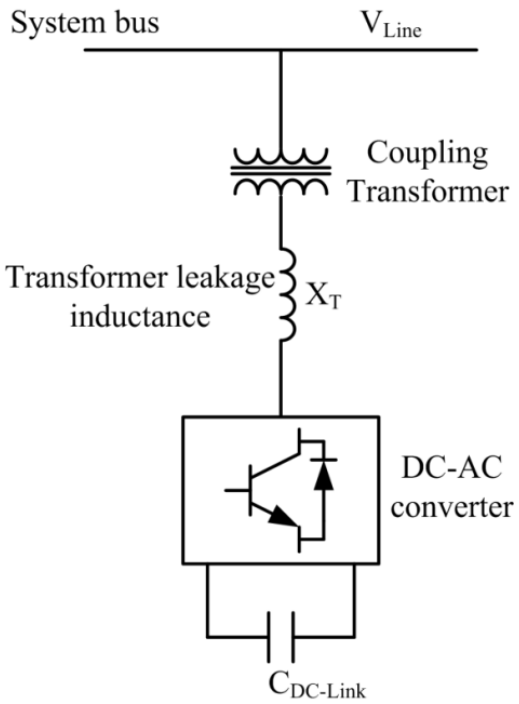

Figure 2.16: Schematic of a Statcom

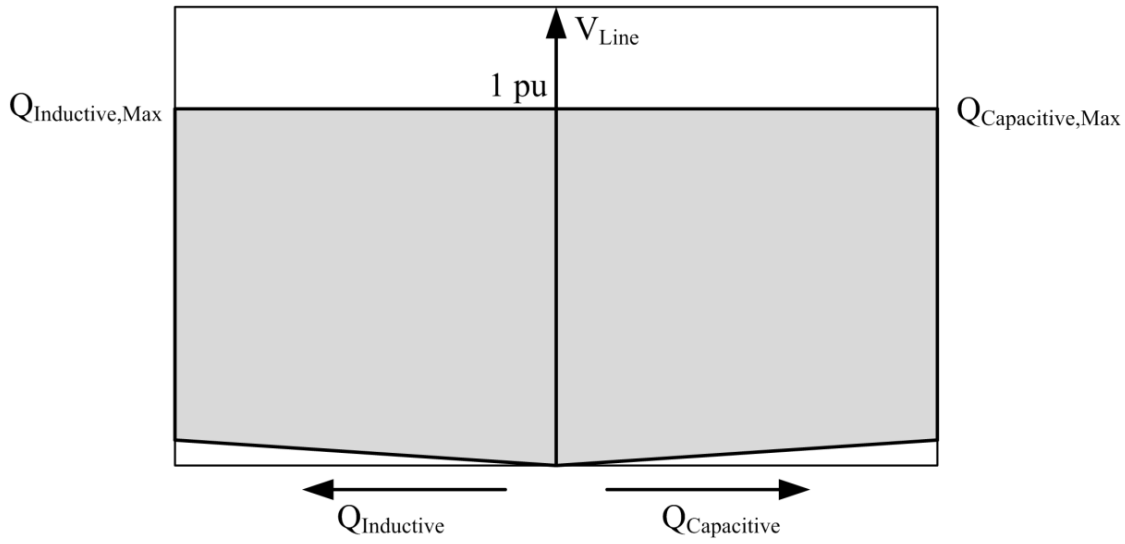

Figure 2.17: Variation of reactive power support capability of Statcom with system voltage

2.4.2.6.2 Series Controllers

Shunt compensation, when applied sufficiently, can theoretically make it possible to transmit power up to the thermal limit of the line, if a large enough angle between the two end voltages can be established. However, shunt compensation is not very effective in controlling the actual transmitted power, which at a defined transmission voltage, is ultimately defined by the transmission line impedance and the angle between the end voltages of the line, as can be seen in (2.19). Line impedance is one of the major factors that limit the amount of power that can be transmitted through a long line. Since transmission line is mainly inductive, series capacitance can be used to cancel a portion of the reactive line impedance and thereby increase the transmittable power.

Thyristor Switched Series Capacitor (TSSC) consists of a number of capacitors each shunted by an anti-parallel thyristor valve as shown in Figure 2.18 [23]. A series capacitor can be inserted in the power circuit by turning off, while it can be bypassed by

turning on the corresponding thyristor pair. The amount of series compensation that has to be injected can be controlled in a stepwise manner by increasing or decreasing the number of series capacitors inserted. Hence if the TSSC system is composed of N series capacitors, each corresponding to X_C amount of reactance, then the line inductance can be varied from X_L-N*X_C to X_L using the TSSC. Figure 2.19 shows the variation of line inductance and the resulting variation in power flow in the line for a TSSC compensated line. TSSC can only provide step-like variation over the line power flow. In practical systems it is often desirable to have a continuous range of control rather than a discrete control steps.

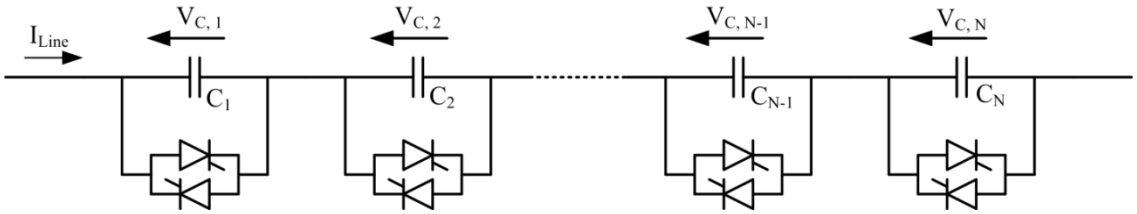

Figure 2.18: Schematic of TSSC

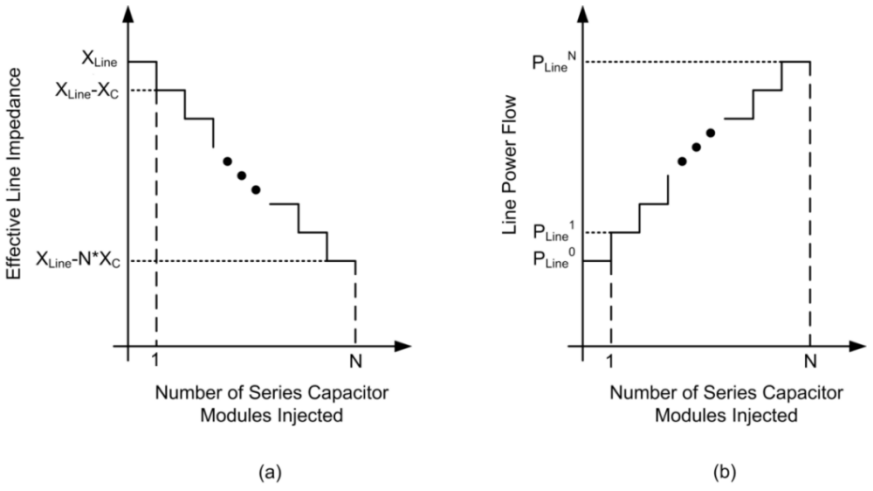

Figure 2.19: Variation of (a) line impedance and (b) line power flow due to TSSC

Thyristor Controlled Series Capacitor (TCSC) can provide a wide range of continuous control over the line impedance and hence the line power flow. The basic schematic of the TSSC is shown in Figure 2.20. The TCSC can be viewed as a tunable parallel LC circuit, whose effective impedance can be controlled by controlling the firing angle of the thyristor valve. The variation of the impedance of a TCSC module with the delay angle of the thyristor firing is shown in Figure 2.21.

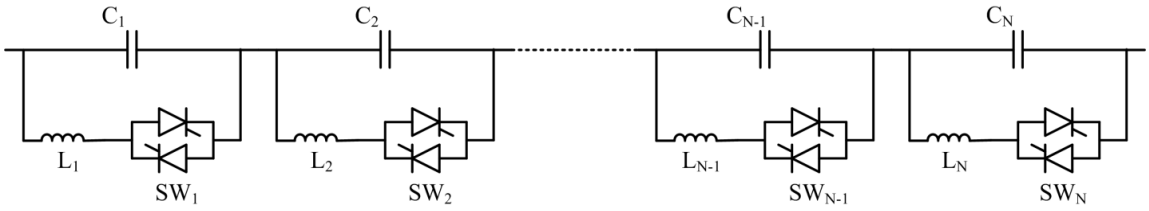

Figure 2.20: Schematic of TCSC (multiple in series)

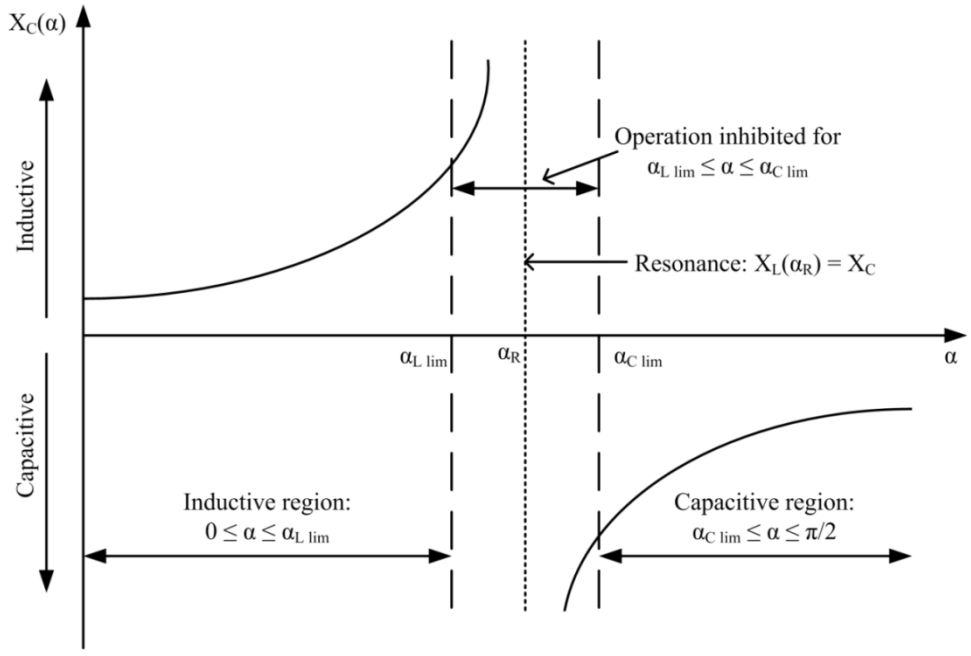

Figure 2.21: Impedance vs. delay angle characteristic of the TCSC

The series capacitive compensation technology has quite a few drawbacks and limitations in terms of actual implementation. The series capacitor may resonate with the line inductance under fault or normal conditions. Series capacitive injection also requires significant real estate and requires additional infrastructure such as isolated platforms, cooling systems, protection and bypass systems. The control also needs to be elaborate to ensure proper handling of startup, shutdown, bypass and fault modes. The distance relay protection of the line is also required to be modified for proper breaker action. The bypass thyristors for the series capacitors has to handle the full fault current, which may be of the order of tens of kilo amperes. The series capacitance may also result in sub-synchronous resonance, which may damage nearby turbine-generator shafts. All these factors make the series capacitor systems to be very complex and expensive. As a result this technology has not achieved much market penetration.

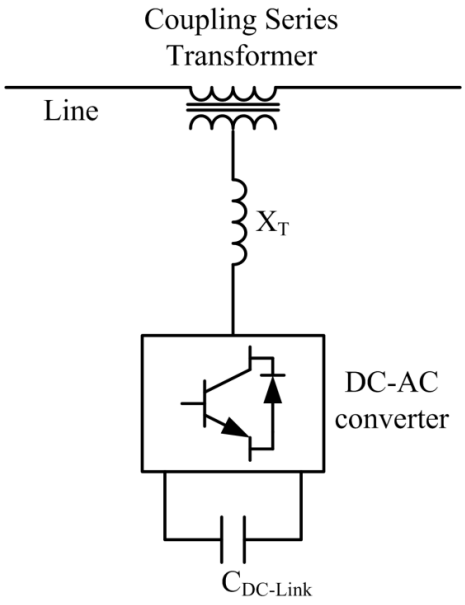

Figure 2.22: Schematic of SSSC

The static synchronous series compensator (SSSC) is a voltage source converter based compensator that can be used to provide series reactive compensation. Figure 2.22 shows the basic schematic of a SSSC, while Figure 2.23 shows the equivalent voltage injection provided by it and the corresponding phasor diagram. The output ac voltage of the voltage source inverter may be controlled to control the line power. Hence to increase line power the output voltage can be controlled so as to emulate that of an equivalent series capacitor. The SSSC being a voltage source, rather than an actual capacitor does not have the resonance issues. However, the SSSC is more expensive as it requires a coupling transformer capable of handling full fault current, DC link capacitor and the power semi-conductor switches.

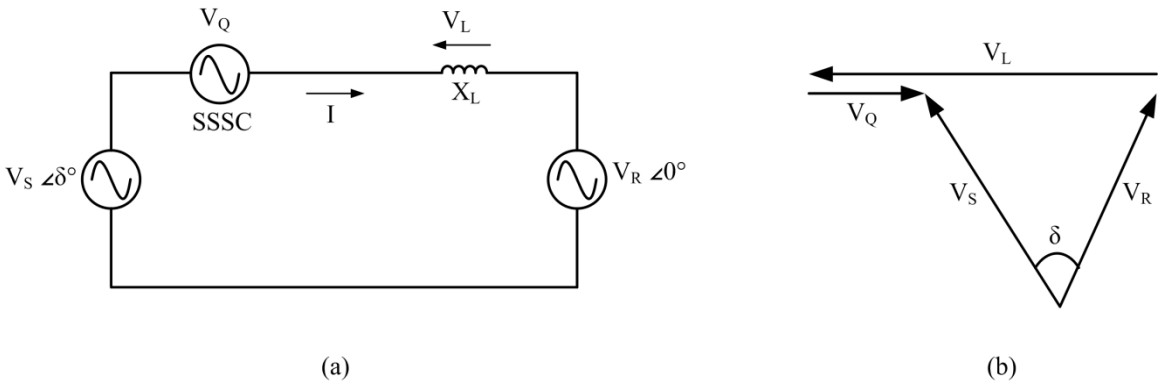

Figure 2.23: (a) Equivalent voltage injection and (b) phasor diagram for a SSSC system

2.4.2.6.3 Unified Power Flow Controller

The unified power flow controller (UPFC) is another voltage source converter based power flow controller [24]. The advantage of the UPFC is that it can control all the three parameters of the line power flow equation – voltage magnitude, voltage angle difference as well as line impedance. Figure 2.24 shows the basic schematic of a UPFC, while its

conceptual equivalent representation in a two bus system, along with the system phasor diagram is shown in Figure 2.25.

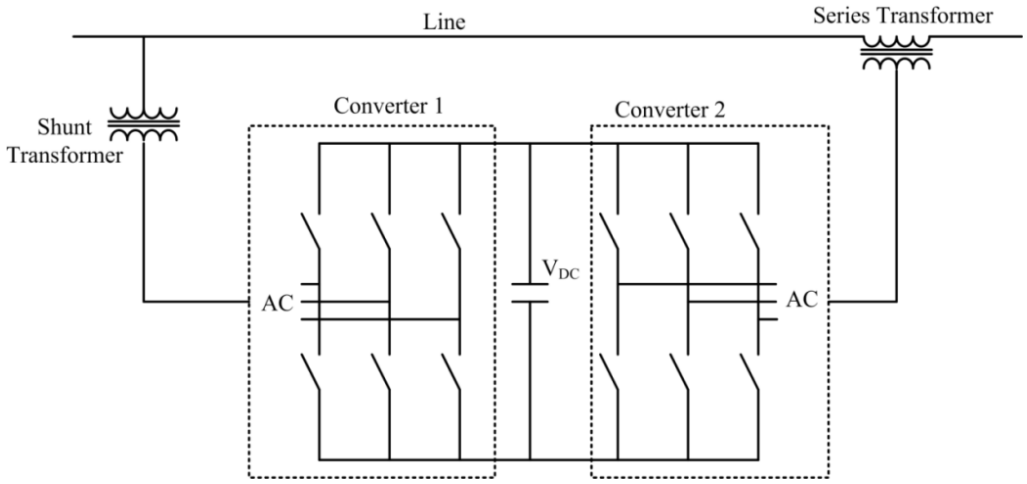

Figure 2.24: Schematic of the UPFC connected to an AC system (shown in single line diagram)

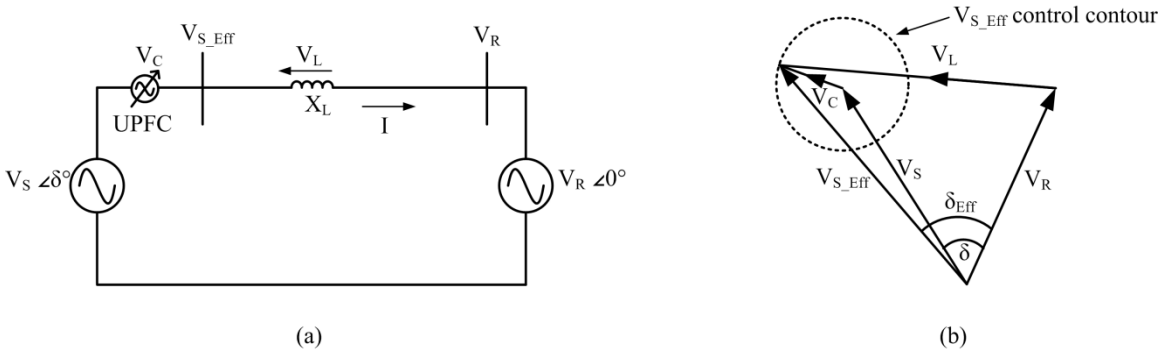

Figure 2.25: (a) Conceptual representation of UPFC in a two bus system and (b) phasor diagram of the system

The UPFC essentially consists of two back to back converters sharing a common DC link. The *Converter 2* of the UPFC is used to inject the desired series voltage through a coupling transformer. The series voltage injected has two components – the direct and the quadrature component. The direct component is in phase, while the quadrature

component is 90° out of phase with the bus voltage. The overall compensation voltage magnitude can be effectively varied between zero to some maximum value, while its angle can be varied between 0° to 360°. The basic function of Converter 1 is to supply or absorb the real power demanded by Converter 2 at the common dc link to support the real power exchange resulting from the series voltage injection. This dc link power demand of Converter 2 is converted back to ac by Converter 1 and coupled to the transmission line via a shunt connected transformer. In addition to the real power need of Converter 2, Converter 1 can also generate or absorb controllable reactive power and therefore provide independent shunt reactive compensation for the line.

Although the UPFC has many attractive features in terms of power flow controllability, the cost and complexity of such a system is very high. The shunt transformers of the UPFC have to be rated for full voltage while the series transformer for full current. The UPFC should be properly designed to handle the worst case fault. The series transformer should be bypassed by a fast acting electronic switch in case of a fault. If this switch is in the high voltage side it will be very expensive and complex. If this bypass switch is in the low voltage side an additional inductor should be provided at the output of the series compensation VSC to prevent it from a dead short across its terminals. This additional inductor however reduces the overall capacitive compensation range and increases the overall inductive compensation range. All these practical design considerations make the UPFC very complex and expensive. As a result till date only three UPFCs have been installed worldwide.

2.4.2.6.4 Back To Back HVDC

The Back To Back (BTB) DC system uses two voltage source converters with a common DC link to control the power flow. The basic schematic of the BTB system is shown in Figure 2.26. The rectifier converts the sending end power to DC, while the inverter converts the DC back to AC. The two AC systems on either side of the DC link are effectively independent of each other in terms of voltage magnitude, voltage phase angle and even frequency. This makes the BTB system very powerful in terms of controllability [25]. The use of semi-conductor based VSCs enables the BTB system to achieve accurate and dynamic control over the line power flow.

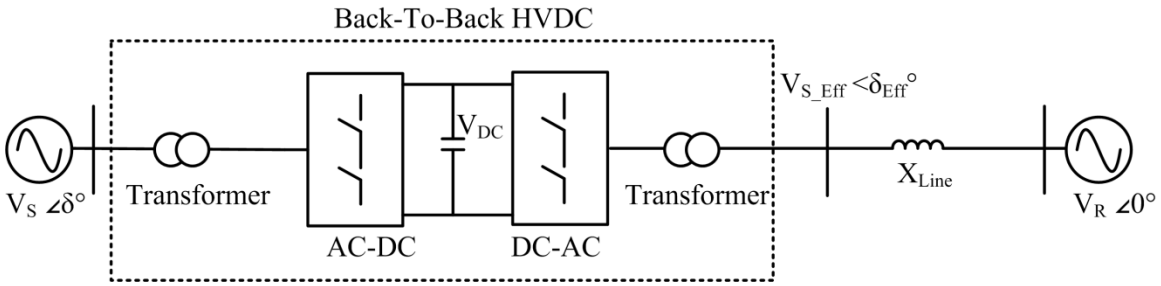

Figure 2.26: Schematic of the BTB system

Although the BTB system provides a very good control over the line power flow, it has many drawbacks and limitations both in the technological as well as the economical frontier. One of the main drawbacks of the BTB system is its cost and complexity. The BTB system requires two bidirectional converters, which can handle full rated power. As a result of the limitation of blocking voltage of power switches it is economically desirable to design these converters for lower voltages. As a result, the system is required to have a step down transformer at each end. Both these transformers have to be rated for full system voltage on the high voltage side and full system power. Also the transformers

should be designed to handle the worst case fault current. The converters of the BTB system can be designed with either thyristors or gate turn off devices like IGBTs or GTOs. Thyristors are the most developed power semiconductor switches. Thyristors with blocking voltage of 12 kV are readily available in the market. On the other hand the maximum voltage blocking rating of presently available IGBTs are only around 6.5 kV. If thyristors are used for the converter design, the number of devices required in series to withstand the secondary voltage can be reduced. This greatly reduces the complexity associated with dynamic voltage sharing among series connected devices. On the other hand thyristors can only be operated at line frequency, since they cannot be turned off forcibly. This makes the filter components more expensive. Also thyristor based BTB requires reactive support from the AC systems on both sides. The required reactive power for a BTB system can be as high as 50-60% of the real power rating [26], thus requiring shunt capacitive compensation on both ends. The problem of reactive power deficiency becomes even more pronounced if the BTB interconnection is performed through a weak link. A system is considered weak if its impedance at the point of interconnection is high or the mechanical inertia is small compared to the tie line power rating [27]. VSCs with turn off capable switches switching at PWM frequencies (multiple kHz) can be used to avoid the reactive power problems. The filter design in such BTB systems is also simplified. However, the design of the power stage of the converter becomes more complicated in these cases. The BTB system like most FACTS system requires to be designed at a substation and requires significant real estate. According to [28], the space required per MW is approximately 40 square meters.

2.5 Direct AC Converters

The concept of direct AC-AC power conversion was first introduced by Venturini more than three decades ago [29]. The traditional concept of these AC-AC converters generally uses voltages of other phases to generate the desired waveform. Such converters generally go by the name of matrix converter [30]. The matrix converter is a forced commutated converter which uses an array of controlled bidirectional switches as the main power elements to create a variable output voltage system with unrestricted frequency. It does not have any dc-link circuit and does not need any large energy storage elements [31].

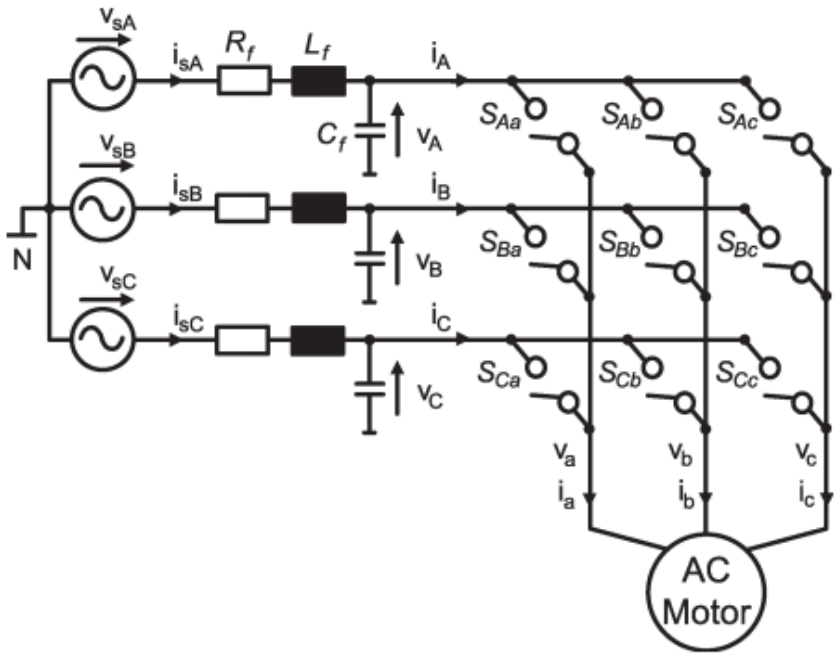

Figure 2.27: Schematic of a 3x3 matrix converter

In general a matrix converter can be defined as a single stage converter, which directly connects an *M* phase voltage source to an *N* phase load using an array of *M x N*

bidirectional switches. The schematic of a 3 x 3 matrix converter is shown in Figure 2.27. This type of matrix converter has generated a lot of interest as it connects a three-phase voltage source with a three-phase load, typically a motor.

The switching function for a matrix converter can be defined as (2.25), while the constraints can be defined mathematically as (2.26). The constraints ensure that the input side of the converter, which is a voltage source, is never short-circuited, while the output side of the converter, which is a current source, is never open-circuited. The mathematical relationship between the input and the output voltages is given by (2.27).

$$\begin{aligned} S_{KJ} &= 0, \text{ when switch } S_{KJ} \text{ is open} \\ &= 1, \text{ when switch } S_{KJ} \text{ is closed} \\ \text{where } J &= \{a, b, c\} \text{ and } K = \{A, B, C\} \end{aligned} \tag{2.25}$$

$$S_{AJ} + S_{BJ} + S_{CJ} = 1, \;\; J = \{a, b, c\} \tag{2.26}$$

$$\begin{bmatrix} V_a \\ V_b \\ V_c \end{bmatrix} = \begin{bmatrix} S_{Aa} & S_{Ba} & S_{Ca} \\ S_{Ab} & S_{Bb} & S_{Cb} \\ S_{Ac} & S_{Bc} & S_{Cc} \end{bmatrix} \begin{bmatrix} V_A \\ V_B \\ V_C \end{bmatrix} \tag{2.27}$$

One of the major issues with direct AC-AC converters is the lack of a free-wheeling path. Care should be taken to avoid short circuiting the input or open circuiting the output. Commutation techniques using current direction or voltage direction are often used for that purpose. Some researchers have also used a hybrid method using both current direction and voltage direction measurements [32].

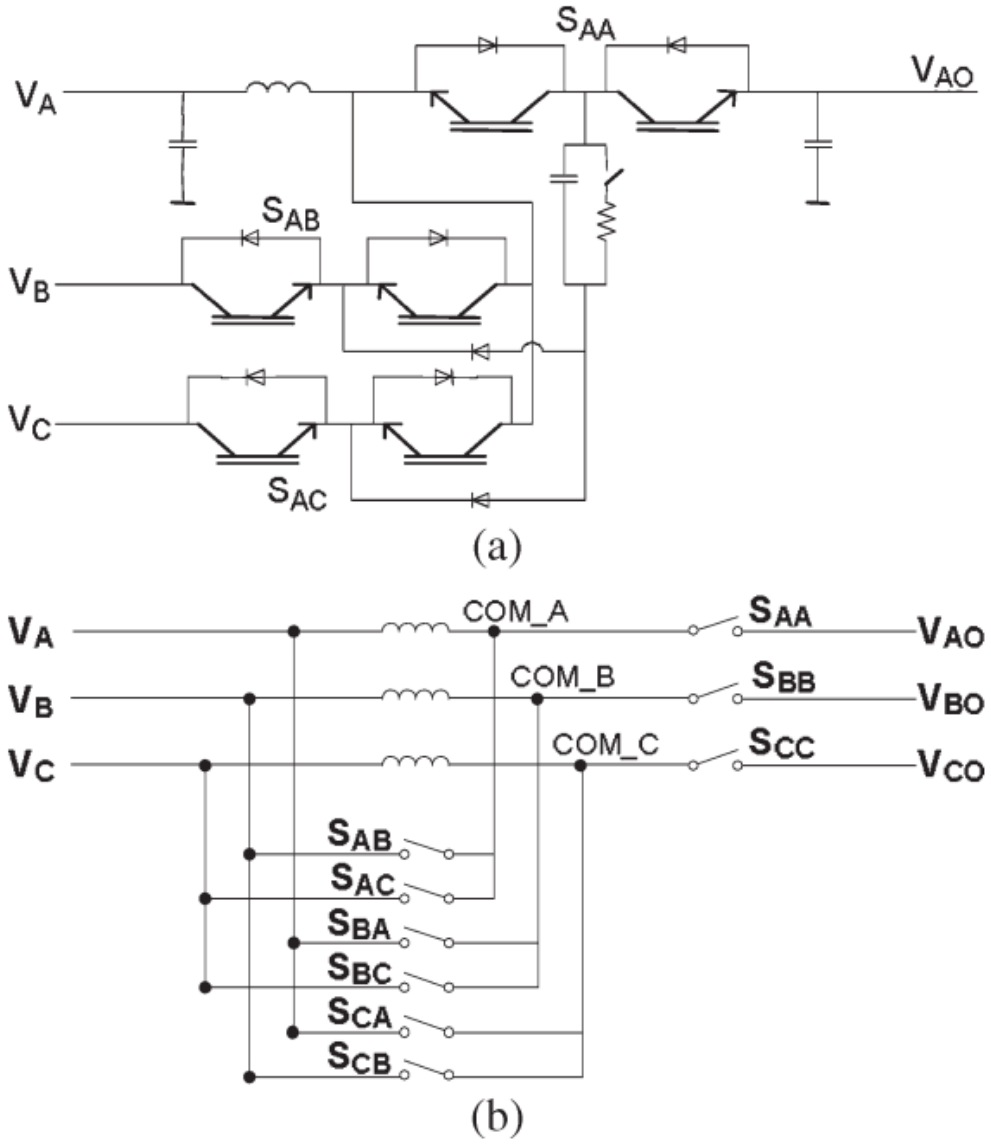

Figure 2.28: (a) Single-phase and (b) a simplified three-phase zero energy sag corrector

The matrix converter is an alternative of VSC based converters, especially for motor drive applications. However many researchers have also used direct AC converters for solving other problems. The authors of [33] used direct AC converters for voltage sag correction. In case of single or two phase voltage sags, the voltages of healthy phases are

used to synthesize voltage waveforms for the sagged phases. The schematic of such a voltage sag corrector is shown in Figure 2.28.

2.6 Conclusion

Although FACTS devices were introduced almost two decades ago and have reached a stage of technological maturity, the market penetration achieved by these devices is very limited. This is because most FACTS devices have some common underlying limitations. Most FACTS devices have high cost, high complexity and low reliability. This is because semi-conductor switches that are presently available can only handle a limited amount of power. Most FACTS projects are targeted towards sub-transmission or transmission level, which requires handling of power that is orders of magnitude greater than the power that can be handled by individual switches. Thus for a realistic FACTS device often tens of these switches have to be connected in series or parallel to effectively realize one high voltage or high current switch. Each of the individual semiconductor switches has a slightly different characteristic, thus controlling them together requires additional circuitry. Also each of these individual semiconductor switches might require different levels of voltage isolation. The driver circuitry of each semiconductor has to be also isolated. The cooling of the semiconductor switches is also a big issue. In most situations forced cooling by de-ionized water is required. Cooling systems is one of the principle sources of failure inception in FACTS systems. Also semiconductor devices have a higher failure rate than other transmission assets like transformers. Hence to ensure that the failure of a few semiconductor switches does not impact the line performance, often redundant switches has to be used. Most converters also use electrolytic capacitors that are also prone to failure. The FACTS devices have to be also

designed for unforeseen events like faults. This leads to considerable over designing of the FACTS system, since it has to be designed for the worst case fault event. All these factors make FACTS systems very complex and expensive. The FACTS devices also require very high maintenance compared to other transmission assets.

In spite of all the redundancies in design, the failure rate of FACTS devices is much higher than that of other transmission assets like lines, breakers, transformers, etc. Effective power flow control is achievable by mostly series FACTS devices. However, most series FACTS controllers are single point injection devices. The failure of these series devices often leads to failure of the line, which reduces the system reliability. Also, from a system perspective, the impact of a few centralized FACTS devices on a large system is not too high. And the high cost and low reliability of the FACTS systems prohibits them from being extensively adopted in the network. As a result, presently there is a need for low cost, reliable power flow controllers in the sub-transmission and transmission sector, which can be used to control the network power flow without compromising on the system reliability.

Chapter 3

3. CONTROLLABLE NETWORK TRANSFORMERS

3.1 Introduction

The objective of the research is to develop a cost-effective dynamic grid controller called the controllable network transformer (CNT) that can be implemented by augmenting existing load tap changing (LTC) transformers with an AC-AC converter. The low market adoption rate of centralized FACTS technologies, in spite of the high technological advancement in this area, calls for a fresh perspective on the grid control problem. The main problem with the centralized FACTS device approach is the difficulty in achieving reliable and cost-effective scaling of power converters to transmission level ratings. An alternate approach of achieving grid control by using distributed "smart" and controllable devices was proposed in [34]. The approach augments existing "dumb" passive system assets with fractionally rated direct AC-AC converters to convert them to "smart" controllable assets, as shown in Figure 3.1. The controllable network transformer is one such smart controllable asset [35].

The proposed approach of using distributed, controllable assets has significant advantages compared to the traditional centralized FACTS approach. Since the proposed approach modifies existing grid assets it is less capital intensive. The use of fractionally rated converters simplifies the power electronics. The use of a direct AC-AC converter, instead of regular DC link inverters eliminates the need for large electrolytic capacitors, which are prone to failure. Direct AC-AC converters also have lower switching losses

than inverters of similar ratings. Further, the proposed approach has a “Fail Normal Mode” of operation, which enables quick bypass of the AC-AC converter in case of a power electronic failure, restoring the grid asset to its normal function. This ensures that a converter failure does not cause a transmission line outage, thus ensuring high reliability. The distributed approach ensures that even in case of a few converter outages, the overall controllability of the system will not change drastically and the system will continue to perform reliably. The CNT is also designed to ensure that the existing grid asset is not subjected to any additional stresses like increased dv/dt or di/dt stresses. Further, in case of an external fault the direct AC converter can be bypassed quickly, thus allowing the existing system protection relays to operate without any hindrance.

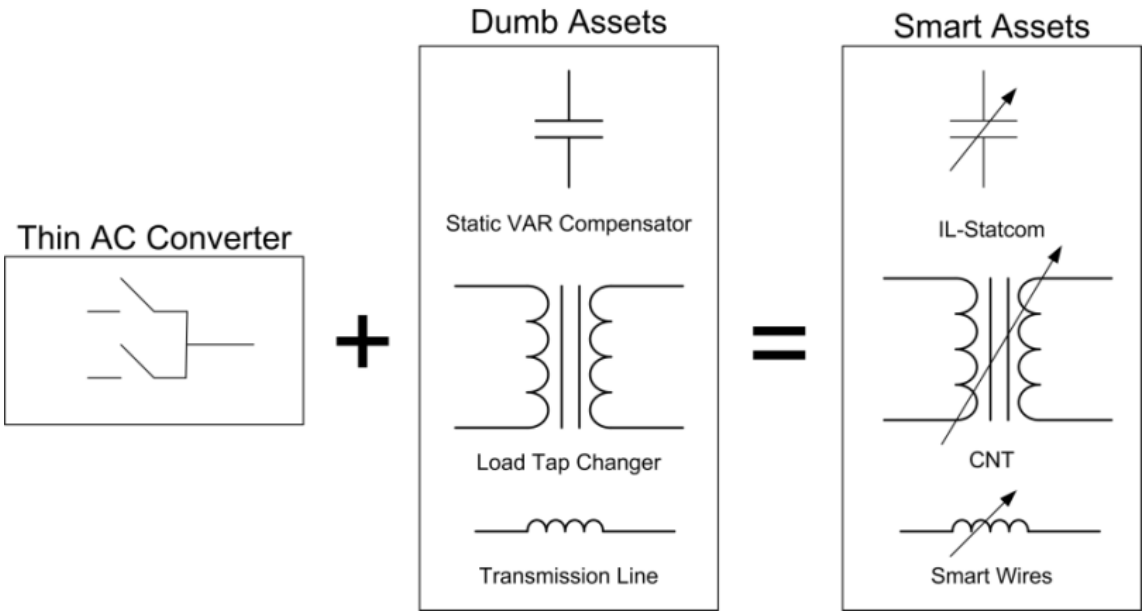

Figure 3.1: Making “dumb” assets “smart”

3.2 CNT Topology

The CNT is realized by augmenting an existing load tap changer (LTC) with a thin ac converter (TACC), as shown in Figure 3.2 [36]. The TACC is realized using bidirectional AC switches S_1 and S_2, and passive filter elements L_f and C_f. In case of a converter failure, the Fail Normal mode can be activated by switching on the anti-parallel thyristor pair T_{12} and bypassing the converter. One of the main advantages of this topology is that the converter can be rated only a fraction of the transformer rating. This is because the switches have to handle only a fraction of the transformer rated voltage. For implementation at transmission or sub-transmission level voltages a multilevel TACC will be required.

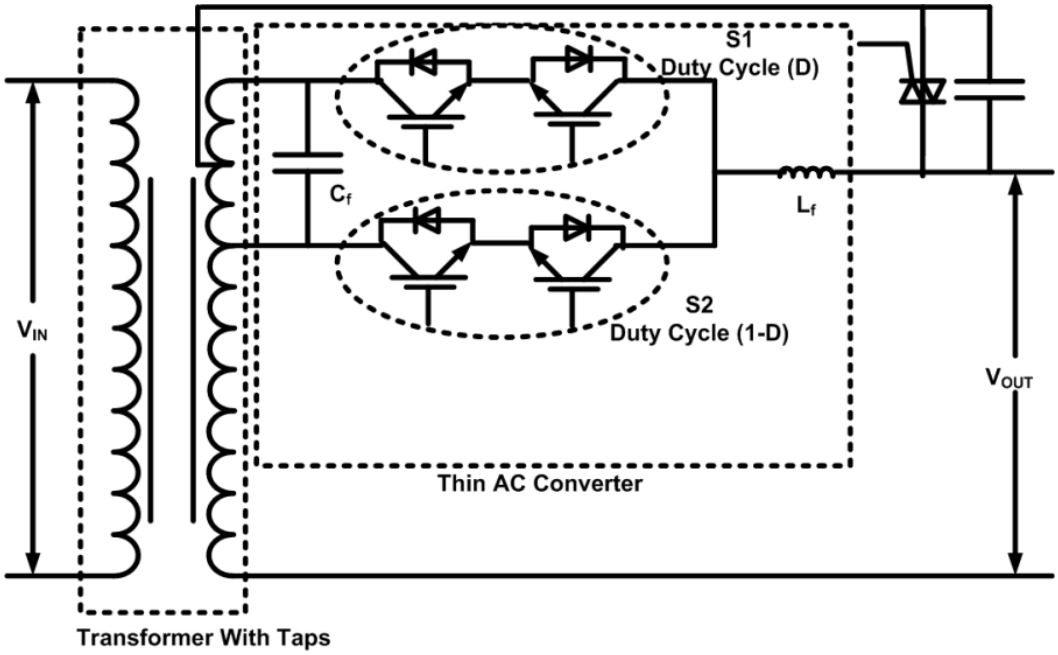

Figure 3.2: Controllable Network Transformer topology

3.3 Basic Operation

Assume that the LTC has off nominal taps at (1+n) pu and (1-n) pu voltage levels. The two switches S_1 and S_2 are operated at fixed duty cycles D and (1-D). When the switch S_1 is on, the turns ratio of the transformer is 1:(1+n), while when the switch S_2 is on it becomes 1:(1-n). By applying fixed duty cycle D, it is possible to control the output voltage magnitude between $\frac{1}{1+n}$ pu to $\frac{1}{1-n}$ pu. However, by using conventional PWM techniques it is not possible to control the phase of the output voltage. This is because there is no energy storage in the circuit, which can provide energy during the zero crossings of the input voltage. The output voltage phase angle in this case is thus the same as that of the input voltage. For controlling the phase of the output voltage, the technique of dual virtual quadrature sources (DVQS) can be applied, which is discussed in the following subsection [37].

3.3.1 Dual Virtual Quadrature Sources

Figure 3.3(a) shows a simple ac chopper circuit. Using conventional PWM techniques, an output voltage of same phase but lesser magnitude, as shown in Figure 3.3(b), can be obtained. Conventional PWM techniques require the duty ratio D to be equal to a constant value K_0. Under this operating condition it is not possible to produce an output voltage with different phase and/or harmonic content, as shown in Figure 3.3(c).

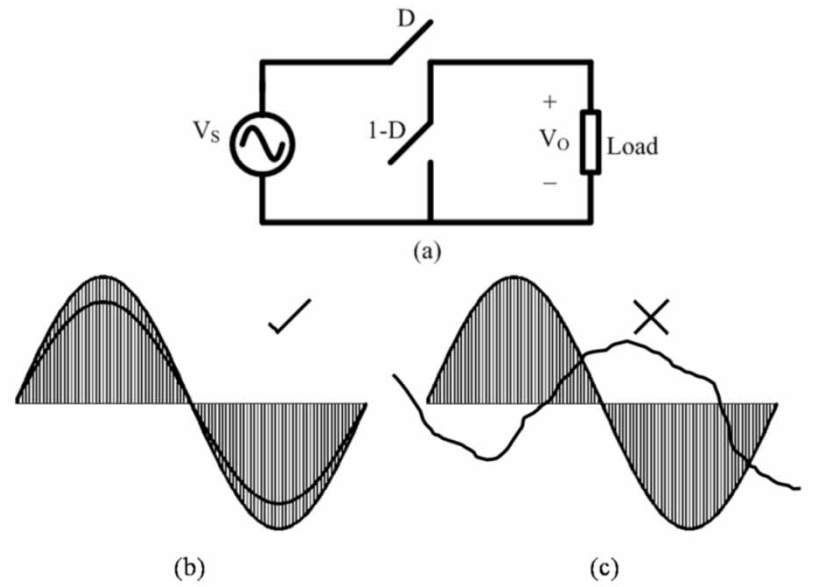

Figure 3.3: AC chopper (a) Circuit topology, (b) Achievable output voltage, (c) Unachievable output voltage using conventional PWM.

$$D = K_0 + K_2 \sin(2\omega t + \Phi) \tag{3.1}$$

$$V_S = V \sin(\omega t) \tag{3.2}$$

$$V_0 = K_0 V \sin(\omega t) + \frac{K_2 V}{2} \cos(\omega t + \Phi) - \frac{K_2 V}{2} \cos(3\omega t + \varphi) \tag{3.3}$$

$$V_d = K_0 V \sin(\omega t) \tag{3.4}$$

$$V_q = \frac{K_2 V}{2} \cos(\omega t + \Phi) \tag{3.5}$$

$$V_3 = -\frac{K_2 V}{2} \cos(3\omega t + \varphi) \tag{3.6}$$

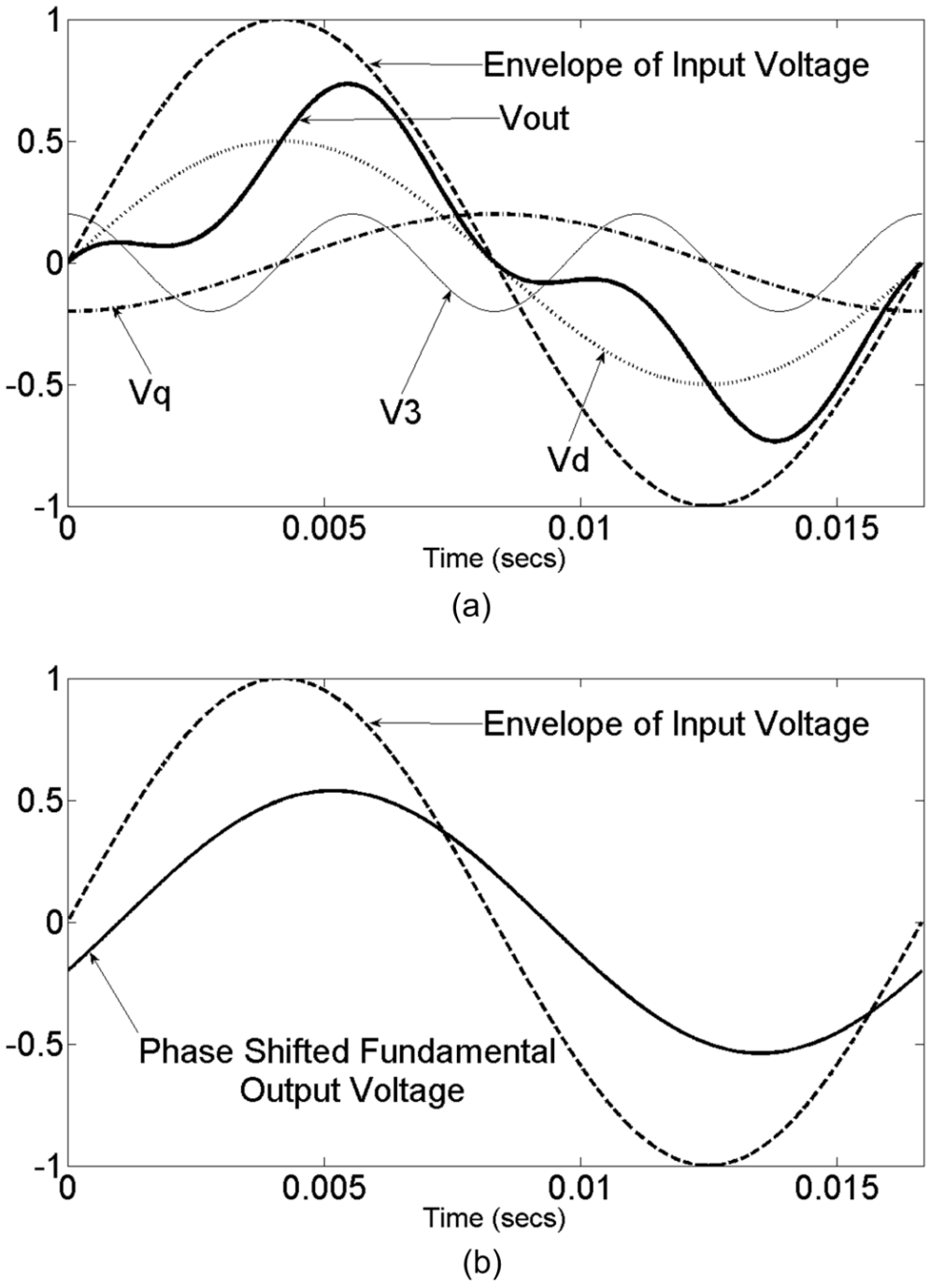

Figure 3.4: Various components of the output voltage obtained using DVQS strategy, (b) Input and phase shifted fundamental output voltage.

The duty ratio D is now modified such that it now has a second harmonic term of magnitude K_2 and phase Φ in addition to the DC component K_0, as shown in (3.1). If the input voltage is a pure sinusoidal wave given by (3.2), then the output voltage obtained in this case can be divided into three components, as given by (3.3). The first component is the output voltage that is in phase with the input voltage (V_d). Additionally two other virtual sources are invoked in quadrature to the input voltage. One of these sources is at fundamental frequency (V_q) while the other one is at the third harmonic frequency (V_3). The sum of all the three components must at all instances of time lie within the envelope of the input voltage. Figure 3.4(a) shows the different components of the output voltage along with the input voltage. The output obtained at the fundamental frequency is the sum of the components V_d and V_q, which can now be phase shifted from the input voltage as shown in Figure 3.4(b). The above method of introducing even harmonic term in the duty ratio to implement DVQS is called Even Harmonic Modulation (EHM) scheme. The EHM scheme can be applied to the controller of the CNT converter to realize DVQS and produce an output voltage with controllable magnitude and phase angle.

3.4 CNT Analysis and Model Derivation

Assume that a CNT, with off nominal tap ratio of n is placed on a line connecting two arbitrary buses, *Bus J* and *Bus K*, as shown in Figure 3.5 [38]. The voltages at these two buses are assumed to be separated by a phase difference of δ^o. The sum of inductance of the transmission line and the transformer reflected to the *Bus K* side is assumed to be *L*. For the purpose of this analysis, the losses in the transmission line and the CNT are neglected.

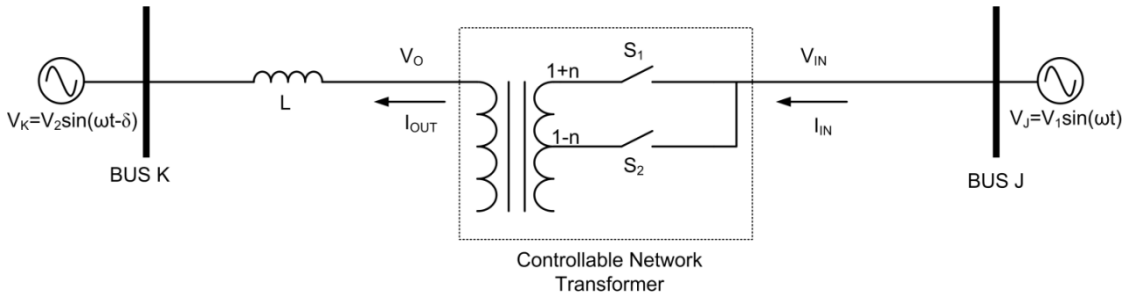

Figure 3.5: CNT model derivation

The DVQS is implemented using the Even Harmonic Modulation (EHM) scheme. The duty cycle of the switch S_1 is given by (3.7), while S_2 is the switch with complimentary switching function. The voltages at the two end buses are given by (3.8) and (3.9). The voltage at the output of the CNT, $\overrightarrow{V_O}$ can be expressed in terms of the input voltage $\overrightarrow{V_{IN}}$, duty cycle $D(t)$ and the off nominal tap ratio n, as shown in (3.10).

$$D(t) = K_0 + K_2 \sin(2\omega t + \Phi) \tag{3.7}$$

$$\overrightarrow{V_J} = \overrightarrow{V_{IN}} = V_1 \sin(\omega t) \tag{3.8}$$

$$\overrightarrow{V_K} = V_2 \sin(\omega t - \delta) \tag{3.9}$$

$$\overrightarrow{V_O} = \left[\frac{D(t)}{1+n} + \frac{1-D(t)}{1-n}\right] * V_{IN} \tag{3.10}$$

Simplification of (3.10) gives (3.11) that shows that $\overrightarrow{V_O}$ consists of a fundamental component and a third harmonic component. The parameters A and B are defined in (3.12) and (3.13). The constants K_0 and K_2 are not fully independent of each other as shown by the constraint equation (3.14). The constraint is required to prevent over

modulation. The secondary current $\overrightarrow{I_O}$, can be expressed as (3.15), where $\overrightarrow{V_O^1}$ is the fundamental component, while $\overrightarrow{V_O^3}$ is the third harmonic component of $\overrightarrow{V_O}$.

$$\overrightarrow{V_O} = V_1(A\sin\omega t - B\cos(\omega t + \Phi)) + BV_1\cos 3\omega t \tag{3.11}$$

$$A = \frac{1 + n - 2K_0 n}{1 - n^2} \tag{3.12}$$

$$B = \frac{nK_2}{1 - n^2} \tag{3.13}$$

$$K_2 \leq min\{K_0, 1 - K_0\} \tag{3.14}$$

$$\overrightarrow{I_O} = \frac{\left(\overrightarrow{V_O^1} - \overrightarrow{V_K}\right)}{j\omega L} + \frac{\overrightarrow{V_O^3}}{j(3\omega)L} \tag{3.15}$$

The expression for $\overrightarrow{I_O}$ can be simplified to (3.16). By principle of conservation of energy, the input and the output currents are related by (3.17). Using (3.16) in (3.17) gives (3.18). From (3.18) it can be seen that the input current consists of fundamental, third harmonic and fifth harmonic components. Since the CNT is made of passive devices and there is no energy storage, the power in the input and the output side should be same instantaneously and on an average basis. This can be verified by comparing the product of (3.11) and (3.16) with that of (3.8) and (3.18).

$$\begin{aligned}\overrightarrow{I_O} = \frac{1}{\omega L}[-AV_1\cos\omega t - BV_1\sin(\omega t + \Phi) + V_2\cos(\omega\mathrm{t} - \delta)] \\ + \frac{V_1}{3\omega L}B\sin(3\omega t + \Phi)\end{aligned} \tag{3.16}$$

$$\overrightarrow{I_{IN}} = \left[\frac{D(t)}{1+n} + \frac{1-D(t)}{1-n}\right] * \overrightarrow{I_O} \tag{3.17}$$

$$\begin{aligned}\overrightarrow{I_{IN}} = \Bigg[&\frac{V_1}{\omega L}\left(-A^2 + \frac{2}{3}B^2\right)\cos\omega t \\ &+ \frac{V_2}{\omega L}(A\cos(\omega t - \delta) - B\sin(\omega t + \Phi + \delta))\Bigg] \\ &+ \left[\frac{BV_1}{\omega L}(2A\sin(3\omega t + \Phi) - B\cos(3\omega t + 2\Phi))\right. \\ &\left. - \frac{BV_2}{\omega L}\sin(3\omega t + \Phi - \delta)\right] + \left[\frac{B^2V_1}{3\omega L}\cos(5\omega t + 2\Phi)\right]\end{aligned} \tag{3.18}$$

The real power through the tie line with CNT is given by (3.19). The sending end and receiving end reactive power equations are given by (3.20) and (3.21). In absence of the CNT, the power flow equations for the line is given by (3.22)-(3.24), which can also be obtained by substituting *A=1, B=0* in (3.19)-(3.21).

$$P_{LINE\_CNT} = \frac{V_1V_2}{\omega L}(A\sin\delta - B\cos(\delta + \Phi)) \tag{3.19}$$

$$Q_{SEND\_CNT} = \frac{V_1}{\omega L}\left[\left(A^2 - \frac{2}{3}B^2\right)V_1 - AV_2\cos\delta + BV_2\sin(\delta + \Phi)\right] \tag{3.20}$$

$$Q_{RECEIVE\_CNT} = \frac{V_2}{\omega L}[V_2 - AV_1\cos\delta - BV_1\sin(\delta + \Phi)] \tag{3.21}$$

$$P_{LINE\_NO\_CNT} = \frac{V_1V_2}{\omega L}\sin\delta \tag{3.22}$$

$$Q_{SEND\_NO\_CNT} = \frac{V_1}{\omega L}[V_1 - V_2\sin\delta] \tag{3.23}$$

$$Q_{RECEIVE\_NO\_CNT} = \frac{V_2}{\omega L}[V_2 - V_1 \sin\delta] \tag{3.24}$$

In the above equations, *Bus J* is assumed to be the sending end, while *Bus K* is the receiving end. Equation (3.19)-(3.21) are very important as they provide some useful insight into the working principles of the CNT. The real power flowing through the tie line is due only to the fundamental voltages and currents. The harmonic voltages and currents do not cause any real power flow. The degree of real and reactive power flow control achievable can also be calculated using (3.19)-(3.21). From (3.12) and (3.13) it is seen that A depends on the dc component K_0 of the duty cycle, while B depends on its second harmonic magnitude K_2. Hence, the line real and reactive power flow formulae can be viewed to be composed of two terms – one which depends on K_0, while the other one depends on K_2 and Φ. Thus by appropriately choosing the duty cycle, the real and reactive power flow through the line can be controlled. The CNT analysis procedure is summarized in Figure 3.6.

The input voltage $\overrightarrow{V_{IN}}$ consists of only the fundamental frequency. The output voltage of the CNT, $\overrightarrow{V_O}$ is obtained by multiplying $\overrightarrow{V_{IN}}$ with the duty cycle $D(t)$, which contains a DC component and a second harmonic component. As a result the output voltage $\overrightarrow{V_O}$ contains a fundamental and a third harmonic component. The output side current is obtained by dividing the voltage difference between the output voltage and the receiving end bus by the line reactance. The presence of fundamental and third harmonic in $\overrightarrow{V_O}$ results in the same frequency content in $\overrightarrow{I_O}$. The input side current $\overrightarrow{I_{IN}}$ is obtained by

multiplying $\overrightarrow{I_O}$ with the duty cycle *D(t)*. As a result $\overrightarrow{I_{IN}}$ is seen to contain fundamental, third and fifth harmonics.

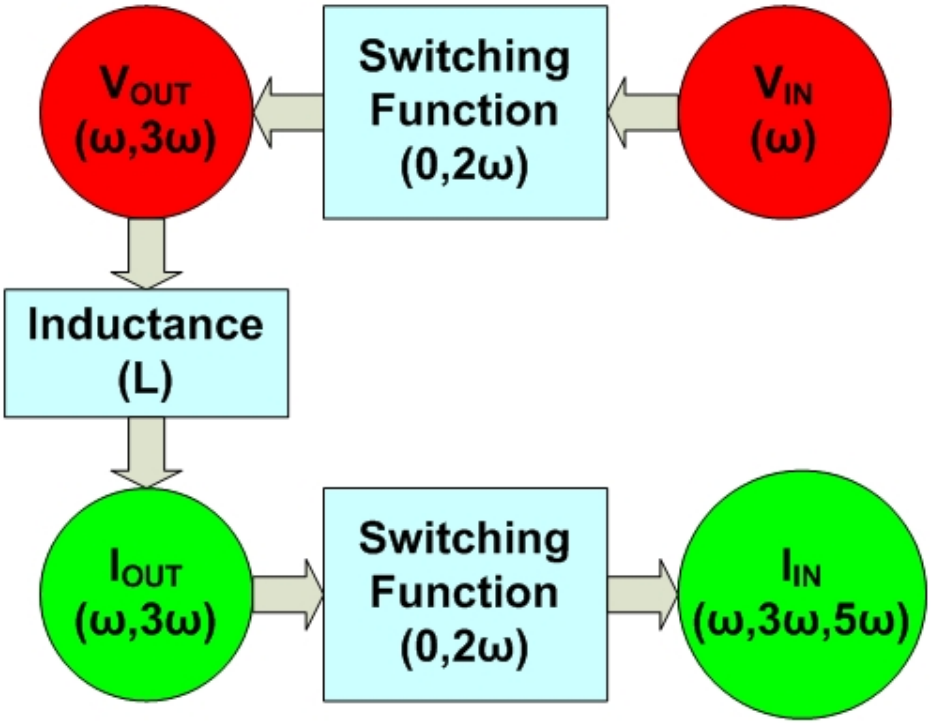

Figure 3.6: CNT analysis methodology

3.5 CNT Control Range Derivation

Using (3.19)-(3.21) the potential controllability that can be achieved by a CNT in a network can be assessed. Often two areas are weakly connected by short tie lines. Consider a tie line of length 10 miles, with line inductance 1.5 mH/mile. The voltage angle deviation between the buses connected by the line is assumed to be 2°. It is to be noted that in a meshed system this angle deviation is a result of the generator dispatch as well as the CNT settings. For the purpose of analysis it is assumed that this angle deviation is held constant. The system is assumed to be at 138 kV. Under normal

conditions the tie line is required to carry very little power. In absence of any power flow controller, the active power through the line will be fixed at 118 MW. The real and reactive power flow controllability achieved by a CNT in this test system is studied.

Suppose a CNT with an off nominal tap ratio of ±10% (n=0.1) is placed on this line. The degree of control achieved by the CNT in the P-Q plane at the sending end, according to (3.19) and (3.20) is shown in Figure 3.7. Using conventional PWM techniques (DC modulation) the CNT can only control active power between 106 MW and 130 MW, as shown by the almost horizontal dashed line in Figure 3.7. Introduction of the EHM scheme allows the active power control go beyond this range and vary from -50 MW to 290 MW. The vertical solid lines in Figure 3.7 show the loci of control achieved by the introduction of second harmonics in the duty ratio function, for a given value of K_0. The overall control area achieved by the CNT is shown by a black dotted border in Figure 3.7.

It is clear from Figure 3.7 that variation of K_2 has little effect on reactive power (Q) while variation of K_0 does not affect real power (P) to a great extent. Figure 3.7 also shows that the range of control achieved by the CNT both for real as well as reactive power is quite high. While the real power can be varied from -50 MW to 290 MW, the reactive power can be varied from -270 MVAR to 420 MVAR. In the absence of a CNT, the real and reactive power through the line is fixed at 118 MW and 2 MVAR respectively as shown in Figure 3.7.

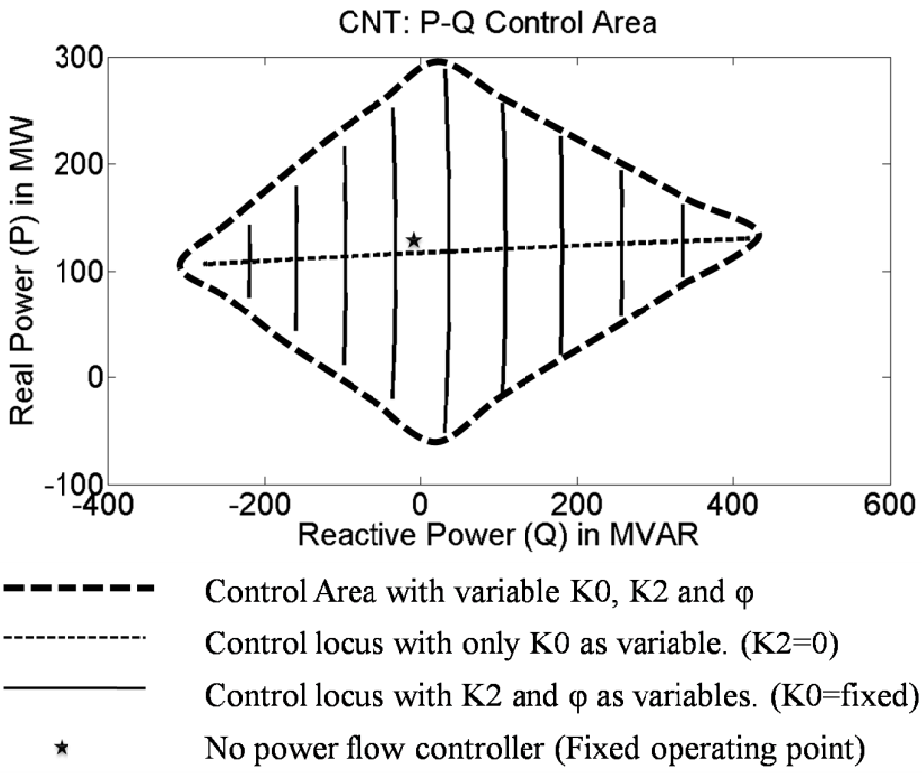

Figure 3.7: Real and reactive power flow control range achieved by the CNT in the test system

Figure 3.8 shows the variation of the control range of a CNT with the converter ratings when other factors like V_1, V_2 and δ are kept constant. It is seen that the control range of the CNT increases with increasing converter rating. The total line rating is assumed to be 450 MVA. From a system planning perspective this situation is quite different from other power flow controllers. In the case of a BTB or VFT type of power flow controller, the system planner has no option but to install a full line power rated device. So, for the above line, to achieve any power flow control a 450 MVA rated BTB or VFT will be required. In contrast, depending on the system requirement, the rating of the CNT to be installed can be varied. For a 23 MVA converter, the CNT can vary the real line power from 75 MW to 160 MW, while for a 45 MVA converter this range

becomes from 33 MW to 202 MW. Hence from a system planner's perspective the CNT provides more options, making it a more attractive solution.

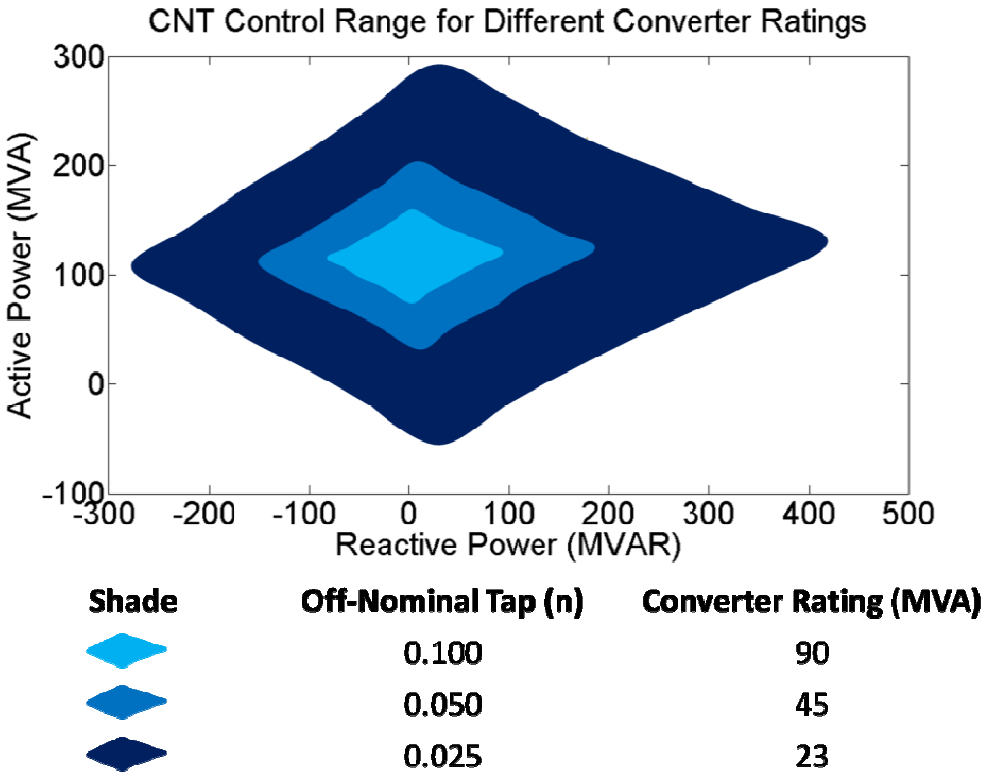

Figure 3.8: CNT control range variation with converter rating

From (3.19) and (3.20) it is clear that the CNT control range also depends on the variable δ, which is the phase angle difference between the two end bus voltages [39]. It is seen from Figure 3.9 that as δ changes, the active control area just shifts along the active power axis while the reactive power control area remains unchanged. It is also noted that the degree of control remains almost unchanged for varying δ. For example if δ = 5°, the active power can be controlled from 126 MW to 466 MW, giving a control range of 340 MW. For δ = -1°, the variation is between -230 MW to 110 MW, hence the control range remaining constant at 340 MW. Theoretically this can be explained as

follows. In (3.19) it is clear that active power varies mostly with B, while A has almost no effect on it. As a result the maximum range of control for a given CNT is given by (3.25), which is independent of δ.

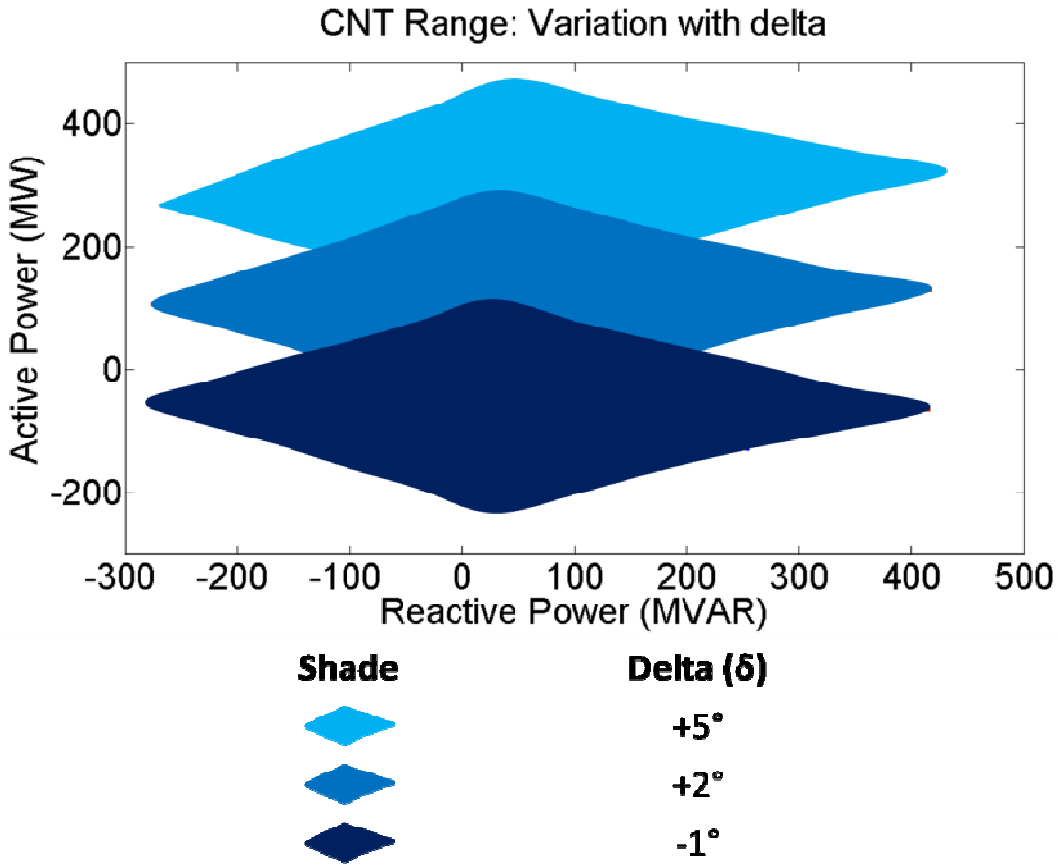

Figure 3.9: CNT control range variation with δ

$$\Delta P_{CNT\ Range} = \frac{V_1 V_2}{\omega L} 2B \tag{3.25}$$

3.6 Basic CNT Simulations

The basic principle for the CNT operation is verified by simulation in this section. The simulations are carries out using Simulink, Matlab.

3.6.1 CNT Power Flow Equation Verification

To verify the analytical power flow formulae derived in the previous section, the system presented in the previous section is simulated. The schematic of the simulated system is shown in Figure 3.10. It is assumed that a CNT is used to control the power flow on a tie line connecting two areas – Area1 and Area2. The system is assumed to be operating at 138 kV, while the voltage phase angle of these two areas is separated by 2°. The tie line is assumed to be 10 miles long with an inductance of 1.5 mH/mile. To simulate a stable system sufficient resistance is introduced in the system. The X/R ratio of the line was assumed to be 10. Figure 3.11 shows the reactive power flowing through the line as the K_0 is varied from 0 to 1 in steps of 0.25, while the K_2 is kept at 0. The results obtained in the simulation show that the reactive power flow at the sending end of the line can be varied from -300 MVAR to 350 MVAR.

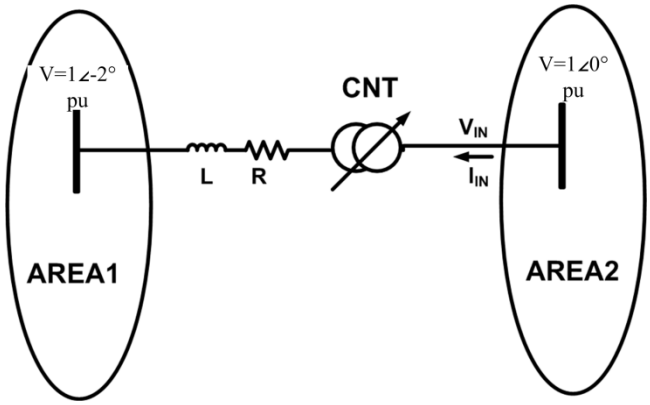

Figure 3.10: Schematic of system simulated in MATLAB

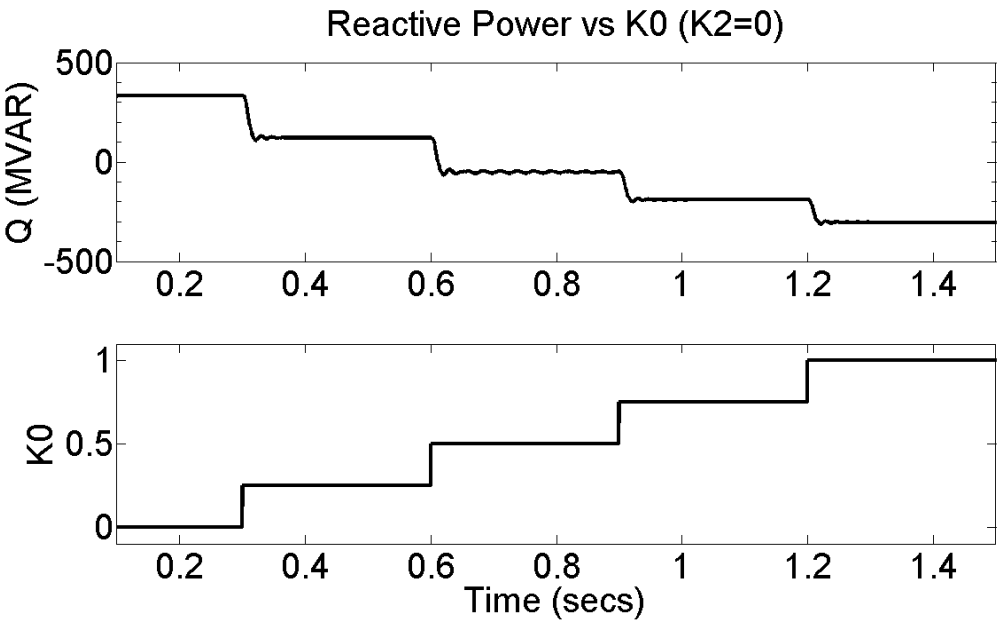

Figure 3.11: Reactive power flow control by variation of K_0 for K_2=0

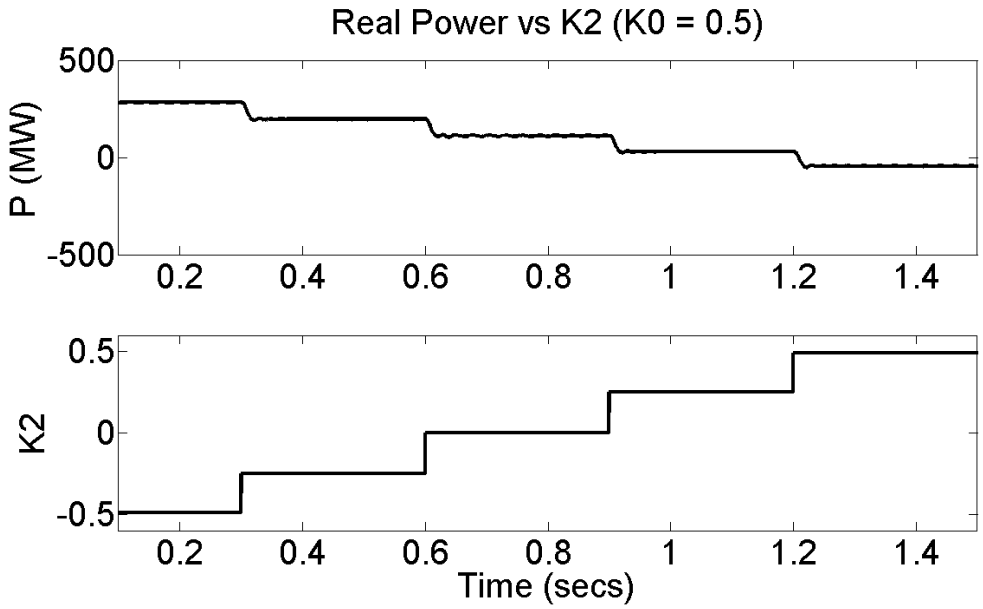

Figure 3.12: Real power flow control by variation of K_2 for K_0=0

The simulation is repeated keeping K_0=0.5 and varying K_2 in steps of 0.25. It is seen from Figure 3.12 that the CNT is able to control the real power from 280 MW to -40

MW, if the value of K_2 is varied from -0.5 to 0.5. Thus in the case of both real and reactive power flow the simulation results closely matches the ones calculated using the derived analytical formulae. The small difference in simulated and calculated power flows can be attributed to the resistances and the non-ideal transformers that were used in the simulation circuit.

3.6.2 Contingency Operation

Often, especially in case of contingencies, it is seen that tie lines carry power from low generation area to high generation area, causing further stress in the low generation area. Bidirectional power flow control on tie lines can prevent such situations, making it a very desirable property for tie lines. The control range achieved by the CNT enables it to do a bidirectional control of power flow under many situations. This is validated by another simulation in Simulink Matlab. The system simulated is the same as shown in Figure 3.10.

It is assumed that under pre-contingency scenario, the angle deviation between the two areas are $\delta=1°$. A loss of generation occurs in Area1. It is assumed that post-contingency the angle deviation between the two areas increase to $\delta=2°$. In absence of a power flow controller in the tie line, under post-fault situation, Area1 is forced to export 120 MW of power. This further aggravates the loss of generation problem of Area1 and might even cause cascading failures. However, in presence of CNT, Area1 can not only stop the export of power, but also can import 40 MW from Area2 through the tie line. This might help alleviate the contingency problem in Area1. The CNT can also control the amount of reactive support required by Area1 through the tie line [40].

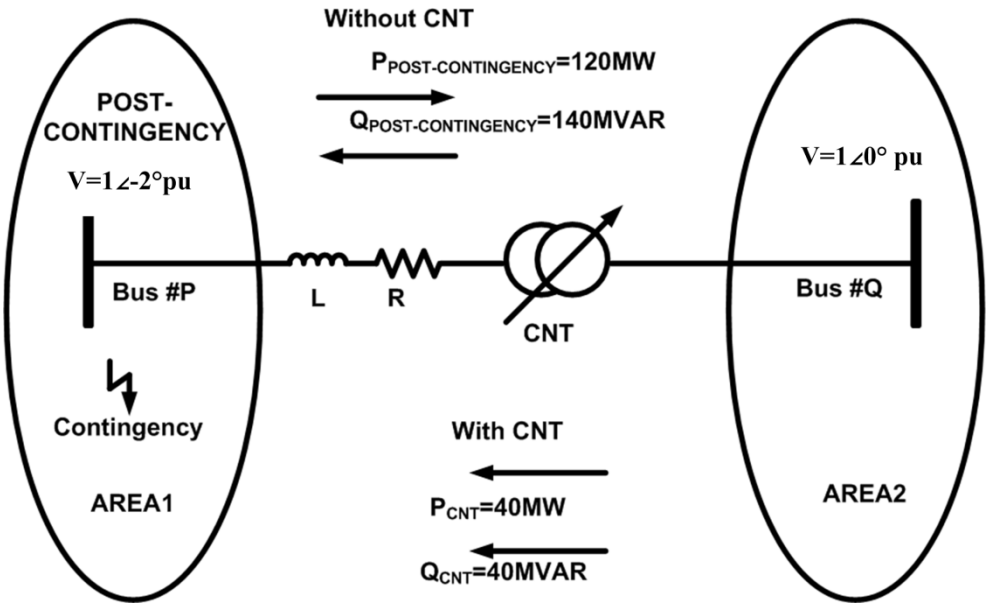

Figure 3.13: Post-contingency real and reactive power flow control by the CNT

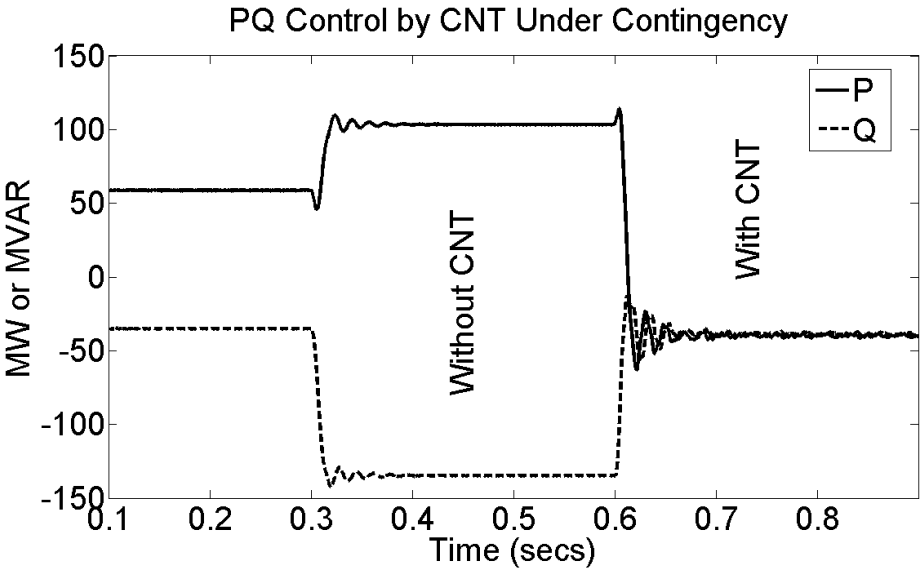

Figure 3.14: Real and reactive power exported from Area1 to Area2

Figure 3.13 summarizes the post-contingency real and reactive power in the tie line with and without CNT. Figure 3.14 shows the real and reactive power through the tie

line. The contingency is assumed to occur at t=0.3s. The effect of contingency on the tie line power without CNT is observed till time t=0.6s, after which the CNT is switched on.

3.7 Hardware Proof of Concept

To validate the CNT operation a prototype CNT rated at 480 V, 2 kVA was built at the Intelligent Power Infrastructure Consortium (IPIC) laboratory at Georgia Tech. The CNT was realized using a standard 480 V / 240 V center tapped transformer as shown by the schematic in Figure 3.15. The output of the CNT is looped back to its input through a resistance and an inductance. It is to be noted that in Figure 3.15, the two voltage sources shown are one and the same. In absence of the CNT no power would flow in the line as it is connected to exactly same voltage at each end. However, with the CNT, both the power flow magnitude as well as the direction can be controlled. From the schematic it is clear that the CNT effectively has an off nominal tap ratio of 25% (n=0.25). The two-level TACC is realized with two ac switches using four IGBTs rated at 100 Amps, 1200 V switching at 10 kHz. A photograph of the experimental setup is shown in Figure 3.16.

Initially the CNT is operated using conventional PWM techniques. Thus the gating signal is assumed to have only a dc component with K_0=0.9. The circuit is kept mostly resistive with R=3.5Ω, while external inductance is kept at zero. The voltage and current waveforms obtained by this method is shown in Figure 3.17. The blue curves represent the input voltage at the transformer primary while the yellow curves are the secondary voltages. The output voltage is shown by the green curves and the line current by the violet curves. It is seen that for an input voltage of about 155 V, the power flowing in the circuit is 1.3 kW.

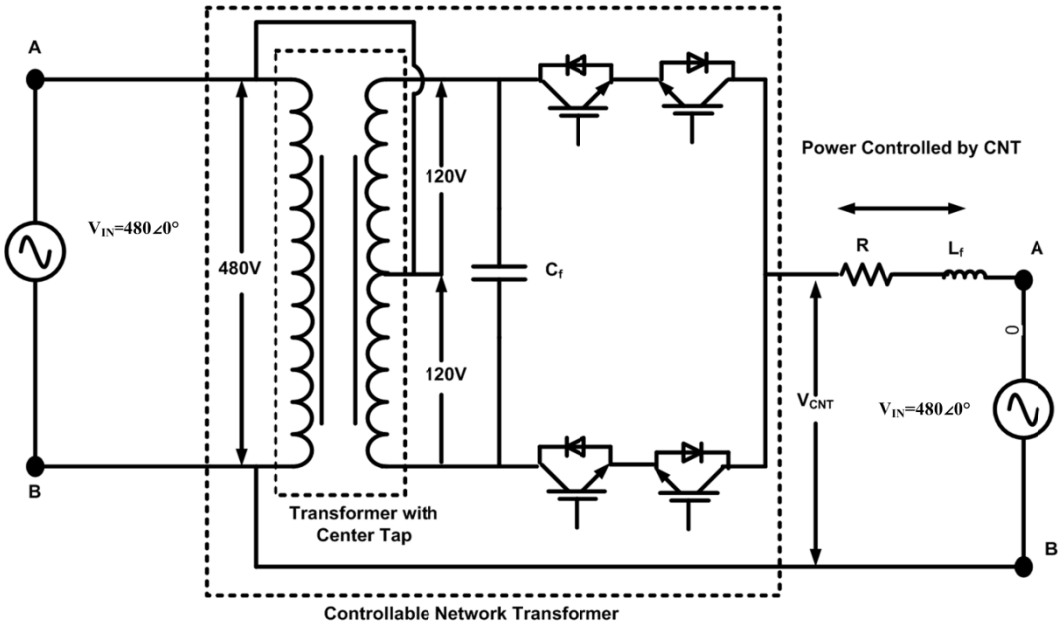

Figure 3.15: Schematic of the 5 kVA CNT experimental setup

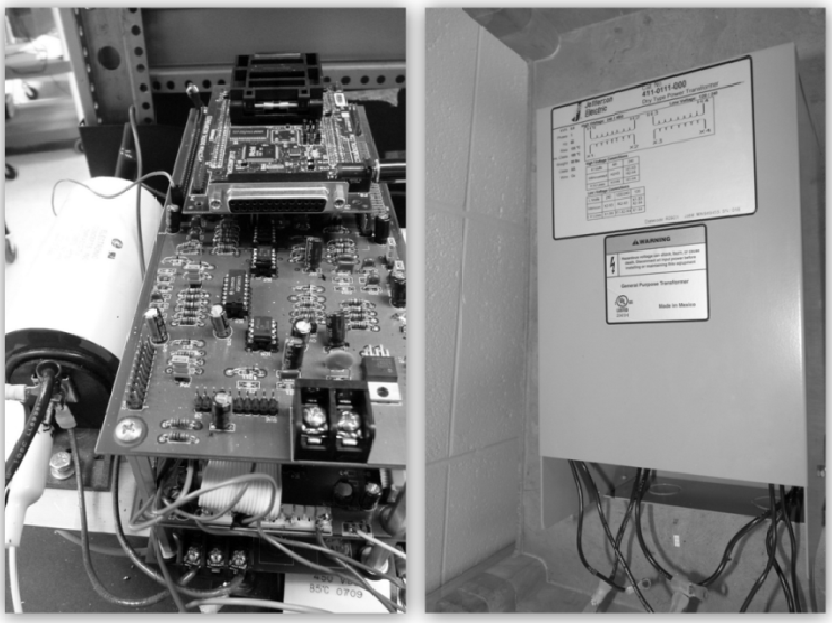

(a) (b)

Figure 3.16: Picture of experimental setup; (a) Two Level AC converter circuit (b): Center Tapped Transformer used as CNT

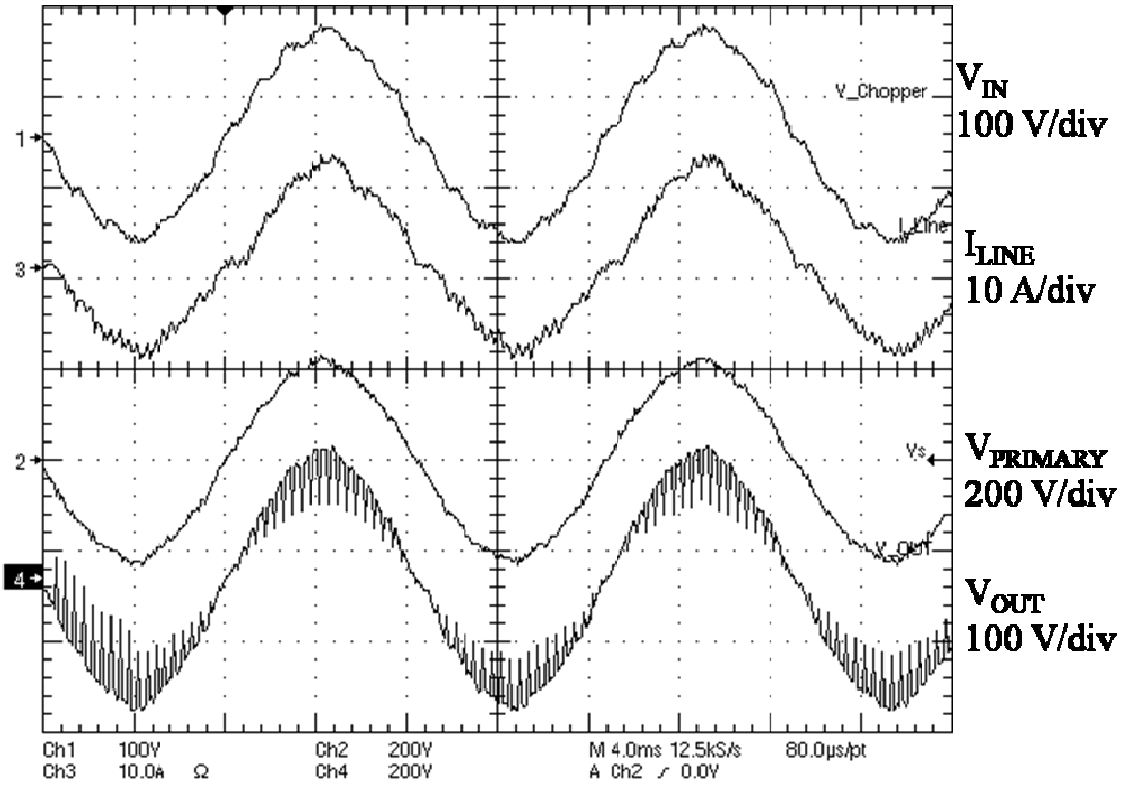

Figure 3.17: Voltage and current waveforms for resistive circuit for K_0=0.9, K_2=0

The CNT is operated at two more operating points. In both these cases the values of K_0 and K_2 are kept constant at 0.5 and 0.2 respectively, while the value of Φ is varied. The circuit for these two operating points is made inductive. Figure 3.18 shows the voltage and currents for Φ=0°, while x shows that for Φ=180°. It is observed that for an input voltage of 80 volts, the CNT can push as much as 260 Watts of power for Φ=0°. For Φ=180° the direction of power flow is reversed and -360 Watts of power flows through the circuit. The reversal of the current phase can be easily seen comparing Figure 3.18 and Figure 3.19.

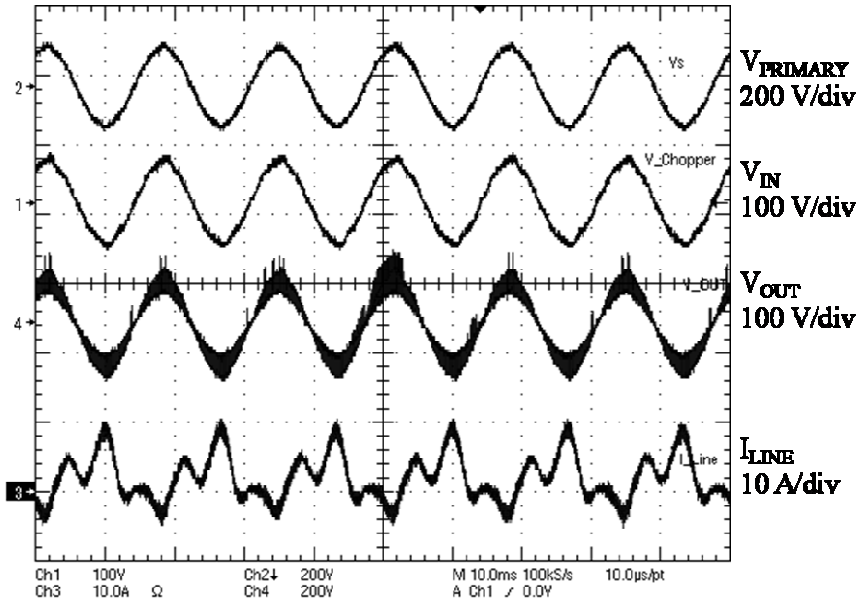

Figure 3.18: Voltage and current waveforms for K_0=0.5, K_2=0.2, Φ=0°

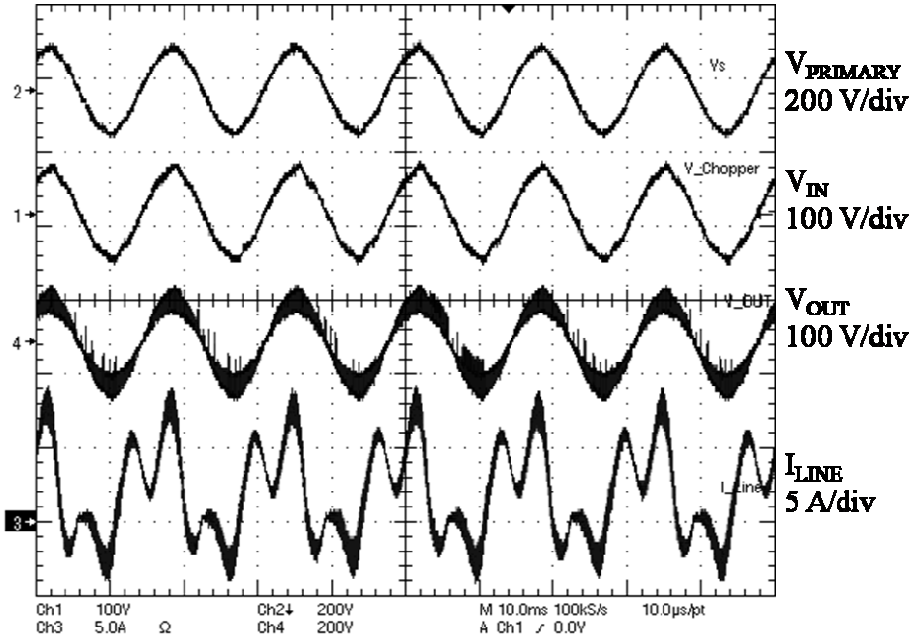

Figure 3.19: Voltage and current waveforms for K_0=0.5, K_2=0.2, Φ=180°

It is seen that the obtained experimental waveforms are in close harmony with the simulated waveforms, shown in Figure 3.20 - Figure 3.22. Hence in absence of any K_2 component, the line current does not have any lower order harmonics. The introduction of the K_2 term helps provide control on real power both in terms of magnitude and direction. However, the K_2 term also introduces third harmonic in the line current.

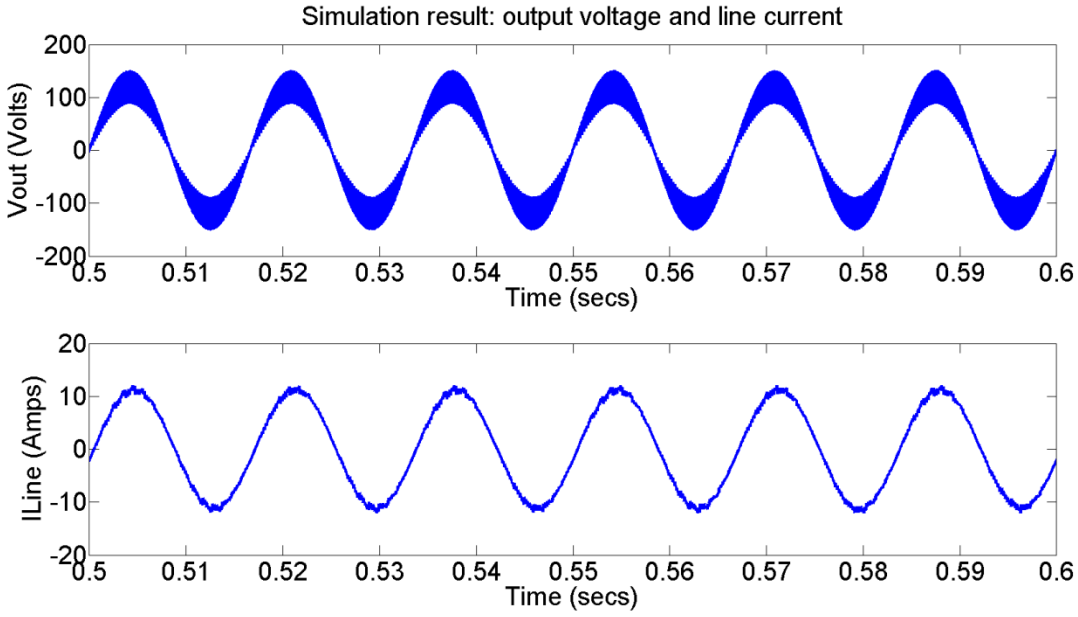

Figure 3.20: Simulated voltage and current waveforms for K_0=0.9, K_2=0.0

At K_0=0.5 and K_2=0, the current in the circuit should be zero. Hence, the control effort required in the form of second harmonic injection is maximum at this point. As a result the current is observed to have significant level of 3rd harmonic. It is possible to reduce the harmonic content in the line current using 3rd harmonic traps. Also, in many utility situations it might be possible to control the power flow to a desired level, using limited amount of harmonic injection.

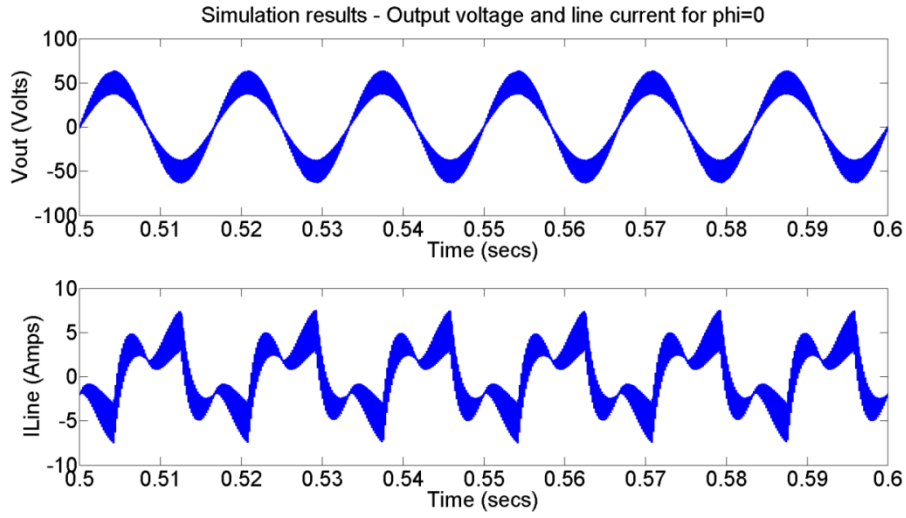

Figure 3.21: Simulated voltage and current waveforms for K_0=0.5, K_2=0.2, Φ=0°

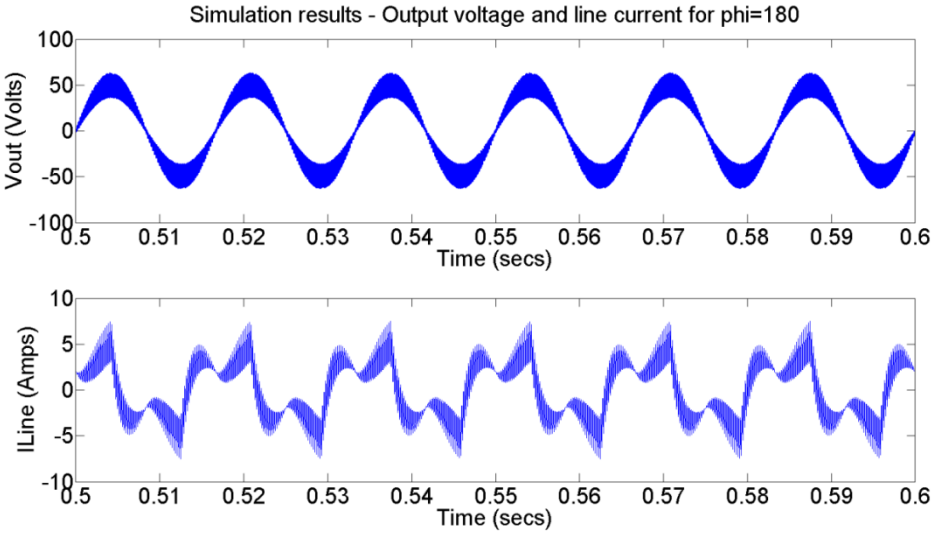

Figure 3.22: Simulated voltage and current waveforms for K_0=0.5, K_2=0.2, Φ=180°

3.8 Conclusions

This chapter introduces the controllable network transformer (CNT), which has several advantages compared to the present state of the art dynamic power flow controllers. The CNT can be realized by augmenting an existing LTC with a fractionally

rated AC-AC converter. The strategy to modify existing grid assets and the use of fractional converters make it quite attractive from the cost perspective. The Fail Normal mode of operation makes it a reliable solution to the power flow problem. The chapter also derives the analytical expressions for active and reactive power flow through a CNT, which are subsequently verified by simulation. The application of the CNT as a tie line power flow controller is also identified and its advantage, especially during contingency conditions, is presented. The principle of operation of the CNT is also verified using a scaled down laboratory prototype.

Although the CNT has many advantages compared to the traditional FACTS based power flow controllers, there are a number of issues that needs to be addressed both from the device as well as from the system perspective, to enable its successful implementation in realistic systems. Firstly although direct AC-AC converter technology is a proven technology for low and medium voltage applications, it is largely unexplored for transmission level voltage and power levels. The absence of switches of sufficient high voltage and current rating will require a multistage converter topology. For multilevel converters, it is necessary to ensure proper dynamic voltage sharing between series connected switches. To achieve bidirectional power flow control, the TACC converter of the CNT has to be built using common emitter or common collector IGBT pairs. Traditional AC-AC converters using these kinds of switches have the disadvantage of not having a freewheeling path, making them prone to high voltage and current stresses. Further, the CNT uses DVQS technique, which gives rise to 3^{rd} harmonic voltages. However, to maintain good power quality it is necessary to prevent significant 3^{rd} harmonic current flow in the transmission circuit. The small frequency gap between the

fundamental and 3rd harmonic makes it a different component for filtering. Further the CNT should also be able to withstand the worst case fault current without causing any line outage, to ensure high reliability.

On the other hand, to meet the network objectives, it is necessary for the system planners to understand the optimal location and size of CNTs required. The system operator should be provided with tools that can easily identify the optimal operating points of the various CNTs in a given network. Finally to ensure that CNT operation does not cause interference with the existing transmission line protection system, it might be necessary to modify the existing distance protection scheme.

Chapter 4

4. IMPACT OF CNTS ON LARGE POWER NETWORKS

4.1 Introduction

This chapter presents in detail the impact of CNTs on large scale power systems. The bidirectional real and reactive power flow control capability of CNT makes it potentially a very important tool for system operators. Thus the impact of CNTs on large systems is studied both under steady state as well as under transient conditions. In steady state the CNT is expected to modify the power flow through a given network. On the other hand since CNT converters are provided with fast switches, it can be an important tool for damping down unwanted system oscillations. Hence the transient response of CNTs in a large system is also studied.

4.2 Test System – Modified IEEE 14 Bus System

The power flow controllability achieved by a CNT makes it potentially an important tool for the system operators. One potential application is its use as a tie line power flow controller. To demonstrate the value added by a CNT in a large system as a tie line controller, a modified IEEE 14 bus system with a CNT controlled tie line is simulated [41]. The impact of the CNT on the system during normal system operation as well as during a contingency is studied in this section [40].

The system in Figure 4.1 consists of two areas – Area1 and Area2, connected through three tie lines – Tie1, Tie2 and Tie3. The system has four generator buses, with two generator buses in each area. It is assumed that the tie line Tie1 is equipped with a CNT

for power flow control. The entire 14 bus system along with the CNT is simulated in PSCAD software.

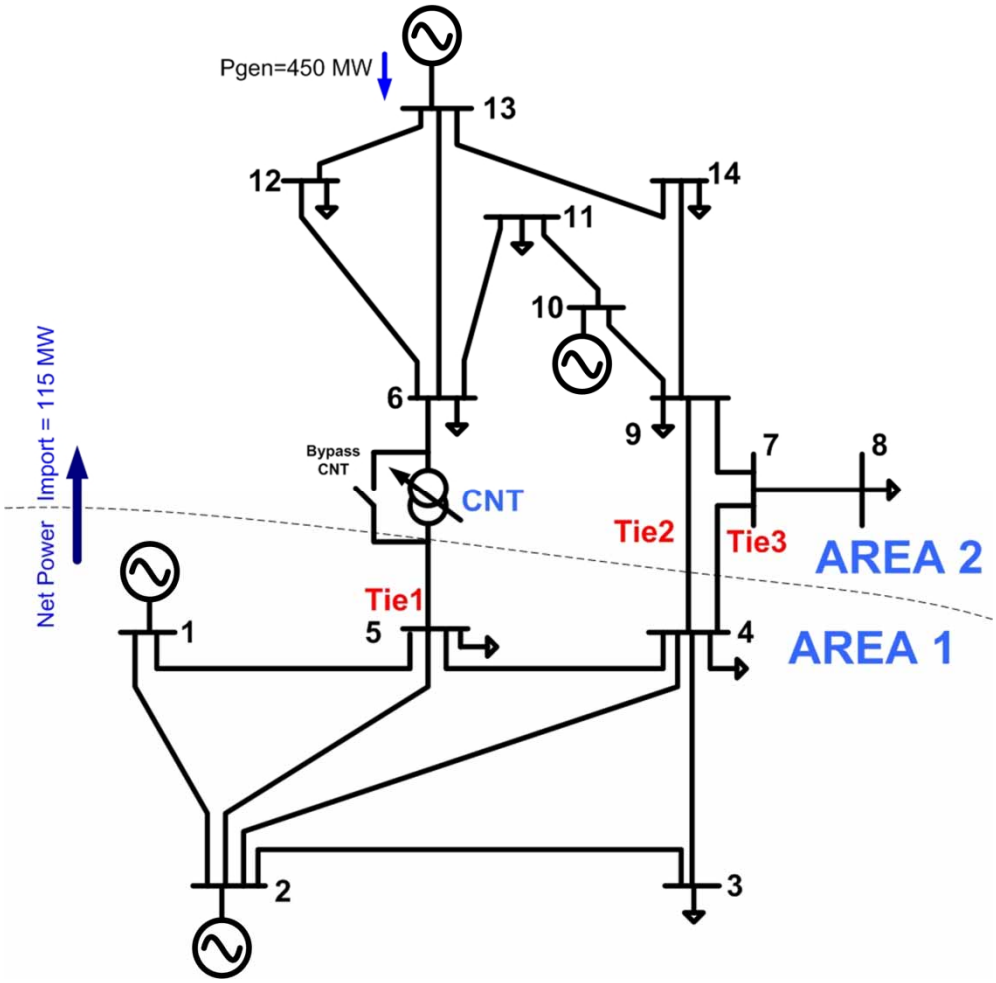

Figure 4.1: Modified IEEE 14 bus system with CNT

The total system load is set to 1620 MW under normal operation. The tie lines are assumed to be rated at 100 MW each. During normal operation it is assumed that the load in Area2 is 1050 MW out of which only 115 MW is imported from Area1 through the tie lines. At this operating point all the tie lines work well within their safe operating limits.

The power through Tie1, Tie2 and Tie3 are 70MW, 14 MW and 31 MW respectively, all of which are directed from Area1 to Area2.

Under normal steady state operations the power generated from each of the generators is fixed. Under this situation the net power transfer between the two areas will be fixed. However, by controlling the CNT the loading of tie line Tie1 can be controlled, which indirectly controls the loading of Tie2 and Tie3. Hence for a particular CNT setting if Tie1 only carries say 50 MW, the rest of the inter-area transferred power i.e. 115-50=65 MW must be carried by Tie2 and Tie3. Clearly, in the absence of the CNT there is no such control possible, which can be easily verified by bypassing the CNT in the simulation.

The power flow control achieved by the CNT in normal operation is first simulated. It is seen that by controlling the CNT, the power through Tie1 can be controlled anywhere between 12 MW to about 130 MW. Thus the CNT can provide a very high range of power flow controllability under normal network operation. This level of control can be highly advantageous for the system operators. The loading of the tie lines under normal network operation for normal, maximum and minimum loading of Tie1 is given in TABLE 4.1. Positive value of power implies power flow from Area1 to Area2.

TABLE 4.1: Loading (in MW) of tie lines under different CNT settings during normal operation for the modified IEEE 14 bus system

	Tie1 (MW)	**Tie2 (MW)**	**Tie3 (MW)**
Tie1 – No Control	70	14	31
Tie1 – Min Loading	12	50	53
Tie1 – Max Loading	129	-22	8

Utilities sometimes use the concept of flowgates, which is essentially a simplified aggregate representation of all the tie lines connecting two areas. The rating of a flowgate is limited by the first line that reaches the thermal limit. In this system for example, in absence of any control, if Tie1 reaches its thermal limit first, when Tie2 and Tie3 are carrying 20 MW and 45 MW, then the rating of the flowgate between Area1 and Area2 is limited to 100+20+45= 165 MW. CNTs can improve the rating of a flowgate, especially in critical situations like during a contingency.

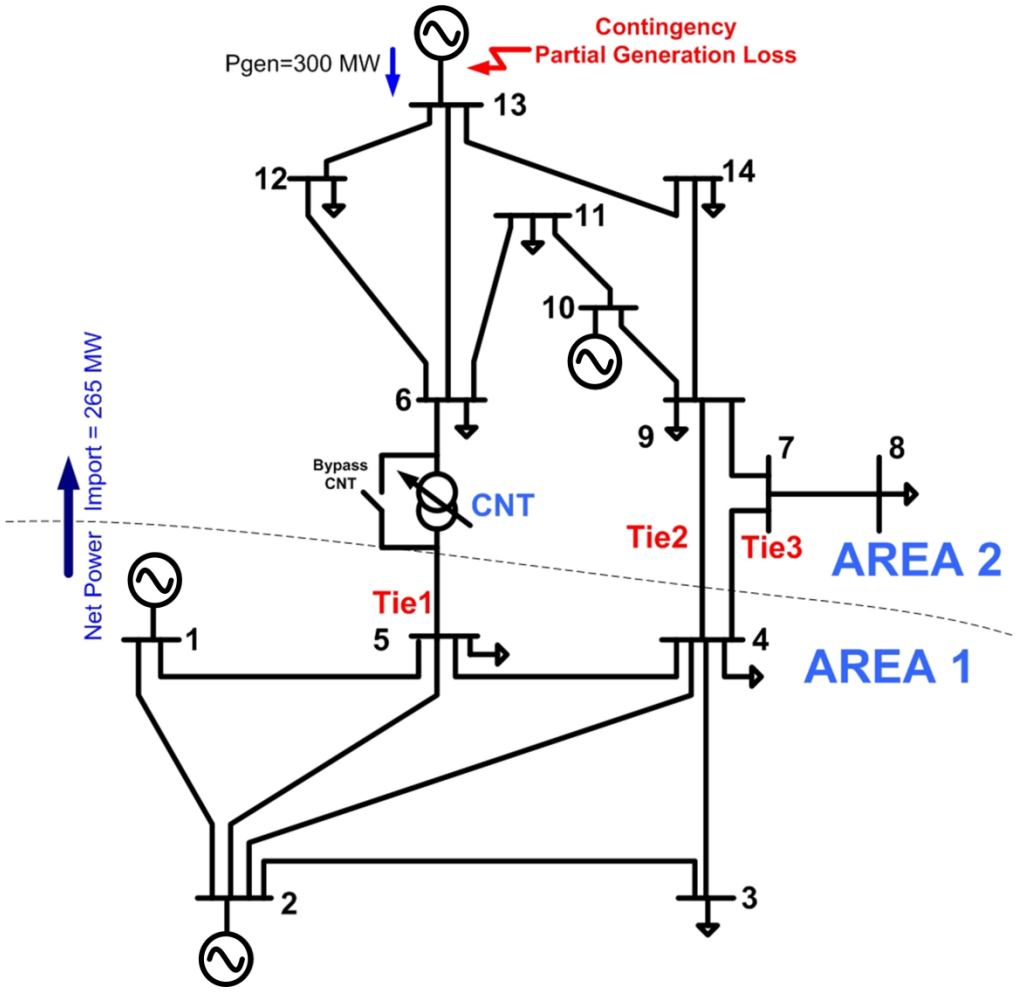

Figure 4.2: Modified IEEE 14 bus system used for post contingency simulation

It is assumed that as a result of a contingency at bus 13, 150 MW of generation is lost, which is about 15% of the load in Area2, as shown in Figure 4.2. To study the worst case scenario, it is assumed that, post-contingency the entire loss in generation is supported by Area1 resulting in a significant increase in power import by Area2. In absence of any power flow controllers it is seen that the power through Tie1 increases to 135 MW, which indicates a 35% overload. Hence in absence of CNT, the tie line can even be tripped, which may also lead to cascading failures and/or islanding followed by load shedding. With the help of a CNT, the contingency situation can be handled. It is seen that if the CNT settings are kept at K0=0.6, K2=0.35, Φ=180º, the power through Tie1 can be controlled below its thermal rating of 100 MW. Additionally it is seen that under this situation the power through all the tie lines can be controlled below their maximum ratings. The loading of the tie lines under the different situations are summarized in TABLE 4.2.

TABLE 4.2: Loading (in MW) of tie lines under different conditions for the modified IEEE 14 bus system

	Tie1 (MW)	**Tie2 (MW)**	**Tie3 (MW)**
Normal Operation	70	14	31
Post Contingency (CNT bypassed)	135	63	67
Post Contingency (CNT controlled)	96	86	83

4.3 Need for Modified Planning and Operation Tools

The previous subsection showed the impact of CNTs in controlling tie line power flow, both under steady state, as well as under contingency scenarios. It is clear from the above example that to extract maximum benefit from the installed CNTs the operating points of the CNTs must be appropriately chosen. Network operators use a host of programs like unit commitment, economic dispatch, loadflow, etc. to find the optimal settings of various network assets like generators, LTCs, etc. CNT being a power flow control asset provides flexibility in terms of real and reactive power flow control. However traditional power system operations programs are incapable of finding optimal settings for networks with CNTs. Similarly traditional power system planning programs cannot be used for determining the optimal location and sizing of the CNTs in a network. It is necessary to develop planning and operation tools, which can handle networks with CNTs. This would enable to correctly assess the impact of CNTs on large area networks.

4.4 Load Flow Algorithm

Two of the main constraints of any power network are the bus voltage and line currents. To ensure reliable operation, it is necessary to maintain all the bus voltages and line currents within their respective limits. Traditionally, the state of a system can be determined from the generator dispatch settings and the load data, using the load flow algorithm [42]. The load flow algorithm also calculates the various bus voltages and line currents for the system operator, and hence is one of the major tools for the system operator. Traditional load flow programs are designed to solve networks with uncontrolled transmission lines. Introduction of power flow controllers like a CNT in one or multiple lines is expected to impact the power flow of the network significantly.

However, power flow equations for CNT controlled lines are different from those for uncontrolled lines. Since the CNT represents a component that does not exist in the actual utility systems today, traditional load flow programs cannot solve load flows for networks with CNTs. For quicker adoption of the CNT technology, it is desirable from the system operator's perspective to have tools such as a modified load flow program, which can solve the load flow problem for a network with CNTs.

Traditionally a load flow algorithm is used for solving the steady state condition of the network [43]. At a given operating point it is assumed that the load demand at all the buses and the generator dispatch for all the generators is known. The load buses of the network are known as PQ buses, since the real and reactive power demand at these buses are known. One generator bus is arbitrarily chosen as the slack bus, whose voltage magnitude is assumed to be 1 pu and the voltage phase angle to be at 0°. All other generator buses are classified as PV buses, since the real power output and the terminal voltage magnitude of these buses are fixed [44]. To solve the system state the voltage magnitude and phase angle of all the buses must be calculated. Hence, for an N bus network with M number of PQ and L number of PV buses, (N-1) number of phase angles and (N-L-1) number of voltage magnitudes are unknown. Since a given bus should be either a slack bus or a PQ or a PV bus, the relationship between M, N and L is given by (3.1).

$$N = M + L + 1 \tag{4.1}$$

The total number of unknowns in the system is (2N-L-2). For solving the load flow problem it is assumed that the real and reactive power flowing into each of the PQ buses

is exactly equal to the load demand. Also the real power flowing out of the PV buses are exactly equal to the power generated by the generator at the given bus.

$$\Delta P_i = -P_i + \sum_{k=1}^{N} |V_i||V_k|(G_{ik}\cos\theta_{ik} + B_{ik}\sin\theta_{ik}) \tag{4.2}$$

$$\Delta Q_i = -Q_i + \sum_{k=1}^{N} |V_i||V_k|(G_{ik}\cos\theta_{ik} - B_{ik}\sin\theta_{ik}) \tag{4.3}$$

The value of ΔP_i should be zero for all the (N-1) buses, while the value of ΔQ_i should be equal to zero for all the M number of PQ buses. Hence the total number of equations is also (2N-L-2), thus the load flow problem has a unique solution. Since these equations are nonlinear, they have to be solved by an iterative method.

If the network state is given by the vector x, and the vector of real and reactive power mismatch is given by f(x), then using the Newton-Raphson method, the system state can be solved using (4.4). It is seen that (4.4) is an iterative equation. The Jacobian matrix J is given by (4.5).

$$X^{(i+1)} = X^{(i)} + J^{-1}f\left(X^{(i)}\right) \tag{4.4}$$

$$J = \begin{bmatrix} \dfrac{\partial P(x)}{\partial \delta} & \dfrac{\partial P(x)}{\partial |V|} \\ \dfrac{\partial Q(x)}{\partial \delta} & \dfrac{\partial Q(x)}{\partial |V|} \end{bmatrix} = \begin{bmatrix} J_1 & J_2 \\ J_3 & J_4 \end{bmatrix} \tag{4.5}$$

4.5 Modified Load Flow Algorithm

Since the equations for real and reactive power flow changes for a CNT controlled line, the Jacobian matrix also needs to be modified [39]. Also it is seen from (3.19)-(3.21) that to evaluate the real and reactive power flowing through a CNT controlled line, apart from the terminal bus conditions, the set point of the CNT converter is also required to be known. Further, it is seen from the CNT power flow equations that although the real power is same at both the sending as well as the receiving end, the reactive power at the two ends are not equal.

It is assumed that for a particular operating point, the settings of all the CNTs in the network are known in addition to the generator dispatch and the load demand. Further, since the CNT power equations were derived for lossless lines, it is assumed that the CNT controlled lines are lossless. For a network with CNT controlled lines, equation (4.2) has to be modified to (4.6). The first summation term is carried out for all the lines connected to the i^{th} bus, which are not controlled by a CNT. The second summation term is for the CNT controlled lines with the i^{th} bus at the sending end, while the third summation term is for the CNT controlled lines with the i^{th} bus at the receiving end. The converter settings of the CNT controlling line between buses i and k are given by the parameters Φ_{ik}, α_{ik} and β_{ik}.

The reactive power flow equation (4.3) can be similarly modified to (4.9) for a network with CNT controlled lines. Using the modified real and reactive bus power flow equations (4.6), (4.9) the Jacobian of the Newton-Raphson method can be modified to accommodate CNTs in the network.

$$\Delta P_i = -P_i + \sum_{\substack{k=1 \\ \{i,k\}\notin CNT}}^{N} |V_i||V_k|(G_{ik}\cos\theta_{ik} + B_{ik}\sin\theta_{ik})$$

$$+ \sum_{\substack{\{i,k\}\in CNT \\ i\in CNT\_SEND}} |V_i||V_k|B_{ik}(\alpha_{ik}\sin\theta_{ik} - \beta_{ik}\cos(\theta_{ik} + \Phi_{ik})) \tag{4.6}$$

$$+ \sum_{\substack{\{i,k\}\in CNT \\ i\in CNT\_RECEIVE}} |V_i||V_k|B_{ik}(\alpha_{ik}\sin\theta_{ik} + \beta_{ik}\cos(\theta_{ik} + \Phi_{ik}))$$

$$\alpha_{ik} = \frac{1 + n_{ik} - 2n_{ik}K0_{ik}}{1 - {n_{ik}}^2} \tag{4.7}$$

$$\beta_{ik} = \frac{n_{ik}K2_{ik}}{1 - {n_{ik}}^2} \tag{4.8}$$

$$\Delta Q_i = -Q_i + \sum_{\substack{k=1 \\ \{i,k\}\notin CNT}}^{N} [|V_i||V_k|(G_{ik}\cos\theta_{ik} - B_{ik}\sin\theta_{ik}) + V_i^2 B_{ik}]$$

$$+ \sum_{\substack{\{i,k\}\in CNT \\ i\in CNT\_SEND}} \left[V_i\left(\alpha_{ik}^2 - \frac{2}{3}\beta_{ik}^2\right) - \alpha_{ik}V_k\cos\theta_{ik}\right.$$

$$\left. + \beta_{ik}V_k\sin(\theta_{ik} + \Phi_{ik})\right]V_i B_{ik} \tag{4.9}$$

$$+ \sum_{\substack{\{i,k\}\in CNT \\ i\in CNT\_RECEIVE}} [V_i - \alpha_{ik}V_k\cos\theta_{ik}$$

$$- \beta_{ik}V_k\sin(\theta_{ik} + \Phi_{ik})]V_i B_{ik}$$

4.5.1 Modifying J_1

The matrix J_1 is the derivative of real power mismatch with respect to the bus voltage angle. To find the J_1 for a given network with CNTs, the derivative of (4.6) has to be taken with respect to the bus voltage angles. For cases where the derivative of real power mismatch of a particular bus has to be calculated with respect to the same bus voltage angle, the resulting formula is given by (4.10). For all other elements of the J_1 matrix, one of the equations (4.11)-(4.13) has to be used. If the line between *bus i* and *bus j* does not have a CNT, equation (4.11) should be used. If the line has a CNT and *bus i* is at the sending end then (4.12) should be used else (4.13) should be used.

$$\frac{\partial \Delta P_i}{\partial \Delta \theta_i} = \sum_{\substack{k=1 \\ \{i,k\} \notin CNT}}^{N} [|V_i||V_k|(-G_{ik}\sin\theta_{ik} + B_{ik}\cos\theta_{ik})] - V_i^2 B_{ii} + \sum_{\substack{\{i,k\} \in CNT \\ i \in CNT\_SEND}} [|V_i||V_k| B_{ik}(\alpha_{ik}\cos\theta_{ik} + \beta_{ik}\sin\theta_{ik})] + \sum_{\substack{\{i,k\} \in CNT \\ i \in CNT\_RECEIVE}} [|V_i||V_k| B_{ik}(\alpha_{ik}\cos\theta_{ik} - \beta_{ik}\sin\theta_{ik})] \tag{4.10}$$

$$\frac{\partial \Delta P_i}{\partial \Delta \theta_k} = |V_i||V_k|(G_{ik}\sin\theta_{ik} - B_{ik}\cos\theta_{ik}) \; for \; \{i,k\} \notin CNT \tag{4.11}$$

$$\frac{\partial \Delta P_i}{\partial \Delta \theta_k} = |V_i||V_k| B_{ik}(-\alpha_{ik}\cos\theta_{ik} - \beta_{ik}\sin\theta_{ik}) \; for \; \{i,k\} \in CNT, i \in CNT\_SEND \tag{4.12}$$

$$\frac{\partial \Delta P_i}{\partial \Delta \theta_k} = |V_i||V_k|B_{ik}(-\alpha_{ik}\cos\theta_{ik} + \beta_{ik}\sin\theta_{ik})\ for\ \{i,k\} \in CNT,$$
$$i \in CNT\_RECEIVE \tag{4.13}$$

4.5.2 Modifying J_2

The matrix J_2 can be similarly modified to accommodate for CNTs in a network. . For elements where the derivative of real power mismatch of a particular bus has to be calculated with respect to the same bus voltage angle, the resulting formula is given by (4.14). If the line between *bus i* and *bus j* does not have a CNT, equation (4.15) should be used. If the line has a CNT and *bus i* is at the sending end then (4.16) should be used else (4.17) should be used.

$$\begin{aligned}\frac{\partial \Delta P_i}{\partial \Delta |V_i|} = & \sum_{\substack{k=1 \\ \{i,k\} \notin CNT}}^{N} [|V_i|(-G_{ik}\sin\theta_{ik} + B_{ik}\cos\theta_{ik})] + |V_i|G_{ii} \\ & + \sum_{\substack{\{i,k\} \in CNT \\ i \in CNT\_SEND}} [|V_i|B_{ik}(\alpha_{ik}\sin\theta_{ik} - \beta_{ik}\cos\theta_{ik})] \\ & + \sum_{\substack{\{i,k\} \in CNT \\ i \in CNT\_RECEIVE}} [|V_i|B_{ik}(\alpha_{ik}\sin\theta_{ik} + \beta_{ik}\cos\theta_{ik})]\end{aligned} \tag{4.14}$$

$$\frac{\partial \Delta P_i}{\partial \Delta |V_k|} = |V_i|(G_{ik}\cos\theta_{ik} + B_{ik}\sin\theta_{ik})\ for\ \{i,k\} \notin CNT \tag{4.15}$$

$$\frac{\partial \Delta P_i}{\partial \Delta |V_k|} = |V_i|B_{ik}(\alpha_{ik}\sin\theta_{ik} - \beta_{ik}\cos\theta_{ik})\ for\ \{i,k\} \in CNT, i \in CNT\_SEND \tag{4.16}$$

$$\frac{\partial \Delta P_i}{\partial \Delta |V_k|} = |V_i| B_{ik} (\alpha_{ik} \sin\theta_{ik} + \beta_{ik} \cos\theta_{ik}) \; for \; \{i,k\} \in CNT, i \in CNT\_RECEIVE \tag{4.17}$$

4.5.3 Modifying J_3

The matrix J_3 is the derivative of reactive power mismatch with respect to the bus voltage angle. For elements where the derivative of reactive power mismatch of a particular bus has to be calculated with respect to the same bus voltage angle, the resulting formula is given by (4.18). If the line between *bus i* and *bus j* does not have a CNT, equation (4.19) should be used. If the line has a CNT and *bus i* is at the sending end then (4.20) should be used else (4.21) should be used.

$$\begin{aligned} \frac{\partial \Delta Q_i}{\partial \Delta \theta_i} = & \sum_{\substack{k=1 \\ \{i,k\} \notin CNT}}^{N} [|V_i||V_k|(G_{ik} \cos\theta_{ik} + B_{ik} \sin\theta_{ik})] \\ & + \sum_{\substack{\{i,k\} \in CNT \\ i \in CNT\_SEND}} [|V_i||V_k| B_{ik} (\alpha_{ik} \sin\theta_{ik} + \beta_{ik} \cos\theta_{ik})] \\ & + \sum_{\substack{\{i,k\} \in CNT \\ i \in CNT\_RECEIVE}} [|V_i||V_k| B_{ik} (\alpha_{ik} \sin\theta_{ik} - \beta_{ik} \cos\theta_{ik})] \end{aligned} \tag{4.18}$$

$$\frac{\partial \Delta Q_i}{\partial \Delta \theta_k} = |V_i||V_k|(-G_{ik} \cos\theta_{ik} - B_{ik} \sin\theta_{ik}) \; for \; \{i,k\} \notin CNT \tag{4.19}$$

$$\frac{\partial \Delta Q_i}{\partial \Delta \theta_k} = |V_i||V_k| B_{ik} (-\alpha_{ik} \sin\theta_{ik} - \beta_{ik} \cos\theta_{ik}) \; for \; \{i,k\} \in CNT, i \in CNT\_SEND \tag{4.20}$$

$$\frac{\partial \Delta Q_i}{\partial \Delta \theta_k} = |V_i||V_k|B_{ik}(-\alpha_{ik}\sin\theta_{ik} + \beta_{ik}\cos\theta_{ik})\ for\ \{i,k\} \in CNT, \quad i \in CNT\_RECEIVE \tag{4.21}$$

4.5.4 Modifying J_4

The matrix J_3 is the derivative of reactive power mismatch with respect to the bus voltage magnitude. For elements where the derivative of reactive power mismatch of a particular bus has to be calculated with respect to the same bus voltage magnitude, the resulting formula is given by (4.22). If the line between *bus i* and *bus j* does not have a CNT, equation (4.23) should be used. If the line has a CNT and *bus i* is at the sending end then (4.24) should be used else (4.25) should be used.

$$\begin{aligned}\frac{\partial \Delta Q_i}{\partial \Delta |V_i|} = & \sum_{\substack{k=1 \\ \{i,k\} \notin CNT}}^{N} [|V_k|(G_{ik}\sin\theta_{ik} - B_{ik}\cos\theta_{ik}) + 2|V_i|B_{ik}] \\ & + \sum_{\substack{\{i,k\} \in CNT \\ i \in CNT\_SEND}} \left[2|V_i|B_{ik}\left(\alpha_{ik}^2 - \frac{2}{3}\beta_{ik}^2\right)\right. \\ & \left. + |V_k|B_{ik}(-\alpha_{ik}\cos\theta_{ik} + \beta_{ik}\sin\theta_{ik})\right] \\ & + \sum_{\substack{\{i,k\} \in CNT \\ i \in CNT\_RECEIVE}} [2|V_i|B_{ik} \\ & + |V_k|B_{ik}(-\alpha_{ik}\cos\theta_{ik} - \beta_{ik}\sin\theta_{ik})]\end{aligned} \tag{4.22}$$

$$\frac{\partial \Delta Q_i}{\partial \Delta |V_k|} = |V_i|(G_{ik}\sin\theta_{ik} - B_{ik}\cos\theta_{ik})\ for\ \{i,k\} \notin CNT \tag{4.23}$$

$$\frac{\partial \Delta Q_i}{\partial \Delta |V_k|} = |V_i| B_{ik}(-\alpha_{ik} \cos\theta_{ik} + \beta_{ik} \sin\theta_{ik}) \; for \; \{i,k\} \in CNT, i \in CNT\_SEND \tag{4.24}$$

$$\frac{\partial \Delta Q_i}{\partial \Delta |V_k|} = |V_i| B_{ik}(-\alpha_{ik} \cos\theta_{ik} - \beta_{ik} \sin\theta_{ik}) \; for \; \{i,k\} \in CNT, i \in CNT\_RECEIVE \tag{4.25}$$

4.5.5 Overall Algorithm

The overall modified load flow algorithm is presented in the form of a flow chart in Figure 4.3. It is seen that the algorithm is essentially still a Newton-Raphson load flow. However at the start of the algorithm, in addition to the regular inputs it also requires the settings of the various CNTs in the network. The settings of a CNT converter are essentially the parameters K_0, K_2 and Φ that are required to set the duty cycle of the converter as shown in (3.7). The output of the load flow algorithm can be used to check if any of the network constraints such as the line loadings or the bus voltages are violated.

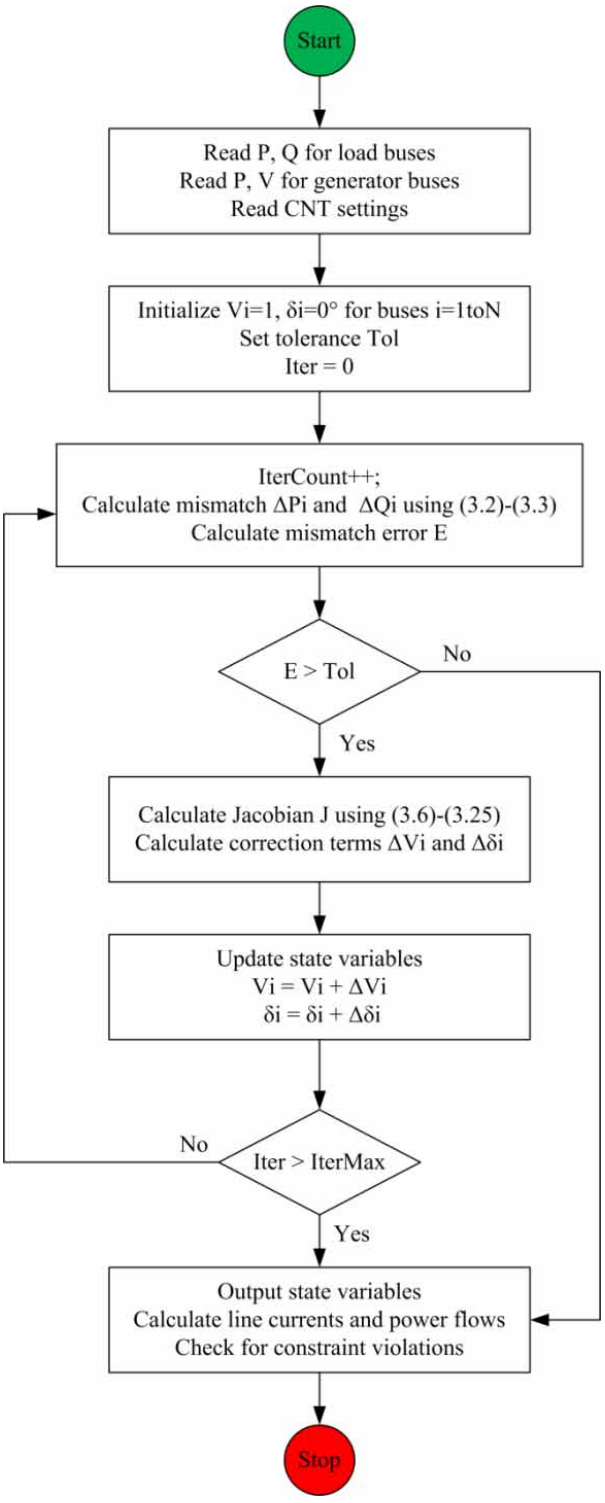

Figure 4.3: Flow chart for modified load flow algorithm

4.5.6 Test System

The modified load flow algorithm is tested on the modified IEEE 30 bus system shown in Figure 4.4. The OPF for the test system is first executed for the situation where the system does not have any CNTs. The resulting generator dispatch is shown in Table 4.3, while the line overloads are listed in Table 4.4. It is seen that lines 2 and 18 are operating at full load, which limits the dispatch from the low cost generators at Bus 1 and Bus 13. The cost of generation for this operating point is seen to be $6525.15 / hour.

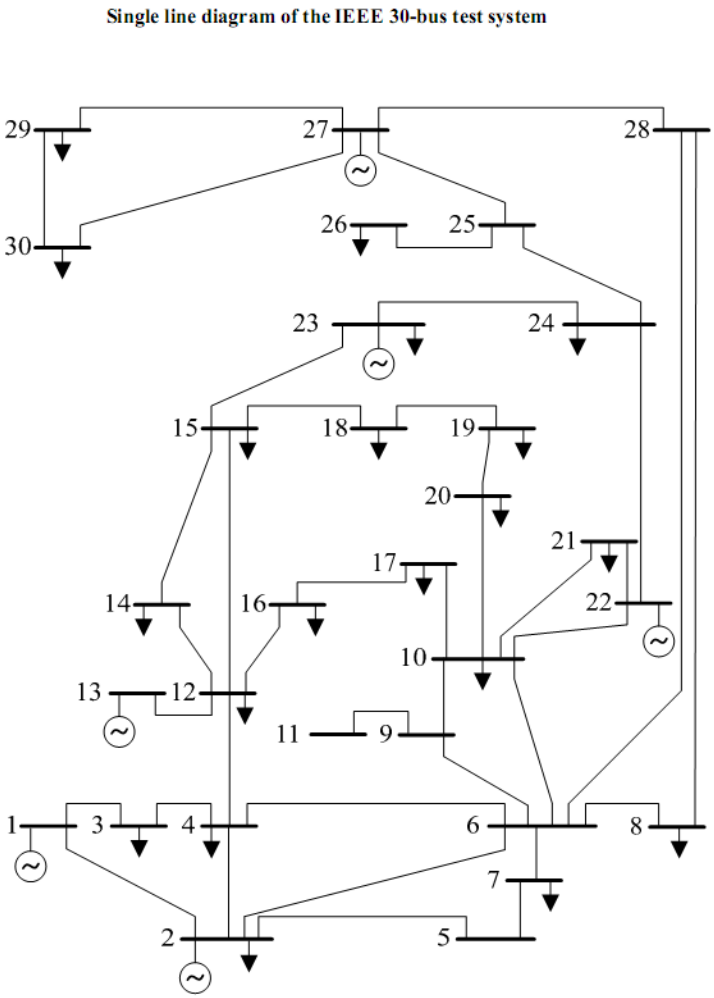

Figure 4.4: Test system - modified IEEE 30 bus system

Table 4.3: OPF generator dispatch for the test system without CNT

Bus No.	P Setting	|V| Setting	$ / MW	$
1	41.33	1.012	60	2479.80
2	0	1.024	84	0
13	25.35	1.027	61	1546.35
22	0	0.985	81	0
23	33.32	1.026	75	2499.00
27	0	0.95	82	0
Total cost of generation				6525.15

Table 4.4: Lines at or near their maximum loading for test system without CNT

Line No.	From Bus	To Bus	MVA	MVA Max
2	1	3	**16**	16
18	12	15	**16**	16

The generator dispatch is kept the same, while the network is now provided with two CNTs – one each on line 2 and line 18. Each CNT is assumed to have ±10% taps; hence the CNT converters are rated at 20% of the line rating. It is seen from

Table 4.5 that if the CNTs are set for $K_0 = 0.55$ and $K_2 = 0.45$, the loading of the lines 12 and 18 is reduced drastically. However, since the generator dispatch is kept unchanged the cost of generation is still $6525.15/hour.

Table 4.5: Loading of selected lines for system with CNTs

Line No.	From Bus	To Bus	MVA	MVA Max
2	1	3	3.9	16
18	12	15	4.3	16

It is clear that installation of the CNTs in the above lines creates extra system throughput for the transmission corridor. The extra throughput of the corridor can be utilized by increasing the dispatch of the low cost generators in Bus 1 and 13. An example of a lower cost generator dispatch is shown in Table 4.6. It is seen that the cost of generation for this operating point is reduced to $6052.70/hour, resulting in a 7.2% decrease compared to the previous case.

It is seen from the above case study that installation of the CNTs in the lines 2 and 18 can reduce the cost of generation for the system. For obtaining the optimal cost, the generators and the CNT settings need to be dispatched in conjunction with each other. This essentially requires development of a modified OPF program for systems with CNTs. Also in this example the location and the CNT converter size are manually chosen and may not be optimal. Further this example only looks at the system benefit for a

particular operating point. The optimal location and sizing decision of the CNT converters must be found by taking into considerations many such operating points. The modified OPF program, along with the program for optimal location and sizing of CNT converter are presented in the latter chapters.

Table 4.6: Lower cost generator dispatch for test system with CNTs

Bus No.	P Setting	|V| Setting	$ / MW	$
1	70.26	1.012	60	4215.60
2	0	1.024	84	0
13	28.10	1.027	61	1714.10
22	0	0.985	81	0
23	1.64	1.026	75	123.00
27	0	0.95	82	0
Total cost of generation				6052.70

4.6 Improving Network Dynamic Stability with CNTs

Reliability is a key metric in the utility industry, and utility systems are typically often operated under N-1 or even N-2 contingency conditions. Hence the network is expected to operate even if the worst contingency occurs. This results in considerable under utilization of existing resources. To study the system limits imposed by

contingencies and system dynamics, a simple single generator connected to an infinite bus system is used, as shown in Figure 4.5 [39]. The system is modeled in the SimPowerSystems toolbox of Matlab [45].

It is assumed that the impedance of the line Tie1 is twice that of Tie2, while the power transferred from the generator to the infinite bus is assumed to be 75 MW. Under this loading condition, a single line to ground fault is simulated at the generator bus, which is cleared after 0.1 seconds. In absence of a CNT the post-fault system is seen to go unstable. In fact it is seen from simulation that for stable post-fault operation, in the absence of the CNT, the inter-area ATC has to be limited to only 70 MW [46].

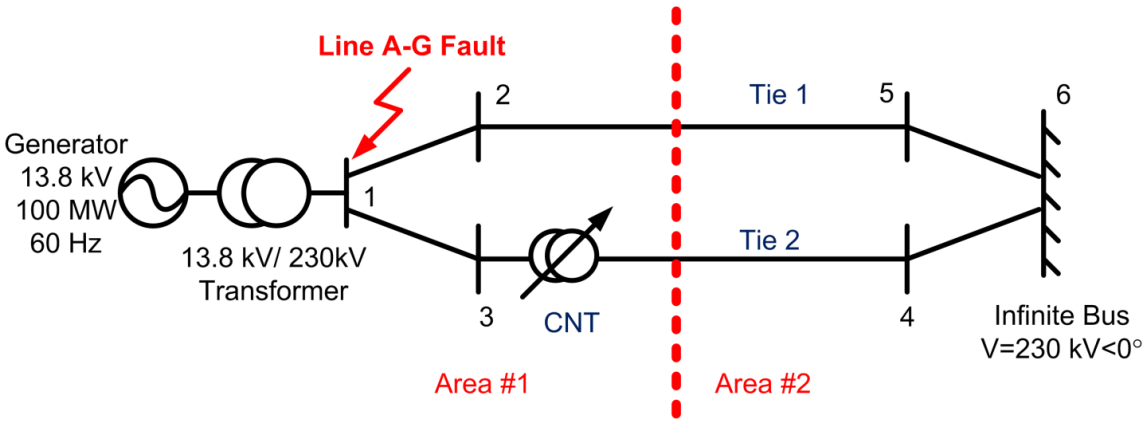

Figure 4.5: Single generator connected to infinite bus system

The CNT converter has fast switches that makes it a potential power oscillation damping device. From Figure 3.7 it is seen that the parameter K_2 has a significant impact on the real power flow through the CNT. Also the condition for preventing over modulation is given by (4). Hence, during damping mode the value of K_0 is fixed at 0.5 to provide maximum degree of freedom for K_2 variation. A bang-bang controller with line

frequency as input is used to provide the dynamic value of K_2. The overall transient control schematic for the CNT is shown in Figure 4.6, and Figure 4.7 shows that even with an inter-area ATC of 90 MW, the post-fault network oscillation can be successfully damped with the CNT converter. Hence with the help of the CNT, the inter-area ATC is increased by as much as 20 MW, which is 29% more than its initial ATC.

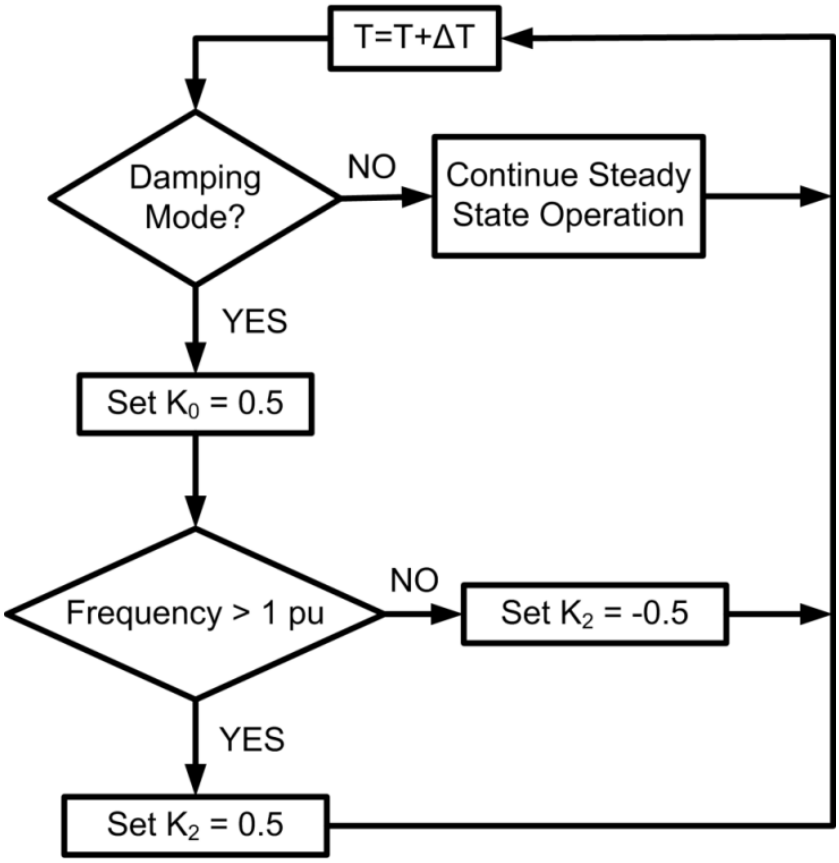

Figure 4.6: CNT damping control strategy

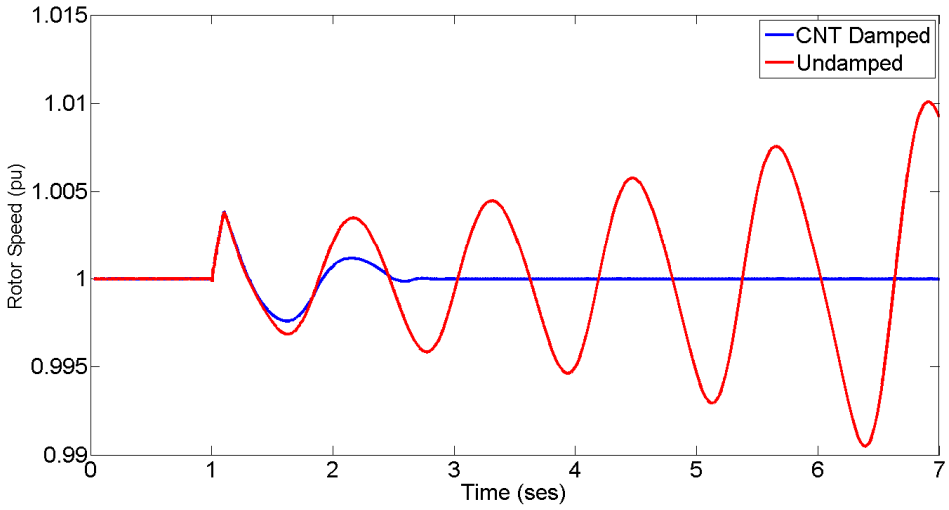

Figure 4.7: Fault response of undamped and CNT damped system

4.7 Conclusions

This chapter addresses the issue of impact of multiple CNTs on a large power network – both under steady state as well as under transient. In steady state, the CNT can be used for various purposes like – enhanced tie line utilization, congestion mitigation, etc. For extracting optimal economic benefits from the CNT technology, especially in large power networks, various problems need to be addressed both at the planning as well as at the power system operation levels. From the planning perspective issues such as the optimal location and sizing of CNTs in a network needs to be solved. On the other hand from the operations perspective issues such as the optimal settings of various CNTs in a network needs to be looked at. Traditional power system planning and operation programs are not equipped to handle the controllability provided by power flow controllers like CNT. This chapter presents in detail the various modifications that are required in the traditional Newton-Raphson loadflow method to make it capable of handling CNTs in a network. The performance of the modified Newton-Raphson method

is then tested on the IEEE 30 bus system. The ability of CNTs to damp power system oscillations in a power network under transient conditions has also been presented in this chapter.

Chapter 5

5. OPTIMAL PLACEMENT AND CONTROL OF CNTs IN A LARGE NETWORK

5.1 Introduction

In Chapter 4 it is shown that the CNT can significantly impact the power flow of a large network. From the network planning perspective it is important to understand these system level impacts and accordingly place the CNTs. On the other hand, from the network operators perspective it is important to optimally set the control points of the CNTs in the network at each time step. In this chapter methodologies for finding the optimal location and optimal control set-points for CNTs in a network will be described. The impact of these optimally placed and controlled CNTs on a test system is also evaluated.

5.2 Optimal Power Flow for Networks with CNTs

The concept of Optimal Power Flow (OPF) for traditional networks is well understood and has been discussed in Chapter 2. The OPF problem is used to find the most economical combination of generation that can be used to meet the load demand of a network without violating any of the constraints. Thus for traditional networks the outputs of the OPF program will be the PV settings of the network generators. On the other hand, for networks with CNTs the set-points of the CNTs are also required to be determined at each time step. Hence for networks with CNTs, the output of the OPF program should not only include the PV set-points of the generators but also the K_0, K_2

set-points for the CNTs in the network. The mathematical formulation of the modified OPF problem is given by (5.1) – (5.3).

$$Min\ (CostOfGeneration) \tag{5.1a}$$

such that

$$P_j^{min} \leq P_j \leq P_j^{max} \qquad j \in [1, N_{gen}] \tag{5.1b}$$

$$Q_j^{min} \leq Q_j \leq Q_j^{max} \qquad j \in [1, N_{gen}] \tag{5.1c}$$

$$V_i^{min} \leq V_i \leq V_i^{max} \qquad i \in [1, N_{bus}] \tag{5.1d}$$

$$\left|S_k^{EndBus1}\right| \leq |S_k^{max}| \qquad k \in [1, N_{line}] \tag{5.1e}$$

$$\left|S_k^{EndBus2}\right| \leq |S_k^{max}| \qquad k \in [1, N_{line}] \tag{5.1f}$$

$$CostofGeneration = f(P_j, V_j, K_0^m, K_2^m) \qquad j \in [1, N_{gen}],\ m \in [1, N_{CNT}] \tag{5.2}$$

$$0 \leq K_0^m \leq 1 \qquad m \in [1, N_{CNT}] \tag{5.3a}$$

$$-K_0^m \leq K_2^m \leq K_0^m \qquad m \in [1, N_{CNT}] \tag{5.3b}$$

The output real and reactive powers of the j^{th} generators are represented by P_j and Q_j respectively. For the j^{th} generator, the limits of the real power are given by P_j^{max} and P_j^{min} while that of the reactive power are given by Q_j^{max} and Q_j^{min}. The bus voltage of the i^{th} bus is given by V_i. For proper voltage regulation this voltage is required to be within V_i^{min}

and V_i^{max}. The apparent powers at the two ends of the k^{th} line are given by $S_k^{EndBus1}$ and $S_k^{EndBus2}$. To ensure operation within the thermal ratings of the k^{th} line it is necessary to ensure that the apparent power flowing through either ends of the line be below the maximum permissible apparent power S_k^{max} of that line. The converter settings of the m^{th} CNT is given by K_0^m and K_2^m. The parameter K_0^m is required to be between zero and unity while K_0^m is required an absolute value less than that of K_0^m in order to prevent over modulation.

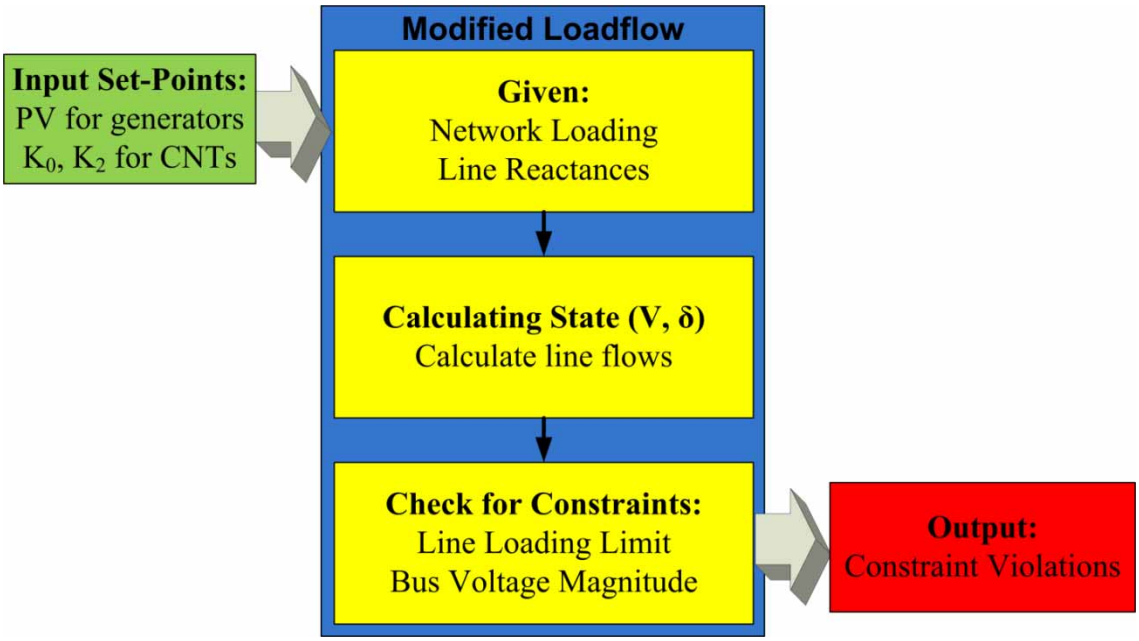

Figure 5.1: Modified loadflow structure

In Chapter 4 the modified loadflow for networks with CNTs have been described. The modified loadflow can calculate the network state for a given generator and CNT dispatch. The structure of the modified loadflow is shown in Figure 5.1. It is seen from Figure 5.1, that the modified loadflow program takes the PV settings of generators and

K_0, K_2 settings for CNTs. The outputs of the program are the network states and the constraint violations.

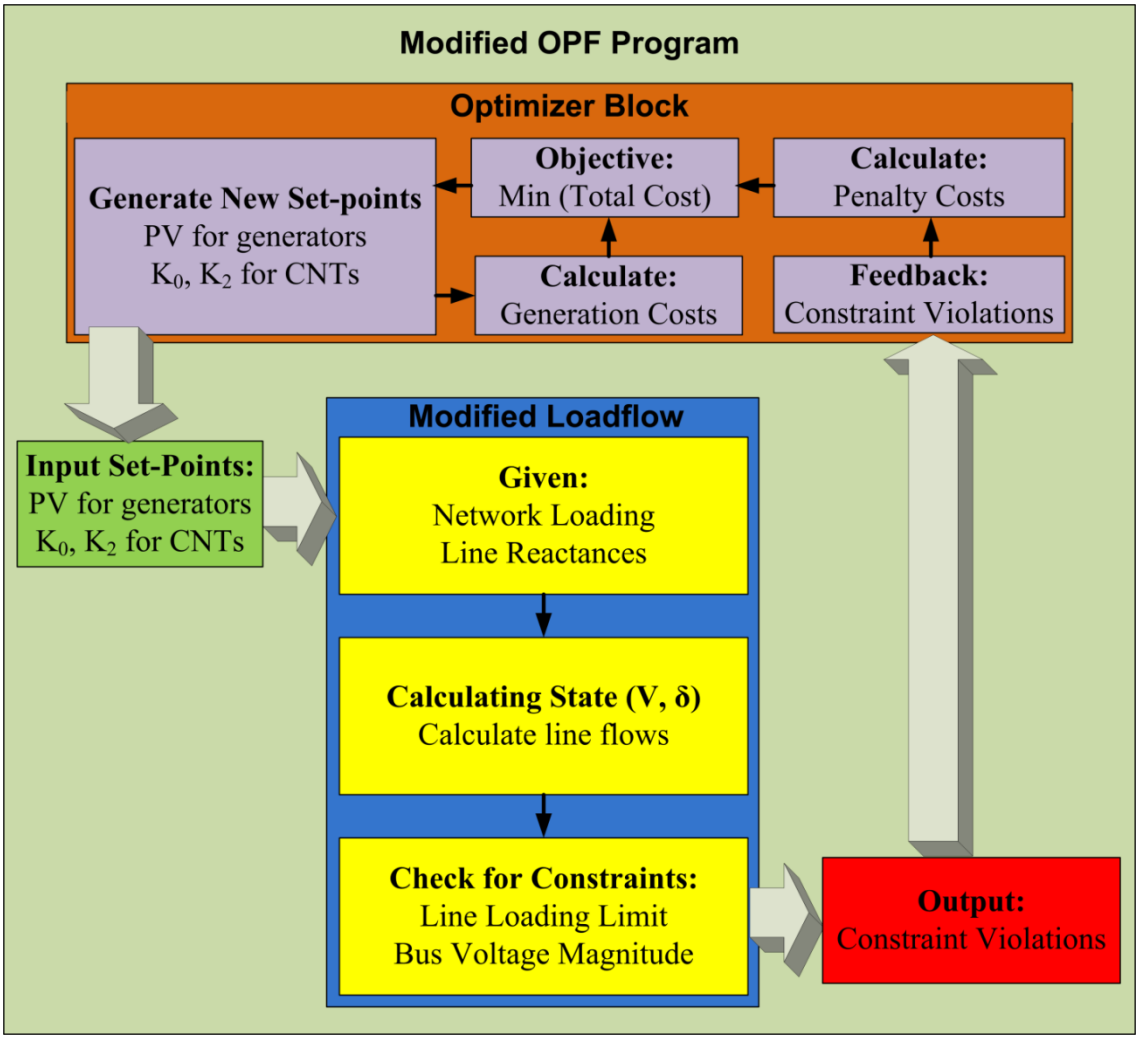

Figure 5.2: Modified OPF structure

The modified OPF program can be built by wrapping an optimizer block around the modified loadflow program, as shown in Figure 5.2. The optimizer block finds the best possible combination of PV settings of generators and K_0, K_2 settings of CNTs to achieve a particular network objective, without causing a constraint violation. In this problem, minimization of the total cost of generation is used as the objective function for the OPF

program. Various network constraints like limits on bus voltage magnitude, maximum line loading capabilities, real and reactive power generation limits, etc. are considered in this problem. In order to avoid a constraint violation the concept of penalty functions are used [47]. For a particular choice of PV settings and K_0, K_2 settings the total cost is calculated as the sum of the cost of generation and the penalty incurred for the particular choice of settings.

5.2.1 Penalty Functions

The penalty function method reduces a constrained optimization problem by an unconstrained problem whose solutions ideally converge to the solution of the original constrained problem [48]. The unconstrained problem is formed by adding a term to the objective function that consists of a penalty parameter and a measure of violation of the constraints. The measure of violation is nonzero when the constraints are violated and is zero in the region where constraints are not violated.

Consider the penalty function for the bus voltage and line current limits. Ideally these penalty functions should look like Figure 5.3 for a cost minimization problem. For line current constraint the penalty function should be zero if the line current is less than the maximum line current rating. For line currents above the limit, the penalty function should tend to infinity. Similarly for the bus voltage constraint, the penalty should be zero if the bus voltage is within the maximum and minimum limits, and should tend to infinity if it outside those limits.

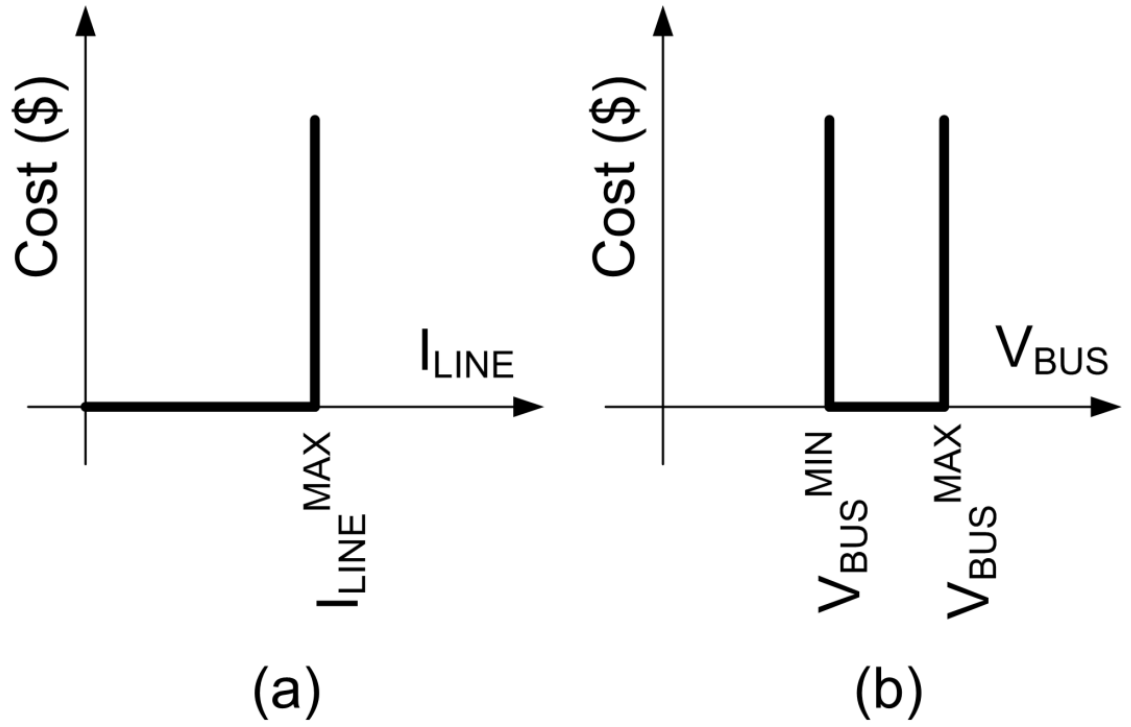

Figure 5.3: Hard penalty function for (a) line current constraint and (b) bus voltage constraint

However, placing such hard penalties often make solving the optimization problem difficult. One way to avoid this issue is to implement what is known as "soft" penalty functions. The soft penalty function allows the penalty factor to increase monotonically as the solution goes further and further away from the allowable limits. The rate of change of the penalty factor can be constant or variable. For this problem the penalty functions are chosen to be quadratic as shown in Figure 5.4. The quadratic penalty function ensures that the penalty factor quickly becomes dominant if a solution drifts away from the allowable range and at the same time it is differentiable.

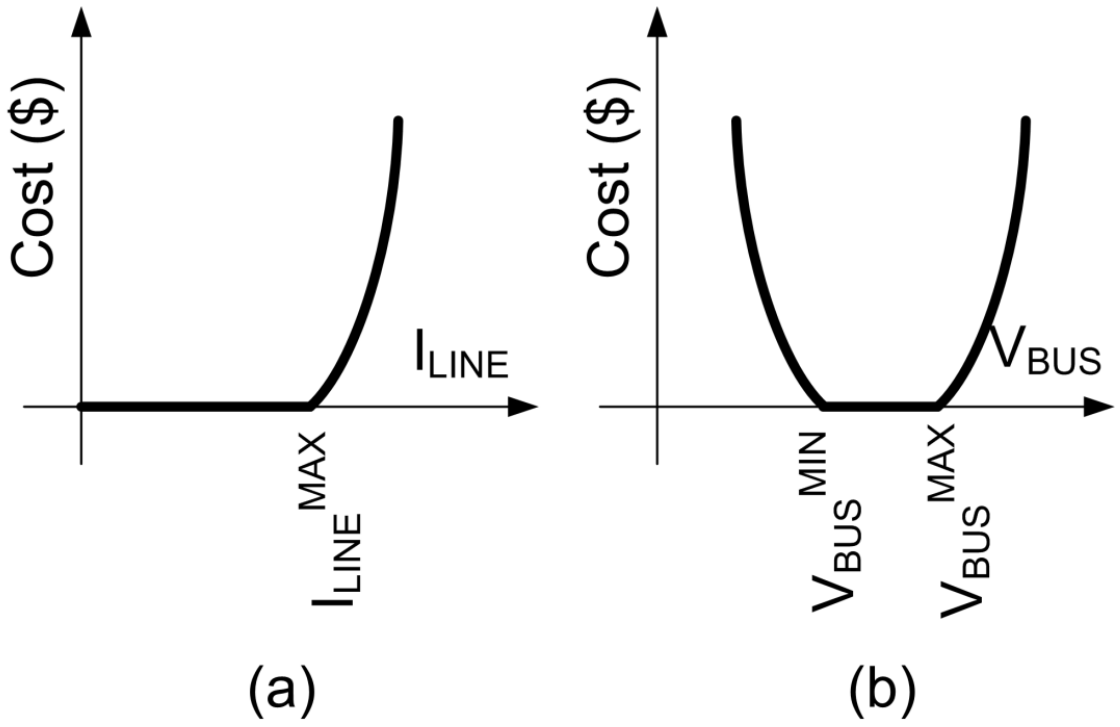

Figure 5.4: Soft penalty function for (a) line current constraint and (b) bus voltage constraint

The choice of the optimizer block is also very important. It is to be noted that the original OPF problem was a multi-objective, non-linear optimization problem with multiple linear and non-linear constraints. The introduction of the penalty function reduced the equivalent problem to a non-linear optimization problem with a single cost function. Particle Swarm Optimization (PSO) technique has been shown to be an excellent tool for solving such problems [49]. In power systems PSO has been used by a number of researchers to solve various kinds of problems including OPF [50]. The PSO has been shown to have many advantages in terms of convergence over other kinds of optimizer like Genetic Algorithm [51]. In this study the PSO has been used as the optimizer block.

5.2.2 Introduction to Particle Swarm Optimization

PSO is a stochastic evolutionary computing algorithm that is generally used for optimization and search problems. The method is based on a population and the interaction of different members of the population. The PSO algorithm was first described by Kennedy and Eberhart [52] and draws its inspiration from the movement of organisms such as a flock of birds or a school of fish.

In a PSO problem each probable solution is called a particle. A cost function is used to define the fitness of these particles [53-57]. At the start of the problem the number of particles is randomly chosen. Initially each particle has a random velocity in the problem search space. In each subsequent iteration the fitness of the particles are calculated according to a predefined cost function. Based on these calculations the best fit particle is chosen. Each of the particles has the capability to remember its best positions and also that of its neighbors. At the end of each iteration the particles update their velocities to move towards the local and global best positions. In order for this algorithm to resemble the movement of real life organisms, a certain amount of stochastic factor is attached to each movement. In an *n* dimensional real number search spaceR^n R^n, at the k^{th} iteration, the i^{th} particle is defined by its position vector $\overrightarrow{x_i}(k) \in R^n \vec{x}_i(k) \in R^n$. This position depends on the position of the particle in the *(k-1)*th iteration and its velocity $\overrightarrow{v_i}(k)$.

$$\overrightarrow{x_i}(k) = \overrightarrow{x_i}(k-1) + \overrightarrow{v_i}(k) \tag{5.5}$$

The velocity of the i^{th} particle at the k^{th} iteration is a combination of its velocity at *(k-1)*th iteration and its distance from the local and the global best positions. The local best position of the ith particle is indicated by p_i while the global best is p_g. The overall

velocity formula is given by (4.5). Because of stability issues it is often desirable to have a limit on the maximum possible velocity of a particle V_{max}. If the velocity of a particle calculated by (4.2) becomes greater than V_{max}, then the velocity is simply taken as V_{max}.

$$\overrightarrow{v_i}(k) = w_i \cdot \overrightarrow{v_i}(k-1) + c_1 \cdot r_1 \cdot \left(p_i - \overrightarrow{x_i}(k-1)\right) + c_2 \cdot r_2 \cdot \left(p_g - \overrightarrow{x_i}(k-1)\right) \tag{5.6}$$

w_i is the inertial constant. Good values are usually slightly less than 1.

c_1, c_2 are the values that represent how much the particles move towards local and global best respectively. They represent cognitive and social components respectively. Usually $c_1=c_2=2$ is a good value.

r_1, r_2 are uniform random numbers between 0 and 1. These numbers introduce the stochastic behavior in the system.

Using the PSO as the optimizer the modified OPF was implemented in software. The programming was done in MATLAB. The detailed program is presented in Appendix A. A couple of case studies are done using this modified OPF software in order to show the application of this software.

5.2.3 OPF Case Study I

The system used for the first case study is shown in Figure 5.5. The seven bus system consists of two generators. The first generator *G1*, located at bus 1 can produce electricity at \$60/MW-hr, while the second generator *G2*, located at bus 7 can produce electricity at \$80/MW-hr. The impedance of the path 1-3-4-6 is half of the impedance of the path 1-2-5-6. The rating of the tie-line *Tie1* is 40 MVA while that of the tie-line *Tie2* is 50 MVA. A load of 90 MW needs to be served at bus 6. The OPF solution of the system (without

any power flow controller) is solved and the resulting bus voltages and power flows are shown in Figure 5.5. It is seen that in absence of a power flow controller generator *G1* can only supply 75 MW of the load since *Tie2* is congested. At this operating point 15 MW of spare capacity is still unused in *Tie1*. Due to the congestion, the system is forced to use the more expensive generator *G2*, to generate the remaining 15 MW.

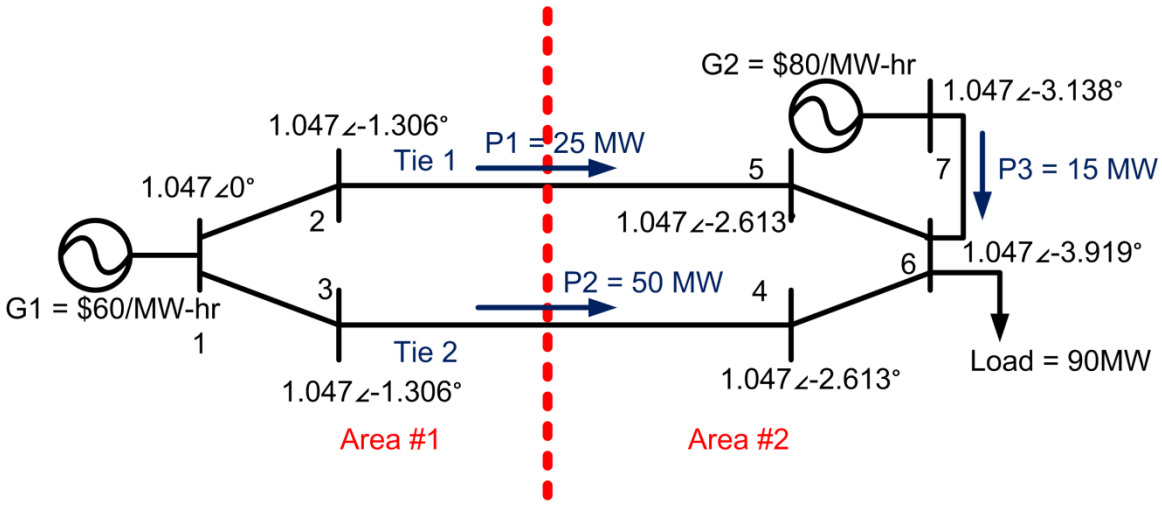

Figure 5.5: Seven bus test system – OPF with no power flow controller

The system is next assumed to have a CNT on *Tie2*. The CNT converters are assumed to be rated at 25% of the *Tie2* rating or 12.5 MVA. The modified OPF program is executed and the results of the simulation are shown in Figure 5.6. It is seen that the system is now able to meet the load using generation from only *G1*. As a result the total cost of generation for the system is reduced from $5700/hr to $5400/hr. The loading of the tie-line Tie1 has been increased from 25 MW to 40 MW with the help of the CNT.

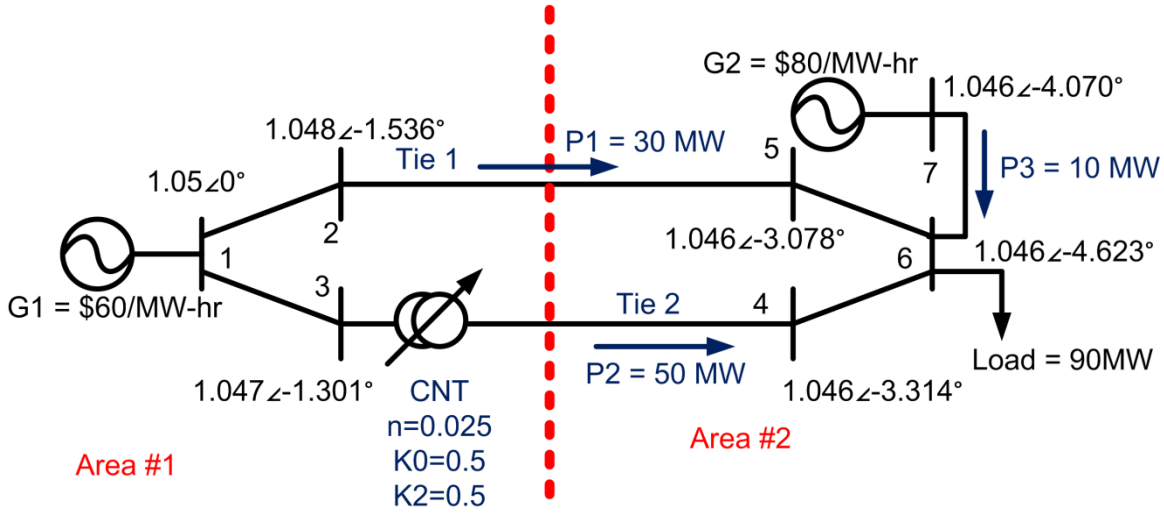

Figure 5.6: Seven bus system – OPF with a CNT on Tie2

5.2.4 OPF Case Study II

The previous case study showed the performance of the modified OPF program for a system having only one CNT. In this case study a bigger system with a larger number of CNTs is examined. For this reason the modified IEEE 30 bus system discussed in Chapter 4.5.6 is used. The system is first studied with no power flow controllers. It is assumed that the total loading of the system is 100 MW. The OPF of the modified IEEE 30 bus system with no power flow controllers is run in MATLAB. The generation costs and the PV settings of the various generators are shown in Table 5.1. The single line diagram of the system, showing the line over-loadings under this condition is presented in Figure 5.7. It is seen that in absence of any power flow controllers lines 2 and 18 are operating at full load. As a result dispatch from low cost generators at Bus 1 and 13 are limited. This increases the overall cost of generation for the system.

Table 5.1: Generator dispatch with no power flow controller for OPF case study II system

Bus No.	P Setting	|V| Setting	$ / MW	$
1	41.33	1.012	60	2479.80
2	0	1.024	84	0
13	25.35	1.027	61	1546.35
22	0	0.985	81	0
23	33.32	1.026	75	2499.00
27	0	0.95	82	0
Total cost of generation				6525.15

CNTs being power flow controllers can help manage system congestions. It is assumed that two CNTs are placed in the network – one each on line 2 and line 18. It is assumed that the installed CNTs have a converter rating of 20% of the line rating. Since each of the lines is rated at 16 MVA, the CNT converters are rated 3.2 MVA each. Using the modified OPF program the system with the two CNTs is simulated. The resulting generator dispatch is shown in Table 5.2. The CNT settings along with the line loadings of line 2 and line 18 are shown in Table 5.3.

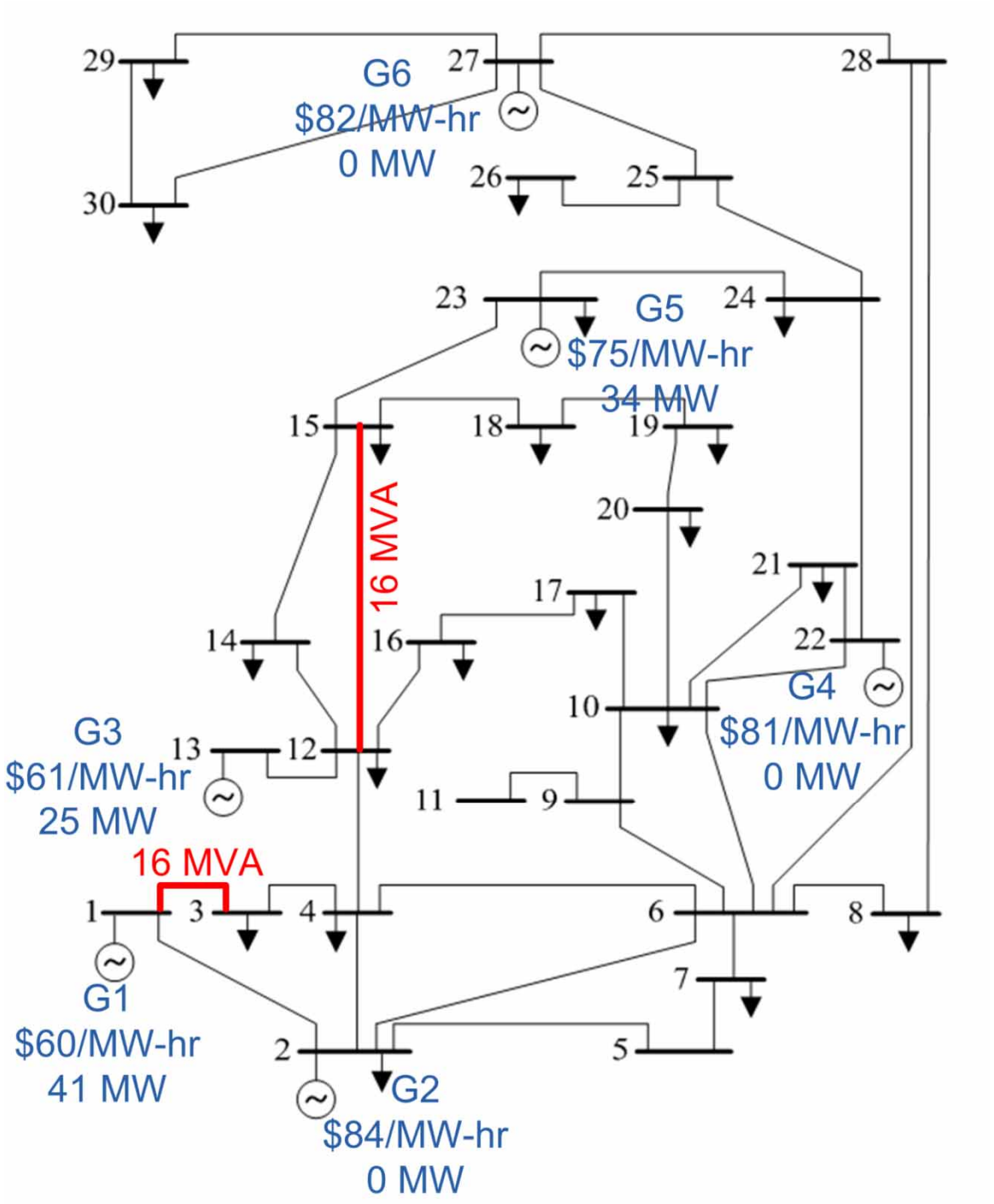

Figure 5.7: IEEE 30 bus system – OPF with no power flow controller

Table 5.2: Generator dispatch with two CNTs for OPF case study II system

Bus No.	P Setting	|V| Setting	$ / MW	$
1	78.65	1.0362	60	4719.00
2	0	1.0500	84	0
13	21.35	1.0197	61	1302.40
22	0	1.0500	81	0
23	0	1.0150	75	0
27	0	0.9830	82	0
Total cost of generation				6021.40

Table 5.3: Line loadings and CNT settings for critical lines

Line No.	From Bus	To Bus	MVA	MVA Max	K_0_set	K_2_set
2	1	3	16	16	0.52	0.56
18	12	15	15.8	16	0.48	0.44

It is seen that for the system with CNTs the power flow through the CNT controlled critical lines can be maintained at or below their maximum rated level. This allows the system to dispatch more of the low-cost generators, thus lowering the overall cost of

generation. It is seen that the cost of generation is lowered from $6525.15/hr (uncontrolled case) to $6021.40/hr (CNT controlled case).

5.3 Optimal Placement and Sizing of CNTs in a Large Network

In the previous section the OPF of the system was performed based on a particular location and sizing assumption of the CNTs. From system planning perspective it is imperative to place the CNTs optimally so that they can be controlled appropriately according to the system requirements. Sizing of the CNT converters is also an important issue. A CNT with a larger converter will have a larger control range and this might help in driving the cost of generation of the system further lower. But on the other hand the cost and complexity of the CNT will also increase with the increasing converter rating. From an economic standpoint it is important to have the correct balance of both the cost of the technology as well as the benefits incurred from it. Payback period, which the time required for the return of investment to repay the original investment, is often regarded as a good measurement of the economic feasibility of a project. In this section a methodology for optimal placement and sizing of CNTs in a large power network, based on the lowest payback period will be presented. The payback period of CNTs would also be compared to that of existing technologies like the Back To Back link.

5.3.1 Setting up the Test System

For the purpose of the study a modified version of the IEEE 30 bus system is used. The detailed data of the test system can be found in Appendix C. The loads of a typical power system are not static but vary with time. The pattern of variation mainly depends both on the time of the day as well as the day of the week [58]. Load data of various

operators like ERCOT are openly available to the public. The normalized load data of ERCOT for the week with highest total loading for the year of 2010 is shown in Figure 5.8. The load data consists of data collected every one hour and hence has 168 points. In this study it is assumed that the loads in the network follow the pattern of the cumulative loads of ERCOT. It is assumed that the peak loading of the test system is 900 MW, which corresponds to the 100% loading in Figure 5.8. In this study it is assumed that the week's data used corresponds to the hottest summer week loading of the system after say 5 years.

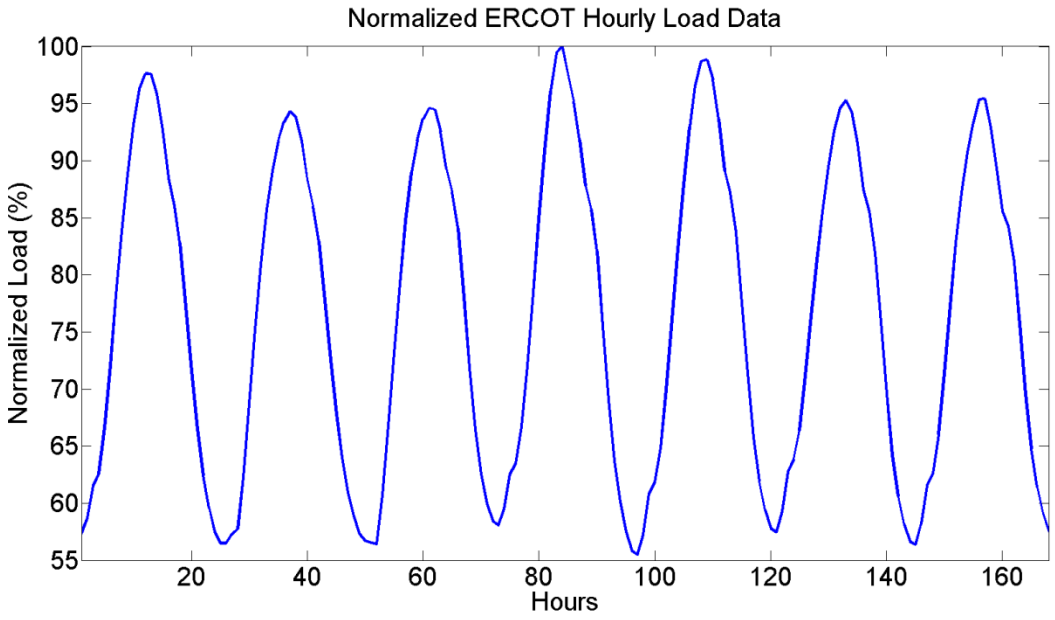

Figure 5.8: Normalized ERCOT hourly load data for a week

The wind generation data on the other hand mostly varies along with the time of the day and does not have a set weekly pattern. For this reason the variation profile of MISO-West wind generators is chosen. It is assumed that the profile repeats itself every 24 hours. The test 30 bus system is assumed to have a wind generator at bus 23 with maximum output capability of 200 MW. The diurnal profile of the wind generator is

shown in Figure 5.9. It is to be noted that for planning purposes it is enough to use average forecasted wind generation. The actual wind generation profile or even the load profile will have a lot more spikes, but those transients would be taken care of by the power-frequency control of the network.

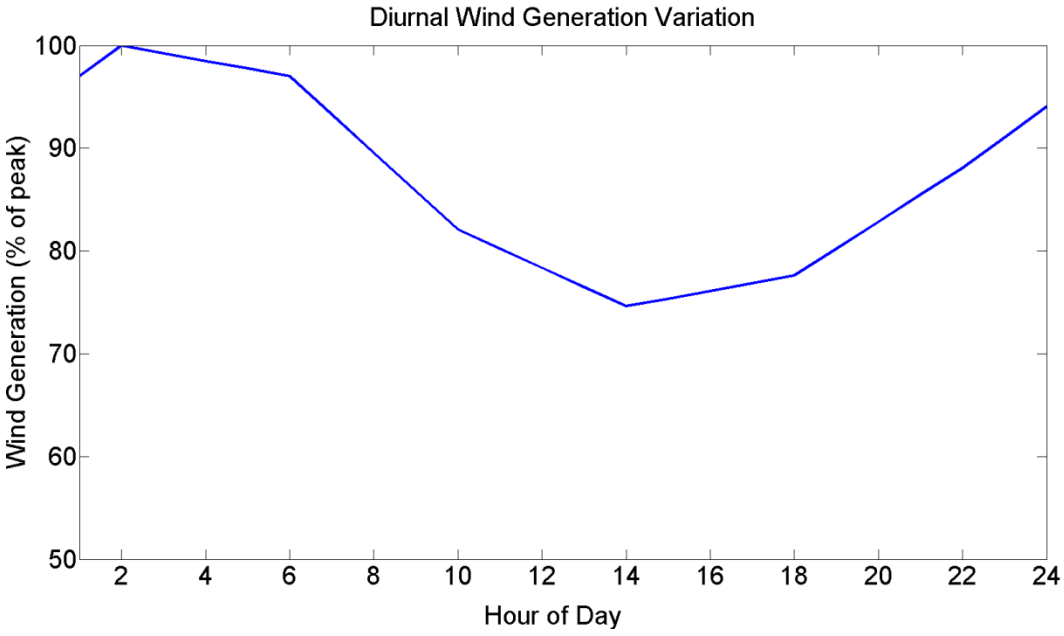

Figure 5.9: Wind generation variation over the day

The test system is assumed to have coal-based generators at buses 1, 2, 13 and 22, while a gas turbine based plant is assumed to be located at bus 27. The cost of the wind based power generation is assumed to be the least, while that of the gas turbine plant is assumed to be the highest. The generation costs of the various generators are shown in Table 5.4.

Table 5.4: Generation costs of various generators

Gen No	Type	Bus No	Cost of Gen ($/MW)
1	Coal	1	70
2	Coal	2	80
3	Coal	13	81
4	Coal	22	71
5	Wind	23	60
6	Gas	27	110

5.3.2 Case A: Evaluating the Test System in Absence of Power Flow Controllers

In this situation it is assumed that the test system does not have any power flow controllers. OPF for the test system is run in MATLAB for all the 168 operating points. The total cost of energy for each of these operating points is determined. Figure 5.10 shows the variation of the hourly generation costs over one week, while Figure 5.11 shows the some lines in the network which are often congested. It is seen that dispatch from low cost generators are mostly hindered by the lines 32 and 34. The average cost of generation of the system comes to $49433/hr making the total generation cost to be $433 M/year.

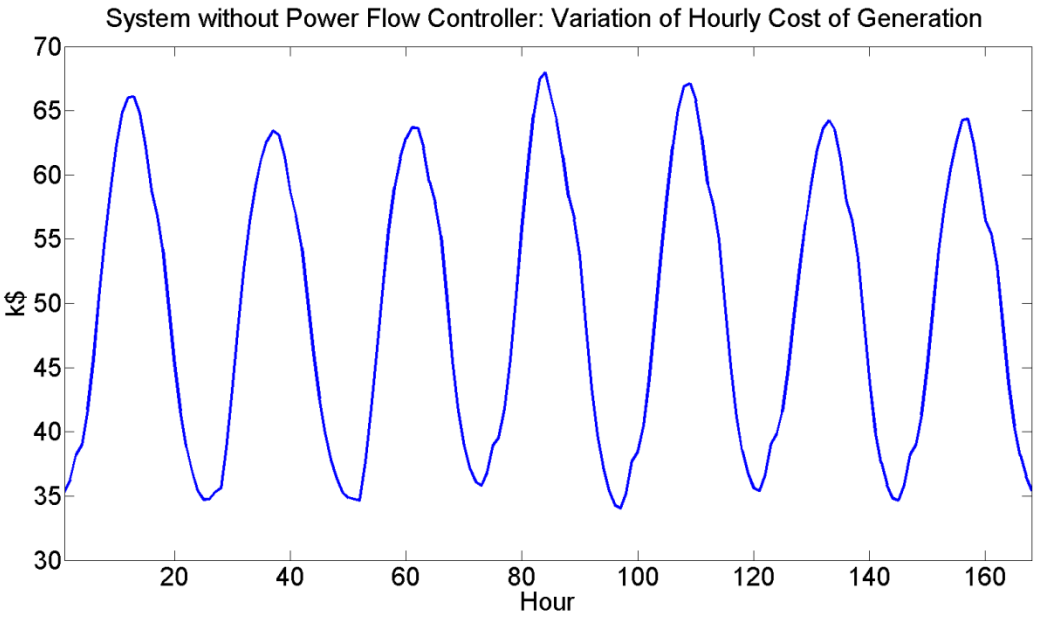

Figure 5.10: Hourly cost of generation for system without power flow controller

Table 5.5: Average energy output of various generators in absence of any power flow controller

Gen No	Bus No	Rating (MW)	Average Energy Output (MW-hr)
1	1	250	134.6
2	2	250	154.3
3	13	250	0.6
4	22	250	212.2
5	23	200 (peak)	115.9
6	27	250	29

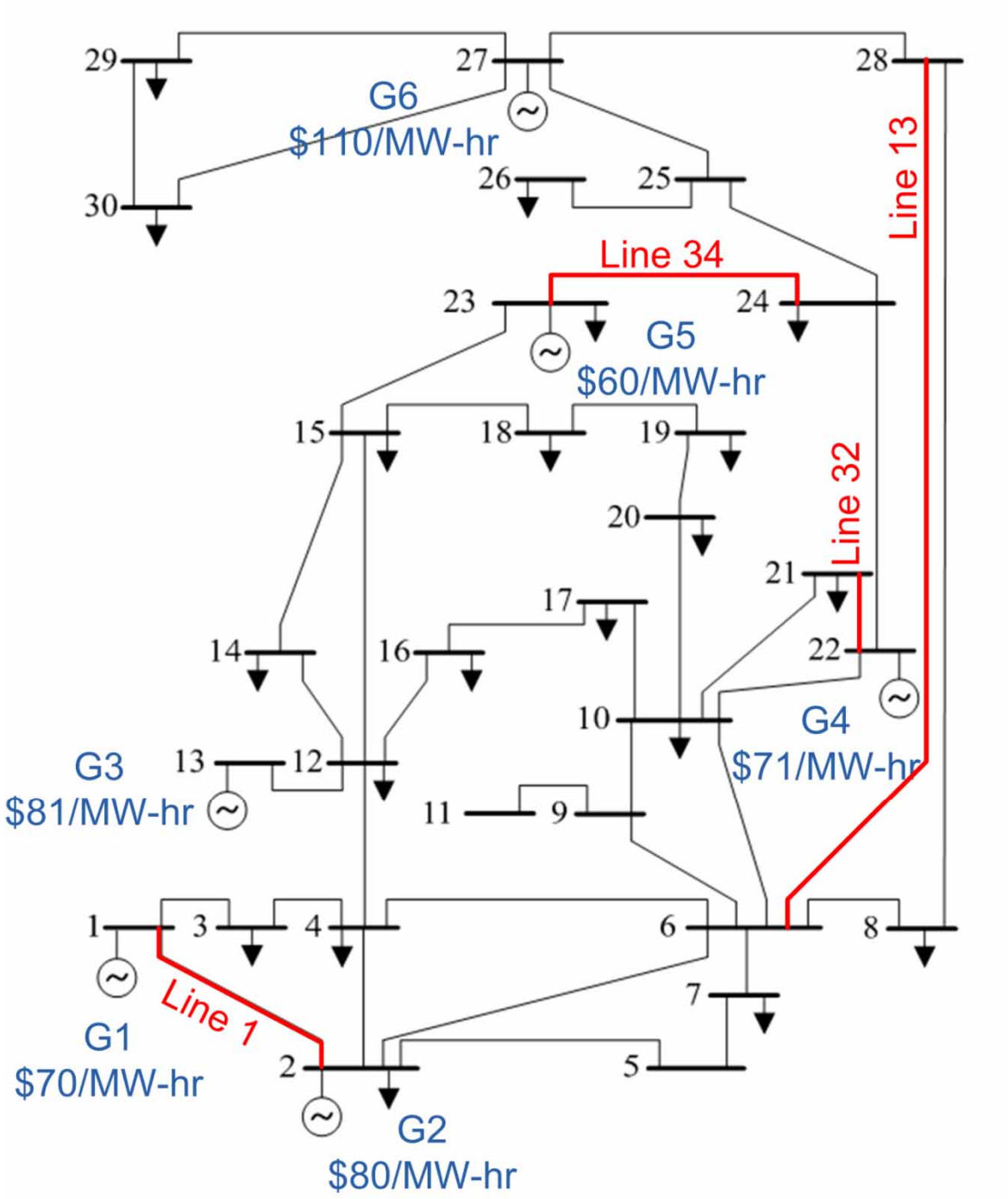

Figure 5.11: Test system with the line overloads in absence of any power flow controllers

Table 5.5 shows the annual energy output of the generators. It is seen that the low cost generator at bus 23 can only output an average power of 115.9 MW due to line

congestions, though it has an average capacity of about 180MW. On the other hand the most expensive generator at bus 27 has an average output power of 29 MW. This drives the cost of generation of the system high.

5.3.3 Methodology of Finding Optimal Placement and Size of CNTs

It is seen that the test system often faces congestions at multiple locations during multiple operating points. Installation of CNTs in the network can help ease some of the congestion and thus help lower the operating costs of the system. The idea of installing one or more CNT devices in a system can be economically feasible if the benefit of the CNT device outweighs its costs. The benefit of installing a power flow controller has been discussed qualitatively in Chapter 1. In this problem the benefit of installing CNTs are measured by the reduced cost of generation for the system. In practical scenarios their might be other benefits such as avoided costs of building new transmission lines, avoided real estate cost, lower time to finish, etc.

It is important to model our costs for the CNT technology properly. A couple of observations are used to model the costs of the CNTs. The cost of each installation should have a significant overhead so as to minimize the total number of such installations. On the other hand cost of each installation should be proportional to the size of the converter. It is seen from Figure 5.11**Error! Reference source not found.** that the congested lines are all of different ratings. Intuitively installing a 10% CNT on a 100 MVA line should be more expensive that putting it on a 50 MVA line. On the other hand the cost of installing a 20% CNT is taken to be twice as the cost of building a 10% CNT on the same line.

Mathematically, it is assumed that the cost incurred as a result of the CNTs will consist of two parts – a fixed cost and a variable cost. The fixed cost is assumed to be proportional to the CNT transformer/line rating (in MVA) while the variable cost is assumed to be proportional to the CNT converter rating (in MVA). If the system requires too many CNT installations the fixed cost of the CNTs in the system would increase, while if the system requires high controllability in some of the lines, the variable cost part would increase.

The optimal placement and sizing program is built by wrapping around a layer of optimizer block around the OPF algorithm. The program structure is shown by the block diagram shown in Figure 5.12. The optimizer is required to generate new sets of possible location and sizes of CNTs. For each location and sizing combination the OPF program is used to find out the total cost of generation over several operating points. The cost of the installation is found out by evaluating the installation costs of the CNTs, while the benefits are found by calculating the reduced cost of generation. Payback period (in years) for a particular plan is calculated as the ratio of costs to benefits. The objective of the upper level optimizer block is to minimize the payback period. PSO is once again chosen as the upper level optimizer due to beneficial features in non-linear search [55]. The overall algorithm is described in Figure 5.13.

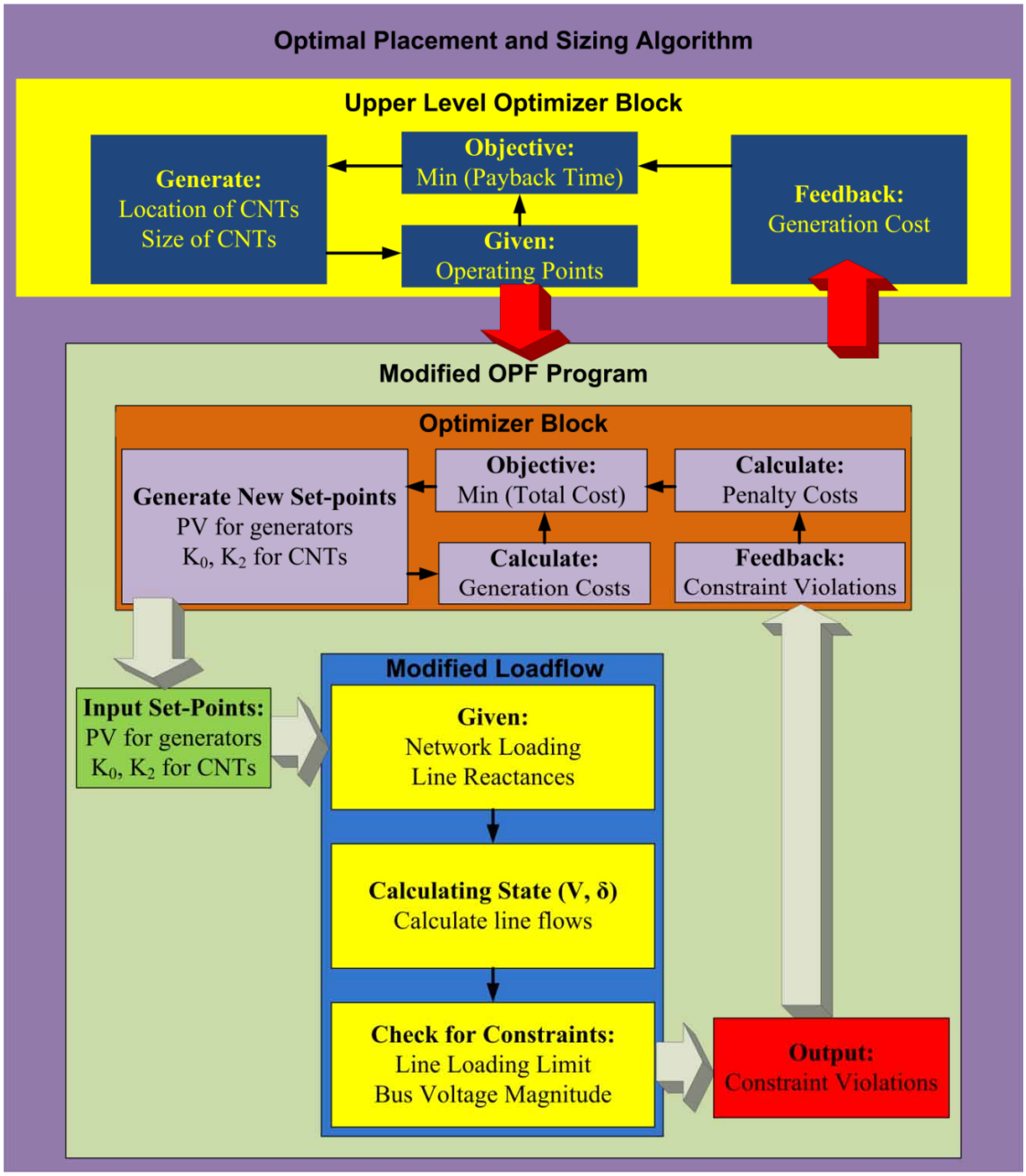

Figure 5.12: Block diagram of the optimal placement and sizing program

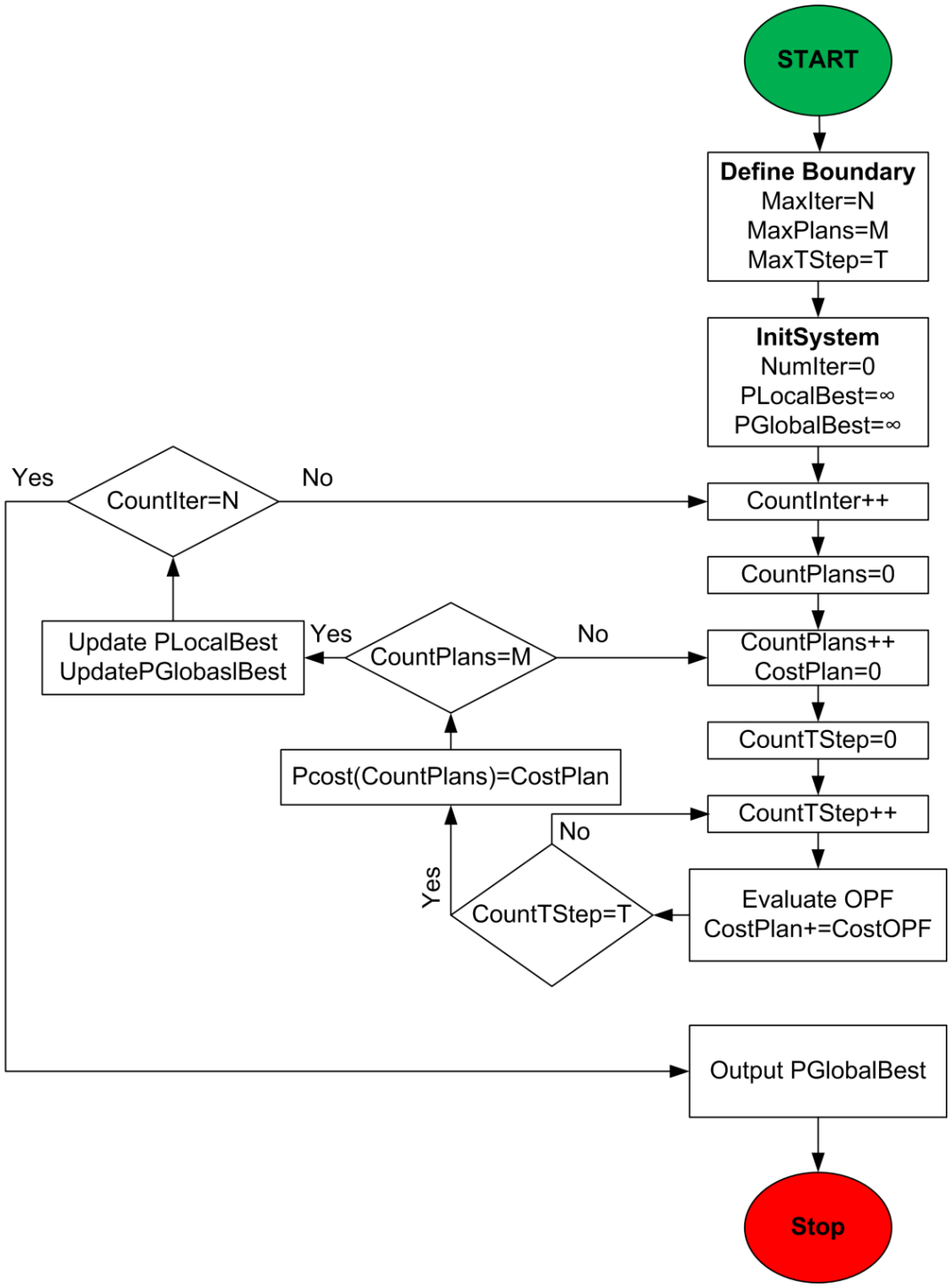

Figure 5.13: Overall algorithm for determining the optimal location and sizing of CNTs

5.3.4 Case B: Evaluating the Test System with Optimally Placed and Sized CNTs

The optimal placement and sizing program is run for the test system. It is assumed that the cost of the CNT installations is of the form (4.4). In utility industry the cost of an FACTS installation varies widely depending on various factors like installation rating, location, real-estate cost, etc. Intuitively it is clear that the cost of a CNT with a larger converter rating will be higher. Also a CNT placed on a higher rated line will have a higher cost than a CNT placed on a lower rated line. This is because the power rating of elements like bypass switches will be proportional to the line rating. It is estimated in [59] that the cost of CNT based power flow controller can be reduced to as low as $35-$50 /kVA using modular converter blocks. In this study a more conservative assumption of the cost estimate of the CNT at $100 / KVA is used. Also it is assumed that the cost of the elements such as bypass switches, etc., the ratings of whom are dependent on the line rating, is 20% of the converter cost. As a result in (4.4), the value of the parameter B is taken as $0.1 Million/MVA, while that of parameter A is taken as $0.02 Million/MVA.

$$Cost = A * LineRating + B * ConverterRating \quad (5.4)$$

It is found that the for the optimal placement the CNTs has to be located at lines 13, 32 and 34 with the converter ratings of 9 MVA, 18 MVA and 6 MVA respectively. This is an interesting result as the program calculates that for the optimal economic benefits CNTs should be placed on the congested lines. The result is in lines with similar optimal placement research done on STATCOM placement [60] and Distributed Series Reactance placement [61]. Intuitively this can be explained as follows. If a CNT placed on an overloaded line, it tries to push the current away from the overloaded line. In case of a

CNT placed on a parallel under-loaded line, it has to pull current from another overloaded line. But, such a CNT controlled line will draw current from all other lines, including the overloaded line. Hence, for mitigating line overload problems CNTs placed on overloaded lines seem to be more effective.

For the calculated optimal placement and sizing of the CNTs, the total installation cost for this configuration is estimated to be $7.9 M. The detailed cost estimate can be seen in Table 5.6. The benefits of the CNTs are acquired in terms of the reduced cost of generation. For this analysis it is assumed that the discount rate is 0%. It is calculated using the modified OPF program that with the optimal placement and sizing of CNTs the cost of generation will reduce to $426.7 M, thus incurring a savings of about $6.3 M every year. Thus the payback period of the CNT installation is estimated to be roughly 1.25 years, which is very small compared to the expected lifetime of typical power flow control technologies.

Table 5.6: Cost estimate for optimal CNT installation

Line No	Line Rating (MVA)	Converter Rating (MVA)	CNT Cost ($ M)
13	80	9	2.5
32	100	18	3.8
34	50	6	1.6
Total Cost of CNTs			7.9

Table 5.7: Comparison of average energy output of the generators in Case A and Case B

Gen No	Case A: Average Energy Output (MW-hr)	Case B: Average Energy Output (MW-hr)
1	134.6	76.8
2	154.3	142.2
3	0.6	3.6
4	212.2	239.9
5	115.9	165.6
6	29	18.5

The reduction in generation cost from *Case A* to *Case B* is due to reduction of energy produced from the high cost generators. The reduction of hourly generation costs is shown in Figure 5.14, while Table 5.7 shows the average energy output from each generator. It is seen that in *Case B* the cost of generation is always lower than that of *Case A*. This is expected as CNTs would allow more generation from low cost generators. The lowest cost generator, *Gen 5* at bus 23 is now able to dispatch an average of 165.6 MW in comparison to just 115.9 MW in Case A. Also there is significant lowering of generation from the high cost generators - *Gen 1, Gen 2 and Gen 6*.

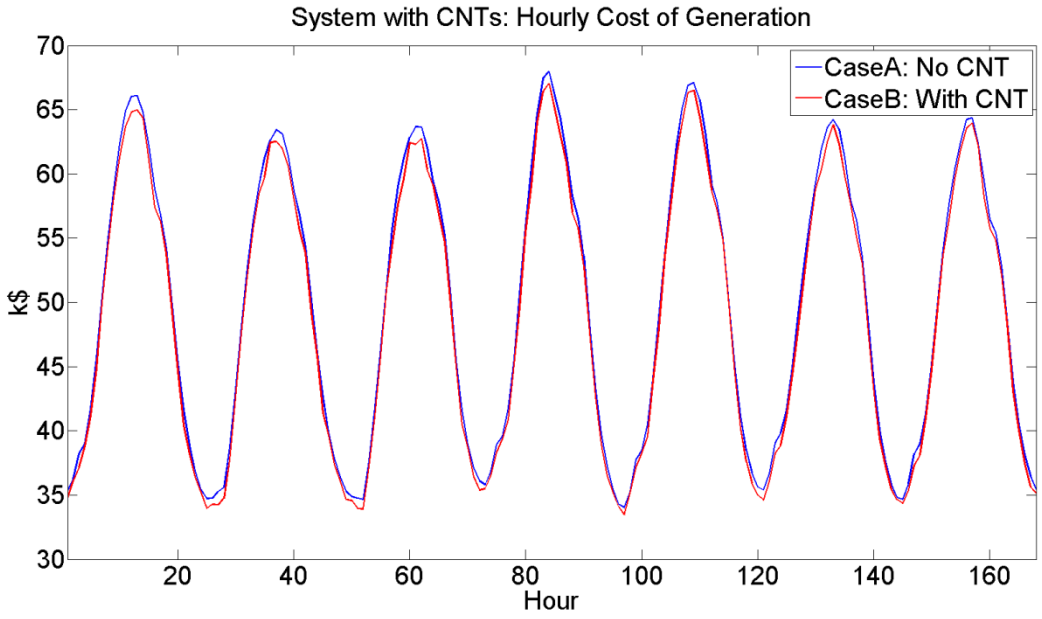

Figure 5.14: Comparison of cost of generation for with and without CNT case

5.3.5 Case C: System with Other Power Flow Controllers

The control achieved by the CNTs in Case B can be achieved by other power flow controllers like the Back-To-Back (BTB) links or the Variable Frequency Transformer (VFT). It is important to compare the benefits of a new technology like CNT in comparison to existing technologies like the BTB or VFT. In this section it is assumed that instead of the three lines being controlled by the CNT, they are controlled using three BTBs. The impact of VFT can be analyzed by simply factoring in the relative cost of the two technologies.

Power flow controllers like the BTB can be assumed to be a constant positive load at the sending end bus and a constant negative load at the receiving end bus. The impact of real and reactive losses on the controlled line is neglected. The equivalent model of the BTB link from an OPF standpoint can be described as shown in Figure 5.15.

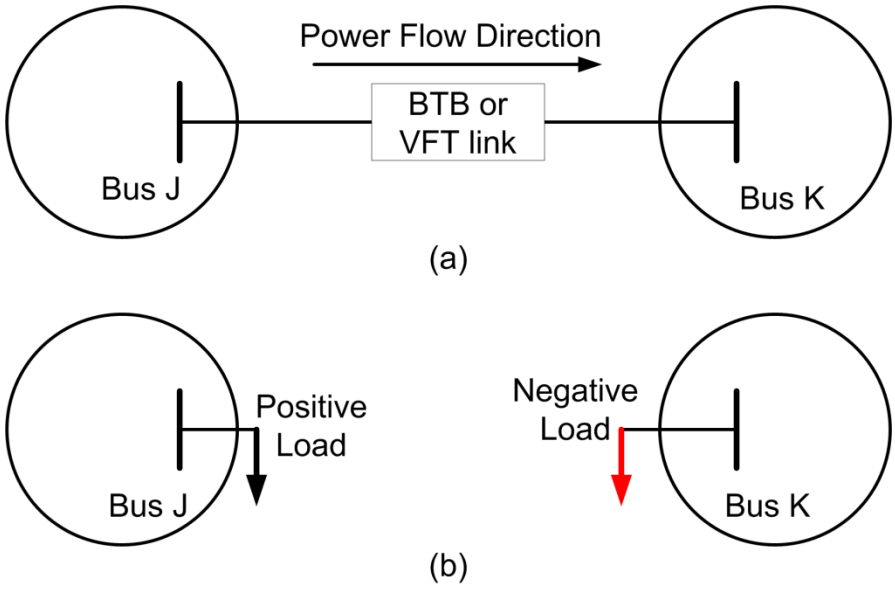

Figure 5.15: Equivalent model of a BTB or VFT from OPF standpoint

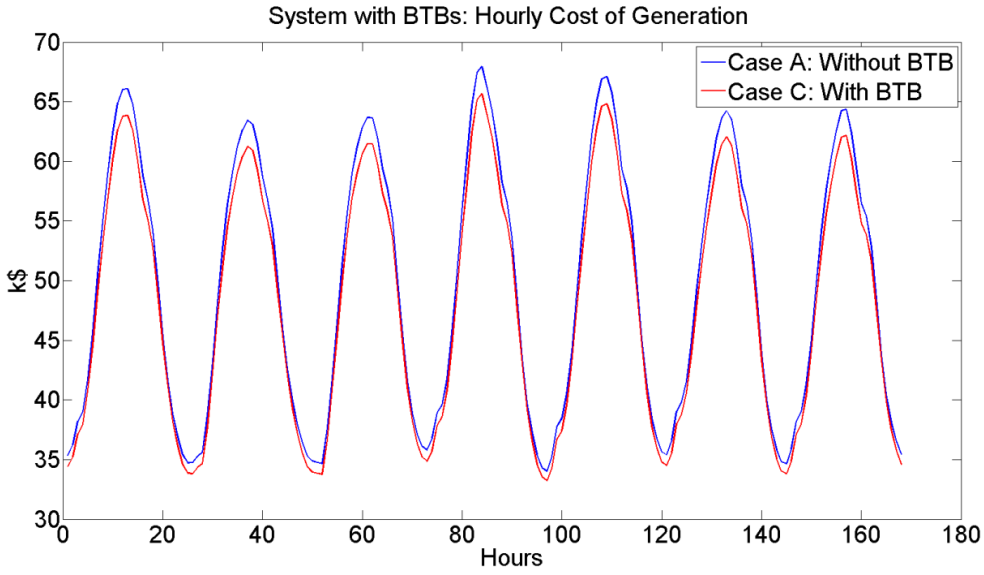

Figure 5.16: Hourly cost of generation for system with BTB links

The test system is assumed to have three BTBs one each on line 13, 32 and 34. Since BTB is not a fractional converter technology, the MVA ratings of each BTB is same as that of the line. Hence the BTBs have to be rated at 80, 100 and 50 MVA respectively. It

is to be noted that the BTBs have two fully rated bi-directional converters. Hence for an 80 MVA BTB, the total rating of the two converters is 160 MVA. In [59] it is estimated that cost of FACTS systems are $170-$300 /kVA. Also [62] and [63] estimates the cost of FACTS converter systems to be about $250 /kVA, while [64] estimates the costs of FACTS devices to be greater than $300 /kVA. In this study the total cost of the BTB system is assumed to be $300 /kVA.

The OPF for the BTB case is again simulated over the week's data. It is seen that the total cost of generation is reduced to $420.9 M, making the annual savings $12.1 M compared to *Case A*. However it is estimated that the costs of BTB technology will be much higher as it requires two fully rated bi-directional converters per line. Using the numbers above it is estimated that the total cost of the BTB solution will be $138 M. Thus the payback period for this technology is estimated to be 11 years, compared to the 1.25 years of the CNT technology.

5.4 Conclusions

The chapter describes the methodology of finding the OPF of a network with multiple CNTs and shows the application of it in two case studies. The methodology for finding the optimal placement and sizing of the CNT in a network is developed next. Using this tool the economic cost-benefit of the CNT technology is studied in a test system. It is found that the optimal place to site CNT installation is on lines which are heavily loaded. Controlling heavily loaded lines can reduce the cost of generation of the system. The study shows that for the test system investments made on CNT technology can be recovered within a period of just 1.25 years. The same test system is assumed to be

installed with BTB links. It is seen that with BTB technology although the cost of generation is further lowered, but the huge investment up-front makes it a risky option. For the test system investments made on BTB is seen to be recoverable in about 11 years, compared to the 1.25 year timeframe for CNT. It is thus concluded that the CNT may be a low risk option for investors compared to some of the present power flow technologies.

Chapter 6

6. CNT FILTER DESIGN

The principle of operation of a CNT is considerably different from that of other FACTS based power flow controllers. Conventional FACTS based devices such as the BTB converters are based on AC-DC-AC power conversion. The two AC systems in these cases are connected via a common DC link, which serves as a low frequency storage element. However, in case of the CNT there are no such low frequency storage elements. Instead in this case the triplen harmonics act as the pseudo-low frequency energy storage element. As a result the CNT topology is not plagued by failures of the low reliability electrolytic capacitors. However, the CNT produces unwanted low frequency triplen harmonic voltages and currents, which may be unacceptable from the utilities standpoint. From equation (3.11) it is seen that the output voltage of the CNT can have third harmonic voltage content of as high as 5%, assuming n=0.1 and K_2=0.5.

6.1 Harmonic Proliferation Caused by the CNT

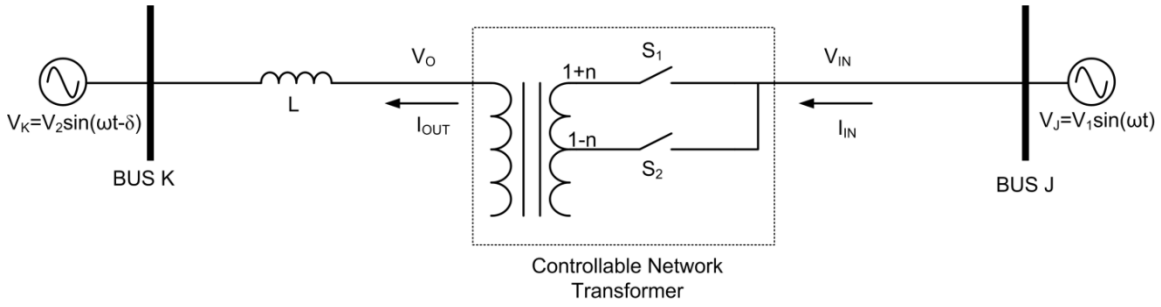

Figure 6.1: Two bus system connected by a CNT controlled tie-line

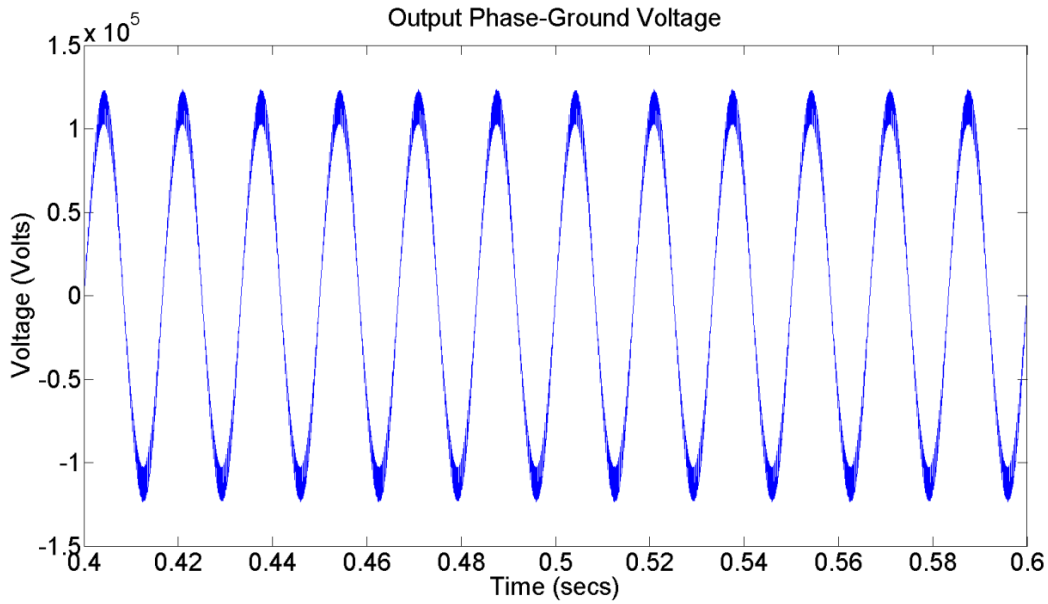

Figure 6.2: Output voltage of the CNT

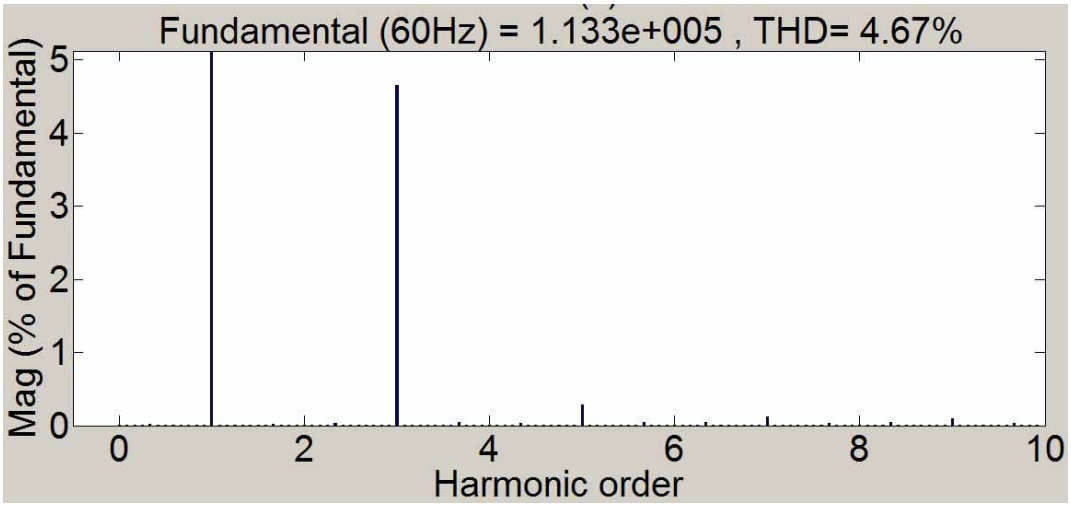

Figure 6.3: Frequency spectrum of the output voltage

Figure 6.1 shows a simple two bus system connected by a CNT controlled tie-line. The voltages of the two areas are assumed to be separated by an angle δ=2°, while the line inductance *L* is assumed to be 15 mH. The CNT is assumed to have 10% taps (n=0.1). The X/R ratio of the line was assumed to be 10. The output voltage and its frequency spectrum for K_0=0.5 and K_2=-0.5, obtained from simulation, are shown in

Figure 6.2 and Figure 6.3 respectively. It is seen that the output voltage has about 4.7% third harmonic as predicted by equation (3.16).

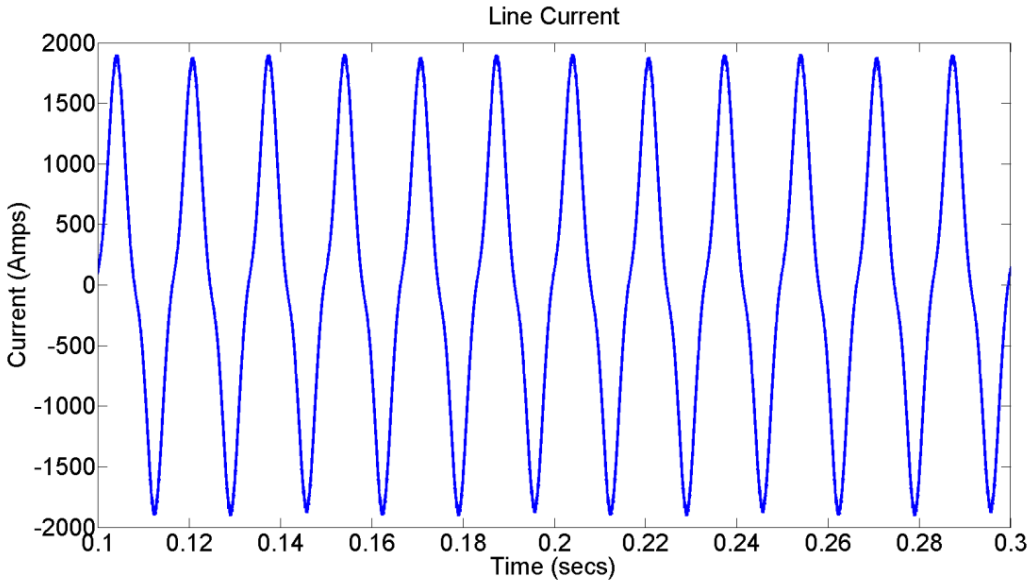

Figure 6.4: Output current of the CNT

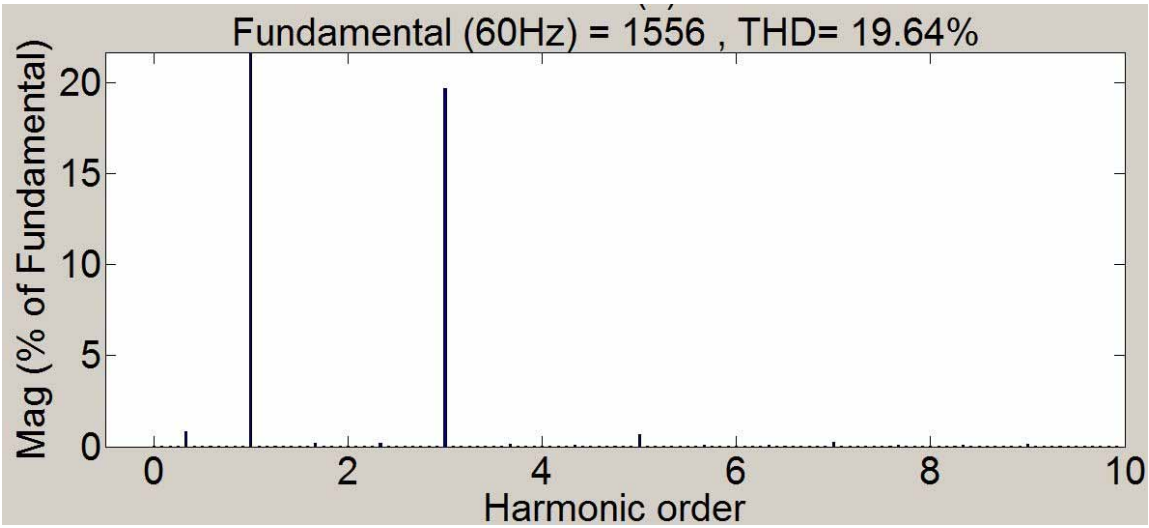

Figure 6.5: Frequency spectrum of the CNT

This 3rd harmonic voltage can cause significant amount of third harmonic currents in the system which is undesirable from power quality perspective. The output current and

its frequency spectrum for the simulated system are shown in Figure 6.4 and Figure 6.5 respectively. It is seen that the output current has about 20% third harmonic content.

From the utility perspective, this high level of harmonic proliferation is unacceptable. Thus it is important to block the flow of this 3rd harmonic current at the output side of the CNT system. The following sub-section describes the various methodologies which can be used for filtering the harmonics produced by the CNT.

6.2 Filtering Options

Using passive L-C trap can be a simple, low-cost solution to the third harmonic problem. The basic topology of the CNT with a passive filter is shown in Figure 6.6.

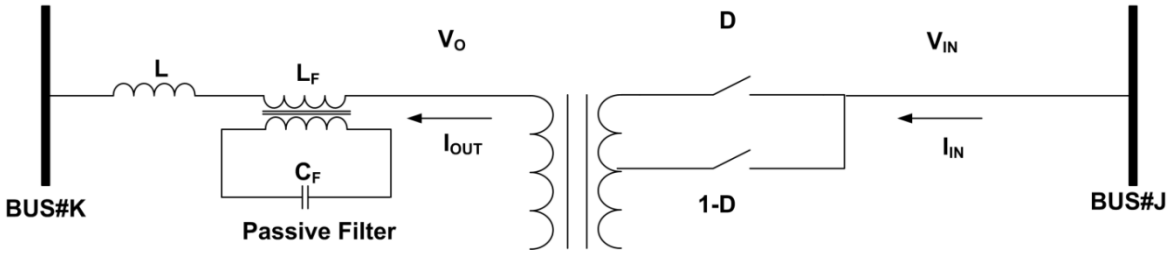

Figure 6.6: CNT with passive filter topology

However practically the LC trap would not be tuned exactly at 180 Hz and the performance of the passive filter will be very limited in a practical scenario. Figure 6.7 shows the output line current in a CNT controlled line, where the output LC passive filter is detuned by 5% (resonating at 189 Hz), while Figure 6.8 shows its frequency spectrum. It is clear from Figure 6.8 that for a practical CNT system, a passive filter would not be a suitable solution.

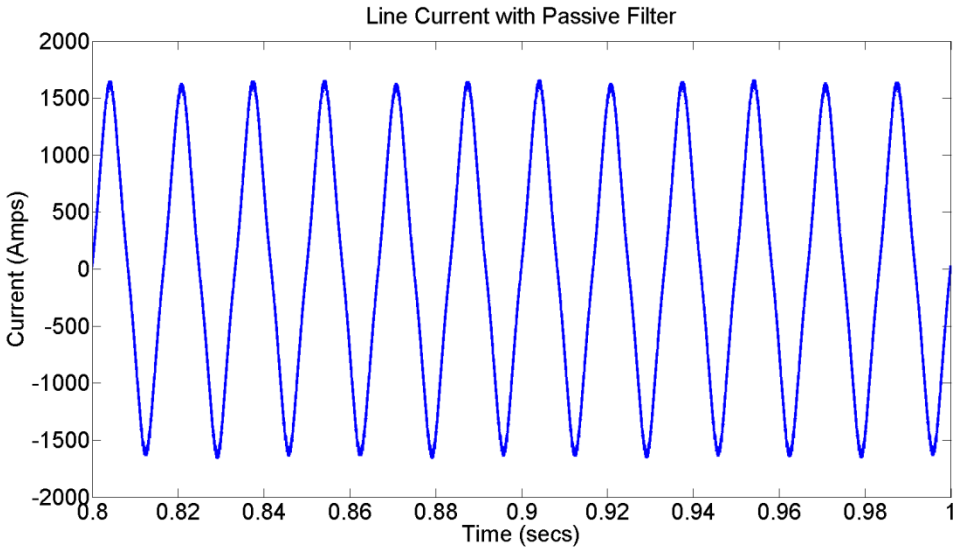

Figure 6.7: Output line current waveform with 5% detuned passive filter

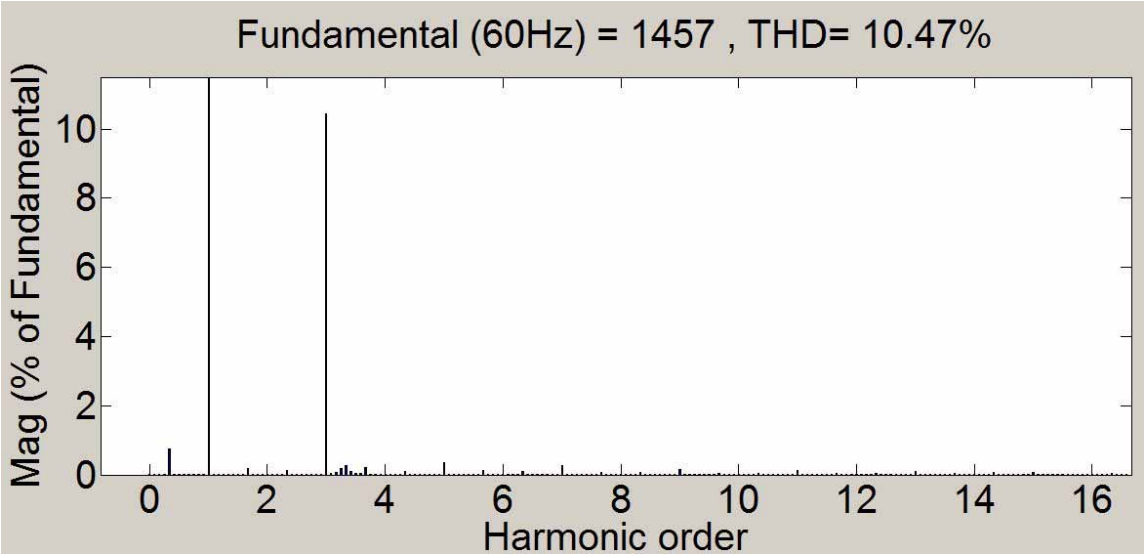

Figure 6.8: Output line current frequency spectrum with 5% detuned passive filter

An active filter topology, as shown in Figure 6.9, can be used to obtain a good dynamic performance and minimize the third harmonic line current. The active filter is used to inject a 3rd harmonic voltage, such that it exactly cancels the 3rd harmonic voltage produced by the CNT. The cost and complexity of such a system, however is expected to be very high [65].

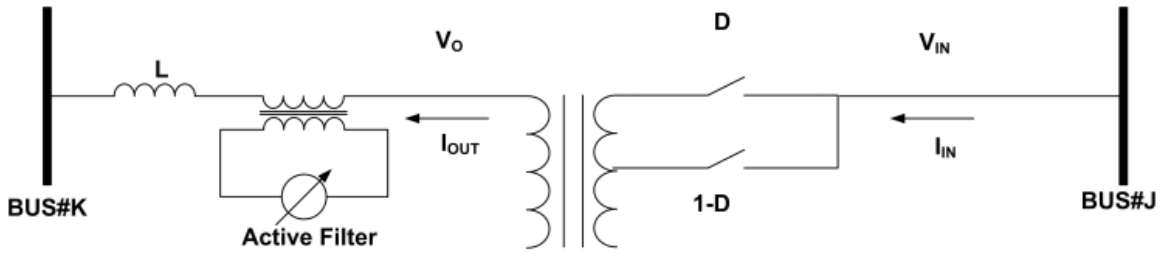

Figure 6.9: Series active filter topology

On the other hand a Hybrid Active Filter (HAF) can provide a good dynamic performance while having a reasonably low cost. The converter is used for providing a small 3rd harmonic voltage which ensures almost perfect dynamic tuning of the LC filter at the 3rd harmonic frequency. The schematic of such a HAF is shown in Figure 6.10. The HAF draws a small amount of real power from the line in order to maintain the DC link voltage. It is estimated that the HAF converter rating can be just a fraction (less than 10%) of the VA rating of the passive components of the LC filter [66].

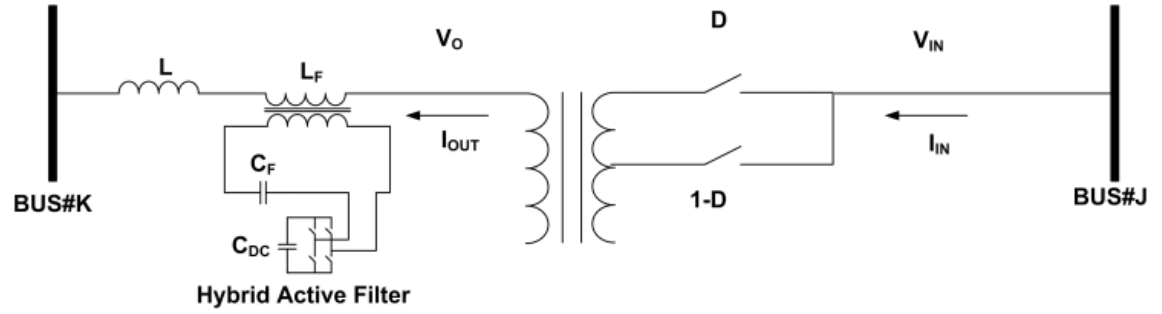

Figure 6.10: Series HAF topology

6.2.1 Controlling the series HAF Filter

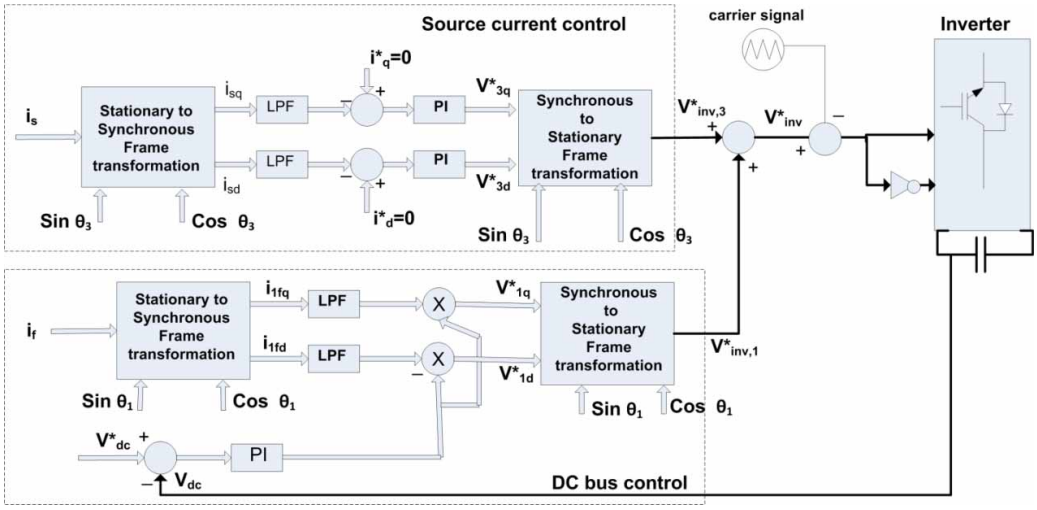

Figure 6.11: HAF control schematic

The control schematic of the HAF is shown in Figure 6.11. It mainly consists of source harmonic current control, dc bus control and pwm generation. The control is achieved in the synchronous reference frame to avoid phase delays associated with PI control of sinusoidal quantities. The objective of the harmonic current control block is to regulate the source 3rd harmonic current (I_{S3}) to zero via negative feedback. The source current (I_S) is measured and transformed into synchronous reference frame at the 3rd harmonic. The transformed current (I_{SD} and I_{SQ}) has a dc value equivalent to that of the third harmonic in the source current. The dc value is extracted with a low pass filter and then compared with a reference value of zero. The current error is fed to PI regulator which in turn generates 3rd harmonic reference voltages for the inverter.

HAF generates 3rd harmonic voltage to block 3rd harmonic current from the source. The terminal voltage and the circulating 3rd harmonic current are not orthogonal, thus real power can flow into or out of the inverter. This real power flow can create fluctuations in

the dc bus voltage. To keep the voltage constant, energy transfer at 3rd harmonic has to be compensated by controlling energy flow at some other harmonic. This is achieved only at the fundamental frequency as choice of any other harmonic would introduce harmonics in the source. There will be a small fundamental current flowing in the inverter, the value of which depends on the impedance of L_F and C_F at the fundamental frequency. The power transfer at the fundamental can be achieved by injecting an in-phase fundamental voltage. The power flow control is achieved by controlling the value of this in-phase fundamental voltage at the inverter terminals. As shown in Figure 6.11, the dc bus voltage is measured and compared with reference value. The error is fed to a PI regulator which generates magnitude reference for the fundamental voltage. The phase command is derived from the fundamental current. The fundamental voltage references from dc bus control block ($V^*_{INV,1}$) are summed up the 3rd harmonic voltage references ($V^*_{INV,3}$) generated by the source harmonic control block. The sum (V^*_{INV}) is compared with the carrier wave to generate pwm pulses.

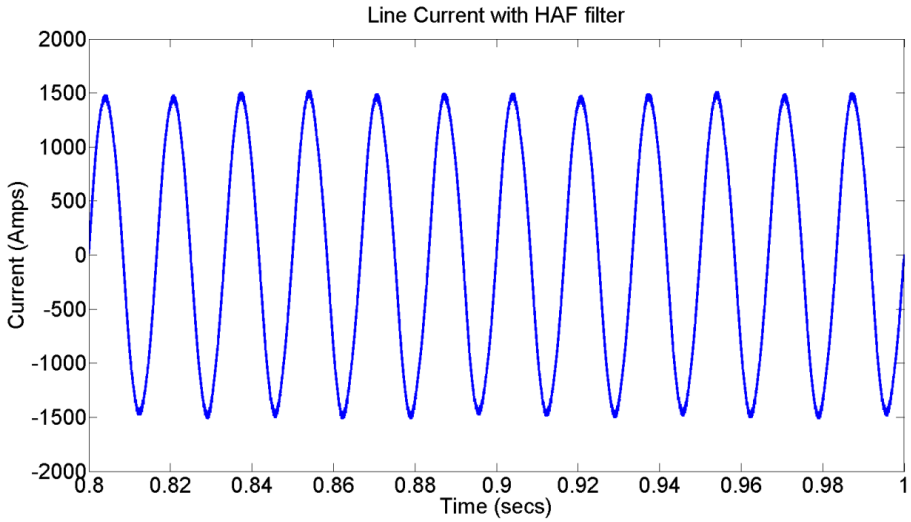

Figure 6.12: Line current with HAF filter

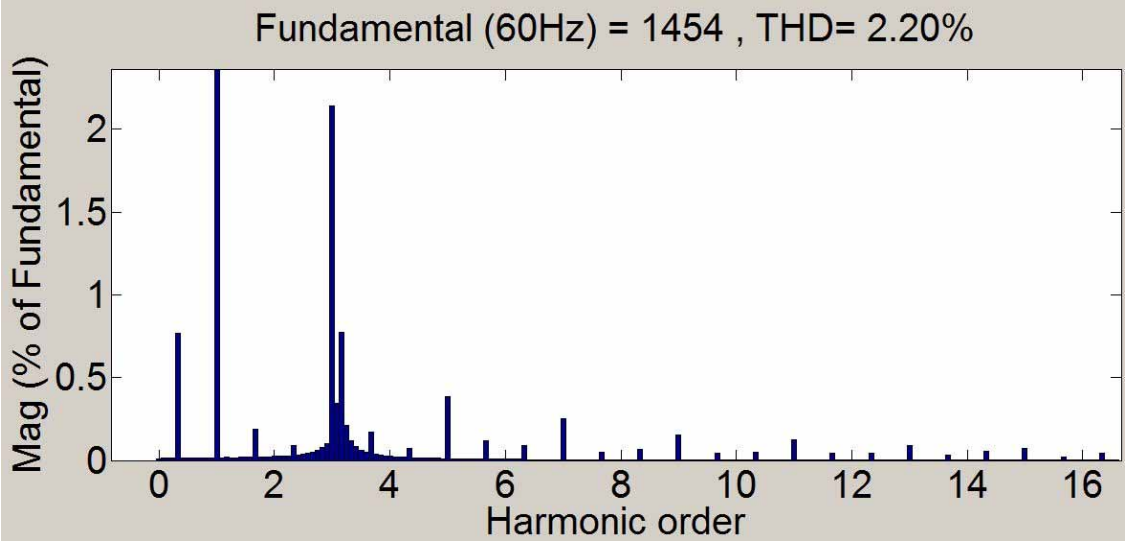

Figure 6.13: Line current frequency spectrum with HAF filter

The output line current and its frequency spectrum for the HAF filter case is shown in Figure 6.12 and Figure 6.13 respectively. It is seen that the HAF filter can reduce the 3rd harmonic content in the line current to about 2.2%, which is acceptable by most utility standards.

6.2.2 Optional Requirement of a Second HAF

Due to the 2nd harmonic content in the duty cycle of the CNT converter, the input and the output currents of the CNT is related as equation (6.1). The HAF shown in Figure 6.10 ensures there is minimal 3rd harmonic content in the output current. However even if the output current has no 3rd harmonic content, the input current will end up having 3rd harmonic content due to the duty ratio term in (6.1).

$$I_{IN} = \left[\frac{D}{1+n} + \frac{1-D}{1-n}\right] * I_O \tag{6.1}$$

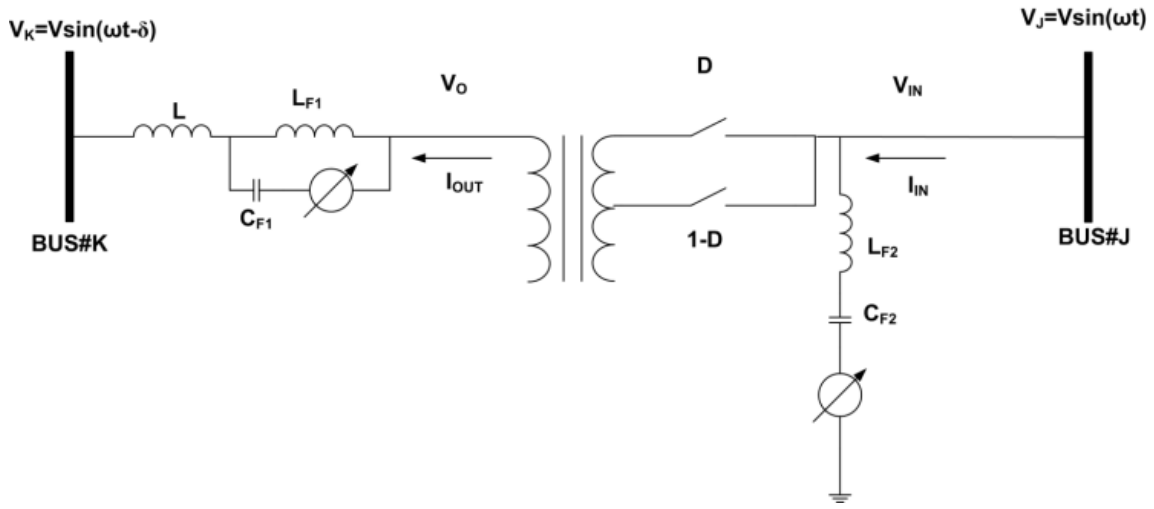

Figure 6.14: CNT with series and shunt HAF filters

The 3rd harmonic current injection in the input side of the CNT can be modeled by an equivalent current source. The magnitude of this 3rd harmonic current can be estimated using the equation (y). The worst case harmonic proliferation would occur for K_2=0.5. For a CNT with taps at ±10% voltage levels (n=0.1), the worst case 3rd harmonic content in the input current is approximately 5%. This level of harmonic proliferation may or may not be acceptable for a given system. Also it is to be noted that the THD of the input current can be lower if K_2 is kept lower. In cases where the input side current harmonics has to be also controlled to very stringent levels, an additional hybrid active shunt filter can be provided at the input side of the CNT, as shown in Figure 6.14.

6.3 Impact of Series Filter on CNT Control Range

The CNT is shown to have a significant control range in the P-Q plane [40] and the control range varies depending on the CNT converter rating and the terminal bus voltages [39]. In this section the impact of the series filter on the CNT control range is studied.

An active series filter would have almost no impact on the CNT control range, since it would inject only a third harmonic voltage. But a HAF filter would appear as an inductance at fundamental frequency and would thus have an impact on the power flow. The filter inductor L_F and the filter capacitor C_F has to be chosen to resonate at around 180 Hz. Intuitively it is clear that L_F should not be too big as it would lower the real power flow in the line. On the other hand if L_F is made too small the VA rating of the passive components of the filter will increase. Higher VA rating of the passive components would lead to increased rating of the HAF converter. Hence an optimal design of the passive components of the filter is required.

In order to find the optimal design for the L_F and the C_F components, the system in Figure 6.10 is considered. The line inductance is once again taken as 15 mH while the 138 kV system is assumed to operate with $\delta=2°$. For the given system different designs of CNT along with an integrated HAF series filter is considered. For a given value of L_F, the corresponding C_F can be found out from the resonance condition. For this design of L_F and C_F, the rating of the CNT converter required in order to achieve a particular active and reactive power control range is calculated. This can be done by using equation (3.19) and (3.20). For this case study the various CNT with integrated HAF systems are designed to have 160 MW and 325 MVAR of real and reactive power control range respectively. It is further assumed that the HAF converter is rated 10% of the sum of the VA ratings of L_F and C_F.

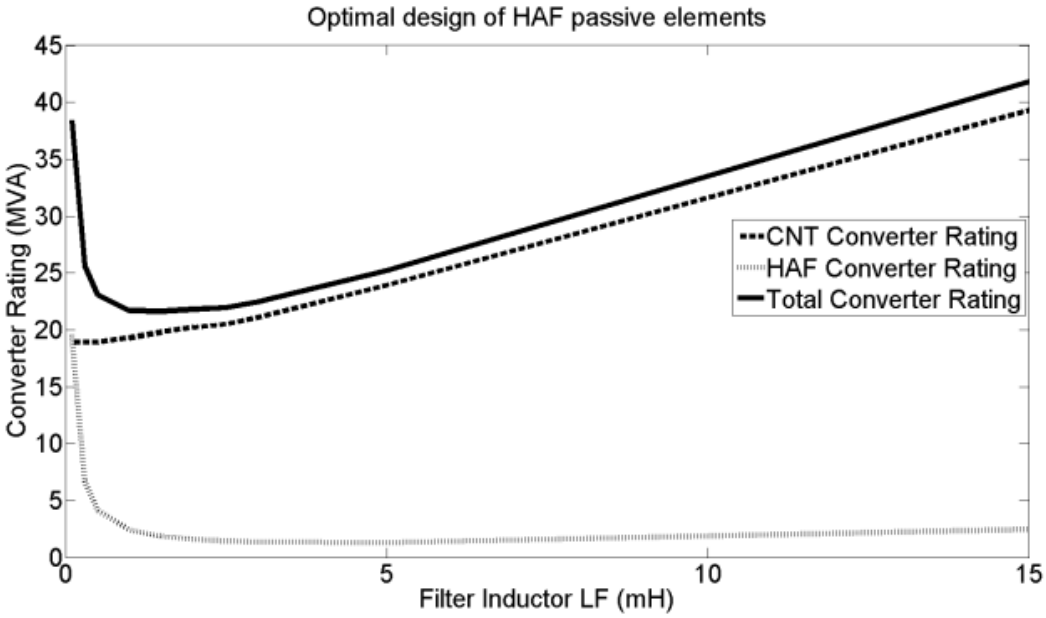

Figure 6.15: Optimizing the passive components of the series HAF

It is important to note that the VA rating of L_F and C_F, not only depend on the circulating 3rd harmonic current, but also on the fundamental current. The sum of the VA rating of the CNT converter and the HAF converter is used as the metric to indicate the best case design. It is seen from Figure 6.15, that the optimal choice of L_F is around 1.5 mH which is 10% of the line inductance.

6.4 Impact of Transformer Winding Configuration on CNT Harmonics

For this analysis the converter connected side of the transformer will be referred to as the primary side. It is assumed that the primary side of the CNT is connected to a pure sinusoidal voltage. In order to achieve Dual Virtual Quadrature Sources (DVQS) technique, the secondary voltage would have a fundamental as well as a 3rd harmonic component. It is clear from the discussion in the previous section that the 3rd harmonics generated by the CNT can be modeled using voltage sources on the secondary side and

current sources on the primary side. The effect of the secondary side 3rd harmonic voltage source can be negated by a series HAF filter, while the impact of the primary side 3rd harmonic current can be negated by a shunt HAF filter.

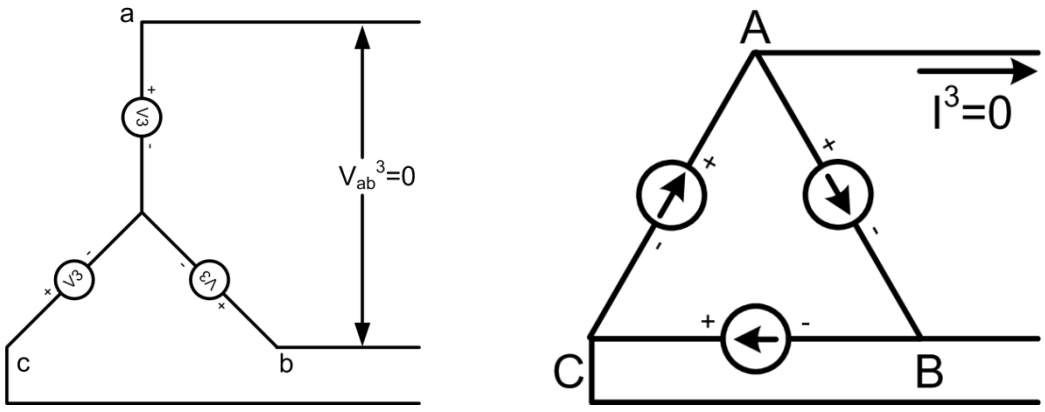

(a) Y connected secondary (b) Δ connected primary

Figure 6.16: CNT winding configurations for 3rd harmonic elimination during balanced operation

The primary and the secondary three phase transformer windings may be connected in Y or Δ configuration. In absence of a harmonic filter, the impact of CNT generated harmonics also depends on the winding configuration of the CNT transformer. For example if the secondary is connected in a Y configuration with neutral not connected, as shown in Figure 6.16(a), then for a balanced three phase system, the line-line voltages will not have any 3rd harmonic component and will thus not have any 3rd harmonic currents flowing in the system. Similarly for a Δ connected primary winding, as shown in Figure 6.16(b) it can be easily seen that under balanced conditions the line current will not have any 3rd harmonic component, though there will be circulating 3rd harmonic current. It must be noted that complete harmonic elimination using Y or Δ winding configuration can be achieved only in situations where the three phase system is

balanced. In practical situations a system may not be completely balanced, which can result in significant harmonic distortions, unless a dynamic filter is used.

6.5 Conclusions

This chapter discusses the impact of the triplen harmonics that are introduced by the CNT in the power system. It is seen that under normal circumstances the harmonic proliferation caused by the CNT is very high. The harmonics in the system can be eliminated by filtering techniques. Passive filters lack the dynamic response that is desirable, while active filters are expensive and complex solutions. HAF filters are low-cost solutions which have reasonably good dynamic response and thus can be used for filtering the harmonics produced by the CNTs. It is shown that for complete elimination of third harmonics two HAF filters are required – one in series on the secondary side and the other in shunt on the primary side. The chapter describes the scheme for closed loop control of the HAF and also shows its successful operation in simulation. The impact of the HAF filter on the P-Q control range of the CNT is also shown. Consequently the methodology of optimal design of the HAF is proposed. The possibility of elimination of third harmonics using appropriate Y or Δ configuration, in case of balanced operation, is also discussed in the chapter.

Chapter 7

7. DESIGN AND TESTING OF A MEDIUM VOLTAGE CNT PROTOTYPE

7.1 Introduction

Conventional power flow controllers are often based on three phase AC-DC-AC converters, compared to the single phase AC-AC converters that are used in the CNT. Although the CNT has many potential benefits over conventional power flow converters, the use of a radically different topology makes it a high risk, high gain approach. This is largely due to the fact that direct AC-AC converters have not been proven in high power applications. Control of high power direct AC-AC converters is considered much more difficult than the corresponding AC-DC-AC converters.

One of the major challenges in high power AC-AC converters is the scaling of the converters to multilevel topologies. The intermediate level voltages have to be precisely controlled to ensure equal distribution of dynamic voltages among all series connected AC switches. Also commutation of AC switches requires special attention as wrong commutation sequence can lead to open circuiting a current source or short circuiting a voltage source. Under those situations, because of the absence of any freewheeling diode paths, snubber paths are used by the converter leading to higher losses and voltage spikes.

The CNT in addition is expected to have another serious point of concern – the high third harmonic generation. Use of DVQS is central to the power flow capability of a

CNT. However use of DVQS leads to generation of third harmonic voltage in the output, which may cause significant third harmonic current to flow in a system, resulting in poor power quality. Such harmonic proliferation is not acceptable in utility industry. Hence it is essential to operate a CNT in conjunction with a third harmonic filter.

The most inexpensive method to filter a signal is by the use of passive LC elements. Since the third harmonic is a very low order harmonic, filtering it using passive solutions would have significant impact on the fundamental, which is not desirable. Besides passive filters have many issues like mismatch between LC components, resonance, etc., which often makes it an undesirable solution for power system applications. An active filter can provide very accurate harmonic cancellation and does not have the above issues of a passive filter. However implementation of an active filter is extremely expensive, especially for transmission level systems. A hybrid active filter (HAF) can be a relatively low cost, effective solution to the third harmonic mitigation problem in CNTs. A HAF employs a fractionally rated converter to simply compensate for the LC mismatch and other non-idealities.

7.2 Experimental System Design

To better understand the limitations and challenges that will be associated with scaling of the CNT technology to high power levels a single phase, medium voltage CNT prototype is built in the IPIC laboratory at the Georgia Tech. The prototype is built with an objective to demonstrate the power flow control capability of the CNT under realistic operating conditions. The CNT prototype is rated at 2.4 kV, 200 kVA and is capable of showing control over both real and reactive power flowing through the line. The CNT

prototype also has an internal third harmonic hybrid active filter (HAF) that ensures low third harmonic content in the line current.

The CNT prototype system is designed such that it can circulate ±200 kVA of power through a line. The schematic of the experimental system is shown in Figure 7.1. The system consists of two 240 V/2400 V transformers – *T1* and *T2*. The primary and secondary windings of each of the transformers are connected in series. The thin ac converter (TACC) is connected across the 240 V winding of *T1*. This helps in realization of a CNT whose taps can be selected between 2400 V and 2640 V. The AC switches are implemented by using two pairs of back to back IGBTs. The upper leg IGBTs are designated as S_{1A} and S_{1B} while the lower leg IGBTS as S_{2A} and S_{2B}. The converter input is smoothed by an input AC capacitor C_F. The output of the TACC is connected with the HAF block.

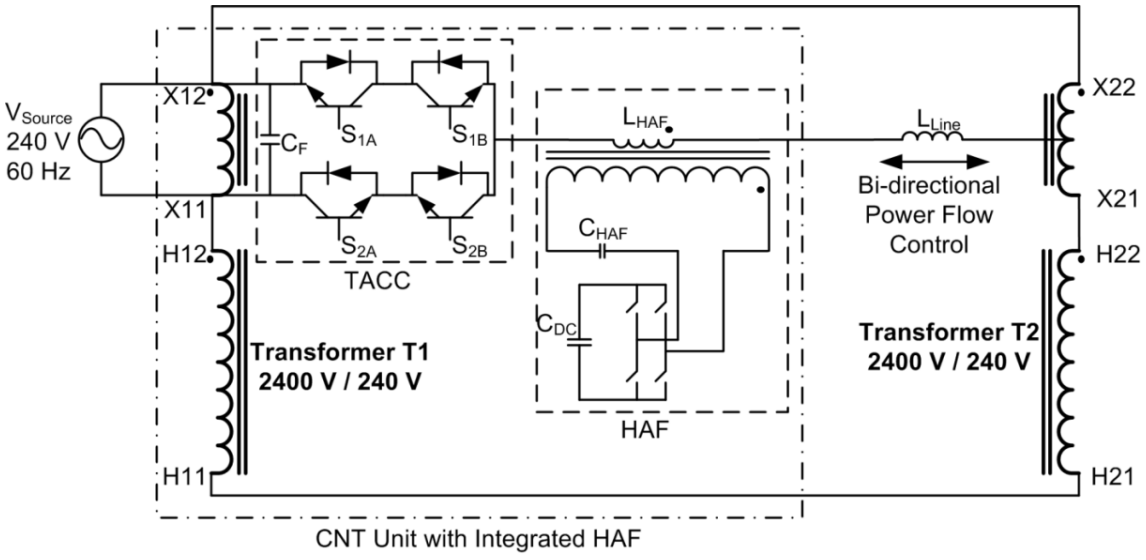

Figure 7.1: Schematic of the 200 kVA CNT prototype unit with integrated HAF

The HAF is essentially an LC trap that is tuned to the third harmonic frequency. The trap has infinite impedance at the third harmonic frequency and hence prevents any third harmonic current from flowing in the circuit. To ensure low current rating of the HAF converter, the HAF is implemented on the high voltage side of a series transformer. The magnetizing inductance of the transformer L_{HAF}, resonates with a AC capacitor C_{HAF} at a frequency close to 180 Hz. The slight mismatch between the actual and the intended resonating frequency is adjusted using the HAF converter.

The output of the HAF unit is series connected with an inductor L_{Line}, which represents the transmission line inductance. The other end of the inductor L_{Line} is connected to the center point of the low voltage winding of transformer *T2*. Thus the line inductor L_{Line} is connected to a constant voltage of 2640 V on one end and the output of the integrated CNT-HAF unit on the other. If the duty ratio of the CNT converter is kept constant at 0.5, then there should not be any real power flow in the line inductor. The experiment aims at showing ±200 kVA power flow along this line inductor with the help of the CNT. The HAF unit helps to minimize the third harmonic content of the line current.

7.3 Detailed Simulation of the Experimental System

To determine the ratings of various active as well as passive components of the experimental system various simulations are carried out using softwares like Matlab, Saber and Solidworks. The Matlab simulations are used to mainly understand the system level impacts of the various active and passive components. It is especially useful in finding the ratings of the various passive components of the system. The various ratings

of the system passive components are summarized in Table 4.1. Figure 7.2 shows the photograph of the converter input filter capacitor (C_F).

Table 7.1: Ratings of Passive Components for the Experimental System

Component	Rating
Converter Input Filter Capacitor (C_F)	200 μF, 500 VAC
HAF Transformer Magnetizing Inductance (L_{HAF})	7.8 mH (HV side)
HAF Resonating Capacitor (C_{HAF})	100 μF, 500 VAC
Line Inductance (L_{LINE})	480 μH
HAF Converter DC Link Capacitor (C_{DC})	20 mF, 200 VDC

The Matlab simulation is also useful in determining the power flow controllability that can be achieved by the resulting CNT prototype system. The experimental system having passive elements rated as shown in Table 7.1 is simulated in Matlab and the CNT converter is controlled at various operating points. The real power flowing through the line inductor can be controlled as shown in Figure 7.3, while the reactive power controllability is shown in Figure 7.4. It is seen that using the designed values of the passives the system is able to show ±200 kW controllability of real power and ±200 kVAR controllability of reactive power.

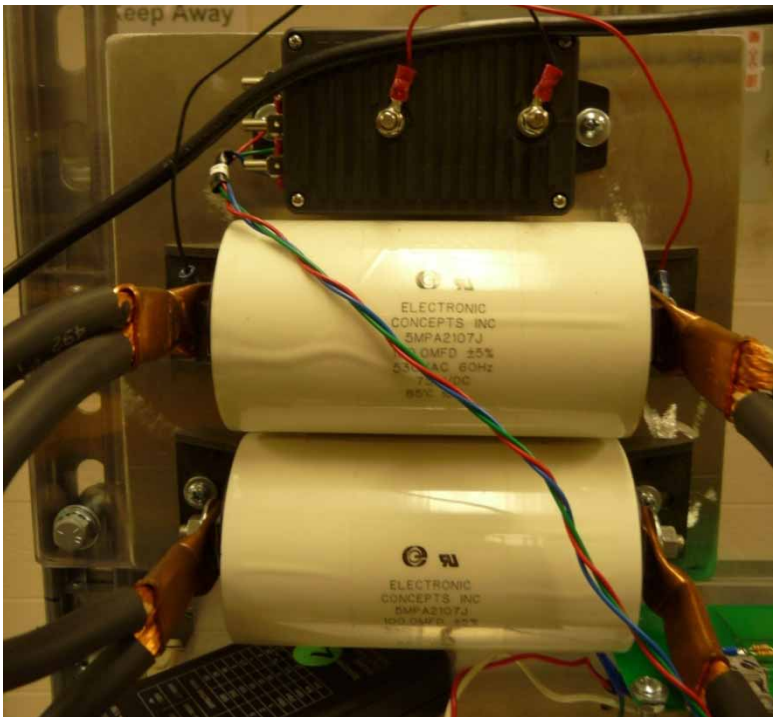

Figure 7.2: Converter input filter capacitor (C_F)

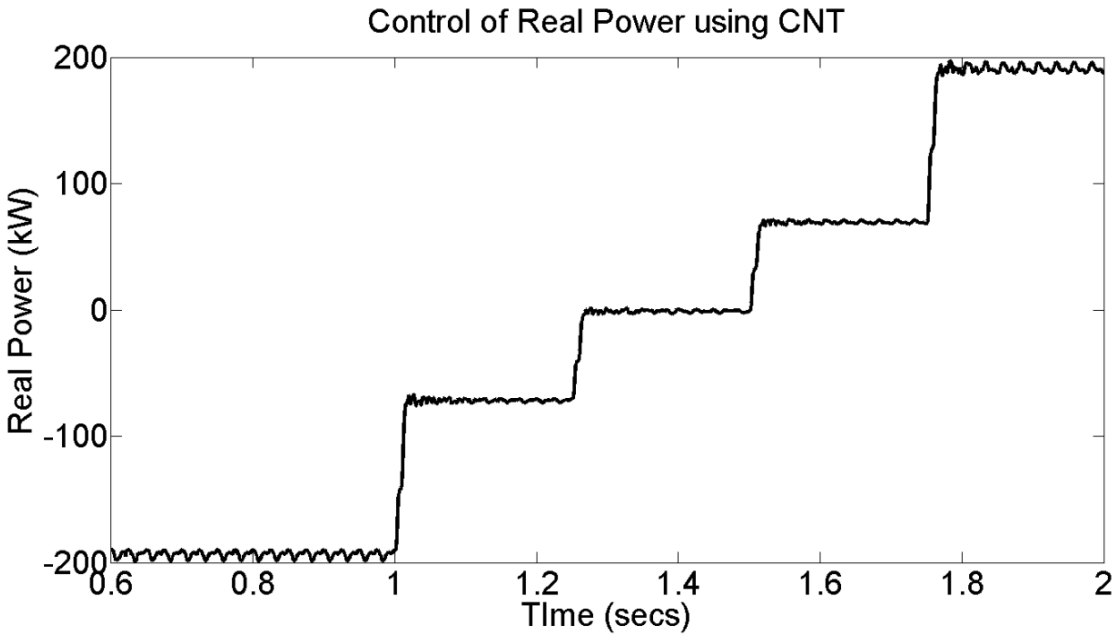

Figure 7.3: Real power controllability achieved by the experimental system

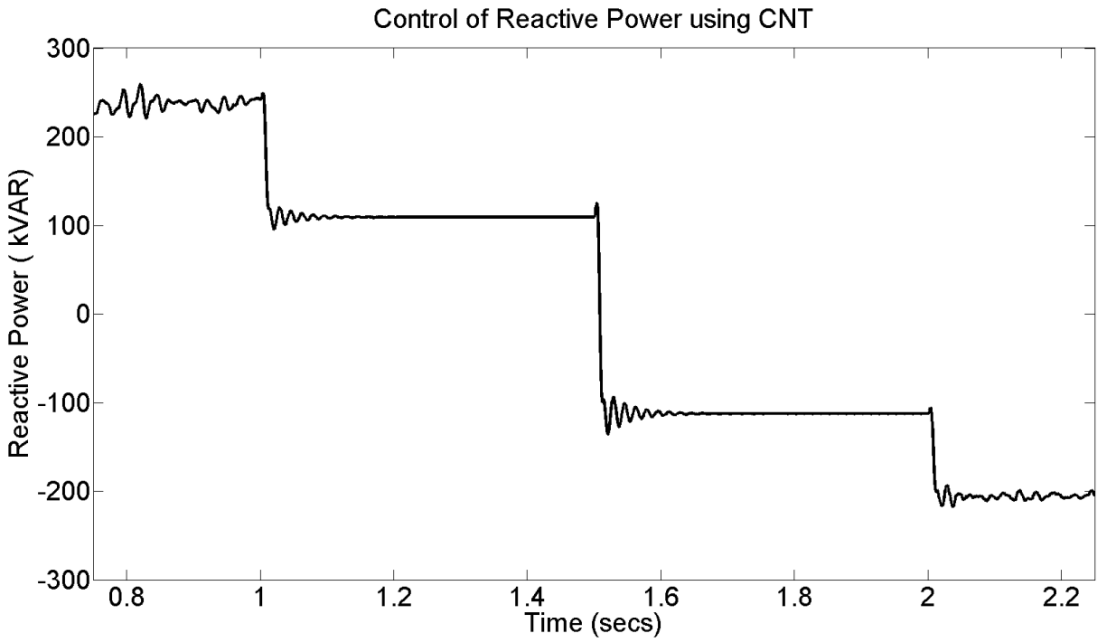

Figure 7.4: Reactive power controllability achieved by the experimental system

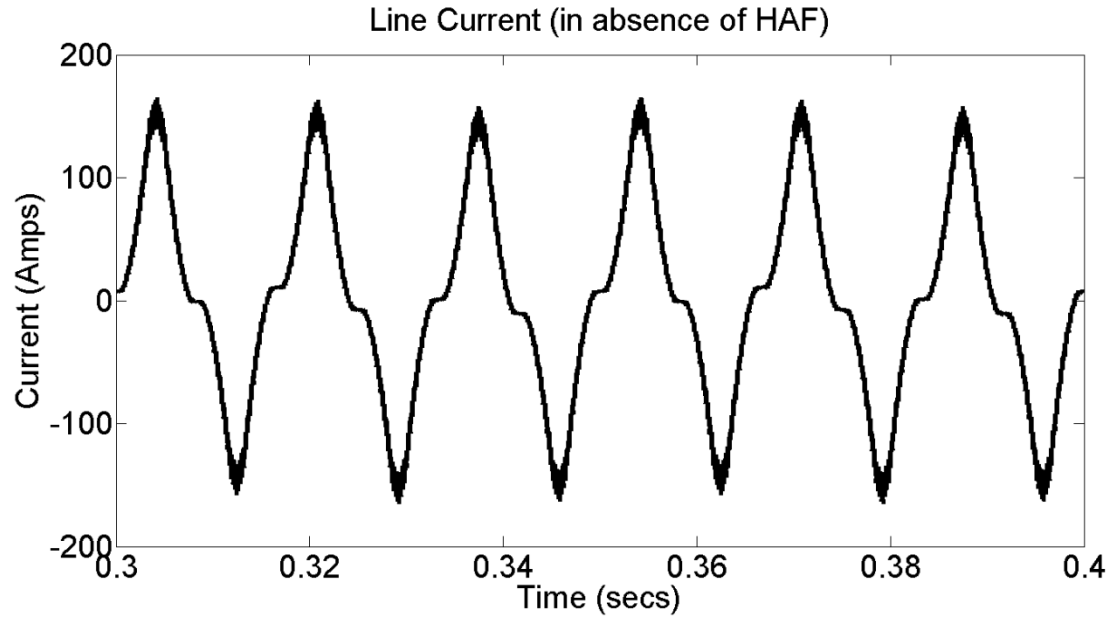

Figure 7.5: Line current with HAF not operational

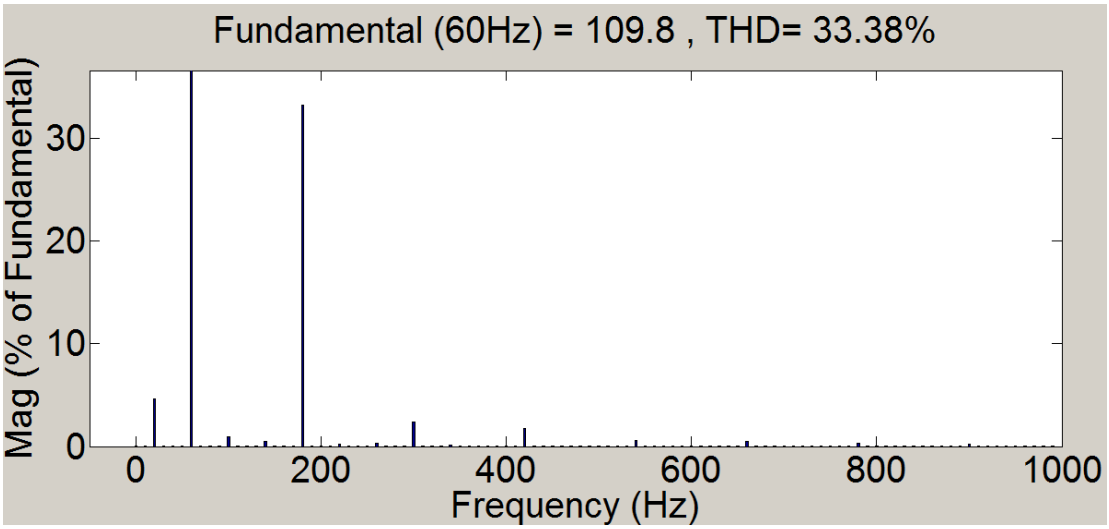

Figure 7.6: Frequency spectrum of the line current with the HAF nonoperational

The Matlab simulation is also helpful in determining the impact of the operation of the HAF circuit. The system is thus simulated with and without the HAF block in the operational mode. In Figure 7.5 the line current of the system is shown, when the HAF is nonoperational. It can be seen that the line current in this case has significant third harmonic content. The amount of harmonic distortion can be quantitatively determined by doing an FFT analysis of the current signal. The frequency spectrum analysis of the line current is shown in Figure 7.6. As can be seen from the Figure 7.6, the line current contains as much as 33% harmonics, mostly at the third harmonic frequency.

The HAF block is used to lower the third harmonic content of the line current to reasonable levels. Figure 7.7 shows the line current of the system, while Figure 7.8 shows the line current frequency spectrum, when the HAF is operational. It can be seen that the harmonic content of the signal has been lowered significantly by the HAF unit. The

resulting Total Harmonic Distortion (THD) of the line current is limited to less than 6% of the fundamental.

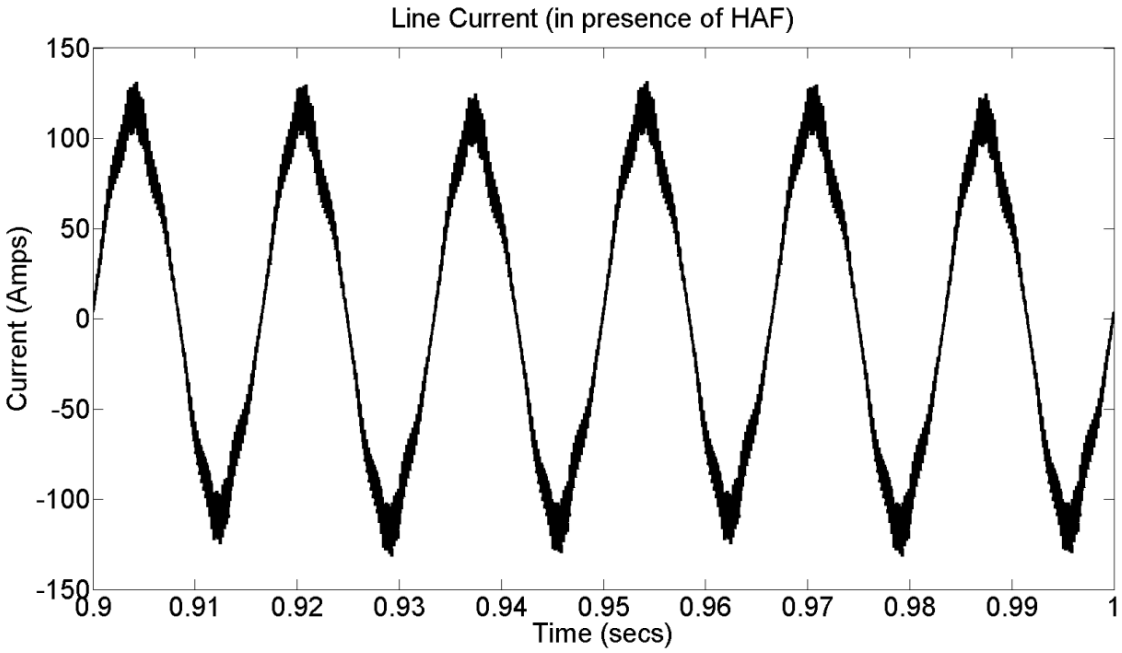

Figure 7.7: Line current with HAF operational

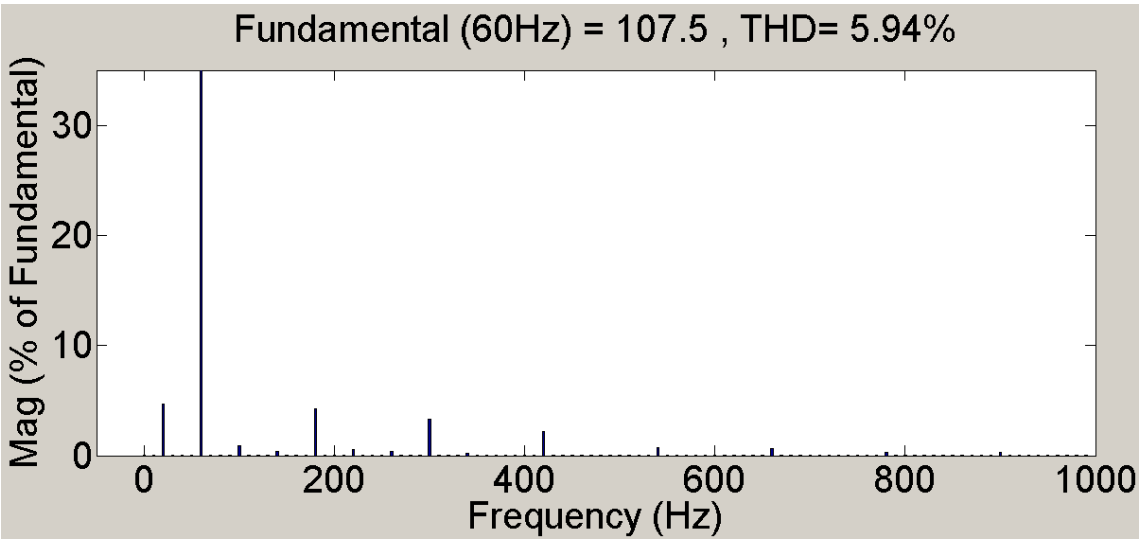

Figure 7.8: Frequency spectrum of the line current with the HAF operational

The HAF converter needs to be rated only a very small fraction of the TACC converter. This can be confirmed from the voltage and current waveforms seen across the HAF converter IGBTs. The maximum voltage across the IGBTs is same as the voltage rating of the dc link capacitor C_{DC} as can be seen from Figure 7.9. The maximum current through the HAF converter IGBTs is expected to be around 30 A, as can be seen from Figure 7.10. Hence IGBTs from International Rectifier (Part Number: IRGP30B60KD-EP) rated for 600 V, 60 A is chosen for the HAF converter.

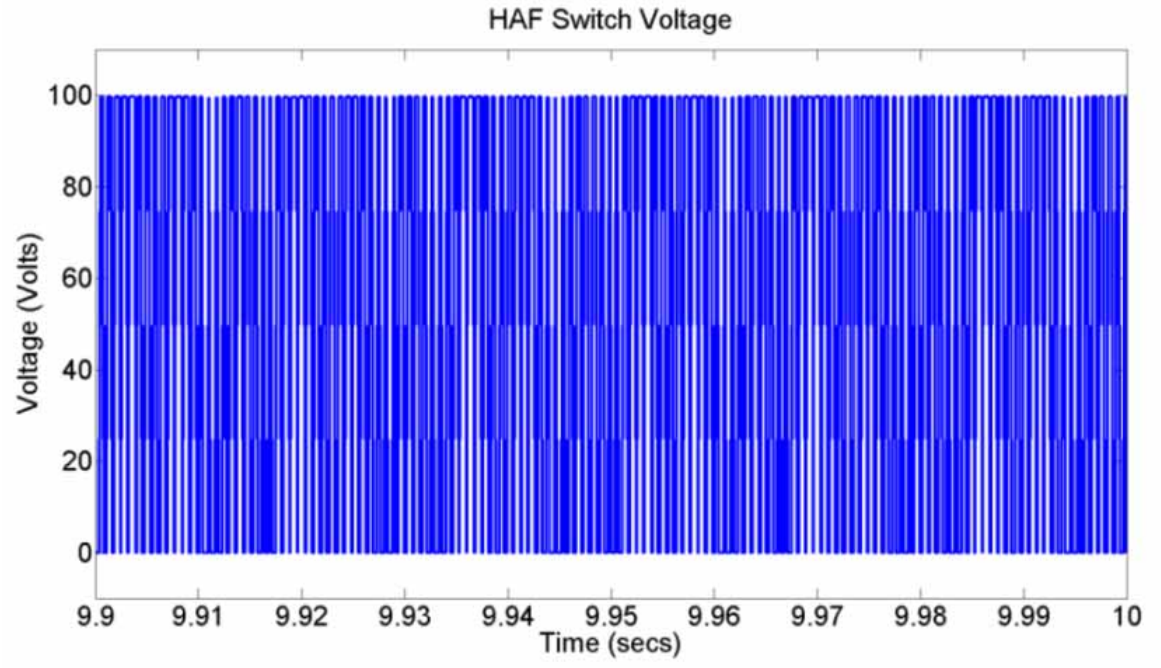

Figure 7.9: Voltage across the HAF converter IGBTs

The dynamic stresses on the active components of the system can be estimated using the detailed simulation in Saber software. The Saber simulation is used in finding an accurate estimate of peak voltage, current, etc. on the TACC converter IGBTs.

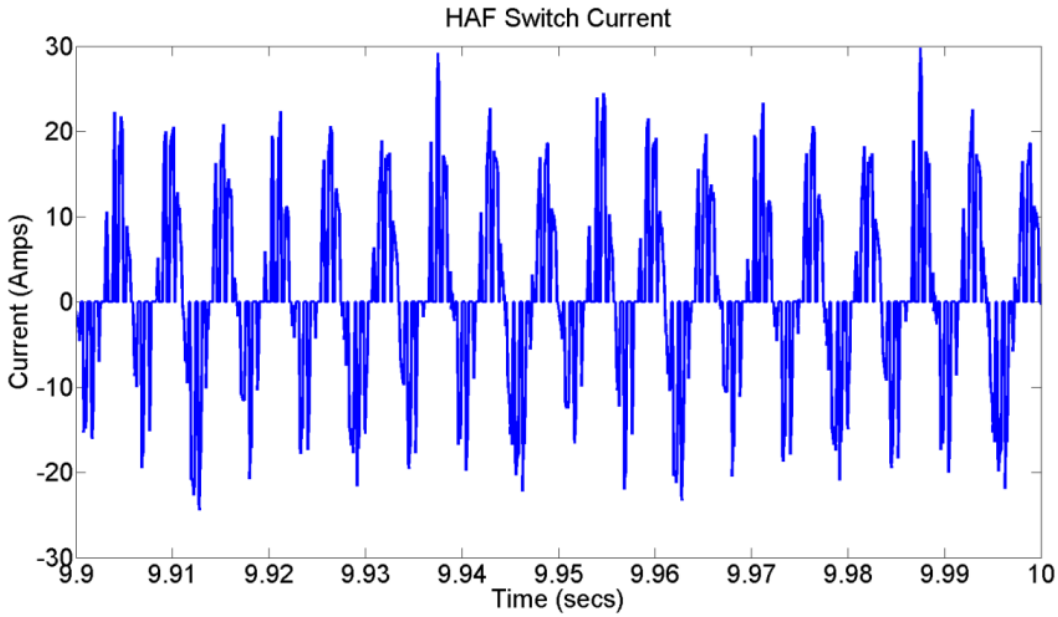

Figure 7.10: Current through the HAF converter IGBTs

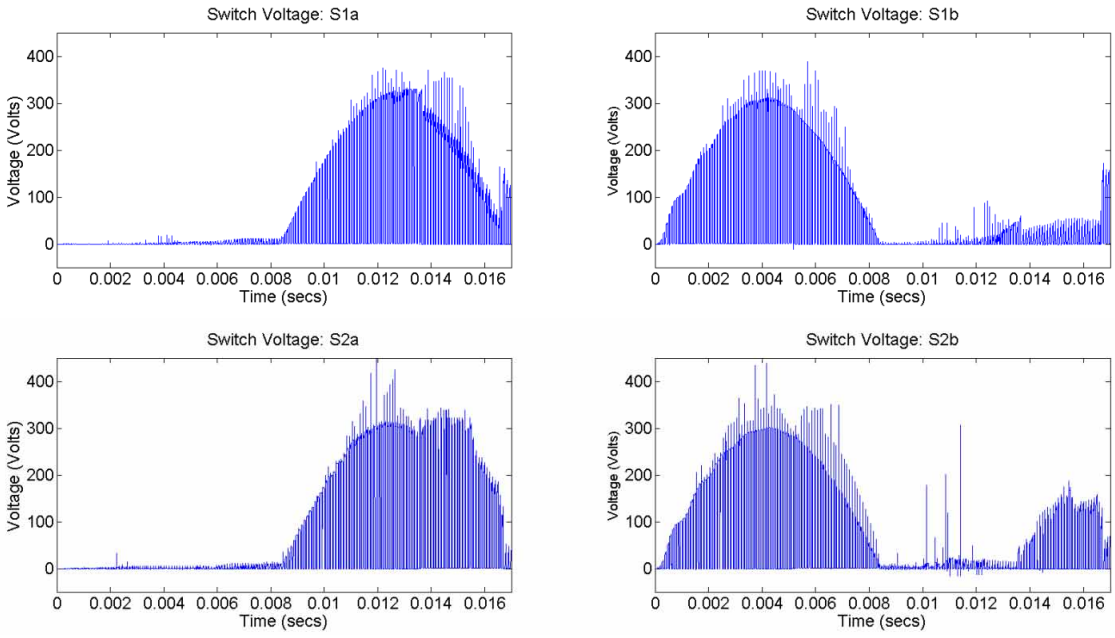

Figure 7.11: Saber simulation showing voltage across TACC IGBTs with passive snubber

The simulation is also used to find the optimal snubber for the switches. A Saber simulation of the TACC converter with passive RCD snubber is built. It is found that for

the optimal design of the snubber circuit, the peak voltage across the TACC IGBTs can be limited to 450 V, as can be seen from Figure 7.11. Powerex IGBTs (Part Number: CM400HA-24A) rated at 1200 V, 400 A are chosen as the TACC converter switches.

7.4 Building the Hardware

For high power converters, one of the major challenges is the proper mechanical layout and building of the converter. On one hand properly addressing issues such as insulation, grounding, etc. help in protection of the equipment. On the other hand a good mechanical layout may also reduce undesirable parasitic elements, which may have otherwise resulted in voltage/current spikes, resonance, etc. Further issues such as thermal management of active and passive elements are also a critical part of the converter design.

For proper estimation of the power loss in the IGBTs of the TACC converter, a switch characterization experiment is required. This is because in AC converters, both the switch blocking voltage and the switch current varies along a sine wave. The IGBT datasheets typically provide switching loss information for only a particular voltage and current. This data is not sufficient for loss estimation of the converter over the full 60 Hz cycle. A lab setup for characterizing the IGBT module (CM400HA-24A) has been setup. The setup schematic for the switch characterization experiment is shown in Figure 7.12, while Figure 7.13 shows the photograph of the setup.

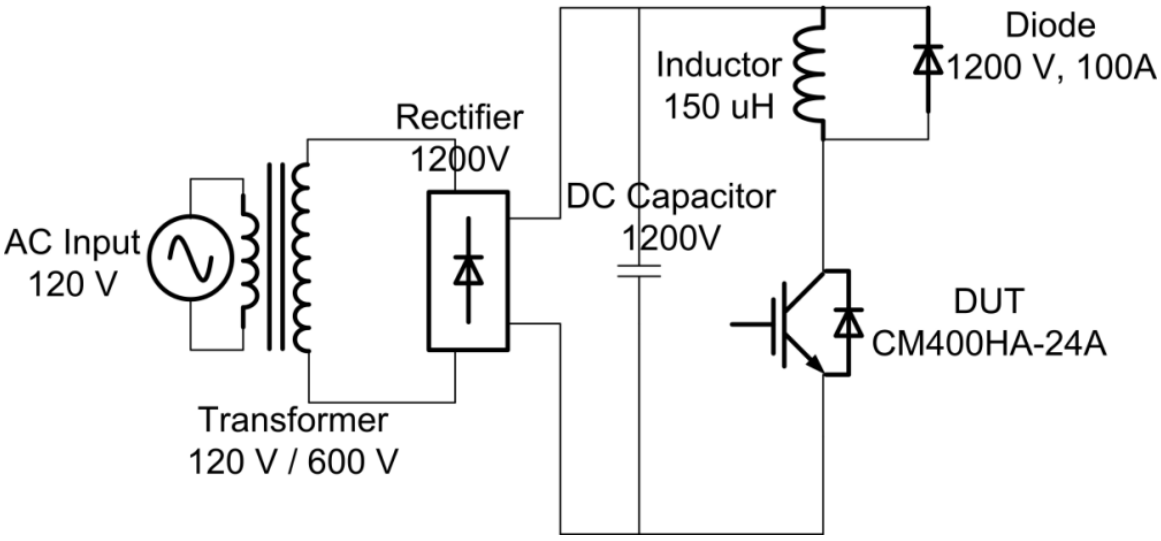

Figure 7.12: Schematic of the switch characterization setup

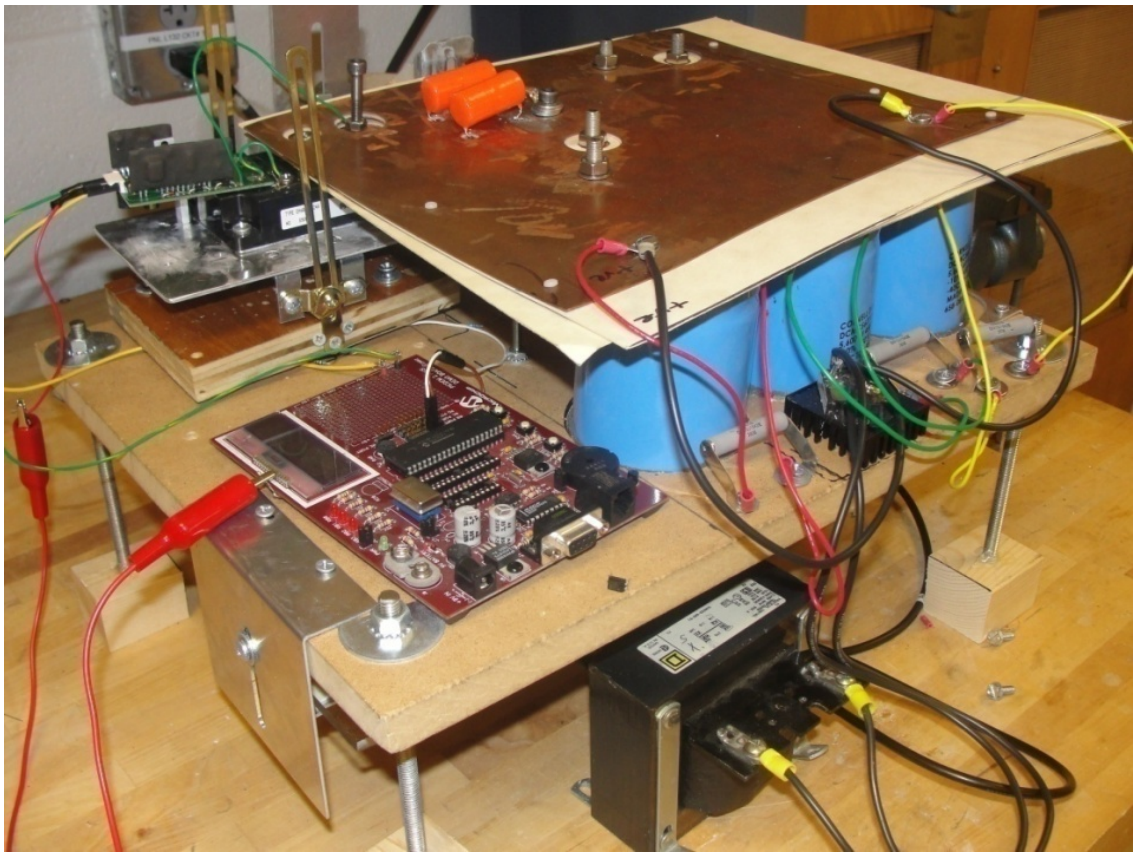

Figure 7.13: Photograph of the switch characterization setup

The choice of gate driver circuit is also a crucial element in the TACC design. Since the TACC converter has to be driven under very high current conditions, Powerex gate driver M57962L, with VLA106_15242 DC-DC converter mounted on BG1A boards is selected. Since the losses in an IGBT depend heavily on the gate resistance, the optimal choice of the gate resistance is found out using the switch characterization experiment.

The IGBT losses are calculated for various operating points. For a particular value of the gate resistance the IGBT losses are calculated over various voltage and current levels. This procedure is repeated for various values of gate resistance. The estimated losses of the IGBTs are stored in a simple Look-Up-Table (LUT) corresponding to each voltage and current levels. From the Matlab simulation the various switching conditions of the TACC devices is recorded over a 60 Hz cycle. The turn-on and turn-off losses stored in the LUT will be then used to estimate the total losses of the TACC over a 60 Hz cycle. The total loss of power in the TACC is proportional to the switching frequency. Hence the loss estimation procedure would help in determining the optimal TACC switching frequency as well as designing the corresponding cooling system (heat sinks and fans) of the TACC.

The results showing the turn-off and turn-on losses for the IGBT module CM400HA-24A for various voltages and currents are shown in Figure 7.14 and Figure 7.15 respectively. The optimal value of the gate resistance is found to be 2 Ω, while the optimal switching frequency is calculated to be 5 kHz. It is estimated that the losses in the TACC converter would not exceed 300 Watts, hence Wakefield Series #1 heat sink

with double fan forced convection, having a thermal resistance of 0.025 °C/W is chosen for the TACC.

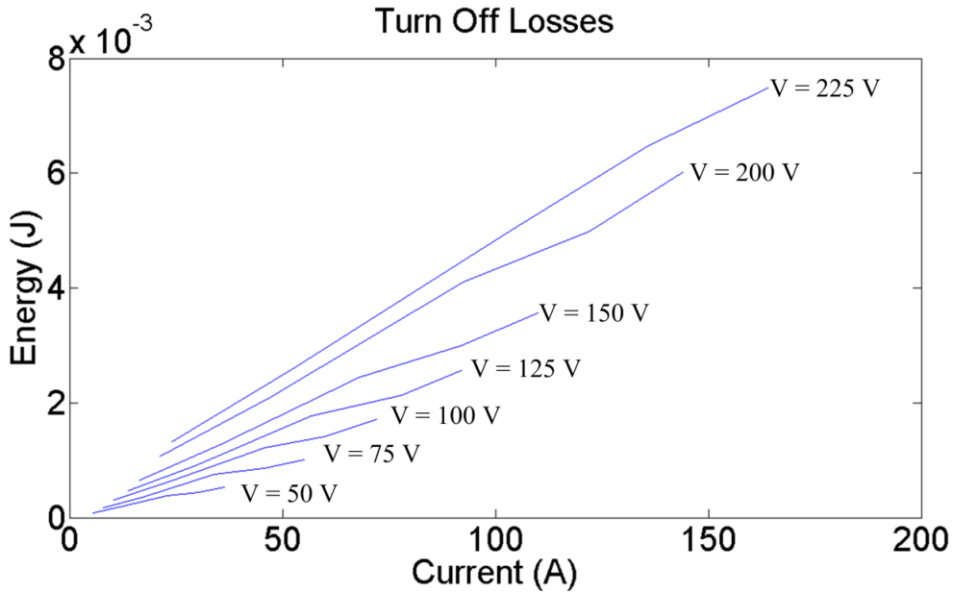

Figure 7.14: Turn-off losses for CM400HA-24A

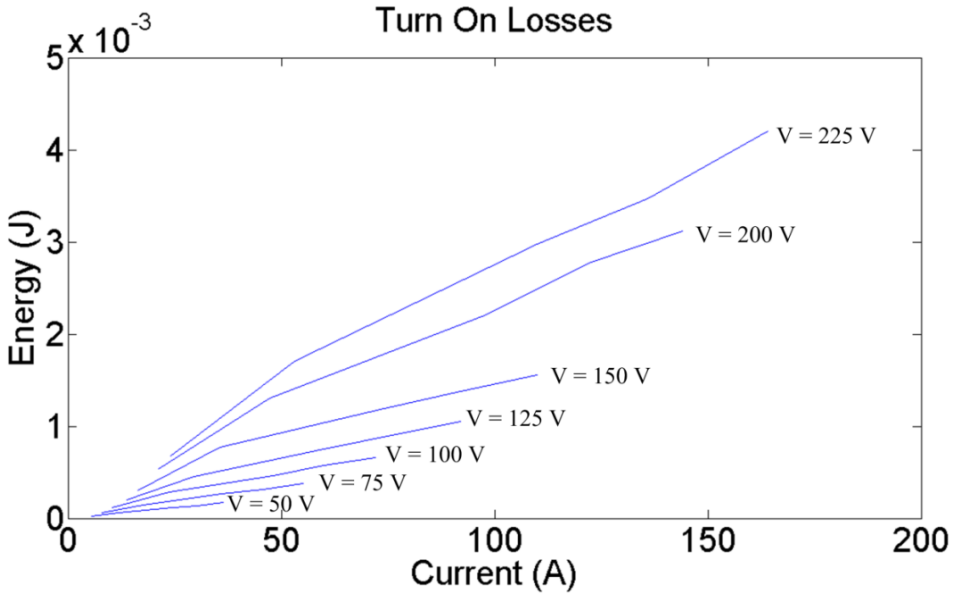

Figure 7.15: Turn-on losses for CM400HA-24A

The mechanical layout of the 200 kVA CNT with integrated HAF unit is designed in Solidworks. The three dimensional layout helps in understanding of various clearances and other space requirements of the experimental setup. Issues such as mounting of various parts such as gate drivers, heat sinks can also be resolved in an early stage. Besides the layout also helps in estimating various factors such as the dimensions of the bus-bars required, estimated length of the power cables, placement of control circuitry, etc. The 3-D concept design of the 200 kVA CNT prototype with integrated HAF is shown in Figure 7.16. The front panel houses the transformer *T1* and the TACC on the heat sink, along with the input capacitors (C_F). The back panel houses the HAF converter along with the line inductor L_{LINE}.

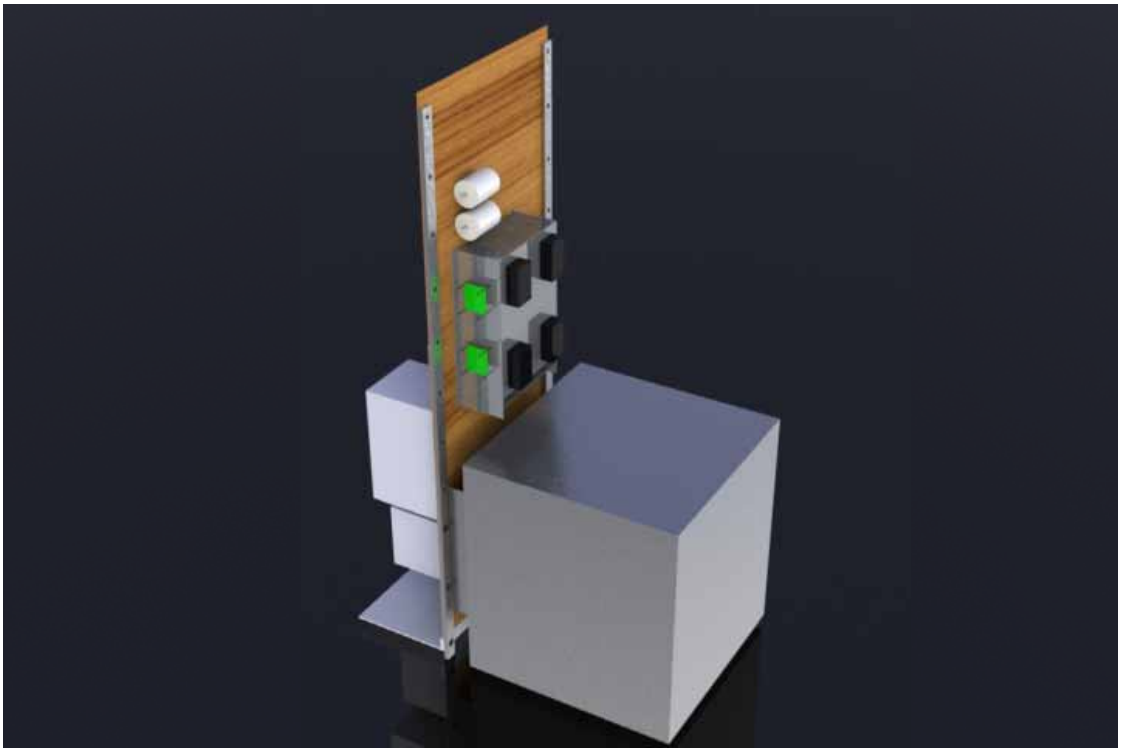

Figure 7.16: Three dimensional concept design of the CNT prototype in Solidworks

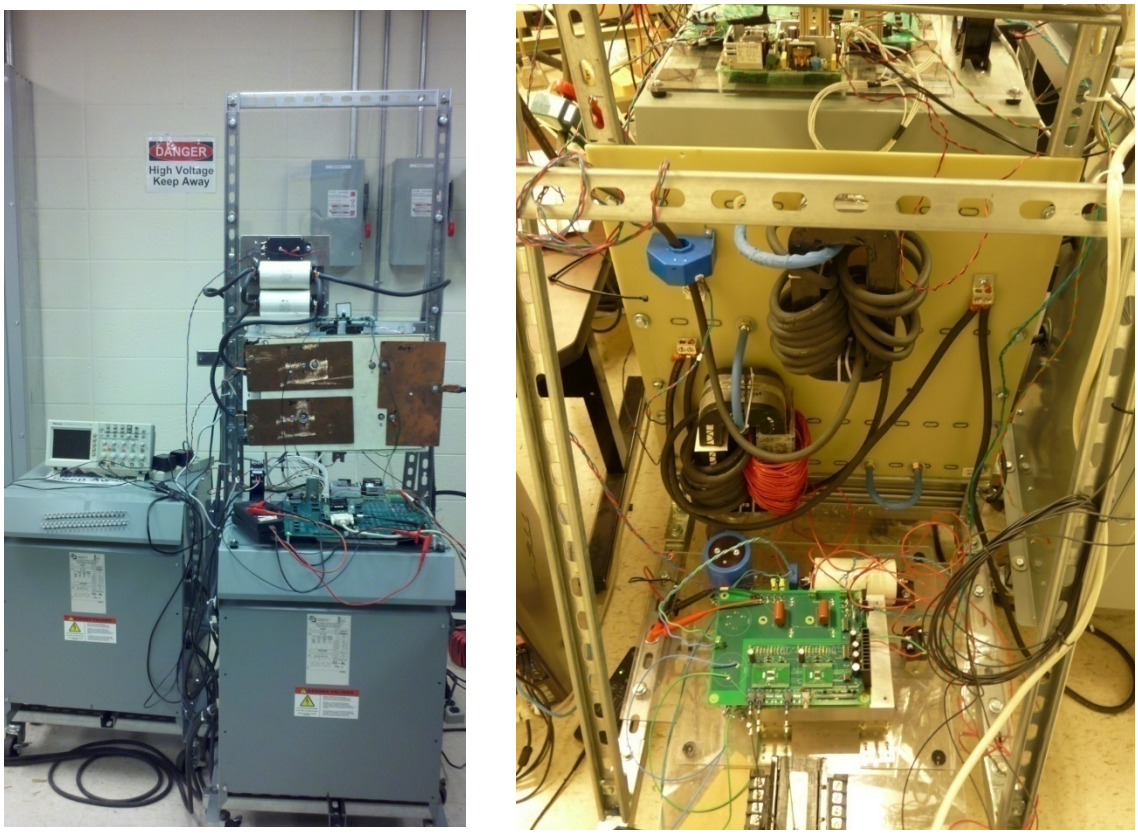

(a) (b)

Figure 7.17: Photograph of the CNT prototype (a) front and (b) rear view

The prototype is built in the IPIC laboratory. Figure 7.17 (a) shows the front view photograph of the CNT prototype experimental setup, while Figure 7.17 (b) shows the rear view.

7.5 Sensors and Control Architecture

The experimental setup is controlled dynamically. The TACC converter is controlled in an open loop while the HAF converter is controlled in a closed loop. The Texas Instruments DSP part number TMS320F2812 is chosen as the controller unit. The controller obtains the state of the system through the sensors. Sensors play a key role in the architecture of any converter – especially for direct AC converters where obtaining

the zero current and/or voltage crossing has critical impact on converter performance. Closed Loop Hall-Effect sensors have high precision and are hence used for the experiment. Figure 7.18 shows a photograph of LEM AV100-750 (750 V maximum rms) and LEM 305-S (300 A maximum rms), which are used as the voltage and current sensors respectively.

Figure 7.18: Photograph of voltage (left) and current (right) sensors used

The readings obtained from the sensors are scaled and level shifted to 0-3 V range to be compatible with the DSP. The DSP uses these measurements to obtain the desired PWM switching waveform for the TACC as well as the HAF converters. The TACC PWM signal is fed to an EEPROM, which is used to generate the gate drive signals for the TACC converter using the correct commutation sequence.

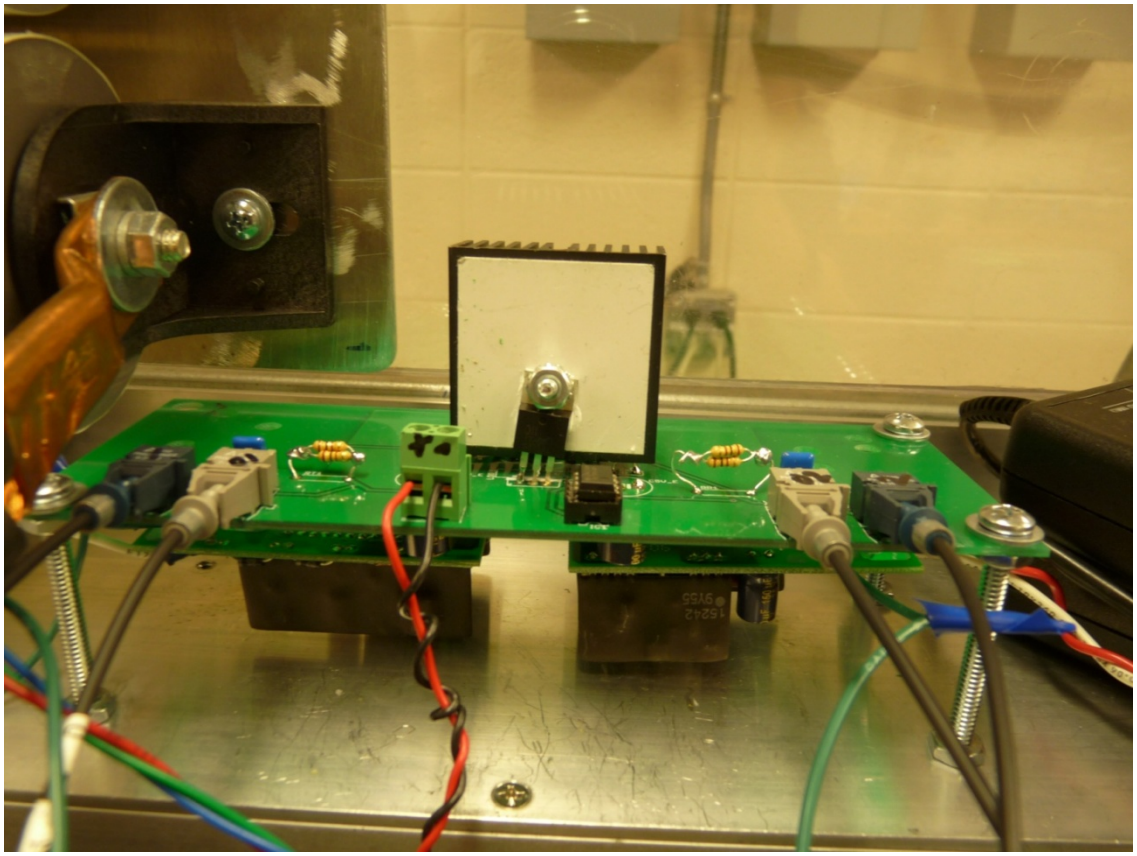

Figure 7.19: Gate driver receiver boards for the TACC IGBTs

The gate driving signals for the TACC and the HAF converters are then transmitted to the respective gate driver boards using fiber optic communication transceivers. The gate drivers are equipped with de-saturation detectors, which help identify possible converter faults. The fault signals are fed back to the main controller board and are used by the Fault Management System to ensure overall equipment protection. Figure 7.19 shows the photograph of one of the gate driver receiver boards which receives the fiber optic communication from the main board and sends the correct gate-emitter voltages to TACC IGBTs.

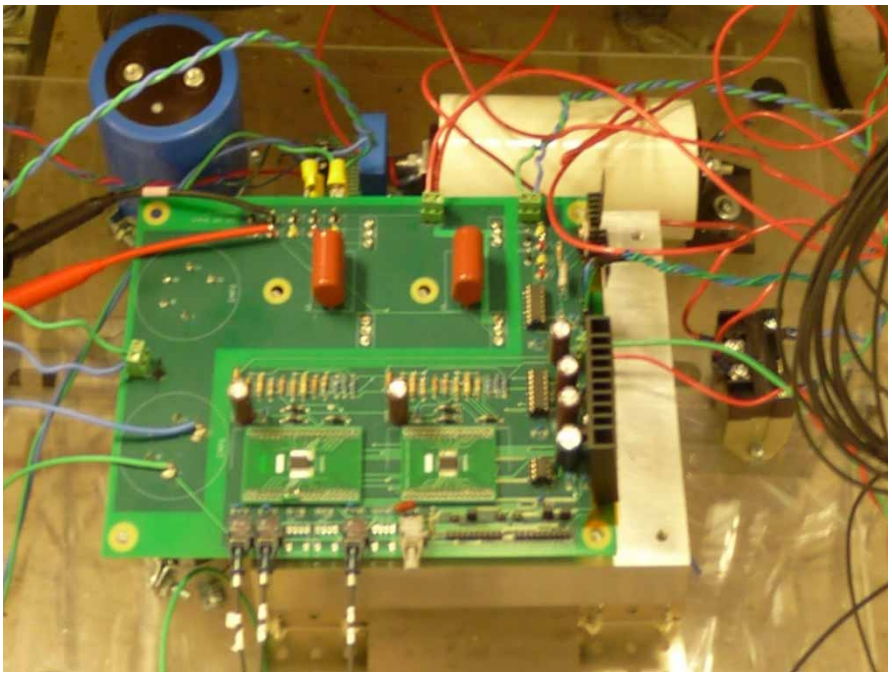

Figure 7.20: HAF converter and HAF gate driver boards

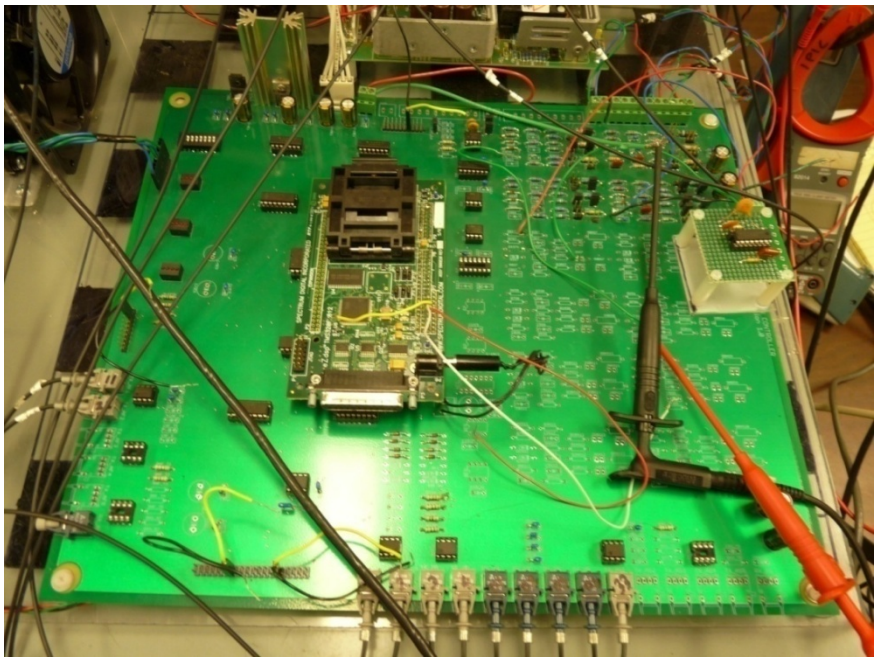

Figure 7.21: DSP mounted control board

Figure 7.20 shows the photograph of the HAF converter along with the HAF gate driver boards. Figure 7.21 shows the photograph of the DSP mounted control board used for controlling the CNT prototype, while the overall control architecture for the experiment is shown in Figure 7.22.

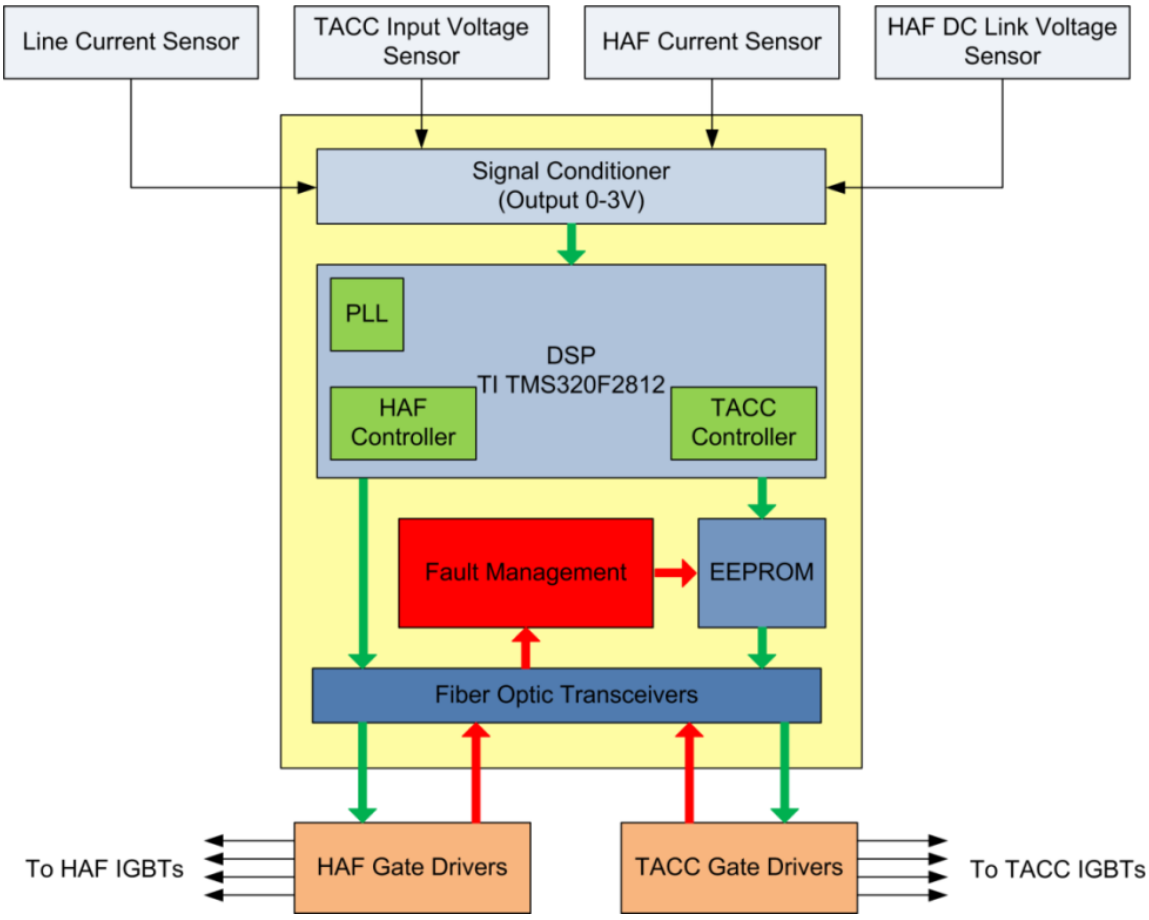

Figure 7.22: Overall control architecture

7.6 Testing Results

The experimental setup is tested in a step by step manner to ensure equipment and personnel safety. Since most of the equipment are built and assembled in the laboratory, special care is taken to ensure compatibility of the individual components with each

other. The setup is first tested for lower voltages and current levels before being tried out at higher voltage and current levels.

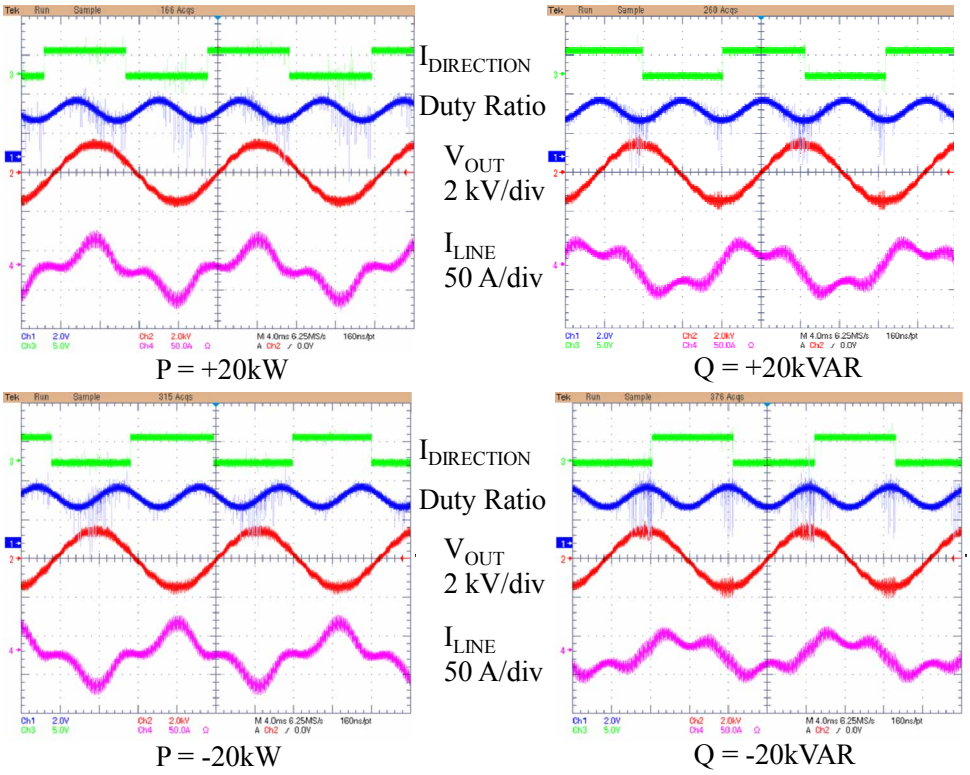

Figure 7.23: Testing the CNT prototype at 20 kVA without the HAF filter

Initially the prototype is testing in absence of the HAF filter. The output voltage and line current waveforms of the CNT at 20 kVA levels are shown in Figure 7.23. The output rms voltage is 1 kV and rms line current is 20 A at this operating point. It is seen from Figure 7.23 that by modifying the duty ratio of the CNT converter, it is possible to change the phase relationship between the voltage and the current. Hence the CNT is shown to be capable of controlling the line power to be fully active or fully reactive in either direction. Although Figure 7.23 shows the four quadrant control capability of the

CNT, it is also seen that the line current has significant third harmonic component in absence of the HAF filter.

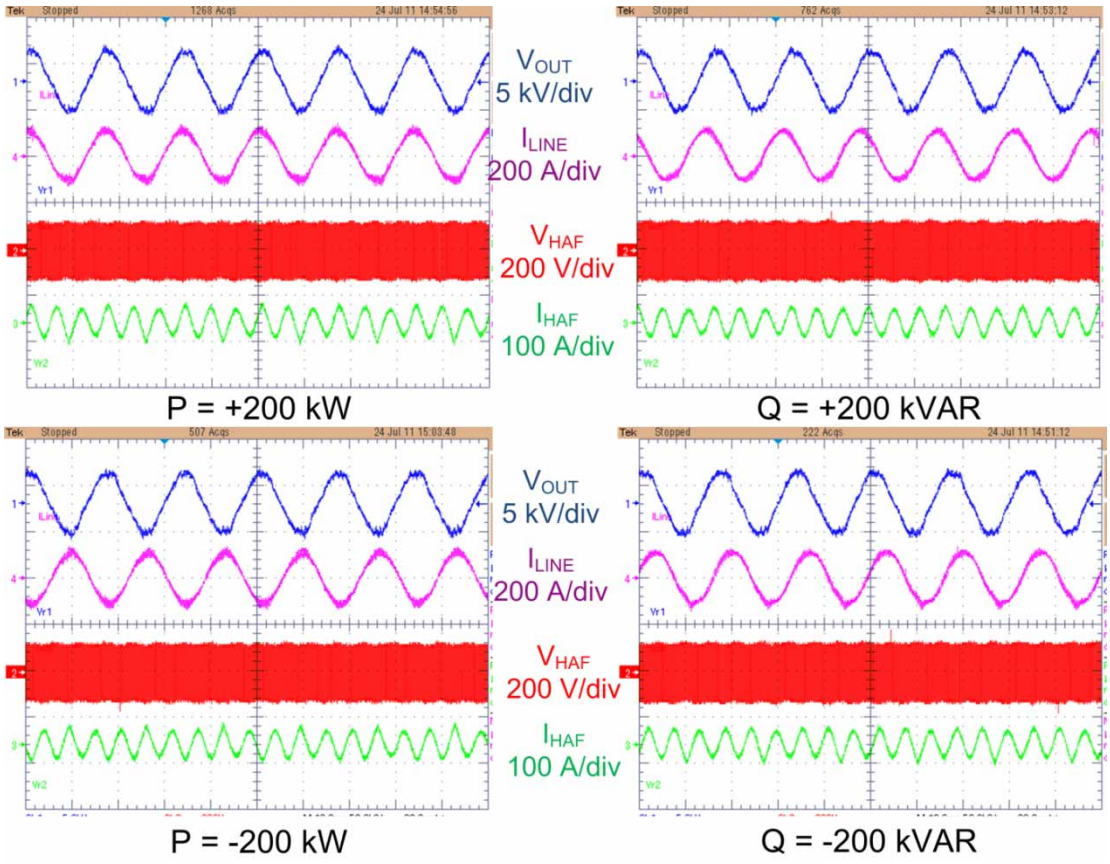

Figure 7.24: Testing the CNT prototype at 200 kVA with the HAF

The testing results of the CNT with the HAF operational are shown in Figure 7.24. It is seen that the CNT can control the line power over all four quadrants. The presence of the HAF filter also ensures very little harmonic content in the line current. The output PWM voltage of the HAF and the third harmonic circulating current in the secondary of the HAF transformer are also shown in the plots. The output voltage at this operating point is 2.4 kV while the line current is 85 A. It is seen that the HAF converter IGBTs have to block around 120 V peak while the circulating third harmonic current is only 21

A rms. As a result the HAF is required to be rated only 2 kVA which is just 1% of the CNT rating.

The THD analysis of the line current is shown in Figure 7.25. It is seen that with the HAF the THD of the current is reduced to just 2.62% which is well within acceptable norms of utilities.

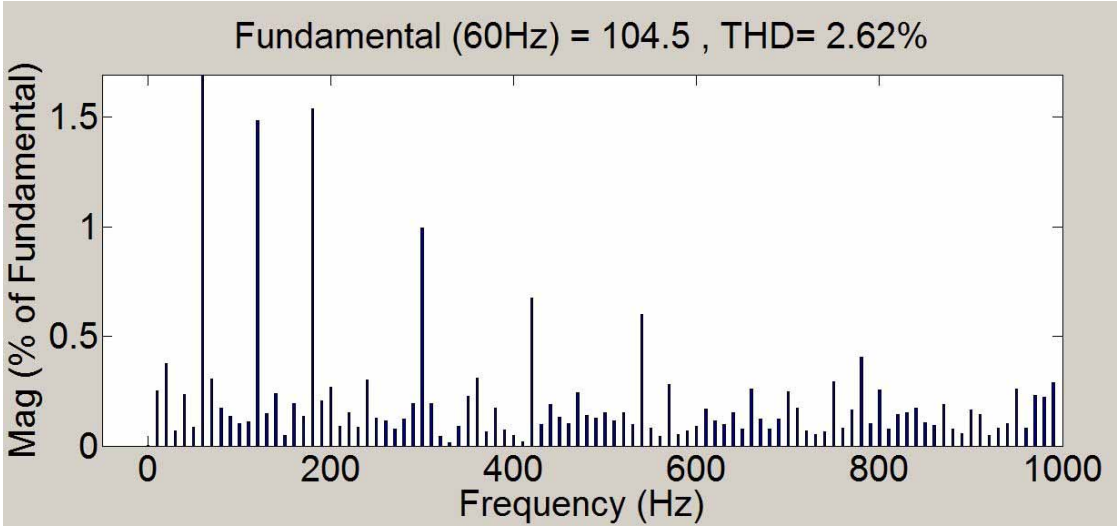

Figure 7.25: THD of the line current

7.7 Loss Calculations

The addition of the TACC and the HAF to the pre-existing LTC has been shown to add a significant control range to the asset, while ensuring compliance with low THD requirements of typical utility systems. However both the TACC and the HAF converters have some losses associated with them. In this section the losses in the TACC and the HAF converters for the experimental prototype is estimated.

The loss in the TACC and the HAF converters are estimated by finding the difference of the power input and power output of the converter. Figure 7.26 shows the voltages and

the currents measured in the experimental schematic for the loss calculation analysis. The measured input and the output voltages for the TACC are marked as *Vm1* and *Vm2* respectively, while the measured input and output currents are marked as *Im1* and *Im2* respectively. Similarly for the HAF, the input and output voltages are labeled as *Vh1* and *Vh2*, while the input and output currents are marked as *Ih1* and *Ih2*. The various voltages and the currents recorded with the CNT running at 180 kVA are shown in Figure 7.27 to Figure 7.34.

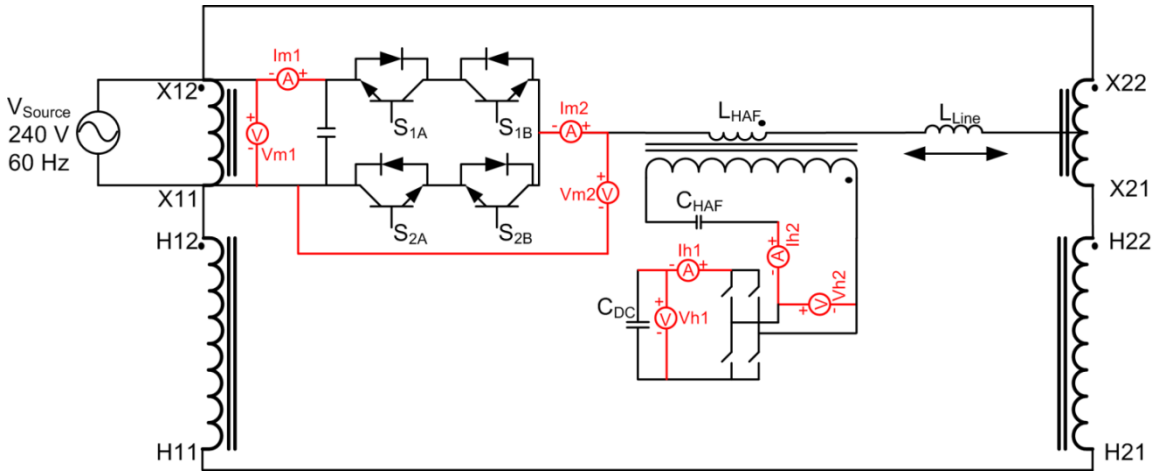

Figure 7.26: Measurements used for loss calculations

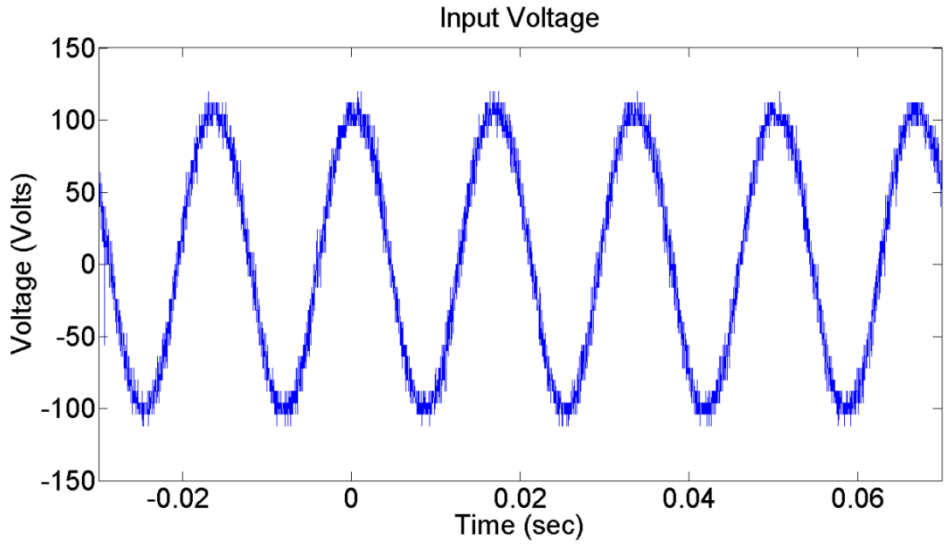

Figure 7.27: Measured TACC input voltage (*Vm1*)

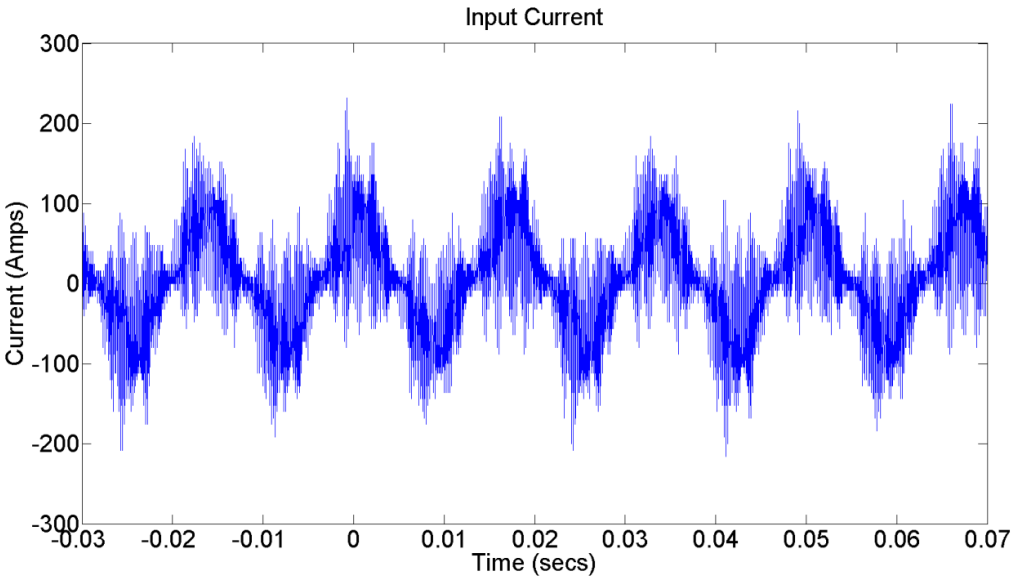

Figure 7.28: Measured TACC input current (*Im1*)

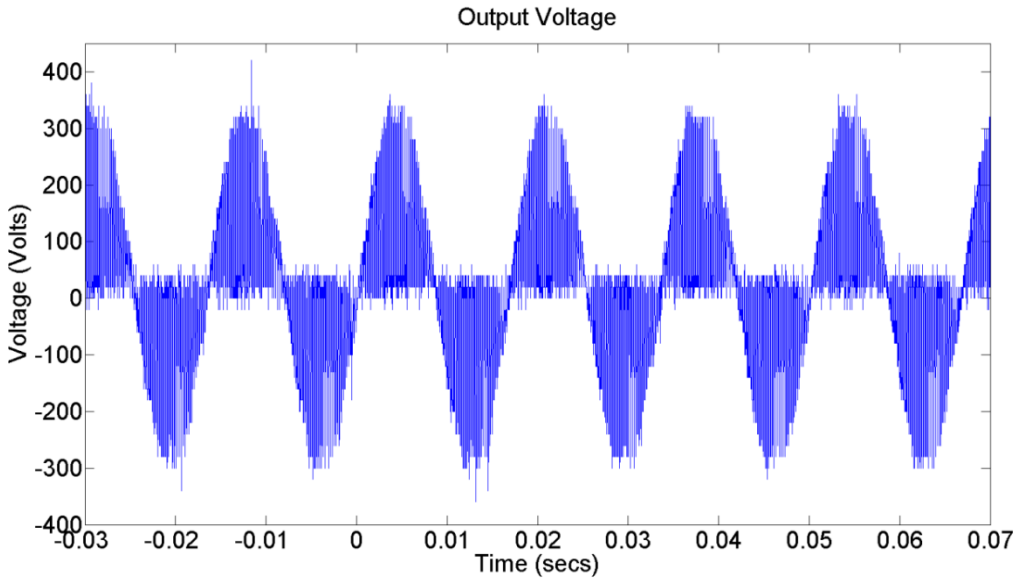

Figure 7.29: Measured TACC output voltage (*Vm2*)

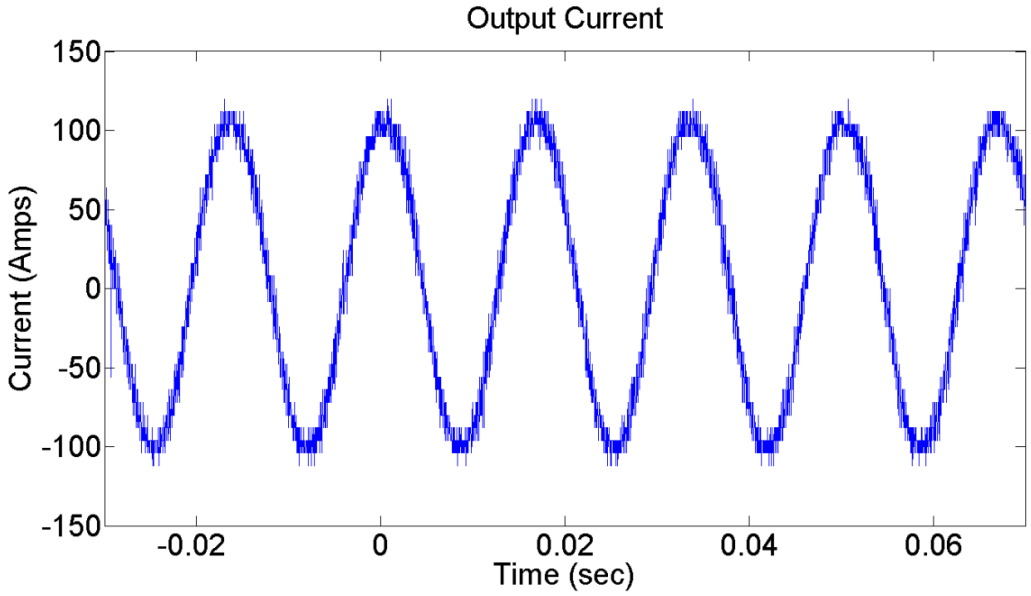

Figure 7.30: Measured TACC output current (*Im2*)

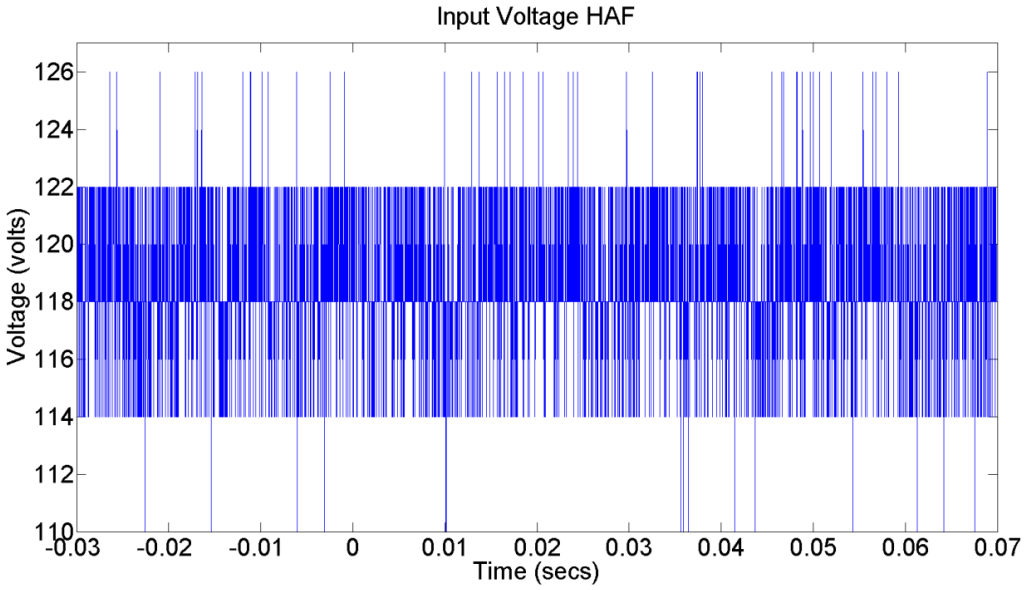

Figure 7.31: Measured HAF input voltage (*Vh1*)

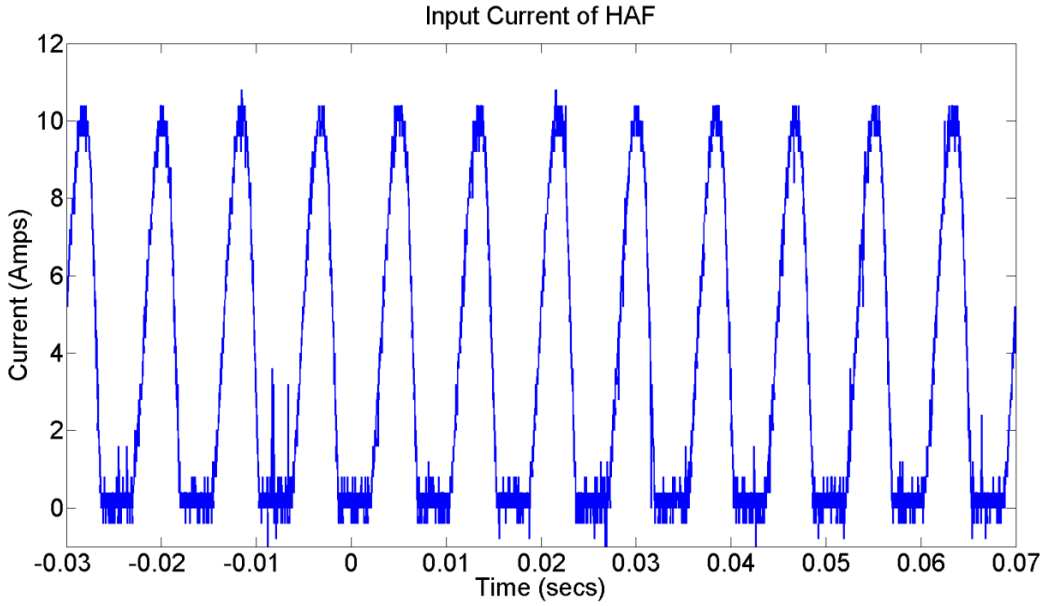

Figure 7.32: Measured HAF input current (*Ih1*)

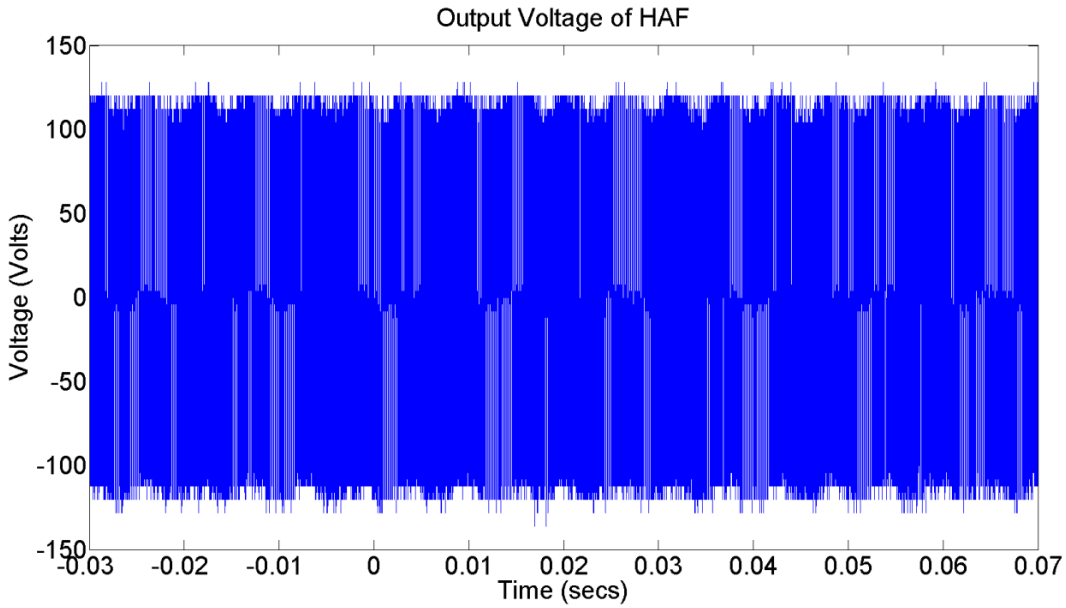

Figure 7.33: Measured HAF output voltage (*Vh2*)

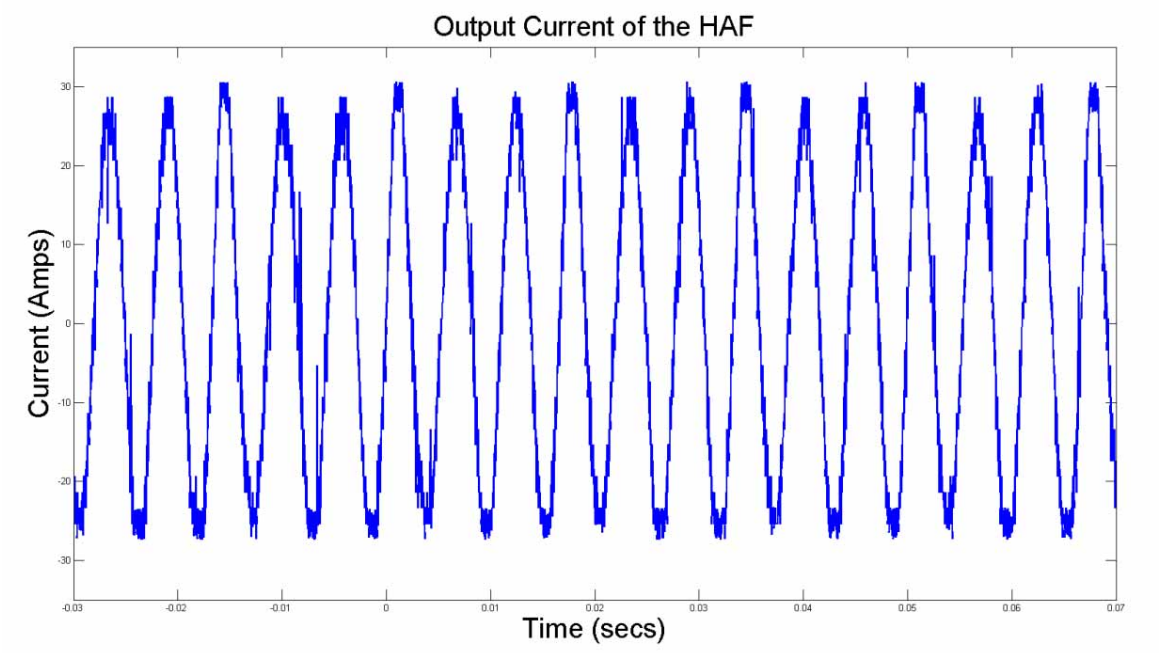

Figure 7.34: Measured HAF output current (*Ih2*)

The obtained voltages and currents are filtered digitally and the power at the input side and the output side is calculated by taking the product of the voltage and the current averaged over 1 second. The loss in the TACC converter is found out to be about 250 Watts. From the device characterization experiment it is estimated that the losses in the TACC should be about 240 W. Thus the loss calculated for the TACC converter is in close agreement to that estimated from the device characterization experiment. On the other hand the losses in the HAF converter are calculated to be about 130 W. Thus the total losses in the converters are 380 W which is only about 0.21 % of the VA throughput of the CNT.

7.8 Dynamic Power Flow Control Demonstration

The experimental set-up is also used to demonstrate the dynamic power flow control capability of the CNT. The phase of the 2^{nd} harmonic content of the duty cycle is varied gradually to achieve the desired power flow control.

Initially the power flow is 100 kW which is changed to about -60 kW within about 20 seconds as shown in Figure 7.35. Similarly by varying the phase of the 2^{nd} harmonic content of the duty cycle in the reverse direction it is possible to change the power flow in the line from -60 kW to 200 kW, as shown in Figure 7.36.

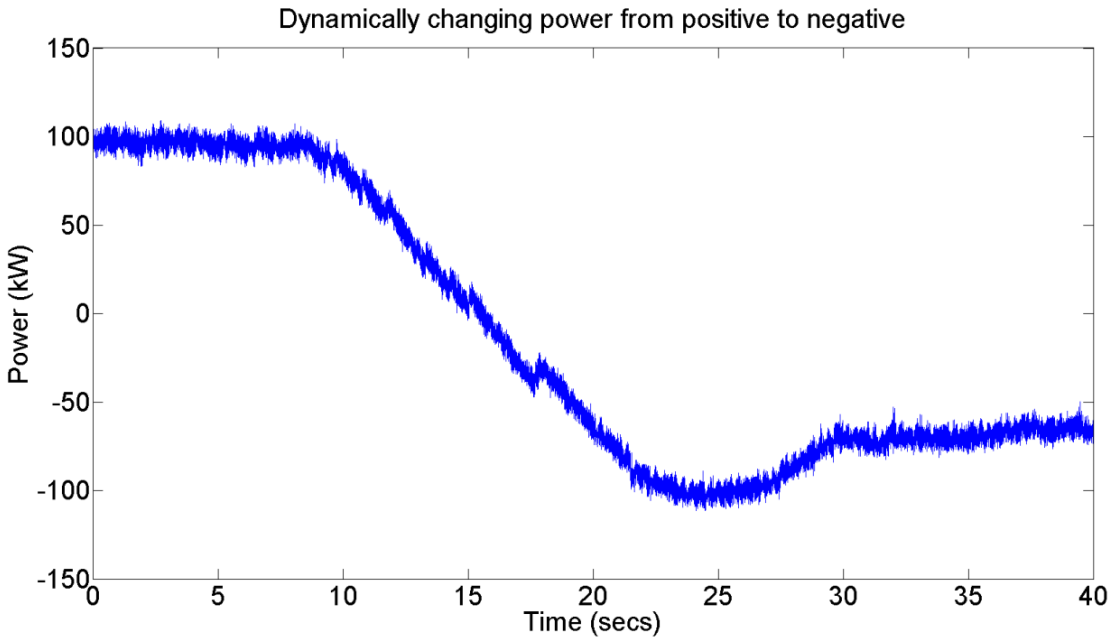

Figure 7.35: Dynamic change of power direction from positive to negative

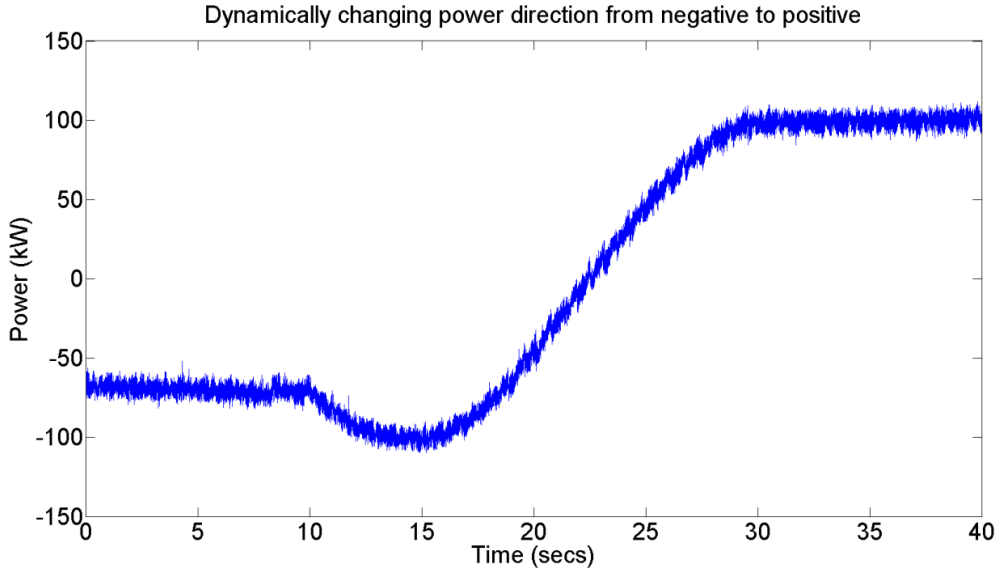

Figure 7.36: Dynamic change of power direction from negative to positive

7.9 Conclusions

The chapter describes the design, implementation and testing of a medium voltage CNT prototype rated at 2.4 kV, 200 kVA. It is seen that for bidirectional control of 200 kVA power it is sufficient to have a direct AC-AC converter rated at just 10% VA rating and a HAF converter of just 1% VA rating. Also the cumulative losses in these converters at rated VA operation are seen to be only 0.21%. These numbers obtained by experiment can be used towards estimating losses and converter VA ratings of CNTs required in transmission systems.

Chapter 8

8. CONTRIBUTIONS AND FUTURE WORK

8.1 Introduction

The dissertation developed a cost-effective, dynamic power flow controller called the Controllable Network Transformer (CNT) that can be used to increase the throughput of the transmission network. Power flow controllers available presently are mostly associated with high cost, high complexity and low reliability. The CNT, which can be realized by augmenting existing Load Tap Changing (LTC) transformers with a direct AC-AC converter, is seen to potentially overcome most of these challenges.

8.2 Conclusions

8.2.1 Steady state model derivation of the CNT

A steady state model for the CNT is developed. The model analytically links the active and reactive power flowing through the CNT with the terminal bus voltages, the line impedance and the CNT converter control parameters. Many dc-link based converters are modeled in synchronous reference frames. As a result for system studies, quantities often have to be converted from the three phase frame to the synchronous reference frame and back. Understanding and interpreting such models can often be complicated. The developed steady state model of the CNT does not require any such synchronous frame conversion and is intuitively easy to understand.

The steady state model of the CNT has proved to be advantageous for various reasons. It can help in understanding the impact of the converter control parameters on the active and reactive power flow. From the system perspective it helps in understanding the impact of change in terminal conditions on power flow. The range of control of the CNT can also be defined with the help of the model. The basic principle of operation of the CNT along with its bi-directional power flow controllability is verified in hardware at low-voltage conditions. The experiment also highlighted the requirement of a third harmonic filter.

8.2.2 Identifying the application space of the CNT

The add-on realization of the CNT is one of the main reasons for potential low-cost implementation. Power networks are often connected to their neighboring systems with tie-lines for reliability purposes. Most of these tie-lines are provided with Load Tap Changers (LTCs) for seasonal control of the reactive power flow. The tie-lines are mainly built for contingency scenarios, whereby neighboring areas can relieve a system under stress. However lack of dynamic control of such tie-lines makes them susceptible to large power oscillations and even eventual disconnection during such contingency scenarios. CNTs are identified as a potential cost-effective tie-line power flow controllers. The improved performance of tie-lines with CNTs under post-contingency scenarios is shown in simulation.

8.2.3 Modified loadflow for the CNT

Traditional Newton-Raphson loadflow tool cannot be used for systems with CNTs as the power flow equations for the CNT controlled lines are modified. A modified Newton-

Raphson loadflow tool is thus developed which is capable of accommodating CNTs. The modified loadflow tool helps in understanding the impact of CNTs on large power networks for a given generator dispatch. The impact of various converter control parameters on the power flow of a large network can also be understood using this tool. The modified tool is tested on a modified IEEE 30 bus system.

8.2.4 Modified OPF for the CNT

The introduction of the CNT in the transmission network makes the power network more flexible. A modified optimal power flow tool is developed which takes advantage of the added transmission system flexibility and finds the most economical combination of generators along with the optimal set-point of the CNTs. In order to ensure compliance of various network constraints the concept of non-linear penalty functions are used. The tool uses the concept of Particle Swarm Optimization (PSO) for searching the most economical and feasible solution. The tool is tested on two different systems – a small 7 bus system and a larger modified IEEE 30 bus system.

8.2.5 Optimal placement of the CNT

In order to extract the maximum benefit for the power network from the CNT technology, the CNTs must be sized and placed optimally. A Particle Swarm Optimization (PSO) based approach is proposed to solve this optimal placement problem. A modified IEEE 30 bus system is taken and its cost of energy is calculated in absence of any power flow controllers. It is seen that for optimally placed CNTs the savings incurred in the form of lower generation cost can be used to pay back for the CNT installations in

just 1.25 years. In comparison, the payback period for traditional power flow controllers like the Back-To-Back was calculated to be about ten times more at 11 years.

8.2.6 Improved system dynamics

The CNT has fast switches which can be used effectively to damp out power system oscillations and transients. This can not only improve the dynamic stability of the system but can also increase the effective Available Transfer Capacity (ATC) of a corridor. The transient oscillation damping can be achieved by a simple bang-bang controller. The proposed transient control is shown to be effective in a simple two bus system.

8.2.7 Optimal third harmonic filter design

The CNT produces third harmonic voltages and currents which must be mitigated by harmonic filters. A hybrid active third harmonic filter is proposed for preventing third harmonic line currents from flowing in the transmission system. The hybrid active filter is a low-cost design having a converter rating of just 1% of the line power. It is also dynamic enough to cancel out the third harmonics in a real system. The Hybrid Active Filter (HAF) with a large inductor is shown to lower the power flow through the CNT controlled line, while that with a small inductor is shown to increase the rating of the HAF. As a result a trade-off is required between the two. An optimal design technique for the harmonic filter has been proposed. For a small test system it was shown that the optimal inductance of the HAF should be about 10% of the line inductance.

8.2.8 Medium voltage implementation

A medium voltage prototype CNT rated at 2.4 kV, 200 kVA with an integrated HAF is designed, built and tested in the laboratory. The prototype CNT is shown to have four

quadrant real-reactive power flow control. The direct AC-AC converter is rated at 10% of the line power while the HAF converter is rated at 1% of the line power. The resulting THD of the line current is shown to be less than 3%. The losses in the AC-AC converter is found to be 240 W, while that in the HAF is found to be 130 W. Thus augmenting the existing LTC with the Thin AC Converter and the HAF is seen to increase the total losses by only 0.21% of the VA throughput. The ability of the CNT to dynamically change the power flow direction over a few seconds has also been demonstrated.

8.3 Contributions

A paper titled "Power flow control in networks using controllable network transformers" was published in the *IEEE Energy Conversion Congress and Exposition, 2009* [36]. This was the initial paper that presented the low frequency modeling technique for the CNT. The paper also showed the real and reactive power flow control capability of the CNT and also presented the low voltage experimental results. This paper was later published at the *IEEE Transactions on Power Electronics, 2010* [38].

A paper titled "Smart tie-line control using Controllable Network Transformers" was published in the *IEEE PES Transmission and Distribution Conference and Exposition, 2010* [40]. The paper highlighted the use of CNT as a cost-effective tie-line power flow controller. It also presented various case studies to show the impact of CNTs on larger networks.

Another paper titled "Increasing inter-area available transfer capacity using controllable network transformers" was published in the *IEEE Energy Conversion Congress and Exposition, 2010* [39].The paper presented the impact of various terminal

conditions of the CNT control range and the ability of the CNT in increasing available transfer capacity of a tie-line corridor. The paper also presented the ability of the CNT to damp power system oscillations.

The work on the medium voltage CNT prototype has been published in the *Energy Conversion Congress and Exposition, 2011* under the title "Design and Testing of a Medium Voltage Controllable Network Transformer Prototype with an Integrated Hybrid Active Filter". The paper presented the details of the design, building and testing of the medium voltage CNT prototype. This paper has been submitted to the *IEEE Transactions on Power Electronics* for review.

An invention disclosure titled, "Transmission Line Power Flow Control using Controllable Network Transformer with Hybrid Active Filter" has been filed with the Georgia Tech Research Institute on January 2011. The disclosure is mainly on the architecture and control of the integrated CNT-HAF system.

Overall the contributions of the research are summarized as follows:

- Development of a low-cost power flow control technology which modifies an existing grid asset.
- Development of a simple steady state model of the CNT which can be used by power system engineers to understand the impact of the CNTs on small or large systems.
- Development of a modified Newton-Raphson loadflow tool that can be used for calculating loadflows of systems with CNTs.

- Development of a modified optimal power flow tool that can be used to find the optimal dispatch of the system generators in conjunction with the optimal steady state set-points of the CNTs.
- Proposed strategy to control CNT under transient conditions such that power system oscillations can be effectively damped.
- Proposed design methodology for an optimal third harmonic hybrid active filter taking the power network parameters and operating condition in consideration.
- Design and validation of a medium voltage implementation of a two-level CNT with an integrated hybrid active filter.

8.4 Recommendations for Future Work

The research presented in this thesis developed a new low-cost power flow controller for the power transmission sector. The proof of concept has been shown with simulation studies on several realistic power networks. Prototypes at low and medium voltages provided validation of the proposed concepts. However, further research and development is required in number of aspects of the technology.

8.4.1 Multi-level AC-AC converters

The CNT technology is targeted towards the transmission sector. The operation of the CNT has been proved at medium voltages, but is yet to be proved at sub-transmission and transmission level voltages, which are of the order of 69 kV – 345 kV. The voltage rating requirement of the thin AC converters for such applications are expected to be in the range of 14 kV – 69 kV, while the power ratings are expected to be of the order of tens of MVAs. The direct AC-AC converter technology has not been proven at such high power

levels. There are significant technological challenges that have to be solved in order to make direct AC converters suitable for such high power levels.

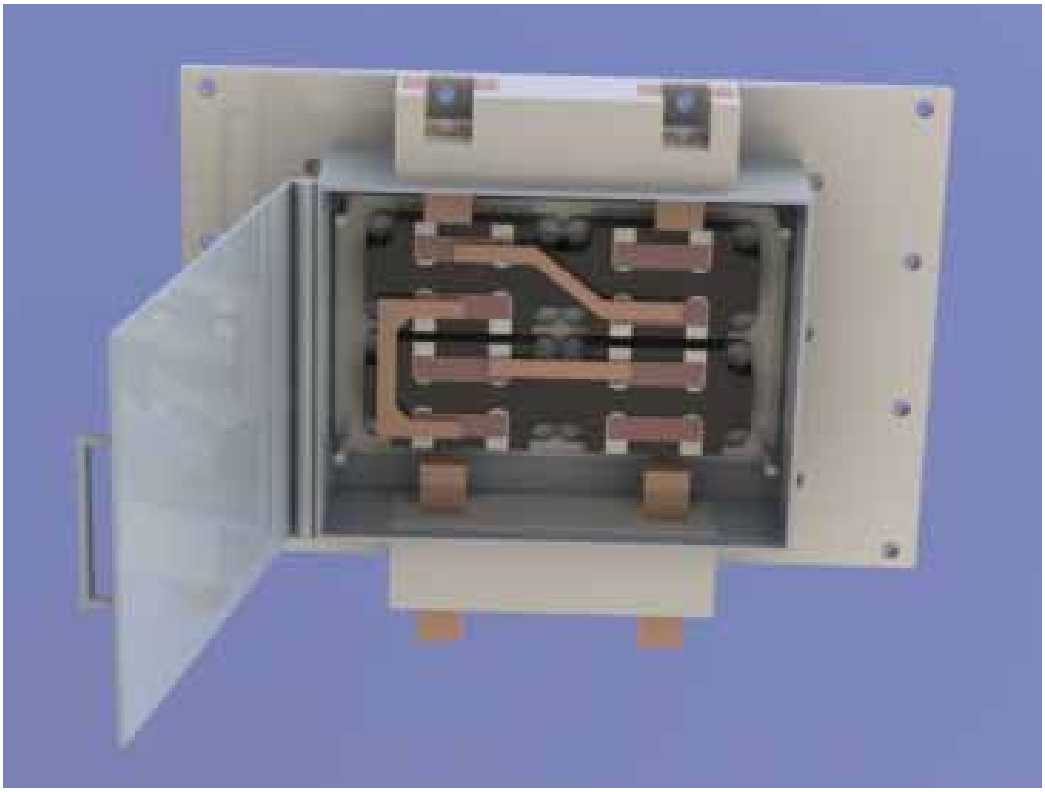

Figure 8.1: 3-D concept diagram of a PEBB cell

The present day individual power electronic switches with turn-off capabilities are not capable of handling blocking voltages higher than 6.6 kV. As a result in order to achieve a blocking voltage of tens of kilovolts, many such devices have to be connected in series. Such multi-level topologies are readily and commercially available for AC-DC-AC converters, but not available for AC-AC converters.

Figure 8.2: 3-D concept diagram of the PEBB assembly

One of the major challenges for multi-level topologies is to ensure even distribution of voltage across all switches especially during transient conditions. For AC-DC-AC converters, the voltage stress across any one such device is constant and hence can be maintained using strategies like the flying capacitor [67-75]. However, for AC-AC converters the voltage across each of the switches varies as a sinusoid. This makes the problem of equal voltage sharing more difficult. The absence of a safe commutation path in case of a switch failure or malfunction makes the problem of scaling direct AC converters a challenging one.

Efforts are on to realize Power Electronic Building Blocks (PEBB) of direct AC converters. The PEBB modules are expected to be directly stackable with each other in order to achieve a high blocking voltage. The 3-D concept diagram of a PEBB cell is shown in Figure 8.1 while that of the PEBB assembly is shown in Figure 8.2 [76]. Also noteworthy is the work towards having an active snubber topology in order to ensure better dynamic voltage sharing between series connected switches in a direct AC converter [77].

8.4.2 Packaging and mechanical design

One of the most critical aspect of any power electronic converter especially for utility application is its packaging and mechanical design. Issues such as cooling, isolation, insulation, etc. have to be taken care of. Cooling by liquids such as de-ionized water requires additional equipments like pumps, reservoir, etc. Further the requirement of real estate and maintenance of such additional equipments adds to the system cost and complexity.

Direct AC converters can have a much lower switching power loss if the commutation is managed properly. It is estimated that at sub-transmission levels the TACC can be packaged to have oil cooling, making the packaging of the system simpler. A concept diagram for such a device is shown in Figure 8.3.

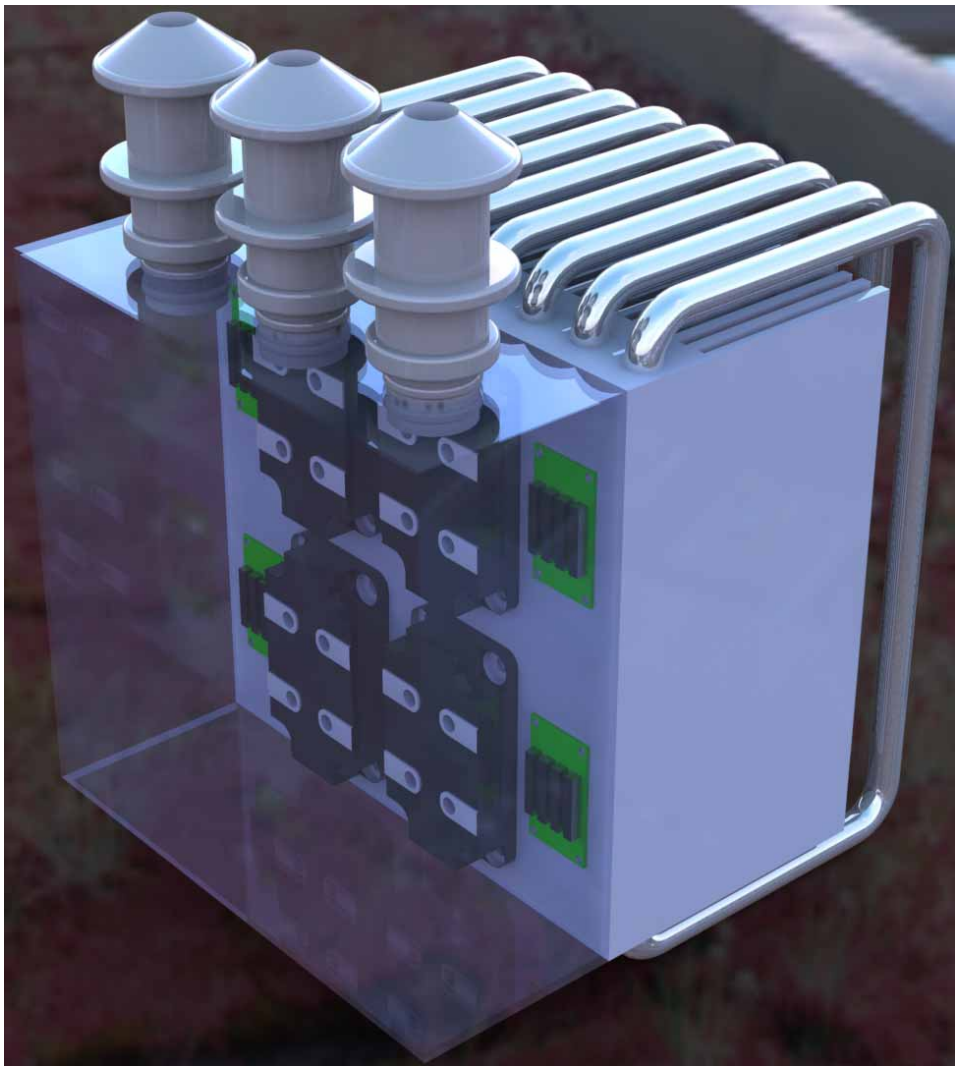

Figure 8.3: 3-D concept diagram of the TACC block with oil cooling

8.4.3 Impact on transformer life

The CNT is realized by augmenting an existing LTC transformer with a TACC converter. Elements such as transformers have a very high reliability and often last for more than 20-25 years. Such high life expectancy is one of the key features of utility assets. The modification of an existing LTC to a CNT will introduce additional stresses

on the LTC due to switching, harmonics, etc. It is thus very important to ascertain that the modification does not significantly cause a loss of life for an existing device.

The HAF filter ensures very low third harmonic current flow. This also ensures that the transformer coils do not have to handle these harmonic currents. But the voltage seen by the transformer coils will have third harmonics. Also the transformer coils will be subjected to switching frequency voltages and currents. A comprehensive study has to be undertaken to understand the impact of these stresses on the transformer life. In some situations it may be possible to de-rate the CNT and thus mitigate the impact of the augmenting the converter.

8.4.4 Alternate fast converging OPF methods

The optimal power flow methodology developed in this thesis uses the concept of particle swarm optimization. Though PSO has many advantages for solving such non-linear search problems, it may take significant time for convergence. It might be important especially for very large systems to develop alternate fast converging OPFs that are based on methods such as Newton-Raphson or Linear Programming or Quadratic Programming. OPF methods for traditional power networks based on such methodologies are already available both commercially as well as in the literature [78-80]. Such methods may sacrifice some level of accuracy but may be able to converge much faster.

8.5 Concluding Remarks

The CNT technology shows a method of converting existing grid assets to make them more controllable and beneficial for the grid. Need for upgrade of the transmission system has been long identified, and policies for renewable integration have further

increased the urgency for such an upgrade. However, the transmission sector remains one of the more conservative sectors. The retrofit approach shown in this research is a cost-effective method of improving the power grid, which consists of a huge number of capital intensive, long-term assets. The incremental capital investment and incremental change in operation of an existing asset offered by the CNT technology makes it an attractive proposition for the power industry. Such small changes distributed over the whole power network may prove to be transformative for the power industry.

Appendix A

MATLAB program for finding OPF for networks with CNTs

```
clear all;
close all;
clc;

timer1=cputime;
LineFile='linedata_case30c';  %'linedataMFpl';
BusFile='busdata_case30c';    %'busdataFpl';
OtherDataFile='otherdata_case30c';    %'otherdataFpl';
linedata=feval(LineFile);
busdata=feval(BusFile);
TotalLoad=sum(busdata(:,7));
NumCNT=max(linedata(:,7));
NT=0.1*ones(NumCNT,1);                    % Taps of CNT
kS=1e4;                                   % Penalties
kV=1e3;
[Vmax Vmin GenCost Vbase Mbase]=feval(OtherDataFile);
[temp1 temp2]= size(GenCost);
NumPV=temp1-1;
PGenMax=GenCost(:,5);
PGenMin=GenCost(:,6);

% kS=Penalty(1);    kV=Penalty(2); Vmax=Penalty(3); Vmin=Penalty(4);
Penalty = [kS kV Vmax Vmin];

N=2*(NumCNT+NumPV)+1;       % Dimension

max_iterations  = 100;
no_of_particles = 20;
dimensions      = N;

delta_min       = -0.003;
delta_max       = 0.003;

c1 = 2;
c2 = 2;

Wmax=0.9;
Wmin=0.4;
max_vel=[0.3; 0.3;  0.3; 0.3; 30; 30; 30; 30; 30; 0.03; 0.03; 0.03; 0.03; 0.03; 0.03;];
```

```
%initialise the particles and teir velocity components

for count_x = 1:no_of_particles
   for count_y = 1: dimensions
      if count_y <= NumCNT                  % K0 Initialize
         particle_position(count_x,count_y) = round(rand*100)/100;
      elseif count_y <= 2*NumCNT            % K2 Initialize
         temp1=particle_position(count_x,count_y-NumCNT);
         temp2=min(temp1,1-temp1);
         particle_position(count_x,count_y) = round((-temp2+2*temp2*rand)*100)/100;
      elseif count_y <= 2*NumCNT+NumPV      % Pgen Initialize
         if count_y-1 >= 2*NumCNT+1
            Pgenalloc=sum(particle_position(count_x,2*NumCNT+1:count_y-1));
         else
            Pgenalloc=0;
         end
         temp1=count_y-2*NumCNT;
         temp2=min(GenCost(temp1+1,5),TotalLoad-Pgenalloc);
         temp3=GenCost(temp1+1,6);
         particle_position(count_x,count_y) = round((temp3+(temp2-
temp3)*rand)*100)/100;
      else
         particle_position(count_x,count_y) = round((Vmin+(Vmax-
Vmin)*rand)*1000)/1000;
      end
      particle_velocity(count_x,count_y) = max_vel(count_y)*rand;
      p_best(count_x,count_y) = particle_position(count_x,count_y);
   end
end

[tempx tempy]=size(GenCost);
gen_init=GenCost(2:tempx,7);
for ind=2:1:tempx
   tempgenbus=GenCost(ind,1);
   v_init(ind-1)=busdata(tempgenbus,3);
end
v_init(ind)=busdata(GenCost(1,1),3);

particle_position(1,:)=[0.55*ones(NumCNT,1); 0*ones(NumCNT,1); gen_init; v_init';];
% particle_position(2,:)=[0.55*ones(NumCNT,1); 0*ones(NumCNT,1); gen_init;
v_init';];
% particle_position(2,1)=0.5; particle_position(2,2)=0.5;
% particle_position(2,4)=46.3543; particle_position(2,6)=12.3166;
```

```
%initialize the p_best_fitness array
for count = 1:no_of_particles
   p_best_fitness(count) = 1e15;
end

%main particle swrm routine
for count = 1:max_iterations

   %find the fitness of each particle
   %change fitness function as per equation requiresd and dimensions
   pseudo=1;
   for count_x = 1:no_of_particles
      K0=particle_position(count_x,1:NumCNT)';
      K2=particle_position(count_x,1+NumCNT:2*NumCNT)';
      SetCNT=[NT K0 K2];
      PVbus=GenCost(2:NumPV+1,1);
      Pgen=particle_position(count_x,1+2*NumCNT:2*NumCNT+NumPV)';
      Vbus=particle_position(count_x,1+2*NumCNT+NumPV:2*(NumCNT+NumPV))';
      SetPV = [PVbus Pgen Vbus];
      SlackV=particle_position(count_x,N);

      %%%% Set time to find loadflow --> else break
      [tCost tOverLoadCost
tOV]=mCNT_cost_2(LineFile,BusFile,SetCNT,SetPV,GenCost,Penalty, SlackV);
      current_fitness(count_x)=tCost;
      %mohmaya=1;
   end
   % ############

   %decide on p_best etc for each particle
   for count_x = 1:no_of_particles
      if current_fitness(count_x) < p_best_fitness(count_x)
         p_best_fitness(count_x) = current_fitness(count_x);
         for count_y = 1:dimensions
            p_best(count_x,count_y) = particle_position(count_x,count_y);
         end
      end
   end

   %decide on the global best among all the particles
   [g_best_val,g_best_index] = min(p_best_fitness);

   %g_best contains the position of teh global best
   for count_y = 1:dimensions
      g_best(count_y) = p_best(g_best_index,count_y);
```

```
    end

    %update the position and velocity components
    for count_x = 1:no_of_particles
        for count_y = 1:dimensions
            p_current(count_y) = particle_position(count_x,count_y);
        end

        for count_y = 1:dimensions
            W=Wmax-(Wmax-Wmin)*count/max_iterations;
            particle_velocity(count_x,count_y) = W*particle_velocity(count_x,count_y) +
c1*rand*(p_best(count_x,count_y)-p_current(count_y)) + c2*rand*(g_best(count_y)-
p_current(count_y));
            if particle_velocity(count_x,count_y) > max_vel(count_y)
                particle_velocity(count_x,count_y)=max_vel(count_y);
            elseif particle_velocity(count_x,count_y) < -max_vel(count_y)
                particle_velocity(count_x,count_y)=-max_vel(count_y);
            end
            particle_position(count_x,count_y) = p_current(count_y)
+particle_velocity(count_x,count_y);

            if count_y <= NumCNT
                if particle_position(count_x,count_y) > 1
                    particle_position(count_x,count_y)=1;
                elseif particle_position(count_x,count_y) < 0
                    particle_position(count_x,count_y) = 0;
                end
            elseif count_y <= 2*NumCNT
                temp1=particle_position(count_x,count_y-NumCNT);
                temp2=min(temp1,1-temp1);
                if particle_position(count_x,count_y) > temp2
                    particle_position(count_x,count_y) = temp2;
                elseif particle_position(count_x,count_y) < -temp2
                    particle_position(count_x,count_y) = -temp2;
                end
            elseif count_y <= 2*NumCNT+NumPV
                temp1=count_y-2*NumCNT;
                temp2=GenCost(temp1+1,5);
                temp3=GenCost(temp1+1,6);
                temp4=particle_position(count_x,count_y);
                if temp4 > temp2
                    particle_position(count_x,count_y)=temp4;
                elseif temp4 < temp3
                    particle_position(count_x,count_y)=temp3;
                end
```

```
            else
               if particle_position(count_x,count_y) > Vmax
                  particle_position(count_x,count_y)=Vmax;
               elseif particle_position(count_x,count_y) < Vmin
                  particle_position(count_x,count_y)=Vmin;
               end
            end
            particle_velocity(count_x,count_y) = - p_current(count_y)
+particle_position(count_x,count_y);
         end
         %pseudo=1;
      end
      %fprintf('%d. %f\n',count,g_best_val);
      %pseudo=0;
end

K0=g_best(1:NumCNT)';
K2=g_best(1+NumCNT:2*NumCNT)';
SetCNT=[NT K0 K2];
PVbus=GenCost(2:NumPV+1,1);
Pgen=g_best(1+2*NumCNT:2*NumCNT+NumPV)';
Vbus=g_best(1+2*NumCNT+NumPV:2*(NumCNT+NumPV))';
SetPV = [PVbus Pgen Vbus];
SlackV=g_best(N);
[BestCost
OverLoadCost]=mCNT_FlowDisplay_2(LineFile,BusFile,SetCNT,SetPV,GenCost,Penal
ty,SlackV);
timer2=cputime-timer1
```

```
function [Cost OverLoadCost
OV]=mCNT_cost_2(LineFile,BusFile,SetCNT,SetPV,GenCost,Penalty,SlackV)

Cost=0;
MVAbase=100;
NT=SetCNT(:,1);
K0=SetCNT(:,2);
K2=SetCNT(:,3);

for ind=1:1:length(NT)
   Alpha(ind)=(1+NT(ind)-2*K0(ind)*NT(ind))/(1-NT(ind)^2);
   Beta(ind)=NT(ind)*K2(ind)/(1-NT(ind)^2);
end

FName=LineFile;     % 'linedataMFpl';
```

```
FName1=BusFile;     %'busdataFpl';
[Y Mode]= ybusppg_mCNT(FName);            % Calling ybusppg.m to get Bus
Admittance Matrix..
busdata=feval(FName1);
baseMVA = 100;              % Base MVA..
bus = busdata(:,1);         % Bus Number..
type = busdata(:,2);        % Type of Bus 1-Slack, 2-PV, 3-PQ..
V = busdata(:,3);           % Specified Voltage..
del = busdata(:,4)*pi/180;         % Voltage Angle..
Pg = busdata(:,5);          % PGi..
Qg = busdata(:,6);          % QGi..
Pl = busdata(:,7);          % PLi..
Ql = busdata(:,8);          % QLi..
Qmin = busdata(:,9);        % Minimum Reactive Power Limit..
Qmax = busdata(:,10);       % Maximum Reactive Power Limit..
nbus = max(bus);            % To get no. of buses..

[temp1 temp2] = size(SetPV);
for ind=1:1:temp1
   pvbus=SetPV(ind,1);
   Pg(pvbus)=SetPV(ind,2);
   V(pvbus)=SetPV(ind,3);
end
V(1)=SlackV;

Slack=find(type==1);
SlackGen=find(GenCost(:,1)==Slack);
ExpectedSlackGen=sum(Pl)-sum(SetPV(:,2));
% if Pgen > GenCost(ind,5)+0.1 || Pgen < GenCost(ind,6)-0.1
% ExpectedSlackGen < GenCost(SlackGen,6)-0.1 || ExpectedSlackGen >
GenCost(SlackGen,5)+0.1
%     Cost=1e8;
%     OverLoadCost=-1;
%     return;
% end

P = Pg - Pl;                % Pi = PGi - PLi..
Q = Qg - Ql;                % Qi = QGi - QLi..
P = P/baseMVA;              % Converting to p.u..
Q = Q/baseMVA;
Qmin = Qmin/baseMVA;
Qmax = Qmax/baseMVA;
Tol = 10;     % Tolerence kept at high value.
Iter = 1;  % iteration starting
Psp = P;
```

```
Qsp = Q;
G = real(Y);    % Conductance..
B = imag(Y);    % Susceptance..

pv = find(type == 2 | type == 1); % Index of PV Buses..
pq = find(type == 3); % Index of PQ Buses..

npv = length(pv); % Number of PV buses..
npq = length(pq); % Number of PQ buses..

IterCount=0;
while (Tol > 1e-8 && IterCount < 1e3)   % Iteration starting..
   IterCount=IterCount+1;
   P = zeros(nbus,1);
   Q = zeros(nbus,1);
   % Calculate P and Q
   for i = 1:nbus
      for k = 1:nbus
         if Mode(i,k) == 0
            P(i) = P(i) + V(i)* V(k)*(G(i,k)*cos(del(i)-del(k)) + B(i,k)*sin(del(i)-del(k)));
            %Q(i) = Q(i) + V(i)* V(k)*(G(i,k)*sin(del(i)-del(k)) - B(i,k)*cos(del(i)-
del(k)));
            if i == k
               bii=-sum(B(i,:));
               Q(i)=Q(i)+V(i)^2*bii;
            else
               Q(i) = Q(i) + V(i)* V(k)*(G(i,k)*sin(del(i)-del(k)) - B(i,k)*cos(del(i)-
del(k))) + V(i)*V(i)*B(i,k);
            end
         elseif Mode(i,k) > 0          % CNT Send => i
            alpha=Alpha(Mode(i,k));
            beta=Beta(Mode(i,k));
            P(i) = P(i) + V(i)*V(k)*B(i,k)*(alpha*sin(del(i)-del(k))-beta*cos(del(i)-
del(k)));
            tempvar=(alpha^2)-(2/3)*(beta^2);
            Q(i) = Q(i) + V(i)*B(i,k)*(V(i)*tempvar-alpha*V(k)*cos(del(i)-
del(k))+beta*V(k)*sin(del(i)-del(k)));
         elseif Mode(i,k) < 0          % CNT Recieve => i
            alpha=Alpha(-Mode(i,k));
            beta=Beta(-Mode(i,k));
            P(i) = P(i) + V(i)*V(k)*B(i,k)*(alpha*sin(del(i)-del(k))+beta*cos(del(i)-
del(k)));
            Q(i) = Q(i) + V(i)*B(i,k)*(V(i)-alpha*V(k)*cos(del(i)-del(k))-
beta*V(k)*sin(del(i)-del(k)));
         else
```

```
            fprintf('Error P,Q\n');
        end
    end
end

% Checking Q-limit violations..
if Iter <= 100 && Iter > 2    % Only checked up to 7th iterations..
    for n = 2:nbus
        if type(n) == 2
            if Q(n) < Qmin(n)
                V(n) = V(n) + 0.001;
            elseif Q(n) > Qmax(n)
                V(n) = V(n) - 0.001;
            end
        end
     end
end

% Calculate change from specified value
dPa = Psp-P;
dQa = Qsp-Q;
k = 1;
dQ = zeros(npq,1);
for i = 1:nbus
    if type(i) == 3
        dQ(k,1) = dQa(i);
        k = k+1;
    end
end
dP = dPa(2:nbus);
M = [dP; dQ];       % Mismatch Vector

% Jacobian
% J1 - Derivative of Real Power Injections with Angles..
J1 = zeros(nbus-1,nbus-1);
for i = 1:(nbus-1)
    m = i+1;
    for k = 1:(nbus-1)
        n = k+1;
        if n == m                % dP(i)/dTheta(i)
            for n = 1:nbus

                if Mode(m,n) == 0
                    J1(i,k) = J1(i,k) + V(m)* V(n)*(-G(m,n)*sin(del(m)-del(n)) +
B(m,n)*cos(del(m)-del(n)));
```

```
                elseif Mode(m,n) > 0
                    alpha=Alpha(Mode(m,n));
                    beta=Beta(Mode(m,n));
                    J1(i,k)=J1(i,k)+V(m)*V(n)*B(m,n)*(alpha*cos(del(m)-
del(n))+beta*sin(del(m)-del(n)));
                elseif Mode(m,n) < 0
                    alpha=Alpha(-Mode(m,n));
                    beta=Beta(-Mode(m,n));
                    J1(i,k)=J1(i,k)+V(m)*V(n)*B(m,n)*(alpha*cos(del(m)-del(n))-
beta*sin(del(m)-del(n)));
                else
                    fprintf('Error J1 Part1\n');
                end

            end
            J1(i,k) = J1(i,k) - V(m)^2*B(m,m);
        else                    % dP(i)/dTheta(k)

            if Mode(m,n) == 0
                J1(i,k) = V(m)* V(n)*(G(m,n)*sin(del(m)-del(n)) - B(m,n)*cos(del(m)-
del(n)));
            elseif Mode(m,n) > 0
                alpha=Alpha(Mode(m,n));
                beta=Beta(Mode(m,n));
                J1(i,k)=V(m)*V(n)*B(m,n)*(-alpha*cos(del(m)-del(n))-beta*sin(del(m)-
del(n)));
            elseif Mode(m,n) < 0
                alpha=Alpha(-Mode(m,n));
                beta=Beta(-Mode(m,n));
                J1(i,k)=V(m)*V(n)*B(m,n)*(-alpha*cos(del(m)-del(n))+beta*sin(del(m)-
del(n)));
            else
                fprintf('Error J1 Part 2\n');
            end

        end
    end
end

% J2 - Derivative of Real Power Injections with V..
J2 = zeros(nbus-1,npq);
for i = 1:(nbus-1)
    m = i+1;
    for k = 1:npq
        n = pq(k);
```

```
        if n == m
            for n = 1:nbus

                if Mode(m,n) == 0
                    J2(i,k) = J2(i,k) + V(n)*(G(m,n)*cos(del(m)-del(n)) + B(m,n)*sin(del(m)-
del(n)));
                elseif Mode(m,n) > 0
                    alpha=Alpha(Mode(m,n));
                    beta=Beta(Mode(m,n));
                    J2(i,k)=J2(i,k)+V(n)*B(m,n)*(alpha*sin(del(m)-del(n)) - beta*cos(del(m)-
del(n)));
                elseif Mode(m,n) < 0
                    alpha=Alpha(-Mode(m,n));
                    beta=Beta(-Mode(m,n));
                    J2(i,k)=J2(i,k)+V(n)*B(m,n)*(alpha*sin(del(m)-del(n)) +
beta*cos(del(m)-del(n)));
                else
                    fprintf('Error J2 Part 1\n');
                end

            end
            J2(i,k) = J2(i,k) + V(m)*G(m,m);
        else

            if Mode(m,n) == 0;
                J2(i,k) = V(m)*(G(m,n)*cos(del(m)-del(n)) + B(m,n)*sin(del(m)-del(n)));
            elseif Mode(m,n) > 0
                alpha=Alpha(Mode(m,n));
                beta=Beta(Mode(m,n));
                J2(i,k)=V(m)*B(m,n)*(alpha*sin(del(m)-del(n)) - beta*cos(del(m)-del(n)));
            elseif Mode(m,n) < 0
                alpha=Alpha(-Mode(m,n));
                beta=Beta(-Mode(m,n));
                J2(i,k)=V(m)*B(m,n)*(alpha*sin(del(m)-del(n)) + beta*cos(del(m)-del(n)));
            else
                fprintf('Error J2 Part 2\n');
            end

        end
    end
end

% J3 - Derivative of Reactive Power Injections with Angles..
J3 = zeros(npq,nbus-1);
for i = 1:npq
```

```
        m = pq(i);
        for k = 1:(nbus-1)
            n = k+1;
            if n == m
                for n = 1:nbus

                    if Mode(m,n) == 0
                        J3(i,k) = J3(i,k) + V(m)* V(n)*(G(m,n)*cos(del(m)-del(n)) +
B(m,n)*sin(del(m)-del(n)));
                    elseif Mode(m,n) > 0
                        alpha=Alpha(Mode(m,n));
                        beta=Beta(Mode(m,n));
                        J3(i,k) = J3(i,k) + V(m)* V(n)*B(m,n)*(alpha*sin(del(m)-del(n)) +
beta*cos(del(m)-del(n)));
                    elseif Mode(m,n) < 0
                        alpha=Alpha(-Mode(m,n));
                        beta=Beta(-Mode(m,n));
                        J3(i,k) = J3(i,k) + V(m)* V(n)*B(m,n)*(alpha*sin(del(m)-del(n)) -
beta*cos(del(m)-del(n)));
                    else
                        fprintf('Error J3 Part1\n');
                    end

                end
                J3(i,k) = J3(i,k) - V(m)^2*G(m,m);
            else

                if Mode(m,n) == 0
                    J3(i,k) = V(m)* V(n)*(-G(m,n)*cos(del(m)-del(n)) - B(m,n)*sin(del(m)-
del(n)));
                elseif Mode(m,n) > 0
                    alpha=Alpha(Mode(m,n));
                    beta=Beta(Mode(m,n));
                    J3(i,k) = V(m)* V(n)*B(m,n)*(- alpha*sin(del(m)-del(n))-beta*cos(del(m)-
del(n)));
                elseif Mode(m,n) < 0
                    alpha=Alpha(-Mode(m,n));
                    beta=Beta(-Mode(m,n));
                    J3(i,k) = V(m)* V(n)*B(m,n)*(- alpha*sin(del(m)-del(n))+beta*cos(del(m)-
del(n)));
                else
                    fprintf('Error J3 Part2\n');
                end

            end
```

```
    end
  end

  % J4 - Derivative of Reactive Power Injections with V..
  J4 = zeros(npq,npq);
  for i = 1:npq
    m = pq(i);
    for k = 1:npq
      n = pq(k);
      if n == m
        for n = 1:nbus

          if Mode(m,n) == 0
            J4(i,k) = J4(i,k) + V(n)*(G(m,n)*sin(del(m)-del(n)) - B(m,n)*cos(del(m)-
del(n))) + 2*V(m)*B(m,n);
          elseif Mode(m,n) > 0
            alpha=Alpha(Mode(m,n));
            beta=Beta(Mode(m,n));
            tempvar=(alpha^2)-(2/3)*(beta^2);
            J4(i,k) = J4(i,k) + 2*V(m)*B(m,n)*tempvar + V(n)*B(m,n)*(-
alpha*cos(del(m)-del(n)) + beta*sin(del(m)-del(n)));
          elseif Mode(m,n) < 0
            alpha=Alpha(-Mode(m,n));
            beta=Beta(-Mode(m,n));
            J4(i,k) = J4(i,k) + 2*V(m)*B(m,n) + V(n)*B(m,n)*(-alpha*cos(del(m)-
del(n)) - beta*sin(del(m)-del(n)));
          else
            fprintf('Error J4 Part1\n');
          end

        end
        bii=-sum(B(m,:));
        J4(i,k) = J4(i,k) - V(m)*B(m,m) + V(m)*bii;
      else

        if Mode(m,n) == 0
          J4(i,k) = V(m)*(G(m,n)*sin(del(m)-del(n)) - B(m,n)*cos(del(m)-del(n)));
        elseif Mode(m,n) > 0
          alpha=Alpha(Mode(m,n));
          beta=Beta(Mode(m,n));
          J4(i,k) = V(m)*B(m,n)*(-alpha*cos(del(m)-del(n)) + beta*sin(del(m)-
del(n)));
        elseif Mode(m,n) < 0
          alpha=Alpha(-Mode(m,n));
          beta=Beta(-Mode(m,n));
```

```
                J4(i,k) = V(m)*B(m,n)*(-alpha*cos(del(m)-del(n)) - beta*sin(del(m)-
del(n)));
            else
                fprintf('Error J4 Part2\n');
            end
        end
    end
end

J = [J1 J2; J3 J4];     % Jacobian

X = inv(J)*M;           % Correction Vector
dTh = X(1:nbus-1);
dV = X(nbus:end);
del(2:nbus) = dTh + del(2:nbus);
k = 1;
for i = 2:nbus
    if type(i) == 3
        V(i) = dV(k) + V(i);
        k = k+1;
    end
end
Iter = Iter + 1;
Tol = max(abs(M));
end

% Iter; % Number of Iterations took..
% V;  % Bus Voltage Magnitudes in p.u ...
% Del = 180/pi*del; % Bus Voltage Angles in Degree...
% disp('-----------------------------');
% disp('|  Bus  |    V    | Angle   | ');
% disp('|  No   |   pu    | Degree  | ');
% disp('-----------------------------');
% for m = 1:nbus
%     fprintf('%4g', m); fprintf('    %8.4f', V(m)); fprintf('    %8.4f', Del(m)); fprintf('\n');
% end
% disp('-----------------------------');

loadflow_mCNT_2;

%%% Calculating GenCost %%%
[temp1 temp2]= size(GenCost);
for ind=1:1:temp1
    genbus=GenCost(ind,1);
    Pgen=Pi(genbus)*MVAbase+Pl(genbus);
```

```
    PgenTemp(ind)=Pgen;
        if Pgen > GenCost(ind,5)+0.1 || Pgen < GenCost(ind,6)-0.1
        Cost=1e15;
        OverLoadCost=-1;
        OV=[];
        return
    end
    GCost(ind)=GenCost(ind,2)*Pgen^2+GenCost(ind,3)*Pgen+GenCost(ind,4);
    GCost(ind)=GenCost(ind,2)*Pgen^2+GenCost(ind,3)*Pgen+GenCost(ind,4);
end
Cost=sum(GCost);

%%% Calculating Penalty Functions %%%
linedata=feval(FName);
LineRating=linedata(:,8)/MVAbase;       % 100 MVA base
kS=Penalty(1);
kV=Penalty(2);
Vmax=Penalty(3);
Vmin=Penalty(4);
OverLoadCost=0;

[temp1 temp2]= size(linedata);
OV=[];
for ind=1:1:temp1
    FromBus=linedata(ind,1);
    ToBus=linedata(ind,2);
    SijFlow=max(abs(Sij(FromBus,ToBus)),abs(Sij(ToBus,FromBus)));
    if SijFlow > LineRating(ind)

%fprintf('BrNo=%d\t%d\t%d\t%f\t%f\n',ind,FromBus,ToBus,SijFlow,LineRating(ind));
        if SijFlow > LineRating(ind)*1.005                    % ### Tolerance
            OverLoadCost=OverLoadCost+kS*(SijFlow/LineRating(ind))^2;
            tempMat=[ind SijFlow LineRating(ind)];
            OV=[OV' tempMat';]';
        end
    end
end

VRegCost=0;
for ind=1:1:length(V)
    if V(ind) > Vmax
        VRegCost=VRegCost+kV*(V(ind)-Vmax)^2;
    elseif V(ind) < Vmin
        VRegCost=VRegCost+kV*(Vmin-V(ind))^2;
    end
```

```
end

Cost=(Cost+OverLoadCost+VRegCost)/1;

% disp(Pi);
% disp(Qi);
```

Appendix B

System parameters in Matpower format for the modified IEEE 30 bus system used in Sections 4.5.6 and 5.2.4.

```
function [baseMVA, bus, gen, branch, areas, gencost] = case30

baseMVA = 100;

%% bus data
%  bus_i  type   Pd  Qd  Gs  Bs  area   Vm  Va  baseKV  zone   Vmax   Vmin
bus = [
   1   3   0     0     0   0     1   1   0   135 1   1.05   0.95;
   2   2   0     0     0   0     1   1   0   135 1   1.05   0.95;
   3   1   0     0     0   0     1   1   0   135 1   1.05   0.95;
   4   1   50    0     0   0     1   1   0   135 1   1.05   0.95;
   5   1   0     0     0   0     1   1   0   135 1   1.05   0.95;
   6   1   0     0     0   0     1   1   0   135 1   1.05   0.95;
   7   1   0     0     0   0     1   1   0   135 1   1.05   0.95;
   8   1   0     0     0   0     1   1   0   135 1   1.05   0.95;
   9   1   0     0     0   0     1   1   0   135 1   1.05   0.95;
   10  1   0     0     0   0     1   1   0   135 1   1.05   0.95;
   11  1   0     0     0   0     1   1   0   135 1   1.05   0.95;
   12  1   0     0     0   0     1   1   0   135 1   1.05   0.95;
   13  2   0     0     0   0     1   1   0   135 1   1.05   0.95;
   14  1   0     0     0   0     1   1   0   135 1   1.05   0.95;
   15  1   50    0     0   0     1   1   0   135 1   1.05   0.95;
   16  1   0     0     0   0     1   1   0   135 1   1.05   0.95;
   17  1   0     0     0   0     1   1   0   135 1   1.05   0.95;
   18  1   0     0     0   0     1   1   0   135 1   1.05   0.95;
   19  1   0     0     0   0     1   1   0   135 1   1.05   0.95;
   20  1   0.0   0     0   0     1   1   0   135 1   1.05   0.95;
   21  1   0.0   0     0   0     1   1   0   135 1   1.05   0.95;
   22  2   0     0     0   0     1   1   0   135 1   1.05   0.95;
   23  2   0.0   0     0   0     1   1   0   135 1   1.05   0.95;
   24  1   0.0   0     0   0.0   1   1   0   135 1   1.05   0.95;
   25  1   0     0     0   0     1   1   0   135 1   1.05   0.95;
   26  1   0.0   0     0   0     1   1   0   135 1   1.05   0.95;
   27  2   0     0     0   0     1   1   0   135 1   1.05   0.95;
   28  1   0     0     0   0     1   1   0   135 1   1.05   0.95;
   29  1   0.0   0     0   0     1   1   0   135 1   1.05   0.95;
```

```
   30  1   0.0    0       0   0       1   1   0   135 1   1.05    0.95;
];

%% generator data
%   bus Pg  Qg  Qmax    Qmin    Vg  mBase   status  Pmax    Pmin
gen = [
   1   23.54   0   150    -20 1   100 1   100 0;
   2   60.97   0   60     -20 1   100 1   100 0;
   13  37      0   44.7   -20 1   100 1   100 0;
   22  21.59  0   62.5   -20 1   100 1   100 0;
   23  19.2    0   40     -20 1   100 1   100 0;
   27  26.91  0   48.7   -20 1   100 1   100 0;
];

%% branch data
%   fbus    tbus    r   x   b   rateA   rateB   rateC   ratio   angle   status
branch = [
   1   2   0.00    0.06    0.00    130 130 130 0   0   1;
   1   3   0.00    0.19    0.00    16  16  16  0   0   1;
   2   4   0.00    0.17    0.00    130 130 130 0   0   1;
   3   4   0.00    0.04    0       130 130 130 0   0   1;
   2   5   0.00    0.2     0.00    130 130 130 0   0   1;
   2   6   0.00    0.18    0.00    65  65  65  0   0   1;
   4   6   0.00    0.04    0       90  90  90  0   0   1;
   5   7   0.00    0.12    0.00    70  70  70  0   0   1;
   6   7   0.00    0.08    0.00    130 130 130 0   0   1;
   6   8   0       0.04    0       32  32  32  0   0   1;
   6   9   0       0.21    0       65  65  65  0   0   1;
   6   10  0       0.56    0       32  32  32  0   0   1;
   9   11  0       0.21    0       65  65  65  0   0   1;
   9   10  0       0.11    0       65  65  65  0   0   1;
   4   12  0       0.26    0       65  65  65  0   0   1;
   12  13  0       0.14    0       65  65  65  0   0   1;
   12  14  0       0.26    0       32  32  32  0   0   1;
   12  15  0.00    0.13    0       16  16  16  0   0   1;
   12  16  0.00    0.2     0       32  32  32  0   0   1;
   14  15  0.00    0.2     0       32  32  32  0   0   1;
   16  17  0.00    0.19    0       16  16  16  0   0   1;
   15  18  0.00    0.22    0       16  16  16  0   0   1;
   18  19  0.00    0.13    0       16  16  16  0   0   1;
   19  20  0.00    0.07    0       32  32  32  0   0   1;
   10  20  0.00    0.21    0       32  32  32  0   0   1;
   10  17  0.00    0.08    0       32  32  32  0   0   1;
   10  21  0.00    0.07    0       32  32  32  0   0   1;
   10  22  0.00    0.15    0       32  32  32  0   0   1;
```

```
   21  22  0      0.02    0      32  32  32  0   0   1;
   15  23  0      0.2     0      65  65  65  0   0   1;
   22  24  0      0.18    0      16  16  16  0   0   1;
   23  24  0.00   0.27    0      65  65  65  0   0   1;
   24  25  0.00   0.33    0      16  16  16  0   0   1;
   25  26  0.00   0.38    0      16  16  16  0   0   1;
   25  27  0      0.21    0      16  16  16  0   0   1;
   28  27  0      0.4     0      65  65  65  0   0   1;
   27  29  0.00   0.42    0      16  16  16  0   0   1;
   27  30  0.00   0.6     0      16  16  16  0   0   1;
   29  30  0.00   0.45    0      16  16  16  0   0   1;
   8   28  0.00   0.2     0.0    32  32  32  0   0   1;
   6   28  0.00   0.06    0.0    32  32  32  0   0   1;
];

%%-----  OPF Data  -----%%
%% area data
areas = [
   1   2;
];

%% generator cost data
%   1   startup shutdown    n   x1  y1  ... xn  yn
%   2   startup shutdown    n   c(n-1)  ... c0
gencost = [
   2   0   0   3   0.0     60      0;
   2   0   0   3   0.0     84      0;
   2   0   0   3   0.0     61      0;
   2   0   0   3   0.0     81      0;
   2   0   0   3   0.0     75      0;
   2   0   0   3   0.0     82      0;
];

return;
```

Appendix C

Parameters of the generator in the 7 bus system used in Sections 4.6.

Table C.1: Generator parameters

Parameter	Value	Unit
Nominal power	100	MW
Line-line voltage	13.8	kV
Nominal frequency	60	Hz
Direct axis reactance (Xd)	1.305	pu
Direct axis transient reactance (Xd')	0.5	pu
Direct axis sub-transient reactance (Xd'')	0.45	pu
Quadrature axis reactance (Xq)	0.65	pu
Quadrature axis transient reactance (Xq')	0.5	pu
Quadrature axis sub-transient reactance (Xq'')	0.18	pu
Direct axis short circuit transient time constant (Td')	1.01	s
Direct axis short circuit sub-transient time constant (Td'')	0.053	s
Quadrature axis open circuit transient time constant (Tqo'')	0.1	s
Stator Resistance (Rs)	2.8544e-3	pu
Coefficient of inertia (H)	3.2	s
Friction facor (F)	0	pu
Number of poles (p)	32	-

Appendix D

System parameters in Matpower format for the 7 bus system used in Sections 5.2.3.

```
function [baseMVA, bus, gen, branch, areas, gencost] = case9
baseMVA = 100;

bus = [
   1   3   0   0   0   0   1   1   0   138 1   1.05    0.95;
   2   1   0   0   0   0   1   1   0   138 1   1.05    0.95;
   3   1   0   0   0   0   1   1   0   138 1   1.05    0.95;
   4   1   0   0   0   0   1   1   0   138 1   1.05    0.95;
   5   1   0   0   0   0   1   1   0   138 1   1.05    0.95;
   6   1   90 0   0   0   1   1   0   138 1   1.05    0.95;
   7   2   0   0   0   0   1   1   0   138 1   1.05    0.95;
];
gen = [
   1   0   0   150 -20 1   100 1   100 0;
   7   25  0   60  -20 1   100 1   100 0;
];
branch = [
   1   2   0   0.10    0   500 500 500 0   0   1;
   1   3   0   0.05    0   500 500 500 0   0   1;
   2   5   0   0.10    0   40  40  40  0   0   1;
   3   4   0   0.05    0   50  50  50  0   0   1;
   4   6   0   0.05    0   500 500 500 0   0   1;
   5   6   0   0.10    0   500 500 500 0   0   1;
   6   7   0   0.10    0   500 500 500 0   0   1;
];
areas = [
   1   5;
];
gencost = [
   2   00  0   3   0.0 60  0;
   2   00  0   3   0.0 80  0;
];

return;
```

Appendix E

System parameters in Matpower format for the modified IEEE 30 bus system used in Sections 5.3.

```
function [baseMVA, bus, gen, branch, areas, gencost] = case_temp88

baseMVA=100;

bus=[
1.000000   3.000000   26.348262  10.000000  0.000000   0.000000   1.000000
1.000000   0.000000   138.000000 1.000000   1.100000   0.900000
2.000000   2.000000   26.348262  10.000000  0.000000   0.000000   1.000000
1.000000   0.000000   138.000000 1.000000   1.100000   0.900000
3.000000   1.000000   26.348262  10.000000  0.000000   0.000000   1.000000
1.000000   0.000000   138.000000 1.000000   1.100000   0.900000
4.000000   1.000000   0.000000   10.000000  0.000000   0.000000   1.000000
1.000000   0.000000   138.000000 1.000000   1.100000   0.900000
5.000000   1.000000   26.348262  10.000000  0.000000   0.000000   1.000000
1.000000   0.000000   138.000000 1.000000   1.100000   0.900000
6.000000   1.000000   0.000000   10.000000  0.000000   0.000000   1.000000
1.000000   0.000000   138.000000 1.000000   1.100000   0.900000
7.000000   1.000000   26.348262  10.000000  0.000000   0.000000   1.000000
1.000000   0.000000   138.000000 1.000000   1.100000   0.900000
8.000000   1.000000   26.348262  10.000000  0.000000   0.000000   1.000000
1.000000   0.000000   138.000000 1.000000   1.100000   0.900000
9.000000   1.000000   26.348262  10.000000  0.000000   0.000000   1.000000
1.000000   0.000000   138.000000 1.000000   1.100000   0.900000
10.000000  1.000000   26.348262  10.000000  0.000000   0.000000   1.000000
1.000000   0.000000   138.000000 1.000000   1.100000   0.900000
11.000000  1.000000   26.348262  10.000000  0.000000   0.000000   1.000000
1.000000   0.000000   138.000000 1.000000   1.100000   0.900000
12.000000  1.000000   26.348262  0.000000   0.000000   0.000000   1.000000
1.000000   0.000000   138.000000 1.000000   1.100000   0.900000
13.000000  2.000000   26.348262  10.000000  0.000000   0.000000   1.000000
1.000000   0.000000   138.000000 1.000000   1.100000   0.900000
14.000000  1.000000   26.348262  0.000000   0.000000   0.000000   1.000000
1.000000   0.000000   138.000000 1.000000   1.100000   0.900000
15.000000  1.000000   26.348262  0.000000   0.000000   0.000000   1.000000
1.000000   0.000000   138.000000 1.000000   1.100000   0.900000
```

```
16.000000   1.000000   26.348262   0.000000   0.000000   0.000000   1.000000
1.000000   0.000000   138.000000  1.000000   1.100000   0.900000
17.000000   1.000000   26.348262   10.000000   0.000000   0.000000   1.000000
1.000000   0.000000   138.000000  1.000000   1.100000   0.900000
18.000000   1.000000   26.348262   0.000000   0.000000   0.000000   1.000000
1.000000   0.000000   138.000000  1.000000   1.100000   0.900000
19.000000   1.000000   26.348262   0.000000   0.000000   0.000000   1.000000
1.000000   0.000000   138.000000  1.000000   1.100000   0.900000
20.000000   1.000000   26.348262   10.000000   0.000000   0.000000   1.000000
1.000000   0.000000   138.000000  1.000000   1.100000   0.900000
21.000000   1.000000   26.348262   0.000000   0.000000   0.000000   1.000000
1.000000   0.000000   138.000000  1.000000   1.100000   0.900000
22.000000   2.000000   26.348262   0.000000   0.000000   0.000000   1.000000
1.000000   0.000000   138.000000  1.000000   1.100000   0.900000
23.000000   2.000000   26.348262   10.000000   0.000000   0.000000   1.000000
1.000000   0.000000   138.000000  1.000000   1.100000   0.900000
24.000000   1.000000   26.348262   10.000000   0.000000   0.000000   1.000000
1.000000   0.000000   138.000000  1.000000   1.100000   0.900000
25.000000   1.000000   26.348262   10.000000   0.000000   0.000000   1.000000
1.000000   0.000000   138.000000  1.000000   1.100000   0.900000
26.000000   1.000000   26.348262   10.000000   0.000000   0.000000   1.000000
1.000000   0.000000   138.000000  1.000000   1.100000   0.900000
27.000000   2.000000   26.348262   10.000000   0.000000   0.000000   1.000000
1.000000   0.000000   138.000000  1.000000   1.100000   0.900000
28.000000   1.000000   26.348262   10.000000   0.000000   0.000000   1.000000
1.000000   0.000000   138.000000  1.000000   1.100000   0.900000
29.000000   1.000000   52.696524   10.000000   0.000000   0.000000   1.000000
1.000000   0.000000   138.000000  1.000000   1.100000   0.900000
30.000000   1.000000   52.696524   10.000000   0.000000   0.000000   1.000000
1.000000   0.000000   138.000000  1.000000   1.100000   0.900000
];

gen=[
1.000000   23.540000   0.000000   200.000000  -100.000000 1.000000   100.000000
1.000000   250.000000  0.000000
2.000000   60.970000   0.000000   200.000000  -100.000000 1.000000   100.000000
1.000000   250.000000  0.000000
13.000000   37.000000   0.000000   200.000000  -100.000000 1.000000   100.000000
1.000000   250.000000  0.000000
22.000000   21.590000   0.000000   200.000000  -100.000000 1.000000   100.000000
1.000000   250.000000  0.000000
23.000000   19.200000   0.000000   200.000000  -100.000000 1.000000   100.000000
1.000000   152.238806  0.000000
27.000000   26.910000   0.000000   200.000000  -100.000000 1.000000   100.000000
1.000000   250.000000  0.000000
```

];

branch=[
1.000000 2.000000 0.000000 0.060000 0.000000 50.000000 50.000000
50.000000 0.000000 0.000000 1.000000
1.000000 3.000000 0.000000 0.190000 0.000000 200.000000 200.000000
200.000000 0.000000 0.000000 1.000000
2.000000 4.000000 0.000000 0.170000 0.000000 200.000000 200.000000
200.000000 0.000000 0.000000 1.000000
3.000000 4.000000 0.000000 0.040000 0.000000 100.000000 100.000000
100.000000 0.000000 0.000000 1.000000
2.000000 5.000000 0.000000 0.200000 0.000000 100.000000 100.000000
100.000000 0.000000 0.000000 1.000000
2.000000 6.000000 0.000000 0.180000 0.000000 200.000000 200.000000
200.000000 0.000000 0.000000 1.000000
4.000000 6.000000 0.000000 0.040000 0.000000 200.000000 200.000000
200.000000 0.000000 0.000000 1.000000
5.000000 7.000000 0.000000 0.120000 0.000000 100.000000 100.000000
100.000000 0.000000 0.000000 1.000000
6.000000 7.000000 0.000000 0.080000 0.000000 100.000000 100.000000
100.000000 0.000000 0.000000 1.000000
6.000000 8.000000 0.000000 0.040000 0.000000 100.000000 100.000000
100.000000 0.000000 0.000000 1.000000
6.000000 9.000000 0.000000 0.210000 0.000000 100.000000 100.000000
100.000000 0.000000 0.000000 1.000000
6.000000 10.000000 0.000000 0.560000 0.000000 100.000000 100.000000
100.000000 0.000000 0.000000 1.000000
6.000000 28.000000 0.000000 0.060000 0.000000 80.000000 80.000000
80.000000 0.000000 0.000000 1.000000
8.000000 28.000000 0.000000 0.200000 0.000000 100.000000 100.000000
100.000000 0.000000 0.000000 1.000000
9.000000 11.000000 0.000000 0.210000 0.000000 100.000000 100.000000
100.000000 0.000000 0.000000 1.000000
9.000000 10.000000 0.000000 0.110000 0.000000 100.000000 100.000000
100.000000 0.000000 0.000000 1.000000
4.000000 12.000000 0.000000 0.260000 0.000000 100.000000 100.000000
100.000000 0.000000 0.000000 1.000000
12.000000 13.000000 0.000000 0.140000 0.000000 400.000000 400.000000
400.000000 0.000000 0.000000 1.000000
12.000000 14.000000 0.000000 0.260000 0.000000 100.000000 100.000000
100.000000 0.000000 0.000000 1.000000
12.000000 15.000000 0.000000 0.130000 0.000000 100.000000 100.000000
100.000000 0.000000 0.000000 1.000000
12.000000 16.000000 0.000000 0.200000 0.000000 100.000000 100.000000
100.000000 0.000000 0.000000 1.000000

```
14.000000   15.000000   0.000000   0.200000   0.000000   100.000000  100.000000
100.000000  0.000000    0.000000   1.000000
16.000000   17.000000   0.000000   0.190000   0.000000   100.000000  100.000000
100.000000  0.000000    0.000000   1.000000
15.000000   18.000000   0.000000   0.220000   0.000000   100.000000  100.000000
100.000000  0.000000    0.000000   1.000000
15.000000   23.000000   0.000000   0.200000   0.000000   200.000000  200.000000
200.000000  0.000000    0.000000   1.000000
18.000000   19.000000   0.000000   0.130000   0.000000   100.000000  100.000000
100.000000  0.000000    0.000000   1.000000
19.000000   20.000000   0.000000   0.070000   0.000000   100.000000  100.000000
100.000000  0.000000    0.000000   1.000000
10.000000   20.000000   0.000000   0.210000   0.000000   100.000000  100.000000
100.000000  0.000000    0.000000   1.000000
10.000000   17.000000   0.000000   0.080000   0.000000   100.000000  100.000000
100.000000  0.000000    0.000000   1.000000
10.000000   21.000000   0.000000   0.070000   0.000000   100.000000  100.000000
100.000000  0.000000    0.000000   1.000000
10.000000   22.000000   0.000000   0.150000   0.000000   100.000000  100.000000
100.000000  0.000000    0.000000   1.000000
21.000000   22.000000   0.000000   0.020000   0.000000   100.000000  100.000000
100.000000  0.000000    0.000000   1.000000
22.000000   24.000000   0.000000   0.180000   0.000000   100.000000  100.000000
100.000000  0.000000    0.000000   1.000000
23.000000   24.000000   0.000000   0.270000   0.000000   50.000000   50.000000
50.000000   0.000000    0.000000   1.000000
24.000000   25.000000   0.000000   0.330000   0.000000   100.000000  100.000000
100.000000  0.000000    0.000000   1.000000
25.000000   26.000000   0.000000   0.380000   0.000000   100.000000  100.000000
100.000000  0.000000    0.000000   1.000000
25.000000   27.000000   0.000000   0.210000   0.000000   100.000000  100.000000
100.000000  0.000000    0.000000   1.000000
28.000000   27.000000   0.000000   0.400000   0.000000   100.000000  100.000000
100.000000  0.000000    0.000000   1.000000
27.000000   29.000000   0.000000   0.420000   0.000000   100.000000  100.000000
100.000000  0.000000    0.000000   1.000000
27.000000   30.000000   0.000000   0.600000   0.000000   100.000000  100.000000
100.000000  0.000000    0.000000   1.000000
29.000000   30.000000   0.000000   0.450000   0.000000   100.000000  100.000000
100.000000  0.000000    0.000000   1.000000
];

areas=[
1.000000    5.000000
];
```

```
gencost=[
2.000000    0.000000    0.000000    3.000000    0.000000    70.000000   0.000000
2.000000    0.000000    0.000000    3.000000    0.000000    80.000000   0.000000
2.000000    0.000000    0.000000    3.000000    0.000000    81.000000   0.000000
2.000000    0.000000    0.000000    3.000000    0.000000    71.000000   0.000000
2.000000    0.000000    0.000000    3.000000    0.000000    60.000000   0.000000
2.000000    0.000000    0.000000    3.000000    0.000000    110.000000  0.000000
];

return;
```

Appendix F

DSP Program for the medium voltage CNT prototype experiment

```
#include "DSP281x_Device.h"     // DSP281x Headerfile Include
File
#include "DSP281x_Examples.h"   // DSP281x Examples Include File
#include "math.h"                // ANSI C Include File
#include "stdlib.h"
#include "IQmathLib.h"
#include "variables.h"


#define N 168   // Number of Samples per period
#define pi 3.14159265358979  // PI
#define    phi_gain 0.001534
#define sine_N 500

// Prototype statements for functions found within this file.
void init_eva(void);
//void init_evb(void);
void InitGPIO(void);
void spi_init(void);
void dac_send(double x,double xmin, double xmax, int channel);
int get_sign(double X, int *s_counter, int aS);
interrupt void t1uf_isr(void);
void haf_init(void);
void haf_tog(void);

// Global counts used in this example
Uint16 i=0,a=0,j,k;
Uint16 is=0, ic=N/4;
Uint16 is2w=0, ic2w=N/4;

int index_i=0;
double Vec[N],sine[N],T,M=0.8;
double s, c, s2w, c2w, OneByN = 1.0/N;

// PLL Variables
double U,V, Yk=0.0, Yk1=0.0;
double Tpmax=5000.0,Tpmin=2000.0;
double Tp=3720.0;
double bp=1, kp=3.0;

// ADC Variables
double Iin, Iin1, Iin2, Ithr=200.0;
double Vin, Vconv, Vthr=200.0;
int tempMODE2;
```

```
// get_sign() variables
int max_count=5,counter1=0, counter2=0, counter3=0;
int aS1=1,aS2=1, aS3=1;

// Main Variables
double D;       // Duty Cycle
int phi=0,delta=0, PHI;
int temp_angle;
double temp2, temp3, temp4;


// Flash Variables
extern Uint16 RamfuncsLoadStart;
extern Uint16 RamfuncsLoadEnd;
extern Uint16 RamfuncsRunStart;

// HAF Control Variables
double Kp_haf=0.055, Ki_haf=0.00005;        //0.11, 0.0001
double V3d_max=0.7, V3d_min=-0.7, V3q_max=0.7, V3q_min=-0.7,
Vdq_max = 0.3;
double HafState=0, HafTimer=0, PosTog=0, Led23Temp=0, Tog3Temp=0;
double Vdc = 5, k_sensor = 100, n_xmer = 8, k3;
double V3_ref, Vdq_ref;
double ILine1d, ILine3d, MILine1d[N], MILine3d[N];
double ILine1q, ILine3q, MILine1q[N], MILine3q[N];
double eh_d,uh_d,uh_d1,eh_d1, Dd, V3d_ref;
double eh_q,uh_q,uh_q1,eh_q1, Dq, V3q_ref;
double sin3theta, cos3theta;

// New PLL variables

double sine_LUT[sine_N];
double onebysine_N = 1.0/sine_N;
double volt_scale = 1.0/1150;
double temp_Vin, temp2_Vin;
int theta_array[4], theta_prev;
double theta_mean;
int theta_index=0, quarter = 1, prev_i = 0;
int theta, Vin_prev=0;



void main(void)
{

// Step 1. Initialize System Control:
// PLL, WatchDog, enable Peripheral Clocks
// This example function is found in the DSP281x_SysCtrl.c file.
   InitSysCtrl();
```

```
// Step 2. Initalize GPIO:

   InitGPIO();

// Step 3. Clear all interrupts and initialize PIE vector table:
// Disable CPU interrupts
   DINT;

     MemCopy(&RamfuncsLoadStart, &RamfuncsLoadEnd,
&RamfuncsRunStart);
     InitFlash();


// Initialize PIE control registers to their default state.
// The default state is all PIE interrupts disabled and flags
// are cleared.
// This function is found in the DSP281x_PieCtrl.c file.
   InitPieCtrl();

   // Disable CPU interrupts and clear all CPU interrupt flags:
   IER = 0x0000;
   IFR = 0x0000;

// Initialize the PIE vector table with pointers to the shell
Interrupt
// Service Routines (ISR).
// This will populate the entire table, even if the interrupt
// is not used in this example.  This is useful for debug
purposes.
// The shell ISR routines are found in DSP281x_DefaultIsr.c.
// This function is found in DSP281x_PieVect.c.
   InitPieVectTable();

// ISR functions found within this file.
   EALLOW;  // This is needed to write to EALLOW protected
register
   PieVectTable.T1UFINT = &t1uf_isr;
   EDIS;    // This is needed to disable write to EALLOW
protected registers


// Step 4. Initialize all the Device Peripherals:
// This function is found in DSP281x_InitPeripherals.c
// InitPeripherals(); // Not required for this example

   AdcRegs.ADCTRL1.bit.ACQ_PS = 0x0;        // S/H width in ADC
module periods
   AdcRegs.ADCTRL1.bit.SEQ_CASC = 1;        // 1  Cascaded mode
```

```
   AdcRegs.ADCTRL1.bit.CONT_RUN = 0;        // Setup start stop
mode
   AdcRegs.ADCTRL3.bit.ADCCLKPS =0x4;       // ADC module clock =
HSPCLK/4*ADC_CKPS   = 25MHz/(1*2) = 12.5MHz
   AdcRegs.ADCMAXCONV.bit.MAX_CONV1 =0xF;   // Setup number of
conv's on SEQ1
   AdcRegs.ADCCHSELSEQ1.bit.CONV00 = 0x0;   // Setup ADCINA1 as
1st SEQ1 conv.
   AdcRegs.ADCCHSELSEQ1.bit.CONV01 = 0x1;   // Setup ADCINA2 as
2st SEQ1 conv.
   AdcRegs.ADCCHSELSEQ1.bit.CONV02 = 0x2;   // Setup ADCINA1 as
1st SEQ1 conv.
   AdcRegs.ADCCHSELSEQ1.bit.CONV03 = 0x3;   // Setup ADCINA2 as
2st SEQ1 conv.
   AdcRegs.ADCCHSELSEQ2.bit.CONV04 = 0x4;   // Setup ADCINA1 as
1st SEQ1 conv.
   AdcRegs.ADCCHSELSEQ2.bit.CONV05 = 0x5;   // Setup ADCINA2 as
2st SEQ1 conv.
   AdcRegs.ADCCHSELSEQ2.bit.CONV06 = 0x6;   // Setup ADCINA1 as
1st SEQ1 conv.
   AdcRegs.ADCCHSELSEQ2.bit.CONV07 = 0x7;   // Setup ADCINA2 as
2st SEQ1 conv.
   AdcRegs.ADCCHSELSEQ3.bit.CONV08 = 0x8;   // Setup ADCINA1 as
1st SEQ1 conv.
   AdcRegs.ADCCHSELSEQ3.bit.CONV09 = 0xE;   // Setup ADCINA2 as
2st SEQ1 conv.
   AdcRegs.ADCCHSELSEQ3.bit.CONV10 = 0xD;   // Setup ADCINA1 as
1st SEQ1 conv.
   AdcRegs.ADCCHSELSEQ3.bit.CONV11 = 0xB;   // Setup ADCINA2 as
2st SEQ1 conv.
   AdcRegs.ADCCHSELSEQ4.bit.CONV12 = 0xC;   // Setup ADCINA1 as
1st SEQ1 conv.
   AdcRegs.ADCCHSELSEQ4.bit.CONV13 = 0xF;   // Setup ADCINA2 as
2st SEQ1 conv.
   AdcRegs.ADCCHSELSEQ4.bit.CONV14 = 0x9;   // Setup ADCINA1 as
1st SEQ1 conv.
   AdcRegs.ADCCHSELSEQ4.bit.CONV15 = 0xA;   // Setup ADCINA2 as
2st SEQ1 conv.



   InitAdc();  // For this example, init the ADC


   init_eva();
   //init_evb();
   spi_init();          // init SPI

     MAIN_FCLR = 0;
```

```
   MODE2=0;
   MODE3=0;
   MODE4=0;
   MODE5=0;
   MODE6=0;

     EGPIO3=0;

   ILine1d = 0.0;
   ILine1q = 0.0;
   ILine3d = 0.0;
   ILine3q = 0.0;

     for(i=0;i<N;i++)
     {
          sine[i] = sin(2.0*pi*i/N);
          Vec[i]     = 0.0;
          MILine1d[i] = 0.0;
          MILine1q[i] = 0.0;
          MILine3d[i] = 0.0;
          MILine3q[i] = 0.0;
     }

    for (i=0;i<sine_N;i++)
     {
        sine_LUT[i] = sin(i*pi*0.5*onebysine_N);
     }
      for (i=0;i<4;i++)
     {
        theta_array[i] = 0.0;
     }

     MAIN_FCLR = 1;



// Enable interrupts required for this example
   PieCtrlRegs.PIECRTL.bit.ENPIE = 1;   // Enable the PIE block
   PieCtrlRegs.PIEIER2.bit.INTx6 = 1;   // Enable PIE Group 2,
INT 6 (T1UF)
   IER=0x2;                             // Enable CPU INT3
   EINT;                                // Enable Global
Interrupts
   ERTM;                                          // Enable Global
realtime interrupt DBGM


  // Just sit and loop forever:
  // PWM pins can be observed with a scope.
  for(;;);       // Triangular Period
```

```
}


void init_eva()
{

    // EVA Configure T1PWM, T2PWM, PWM1-PWM6
    // Initalize the timers
    // Initalize EVA Timer1
    EvaRegs.T1PR = Tp;           // Timer1 period
    EvaRegs.T1CMPR = 0x3C00;     // Timer1 compare
    EvaRegs.T1CNT = 0x0000;      // Timer1 counter

    // TMODE = continuous up/down
    // Timer enable
    // Timer compare enable
    EvaRegs.T1CON.all = 0x0842;


  // Initalize EVA Timer2 Timer2 period
      EvaRegs.T2PR = 2*Tp;             // Timer2 period
      EvaRegs.T2CMPR = 0x03C0;     // Timer2 compare
      EvaRegs.T2CNT = 0x0000;      // Timer2 counter
  // TMODE = continuous up/down
  // Timer enable
  // Timer compare enable
  EvaRegs.T2CON.all = 0x0842;

  // Setup T2PWM
  // Drive T2 PWM by compare logic
      EvaRegs.GPTCONA.bit.TCMPOE = 1;
  // Polarity of GP Timer 2 Compare = Active high
      EvaRegs.GPTCONA.bit.T2PIN = 2;
 // Polarity of GP Timer 2 Compare = Active high
      EvaRegs.GPTCONA.bit.T1PIN = 1;


    // Enable Period interrupt bits for GP timer 1
      EvaRegs.EVAIMRA.bit.T1UFINT = 1;
      EvaRegs.EVAIFRA.bit.T1UFINT = 1;

    // Enable compare for PWM1-PWM6
    EvaRegs.CMPR1 = 0x0C00;
    EvaRegs.CMPR2 = 0x75A;
    EvaRegs.CMPR3 = 0x75A;


    // Compare action control.  Action that takes place
```

```
    // on a cmpare event
    // output pin 1 CMPR1 - active low
    // output pin 2 CMPR1 - active high
    // output pin 3 CMPR2 - active low
    // output pin 4 CMPR2 - active high
    // output pin 5 CMPR3 - active low
    // output pin 6 CMPR3 - active high
     //** SE DEBEN ENVIAR LOS PULSOS NEGADOS**//
    EvaRegs.ACTRA.all = 0x0666;
    EvaRegs.DBTCONA.all = 0x0000; // Disable deadband
    EvaRegs.COMCONA.all = 0xA600;
}

int get_sign(double X, int *s_counter, int aS)

{
     int iS;
     int aux_count;

     aux_count = *s_counter;

     iS=X>=0;                          // Instant Sign

     if(aS)                                 // If Actual Sign is
1...
     {
          if(iS) aux_count=0;          // and the Instant Sign is
1 then the counter is 0
          else aux_count++;            // else the sign count
starts
     }
     else                              // If Actual Sign is not
1...
     {
          if(iS) aux_count++;          // and the Instant Sign is
1 then the sign count starts
          else aux_count=0;            // else the sign counter is
0
     }

     if (aux_count>=max_count)   // If the sign counter reaches
the max_count value, then...
     {
          aS=1-aS;                     // the Actual Sign Changes
(from 1 to 0 or from 0 to 1)
          aux_count=0;                 // and the sign counter
must be reset to 0.
     }

     *s_counter = aux_count;
```

```
     return aS;
//GpioDataRegs.GPADAT.bit.GPIOA8 = aS;

}

void spi_init()
{
     SpiaRegs.SPICCR.all =0x000F;                 // Reset on,
rising edge, 16-bit char bits
     SpiaRegs.SPICTL.all =0x000E;               // Enable master
mode, delay phase,
                                                 // enable talk,
and SPI int disabled.
     SpiaRegs.SPIBRR =0x000A;

    SpiaRegs.SPICCR.all =0x009F;               // Relinquish SPI
from Reset
    SpiaRegs.SPIPRI.bit.FREE = 1;                // Set so
breakpoints don't disturb xmission
}


void dac_send(double x,double xmin, double xmax, int channel)

{
    double Ftest, offset,span;
     Uint16 data,AB;
     if(x<xmin)x=xmin;
     if(x>xmax)x=xmax;
     offset = - xmin;
     span = xmax-xmin;
    Ftest=(x + offset)/span*511.0;
     data = ((int)(Ftest))<<7;
     if (channel == 2) AB= 1024;
     else AB=0;
    SpiaRegs.SPIDAT= AB + 768 + (data>>8);
}



void InitGPIO(void)

{
   EALLOW;

   // Initialize all GP as inputs

    GpioMuxRegs.GPAMUX.all = 0x0000;                  // GPIOA
registers as I/O
```

```
    GpioMuxRegs.GPADIR.all = 0x0000;                    // Set
pins as inputs

    GpioMuxRegs.GPBMUX.all = 0x0000;                    // GPIOB
registers as I/O
    GpioMuxRegs.GPBDIR.all = 0x0000;                    // Set
pins as inputs

    GpioMuxRegs.GPDMUX.all = 0x0000;                    // GPIOD
registers as I/O
    GpioMuxRegs.GPDDIR.all = 0x0000;                    // Set
pins as inputs

     GpioMuxRegs.GPEMUX.all = 0x0000;                   // GPIOE
registers as I/O
    GpioMuxRegs.GPEDIR.all = 0x0000;                    // Set
pins as inputs

    GpioMuxRegs.GPFMUX.all = 0x0000;                    // GPIOF
registers as I/O
    GpioMuxRegs.GPFDIR.all = 0x0000;                  // Set pins
as inputs

    GpioMuxRegs.GPGMUX.all = 0x0000;                    // GPIOG
registers as I/O
    GpioMuxRegs.GPGDIR.all = 0x0000;                    // Set
pins as inputs


/**** Setting LEDs pins as DSP outputs ****/

// LED21 corresponds to the GPIOE0 (P8-5)
     GpioMuxRegs.GPEDIR.bit.GPIOE0 = 1;                      //
Set GPIOE0 as output

// LED22 corresponds to the GPIOA9 (P8-7)
     GpioMuxRegs.GPADIR.bit.GPIOA9 = 1;                      //
Set GPIOA9 as output

// LED23 corresponds to the GPIOA15 (P7-3)
     GpioMuxRegs.GPADIR.bit.GPIOA15 = 1;                     //
Set GPIOA15 as output

// LED24 corresponds to the GPIOD1 (P7-4)
     GpioMuxRegs.GPDDIR.bit.GPIOD1 = 1;                      //
Set GPIOD1 as output

/**** Setting DAC pins as DSP SPI function ****/

// CLK corresponds to the SPICLKA (P8-25)
```

```
     GpioMuxRegs.GPFMUX.bit.SPICLKA_GPIOF2 = 1;       // SPICLKA
register as SPI function

// Enable corresponds to the SPISTEA (P8-26)
     GpioMuxRegs.GPFMUX.bit.SPISTEA_GPIOF3 = 1;       // SPISTEA
register as SPI function

// Data corresponds to the SPISIMOA (P8-23)
     GpioMuxRegs.GPFMUX.bit.SPISIMOA_GPIOF0 = 1;      //
SPISIMOA register as SPI function

/**** Setting EEPROM pins as DSP outpus ****/
// Main PWM (MODE1) corresponds to the T2PWM (P8-16)
     GpioMuxRegs.GPAMUX.bit.T2PWM_GPIOA7 = 1;         // T2PWM
register as PWM function

// MODE2 corresponds to the GPIOA6 (P8-15)
     GpioMuxRegs.GPADIR.bit.GPIOA6 = 1;                    //
Set GPIOA6 as output

// MODE3 corresponds to the GPIOA5 (P8-14)
     GpioMuxRegs.GPADIR.bit.GPIOA5 = 1;                    //
Set GPIOA5 as output

// MODE4 corresponds to the GPIOA4 (P8-13)
     GpioMuxRegs.GPADIR.bit.GPIOA4 = 1;                    //
Set GPIOA4 as output

// MODE5 corresponds to the GPIOF13 (P4-8)
     GpioMuxRegs.GPFDIR.bit.GPIOF13 = 1;                   //
Set GPIOF13 as output

// MODE6 corresponds to the GPIOF12 (P4-7)
     GpioMuxRegs.GPFDIR.bit.GPIOF12 = 1;                   //
Set GPIOF12 as output


/**** Setting EGPIO pins as outputs ****/

// EGPIO1 corresponds to the GPIOF4
     GpioMuxRegs.GPFDIR.bit.GPIOF4 = 1;                    //
Set GPIOF4 as output
// EGPIO2 corresponds to the GPIOF5
     GpioMuxRegs.GPFDIR.bit.GPIOF5 = 1;                    //
Set GPI0F5 as output
// EGPIO3 corresponds to the GPIOA11
     GpioMuxRegs.GPADIR.bit.GPIOA11 = 1;                   //
Set GPIOA11 as output
// EGPIO4 corresponds to the GPIOA12
```

```
     GpioMuxRegs.GPADIR.bit.GPIOA12 = 1;                    //
Set GPIOA12 as output
// EGPIO5 PIN IS DUPLICATED, SHOULD NOT BE USED
// EGPIO6 corresponds to the GPIOF1
     GpioMuxRegs.GPFDIR.bit.GPIOF1 = 1;                     //
Set GPIOF1 as output
// EGPIO7 corresponds to the GPIOF6
     GpioMuxRegs.GPFDIR.bit.GPIOF6 = 1;                     //
Set GPIOF6 as output
// EGPIO8 corresponds to the GPIOF7
     GpioMuxRegs.GPFDIR.bit.GPIOF7 = 1;                     //
Set GPIOF7 as output
// EGPIO9 corresponds to the GPIOD0
     GpioMuxRegs.GPDDIR.bit.GPIOD0 = 1;                     //
Set GPIOD0 as output
// EGPIO10 corresponds to the GPIOD5
     GpioMuxRegs.GPDDIR.bit.GPIOD5 = 1;                     //
Set GPIOD5 as output


  /**** Setting Fault Clear pins ****/

// MAIN_FCLR corresponds to the GPIOB8 (P8-36)
     GpioMuxRegs.GPBDIR.bit.GPIOB8 = 1;                     //
Set GPIOB8 as output
// AS_FCLR corresponds to the GPIOB5 (P8-35)
     GpioMuxRegs.GPBDIR.bit.GPIOB5 = 1;                     //
Set GPIOB5 as output
// AF_FCLR corresponds to the GPIOF11 (P4-6)
     GpioMuxRegs.GPFDIR.bit.GPIOF11 = 1;                    //
Set GPIOF11 as output


/**** Setting Active Filter (Harmonic Trap) pins as DSP PWM
outputs ****/

// AF_PWM1 corresponds to the PWM1 (P8-9)
     GpioMuxRegs.GPAMUX.bit.PWM1_GPIOA0 = 1;                //
PWM1 register as PWM function
// AF_PWM2 corresponds to the PWM2 (P8-10)
     GpioMuxRegs.GPAMUX.bit.PWM2_GPIOA1 = 1;                //
PWM2 register as PWM function
// AF_PWM3 corresponds to the PWM3 (P8-11)
     GpioMuxRegs.GPAMUX.bit.PWM3_GPIOA2 = 1;                //
PWM3 register as PWM function
// AF_PWM4 corresponds to the PWM4 (P8-12)
     GpioMuxRegs.GPAMUX.bit.PWM4_GPIOA3 = 1;                //
PWM4 register as PWM function
```

```
/**** Setting Active Snubber pins as DSP PWM outputs ****/

// AS_PWM1 corresponds to the PWM7 (P8-30)
     GpioMuxRegs.GPBMUX.bit.PWM7_GPIOB0 = 1;                //
PWM7 register as PWM function
// AS_PWM2 corresponds to the PWM7 (P8-31)
     GpioMuxRegs.GPBMUX.bit.PWM8_GPIOB1 = 1;                //
PWM8 register as PWM function
// AS_PWM3 corresponds to the PWM7 (P8-32)
     GpioMuxRegs.GPBMUX.bit.PWM9_GPIOB2 = 1;                //
PWM9 register as PWM function
// AS_PWM4 corresponds to the PWM7 (P8-33)
     GpioMuxRegs.GPBMUX.bit.PWM10_GPIOB3 = 1;          // PWM10
register as PWM function


/**** Setting START pins as outputs ****/

// START1 corresponds to the GPIOB13 (P7-5)
     GpioMuxRegs.GPBDIR.bit.GPIOB13 = 1;                    //
Set GPIOB13 as output
// START2 corresponds to the GPIOB14 (P7-6)
     GpioMuxRegs.GPBDIR.bit.GPIOB14 = 1;                    //
Set GPI0B14 as output
// START3 corresponds to the GPIOB15 (P7-7)
     GpioMuxRegs.GPBDIR.bit.GPIOB15 = 1;                    //
Set GPIOB15 as output
// START4 corresponds to the GPIOD6 (P7-8)
     GpioMuxRegs.GPDDIR.bit.GPIOD6 = 1;                     //
Set GPIOD6 as output



   EDIS;

}


// ISR's used in this example
// INT 2.6
interrupt void t1uf_isr(void)     // EV-A
{
    EGPIO2=1;
     //GpioDataRegs.GPADAT.bit.GPIOA10 = 1;
     EvaRegs.T1PR = Tp;
     //  ADC Code
     AdcRegs.ADCST.bit.INT_SEQ1_CLR = 1;
    // Review ADC input 1
     AdcRegs.ADCTRL2.bit.RST_SEQ1=1;
```

```
      AdcRegs.ADCTRL2.bit.SOC_SEQ1=1;// start of secuence by
software
      //Put results on variables
      // AdcRegs.ADCRESULT0 has 16 bits, where the first 4 LSB
are not data
      // Vin 2048 - (-)2047

      //    PHI = phi_gain*(AdcRegs.ADCRESULT13>>4);
     PHI = (int)(0.5*(AdcRegs.ADCRESULT13>>4));
      Vin = (double)(AdcRegs.ADCRESULT14>>4) - 2140.0;
      Iin = (double)(AdcRegs.ADCRESULT1>>4) - 2150.0;
      Vconv= (double)(AdcRegs.ADCRESULT11>>4) - 2130.0;
      //Iin1 = Iin + 100;
      //Iin2 = Iin - 100;



      Tp= 3720;

      if ((Vin_prev < 0) && (Vin > 0))
      {
            theta = 0;
      }
      else
      {
            theta = theta + 12;
      }

      Vin_prev = Vin;


      if(is == 0)
      {
            if ((PHI-phi)> 64) delta = 1;                // Changed
from 6 to 1
            else if ((PHI-phi)< -64) delta = -1;
            else delta = 0;
            phi = phi + delta;
      }

      temp_angle = 2*theta+phi;

     while(temp_angle >= 2000)
      { temp_angle -= 2000; }

     if (temp_angle < 500)
        { temp2 = sine_LUT[temp_angle];}
      else if (temp_angle < 1000)
        { temp2 = sine_LUT[999 - temp_angle];}
     else if (temp_angle < 1500)
```

```
        { temp2 = -sine_LUT[temp_angle - 1000];}
      else
        { temp2 = -sine_LUT[1999 - temp_angle];}


    //D = 0.50  + 0.10*temp2;
      D = 0.50  + 0.21*temp2;

      tempMODE2=0;
      if ((Iin < Ithr) && (Iin > -Ithr))
      {
            if (Vconv > Vthr)
                  {
                        tempMODE2 = 1;        //Voltage Commutation
                        MODE4 = 1;       //Positive Voltage
                  }
            else if (Vconv < -Vthr)
                  {
                        tempMODE2 = 1;        //Voltage Commutation
                        MODE4 = 0;       //Negative Voltage
                  }
            //MODE2=1;
      }

      aS1 = get_sign(Iin, &counter1, aS1);
      MODE2=tempMODE2;
      //MODE2=1; tempMODE2=1;
      if (tempMODE2 == 0)                   // Current
Commutation
      {
            MODE4=aS1;
      }
//    MODE5=aS2;
//    MODE6=aS3;

      temp_angle = 3*theta;

    while(temp_angle >= 2000)
      { temp_angle -= 2000; }

    if (temp_angle < 500)
        { temp3 = sine_LUT[temp_angle];}
      else if (temp_angle < 1000)
        { temp3 = sine_LUT[999 - temp_angle];}
    else if (temp_angle < 1500)
        { temp3 = -sine_LUT[temp_angle - 1000];}
      else
        { temp3 = -sine_LUT[1999 - temp_angle];}

    temp_angle = 3*theta+500;
```

```
    while(temp_angle >= 2000)
      { temp_angle -= 2000; }

      dac_send(temp_angle, 0.01, 2000 ,1);

    if (temp_angle < 500)
       { temp4 = sine_LUT[temp_angle];}
      else if (temp_angle < 1000)
       { temp4 = sine_LUT[999 - temp_angle];}
    else if (temp_angle < 1500)
       { temp4 = -sine_LUT[temp_angle - 1000];}
      else
       { temp4 = -sine_LUT[1999 - temp_angle];}


 // calculating third harmonic line current

    sin3theta = temp3;
      cos3theta = temp4;

      Dd= 2.0*Iin*sin3theta*OneByN;
      ILine3d = ILine3d-MILine3d[is]+Dd;
      MILine3d[is]= Dd;

    Dq= 2.0*Iin*cos3theta*OneByN;
      ILine3q = ILine3q-MILine3q[is]+Dq;
      MILine3q[is]= Dq;

      // dq axis PI controller
      eh_d  = -ILine3q*0.0033;
      // Present Time Error
      uh_d  = uh_d + Ki_haf*(eh_d1+eh_d)*0.5;                //
Present Time Output
      eh_d1 = eh_d;
      // Past Time Error
      V3d_ref = uh_d + Kp_haf*eh_d ;

      eh_q  = ILine3d*0.0033;
      // Present Time Error
      uh_q  = uh_q + Ki_haf*(eh_q1+eh_q)*0.5;                //
Present Time Output
      eh_q1 = eh_q;
      // Past Time Error
      V3q_ref = uh_q + Kp_haf*eh_q ;

      // Vd and Vq individual limits

      if (uh_d > V3d_max)                    // Changed from
V3d_ref
```

```
      { uh_d = V3d_max; }
      else if (uh_d < V3d_min)
      { uh_d = V3d_min; }
      if (uh_q > V3q_max)                    // Changed from
V3q_ref
      { uh_q = V3q_max; }
      else if (uh_q < V3q_min)
      { uh_q = V3q_min; }


      if (HafState < 4)
      {
           haf_init();
      }
      if ((LED23 == 0) && (TOG3 == 1))
      {
           PosTog = 1;
      }
      else if ((LED23 == 1) && (TOG3 == 0))
      {
           PosTog = -1;
      }

      if (PosTog != 0)
      {
           haf_tog();
      }

      //dac_send(phi,0.1, 7.0 ,1);
      //dac_send(uh_d, V3d_min, V3d_max ,1);
      //dac_send(Vin, -2048.0, +2048.0 , 2);

      LED21=TOG1;
      LED22=TOG2;
      LED23=TOG3;
      LED24=TOG4;

      MODE3=TOG1;

      if (FM == 1)          // Disable in case of a fault
      {
           MODE3 = 0;
      }

      is++;
      if(is==N) is=0;

      //    GpioDataRegs.GPADAT.bit.GPIOA9 = sine[indexs0]>0;

      MainPWM = D*2*Tp;
```

```
        // Enable more interrupts from this timer
        EvaRegs.EVAIMRA.bit.T1UFINT = 1;

        // Note: To be safe, use a mask value to write to the
entire
        // EVAIFRB register.  Writing to one bit will cause a
read-modify-write
        // operation that may have the result of writing 1's to
clear
        // bits other then those intended.
        EvaRegs.EVAIFRA.all = BIT9;

        // Acknowledge interrupt to receive more interrupts from
PIE group 2
       PieCtrlRegs.PIEACK.all = PIEACK_GROUP2;
      EGPIO2=0;

}

void haf_init(void)
{

      // Switch off LED
      LED23 = 0;

      // Initializing sequence for gate driver, charging Boot Cap
      if (HafState == 0)
      {
            FCLR = 1;
            HafState++;
      }
      else if (HafState == 1)
      {
            EvaRegs.ACTRA.all = 0x069F;
            HafState++;
      }
      else if (HafState == 2)
      {
            EvaRegs.ACTRA.all = 0x0690;
            HafState++;
      }
      else if (HafState == 3)
      {
            FCLR = 0;
            HafState++;
      }
```

```
}

void haf_tog(void)
{

double temp;
      if (PosTog == 1)
      {
            // Glow LED
            LED23 = 1;

            if (HafState == 4)
            {
                  // Wait for 100 ms for contactor to turn on
                  // Re-initialize PI errors to zero
                  HafTimer++;
                  if (HafTimer == 1000)
                  {
                        HafState++;
                        uh_d = 0.0;
                        uh_q = 0.0;
                        eh_d1 = 0.0;
                        eh_q1 = 0.0;
                        HafTimer = 0;
                        EvaRegs.ACTRA.all = 0x0696;
                  }
            }
            else if (HafState == 5)
            {

            V3_ref = V3d_ref*sin3theta+V3q_ref*cos3theta;
                  //EvaRegs.CMPR1 = 9*Tp/10;
                  temp =  Tp-Tp*0.5*(V3_ref + 1);
                  if (temp > Tp)
                  {
                        temp = Tp;
                  }
          else if (temp < 0)
             {
                  temp = 0;
             }

                  EvaRegs.CMPR1 = temp;
                  //EvaRegs.CMPR1 = 9*Tp/10;
            }
      }
      else
      {
            // Negative Toggle, switch HAF off
            LED23 = 0;
```

```
            if (HafState == 5)
            {
                  EvaRegs.CMPR1 = 0;
                  //EvaRegs.CMPR2 = Tp;
                  HafState = 4;
                  //EGPIO2 = 0;
                  //LED23 = TOG3;
                  EvaRegs.ACTRA.all = 0x0690;
            }
      }
}


//===========================================================================
============
// No more.
//===========================================================================
============
```

Appendix G

EEPROM data generator in Matlab for the medium voltage experiment

```
clear all
close all
clc

A = xlsread('EEPROM.xls','MODE 6')

%A=[NaN(max(size(A)),1) A];
AA=A;

[n,m]=size(A);

Ha=[];
Hd=[];
k=1;

for i=1:n
    N=find(isnan(A(i,:)));
    V=0:2^length(N)-1;
    T=dec2bin(V);
    [x,y]=size(T);
    for j=1:x
        R=[];
        for l=1:y
            R(l)=str2num(T(j,l));
        end
        AA(k,:)=A(i,:);
        AA(k,N)=R;
        k=k+1;
    end
end

[n,m]=size(AA);

B=2.^(10:-1:0);
C=2.^(7:-1:0);

for i=1:n
    D=dot(AA(i,1:11),B);
    E=dot(AA(i,12:19),C);
    Ha=[Ha; dec2hex(D,4)];
    Hd=[Hd; dec2hex(E,2)];
end

save address Ha Hd
```

```
clear all
close all
clc

load address

N=length(Ha);

fid=fopen('eeprom.hex','w');

for i=1:N
    str=[':01' Ha(i,:) '00' Hd(i,:) 'FF'];
    fwrite(fid,str,'char');
    fprintf(fid,'\r\n');
end

fwrite(fid,':00000001FF','char');

fclose(fid)
```

Appendix H

PCB layout of the signal conditioning board for the medium voltage experiment

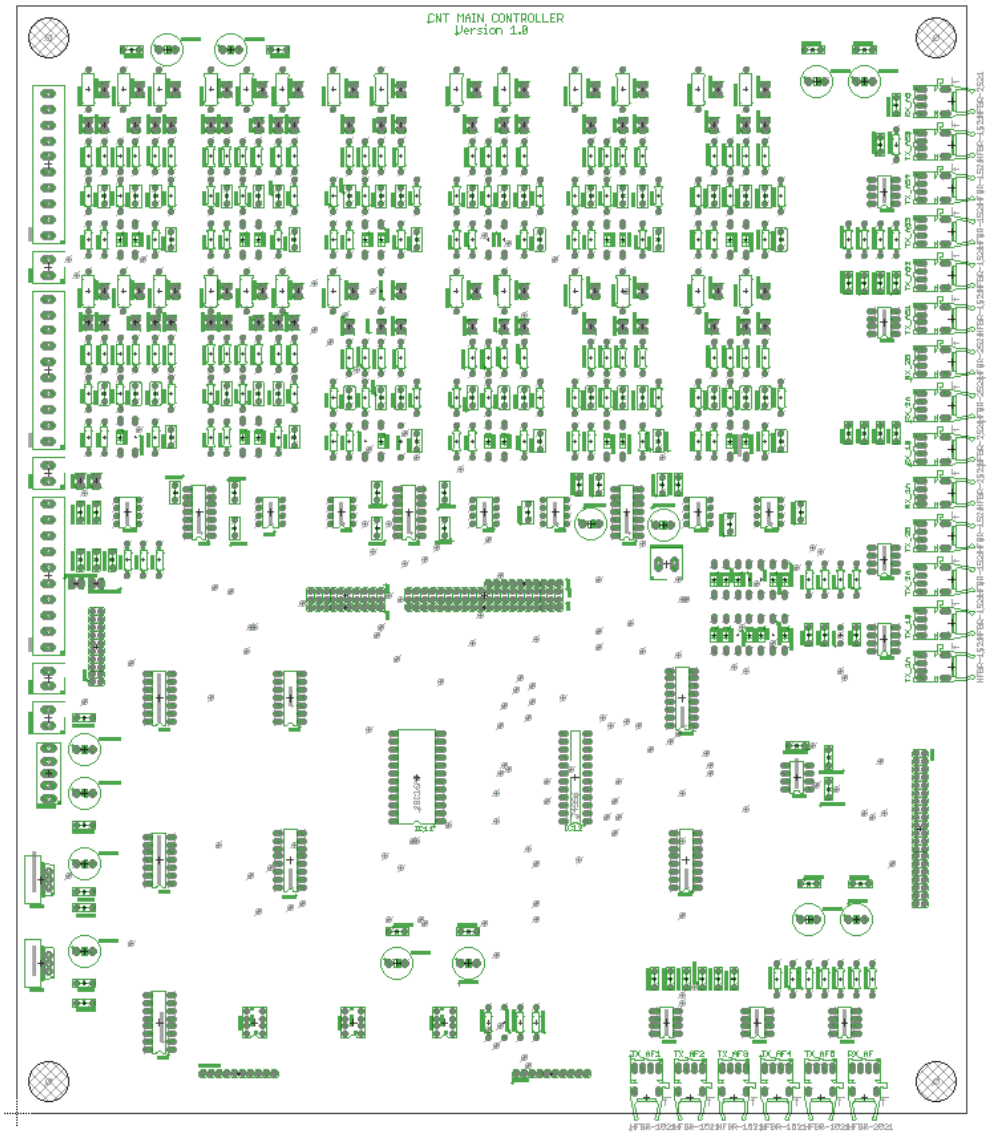

Figure H.1: PCB layout of the signal conditioning board

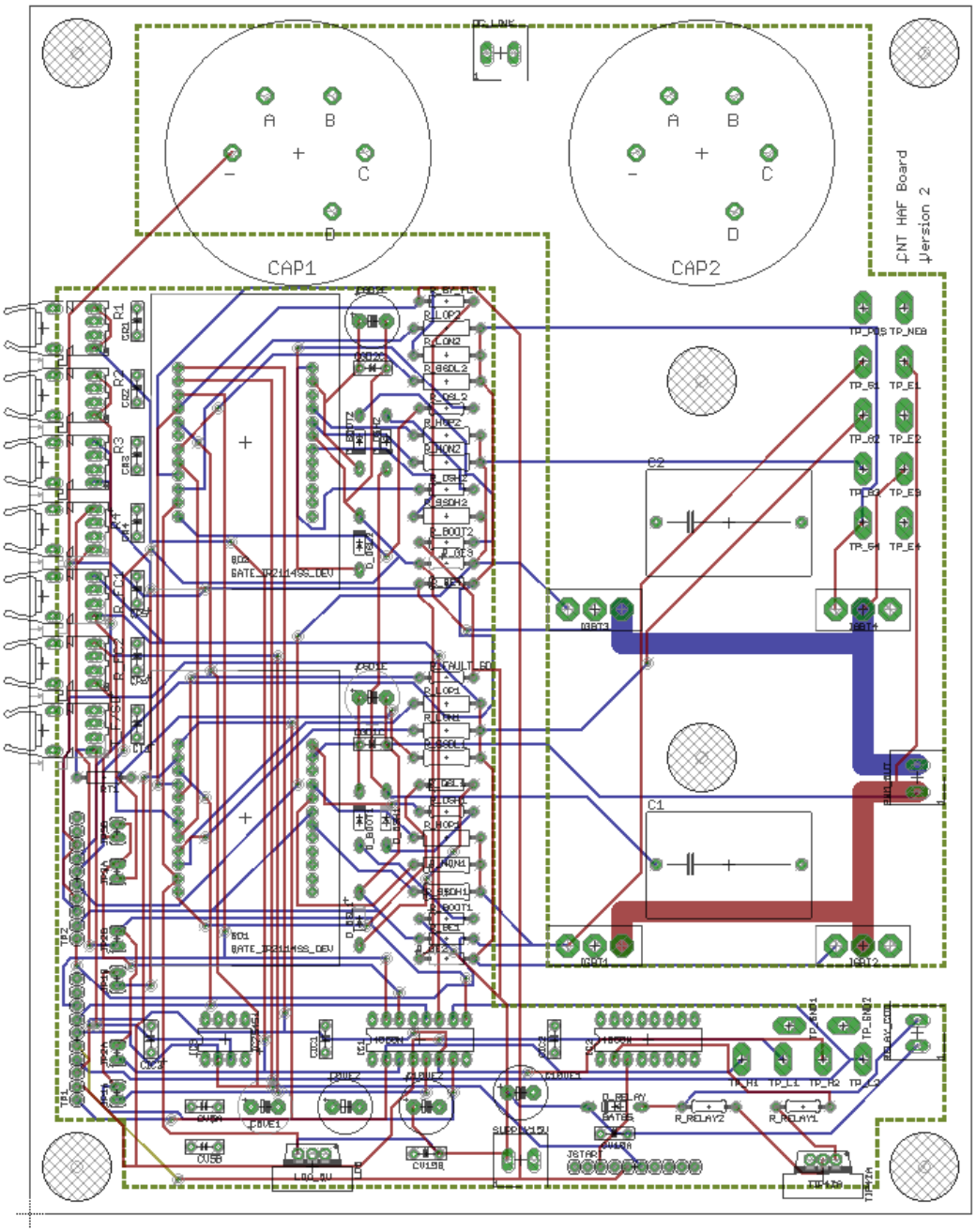

Figure H.2: PCB layout of the hybrid active filter gate driver board

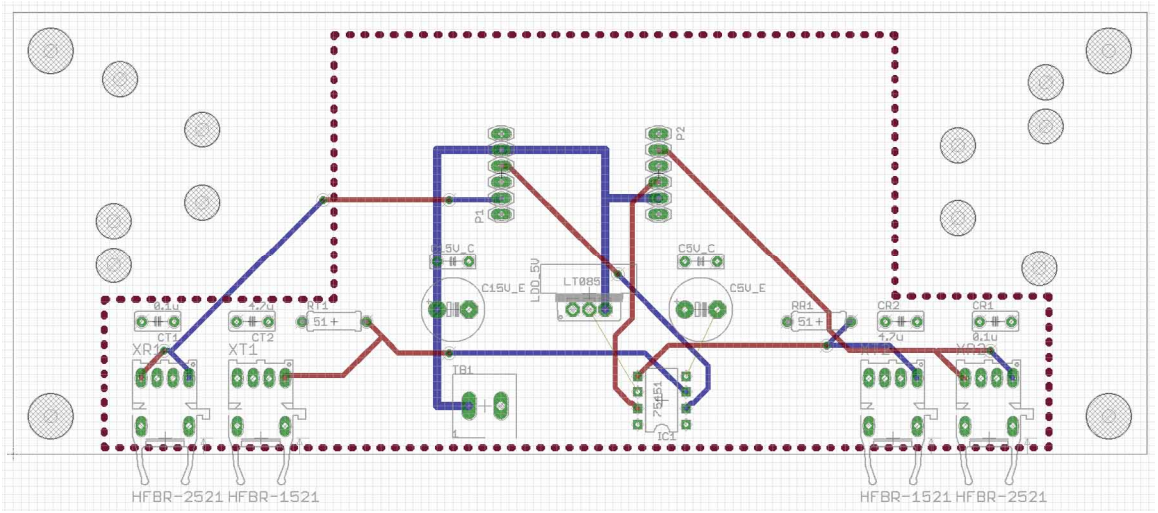

Figure H.3: PCB layout of the TACC gate signal receiver board

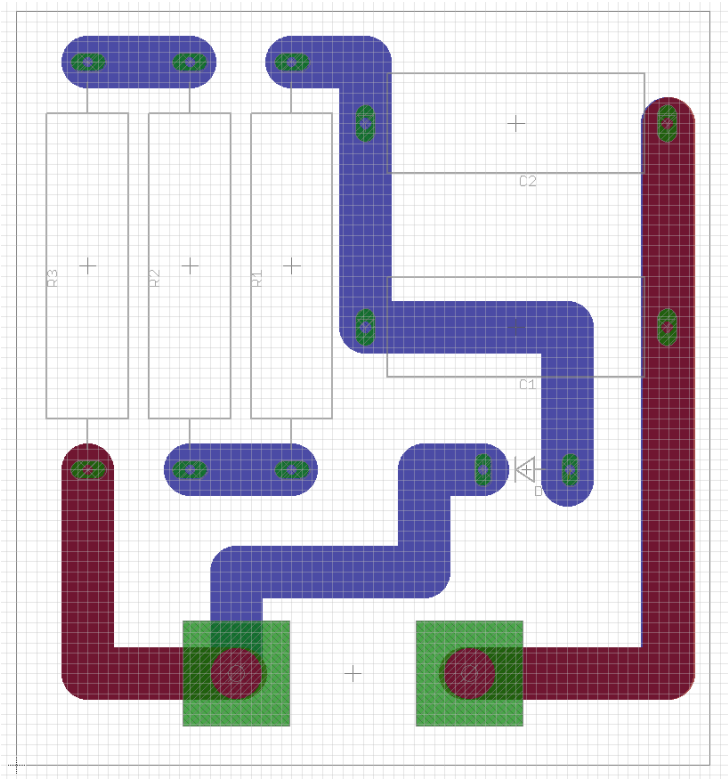

Figure H.4: PCB layout of the TACC snubber board

REFERENCES

[1] Website of US Energy Information Administration http://www.eia.doe.gov/electricity/data.cfm

[2] National electric transmission congestion study, Dec 2009, US Department of Energy

[3] Website of Energy efficiency & Renewable Energy, US Department of Energy http://apps1.eere.energy.gov/states/maps/renewable_portfolio_states.cfm

[4] Website of the Regional Greenhouse Gas Initiative http://www.rggi.org/home

[5] Website of Govtrack.us http://www.govtrack.us/congress/bill.xpd?bill=h111-2454

[6] R. Wiser, G. Barbose, "Renewable Portfolio Standards in the United States: A status report with data through 2007", Lawrence Berkeley National Laboratory

[7] "Green super highways: building a path to America's clean energy future", American Wind Energy Association and the Solar Energy Industries Association

[8] Mike Sloan, "Texas wind: a bit of history", Virtus Energy Research Associates, available at http://www.treia.org/assets/documents/A%20bit%20of%20history.pdf

[9] W. W. Hogan, "Financial transmission right incentives: applications beyond hedging", Harvard Electricity Policy Group, May 2002

[10] H. Johal, D. Divan, "Current Limiting Conductors: A Distributed Approach for Increasing T&D System Capacity and Enhancing Reliability", IEEE PES Transmission and Distribution Conference and Exhibition, 2005/2006 , Pages 1127-1133

[11] Data from AEP website http://www.aep.com/about/transmission/docs/transmission-facts.pdf

[12] H. H. Happ, "Optimal Power Dispatch", IEEE Transactions on Power Apparatus and Systems, Volume: PAS-93 , Issue: 3 Publication Year: 1974 , Page(s): 820 – 830

[13] O. J. M. Smith, "Power System State Estimation", IEEE Transactions on Power Apparatus and Systems, Volume: PAS-89 , Issue: 3 , Publication Year: 1970 , Page(s): 363 – 379

[14] S. S. Sharif, J. H. Taylor, E. F. Hill, "On-line optimal reactive power flow by energy loss minimization", Proceedings of the 35th IEEE Decision and Control, 1996., Publication Year: 1996 , Page(s): 3851 - 3856 vol.4

[15] N. G. Hingorani, L. Gyugyi, “Understanding FACTS – Concepts and Technology of Flexible AC Transmission Systems”, IEEE press

[16] D. M. Getson, “On-load tap changers”, available at ABB website, http://www05.abb.com/global/scot/scot252.nsf/veritydisplay/f741130363e7c6de85256d6f007aade1/$file/030129_on-load.pdf

[17] W. J. Lyman, "Controlling Power Flow with Phase Shifting Equipment", AIEE transactions, volume 49, 1930, page 825.

[18] K. K. Sen, M. L. Sen;, "Introducing the family of "Sen" transformers: a set of power flow controlling transformers", 2002 IEEE Power Engineering Society Summer Meeting, Volume: 1

[19] R. J. Piwko, E. V. Larsen, C. A. Wegner, "Variable frequency transformer - a new alternative for asynchronous power transfer", 2005 IEEE Power Engineering Society Inaugural Conference and Exposition in Africa, Page(s): 393 – 398

[20] F. Iliceto, E. Cinieri, "Comparative analysis of series and shunt compensation schemes for AC transmission systems", IEEE Transactions on Power Apparatus and Systems, Volume: 96 , Issue: 6 , Publication Year: 1977 , Page(s): 1819 – 1830

[21] S. Mori, K. Matsuno, T. Hasegawa, S. Ohnishi, M. Takeda, M. Seto, S. Murakami, F. Ishiguro, "Development of a large static VAr generator using self-commutated inverters for improving power system stability", IEEE Transactions on Power Systems, Volume: 8 , Issue: 1, Publication Year: 1993 , Page(s): 371 – 377

[22] P. Petitclair, Y. Besanger, S. Bacha, N. Hadjsaid, "FACTS modelling and control: applications to the insertion of a STATCOM on power system", IEEE Industry Applications Conference, 1997, Volume: 3, Publication Year: 1997 , Page(s): 2213 – 2217

[23] L. Gyugyi. "Solid state control of electric power in AC transmission systems", EECPS, Capri, May1989.

[24] L. Gyugyi, C. D. Schauder, S. L. Williams, T. R. Rietman, D. R. Torgerson, A. Edris, "The unified power flow controller: a new approach to power transmission control", IEEE Transactions on Power Delivery, Volume: 10 , Issue: 2 Publication Year: 1995 , Page(s): 1085 – 1097

[25] M. H. Baker, R. P. Burgess, "Design and experience of a back-to-back HVDC link in western Canada", International Conference on Advances in Power System Control, Operation and Management, 1991, Page(s): 686 - 693 vol.2

[26] P. Kundur, "Power System Stability and Control", McGraw-Hill, 1994, pp. 463 – 580.

[27] CIGRE and IEEE Joint Task Force Report, “Guide for planning DC links terminating at AC locations having low short-circuit capacities, Part I: AC/DC interaction phenomena,” CIGRE Publication 68, June 1992.

[28] G. Schmidt, B. Fiegl, S. Kolbeck, “HVDC transmission and the environment,” Power Engineering Journal, vol. 10, no. 5, Oct. 1996, pp. 204 – 210.

[29] M. Venturini, “A new sine wave in sine wave out, conversion technique which eliminates reactive elements,” in Proc. Powercon 7, 1980, pp.E3/1–E3/15

[30] M. Rivera, R. Vargas, J. Espinoza, and J. Rodriguez, “Behavior of the predictive DTC based matrix converter under unbalanced AC-supply,” in Proc. IEEE Power Electron. Spec. Conf., Sep.2007, pp.202–207.

[31] J. Rodriguez, M. Rivera, J. W. Kolar, P. W. Wheeler, "A Review of Control and Modulation Methods for Matrix Converters", IEEE Transactions on Industrial Electronics, Jan 2012.

[32] N. Burany, “Safe Control of Four-Quadrant Switches,” Conference Records of IEEE-IAS Annual Meeting, 1989, pp. 1190-1194.

[33] A. Prasai, D. M. Divan, "Zero-Energy Sag Correctors — Optimizing Dynamic Voltage Restorers for Industrial Applications", Ieee Transactions On Industry Applications, Vol.44, No.6, November / December 2008

[34] D. Divan, J. Sastry, A. Prasai, H. Johal, "Thin AC converters — A new approach for making existing grid assets smart and controllable", IEEE Power Electronics Specialists Conference, 2008. PESC 2008, 15-19 June 2008 Page(s):1695 - 1701.

[35] D. Divan, J. Sastry, "Controllable Network Transformers", IEEE Power Electronics Specialists Conference, 2008. PESC 2008. 15-19 June 2008 Page(s):2340 – 2345

[36] D. Das, D. Divan, "Power flow control in networks using controllable network transformers", IEEE Energy Conversion Congress and Exposition, 2009, Publication Year: 2009 , Page(s): 2224 – 2231

[37] D. Divan, J. Sastry, “Voltage Synthesis Using Dual Virtual Quadrature Sources- A New Concept in AC Power Conversion”, IEEE Power Electronics Specialists Conference (PESC), June 2007. pp. 2678-2684.

[38] D. Das, D. M. Divan, R. G. Harley, "Power Flow Control in Networks Using Controllable Network Transformers", IEEE Transactions on Power Electronics, Volume: 25 , Issue: 7, Publication Year: 2010 , Page(s): 1753 – 1760

[39] D. Das, D. Divan, R. G. Harley, "Increasing inter-area available transfer capacity using controllable network transformers", IEEE Energy Conversion Congress and Exposition (ECCE), 2010, Publication Year: 2010 , Page(s): 3618 – 3625

[40] D. Das, D. Divan, R. G. Harley, "Smart tie line control using Controllable Network Transformers", IEEE PES Transmission and Distribution Conference and Exposition, 2010, Publication Year: 2010

[41] Power systems test case archive, electrical Engineering, University of Washington, available at website, http://www.ee.washington.edu/research/pstca/

[42] Website of ETAP, http://etap.com/load-flow-analysis/load-flow-analysis.htm

[43] R. G. Wasley, M. A. Shlash, "Newton-Raphson algorithm for 3-phase load flow", Proceedings of the Institution of Electrical Engineers, Volume: 121 , Issue: 7, Publication Year: 1974 , Page(s): 630 – 638

[44] http://www.ece.mtu.edu/faculty/bamork/EE5200_F02/NRLF.pdf

[45] Website of Matlab, http://www.mathworks.com/products/simpower/

[46] A. A. Fouad, K. T. Khu, "Damping of Torsional Oscillations in Power Systems with Series-Compensated Lines", IEEE Transactions on Power Apparatus and Systems, Volume: PAS-97 , Issue: 3 Publication Year: 1978 , Page(s): 744 – 753

[47] J T Richardson M R Palmer G Liepins and M Hilliard, "Some guidelines for genetic algorithms with penalty functions", Proceedings of the Third International Conference on Genetic Algorithms 1989, 191-197

[48] A. E. Smith and D. M. Tate, "Genetic optimization using a penalty function", Proceedings of the Fifth International Conference on Genetic Algorithms, 1993, 499-505

[49] P. E. Onate Yumbla, J. M. Ramirez, C. A. Coello Coello, "Optimal Power Flow Subject to Security Constraints Solved With a Particle Swarm Optimizer", IEEE Transactions on Power Systems, Volume: 23 , Issue: 1, Publication Year: 2008 , Page(s): 33 - 40

[50] N. Mo, Z. Y. Zou, K. W. Chan, T. Y. G. Pong, "Transient stability constrained optimal power flow using particle swarm optimisation", IET Generation, Transmission & Distribution, Volume: 1 , Issue: 3, Publication Year: 2007 , Page(s): 476 - 483

[51] Sailaja M. Kumari, G. Priyanka, M. Sydulu, "Comparison of Genetic Algorithms and Particle Swarm Optimization for Optimal Power Flow Including FACTS devices", Power Tech, 2007 IEEE Lausanne, Publication Year: 2007 , Page(s): 1105 - 1110

[52] J. Kennedy, and R. Eberhart, "Particle swarm optimization," in Proc. IEEE Int. Conf. Neural Networks, vol. 4, 1995, pp. 1942-1948.

[53] Z. Gaing, “Particle swarm optimization to solving the economic dispatch considering the generator constraints”, IEEE Transactions on Power Systems, vol. 18, issue 3, pp. 1187-1195, Aug. 2003.

[54] J. Park, K. Lee, J. Shin, K. Y. Lee, “A particle swarm optimization for economic dispatch with nonsmooth cost functions,” IEEE Transactions on Power Systems, vol. 20, issue 1, pp. 34-42, Feb. 2005.

[55] M. A. Abido, “Multiobjective particle swarm for environmental/economic dispatch problem,” Proc. Of International Power Engineering Conference (IPEC 2007), pp. 1385-1390, Dec. 2007.

[56] A. Parastar, A. Pirayesh, J. Nikoukar, “Optimal location of FACTS devices in a power system using modified particle swarm optimization”, Proc. Of International Universities Power Engineering Conference, pp. 1122-1128, Sept. 2007.

[57] G. I. Rashed, H. I. Shaheen, S. J. Cheng, “Optimal Location and Parameter Setting of TCSC by Both Genetic Algorithm and Particle Swarm Optimization”, Proc. Of IEEE Conf. on Industrial Electronics and Application, pp. 1141-1147, May 2007.

[58] Y. D. Valle, J. C. Hernandez, G. K. Venayagamoorthy, R. G. Harley, "Multiple STATCOM Allocation and Sizing Using Particle Swarm Optimization", IEEE Power Systems Conference and Exposition, 2006.

[59] D. Divan, et al., “Dynamic Control of Grid Assets Using Direct AC Converter Cells”, research proposal submitted to ARPA-E, July 2010.

[60] D. Das, A. Prasai, R. G. Harley, D. Divan, "Optimal placement of Distributed Facts devices in power networks Using Particle Swarm Optimization", IEEE Energy Conversion Congress and Exposition, 2009.

[61] R. Inzunza, H. Akagi, "A 6.6-kV transformerless shunt hybrid active filter for installation on a power distribution system", IEEE Transactions on Power Electronics, Volume: 20 , Issue: 4,Publication Year: 2005 , Page(s): 893 – 900

[62] CAEM study report, “Chips, hits, bits & bytes: Tools for Transmission” available online at http://www.caem.org/website/pdf/Grid%20Background.pdf

[63] P. F. RIBEIRO, M. L. CROW, "Energy Storage Systems for Advanced Power Applications", available online at http://www.calvin.edu/~pribeiro/misc/Papers%20Published/energy%20storage%20systems.pdf

[64] D. Divan, "Distributed Intelligent Power Networks – A New Concept for Improving T&D System Utilization and Performance", available online at http://www.ece.cmu.edu/~electriconf/2004/Divan_CMU-paper2-11-041.pdf

[65] S. Bhattacharya, Po-Tai Cheng; D. M. Divan, "Hybrid solutions for improving passive filter performance in high power applications", IEEE Transactions on Industry Applications, Volume: 33 , Issue: 3, Publication Year: 1997 , Page(s): 732 – 747

[66] Y. Liang, C. O. Nwankpa, "A power-line conditioner based on flying-capacitor multilevel voltage-source converter with phase-shift SPWM", IEEE Transactions on Industry Applications, Year 2000, Volume: 36 , Issue: 4

[67] G. P. Adam, et al., "Capacitor Balance Issues of the Diode-Clamped Multilevel Inverter Operated in a Quasi Two-State Mode," Industrial Electronics, IEEE Transactions on, vol. 55, pp. 3088-3099, 2008.

[68] S. J. Huang and J. C. Wu, "Design and operation of cascaded active power filters for the reduction of harmonic distortions in a power system," Generation, Transmission and Distribution, IEE Proceedings-, vol. 146, pp. 193-199, 1999.

[69] G. P. Adam, O. Anaya-Lara, G. Burt, S.J. Finney, B.W. Williams and J. McDonald, “Comparison between Two VSCHVDC Transmission Systems Technologies: Modular and Neutral Point Clamped Multilevel Converter,” 13th Annual conference of the IEEE Industrial Electronic Society IECON2009, Porto-Portugal, 3rd -5th November 2009.

[70] M. P. Bahrman and B. K. Johnson, “The ABCs of HVDC Transmission Technologies: An Overview of High Voltage Direct Current Systems and Applications,” IEEE Power and Energy Magazine, March/April 2007, pp. 32-44.

[71] R. Inzunza and H. Akagi, "A 6.6-kV transformerless shunt hybrid active filter for installation on a power distribution system," Power Electronics, IEEE Transactions on, vol. 20, pp. 893-900, 2005.

[72] H. Akagi, "Keynote speech - active filters and energy storage systems for power conditioning in japan," in Power Electronics Systems and Applications, 2004. Proceedings. 2004 First International Conference on, 2004, pp. 78-79.

[73] H. Akagi and T. Hatada, "Voltage Balancing Control for a Three-Level Diode-Clamped Converter in a Medium-Voltage Transformerless Hybrid Active Filter," Power Electronics, IEEE Transactions on, vol. 24, pp. 571-579, 2009.

[74] H. Akagi, et al., "Control and Performance of a Transformerless Cascade PWM STATCOM With Star Configuration," Industry Applications, IEEE Transactions on, vol. 43, pp. 1041-1049,2007.

[75] S. Fukuda, et al., "Control Strategies of a Hybrid Multilevel Converter for Expanding Adjustable Output Voltage Range,"Industry Applications, IEEE Transactions on, vol. 45, pp. 827-835, 2009.

[76] D. Divan, J. R. Mayor, F. Lambert, “Dynamic Control of Grid Assets Using Direct AC Converter Cells”, available on ARPA-E website at http://arpa-e.energy.gov/LinkClick.aspx?fileticket=D8FbTmhTQI4%3D&tabid=416

[77] A. Prasai, D. M. Divan, “Active AC Snubber for Direct AC/AC Power Converters”, IEEE Energy Conversion Congress and Exposition (ECCE), 2011.

[78] H.W. Dommel, W. F. Tinney, "Optimal Power Flow Solutions", IEEE Transactions on Power Apparatus and Systems, 1968, Volume PAS-87, Issue: 10

[79] J. Peschon, D. W. Bree Jr., L. P. Hajdu, "Optimal power-flow solutions for power system planning", Proceedings of the IEEE, Volume: 60 , Issue: 1, Publication Year: 1972

[80] A. G. Bakirtzis, P. N. Biskas, C. E. Zoumas, V. Petridis, "Optimal power flow by enhanced genetic algorithm", IEEE Transactions on Power Systems, Volume: 17 , Issue: 2, Publication Year: 2002 , Page(s): 229 – 236